

# Equation of Motion Method to strongly correlated Fermi systems and Extended RPA approaches

P. Schuck

*Université Paris-Saclay, CNRS-IN2P3, IJCLab, 91405 Orsay, France and  
Université Grenoble Alpes, CNRS, LPMMC, 38000 Grenoble, France*

D.S. Delion

*"Horia Hulubei" National Institute of Physics and Nuclear Engineering,  
407 Atomistilor, RO-077125 Bucharest-Magurele, România and  
Academy of Romanian Scientists, 3 Ilfov RO-050044, Bucharest, România*

J. Dukelsky

*Instituto de Estructura de la Materia, CSIC, Serrano 123, E-28006 Madrid, Spain*

M. Jemai

*Laboratory of Advanced Materials and Quantum Phenomena,  
Physics Department, FST, El-Manar University, 2092 Tunis, Tunisia  
ISSATM, Carthage University, Avenue de la République P.O. Box 77-1054 Amilcar, Tunis, Tunisia*

E. Litvinova

*Department of Physics, Western Michigan University, Kalamazoo, MI 49008, USA  
National Superconducting Cyclotron Laboratory, Michigan State University, East Lansing, MI 48824, USA and  
GANIL, CEA/DRF-CNRS/IN2P3, F-14076 Caen, France*

G. Röpke

*Universität Rostock, FB Physik, Universitätspatz, D-18051 Rostock, Germany*

M. Tohyama

*Kyorin University School of Medicine, Mitaka, Tokyo 181-8611, Japan*

(Dated: September 1, 2020)

The status of different extensions of the Random Phase Approximation (RPA) is reviewed. The general framework is given within the Equation of Motion Method and the equivalent Green's function approach for the so-called Self-Consistent RPA (SCRPA). The role of the Pauli principle is analyzed. A comparison among various approaches to include Pauli correlations, in particular, renormalized RPA (r-RPA), is performed. The thermodynamic properties of nuclear matter are studied with several cluster approximations for the self-energy of the single-particle Dyson equation. More particle RPA's are shortly discussed with a particular attention to the  $\alpha$ -particle condensate. Results obtained concerning the Three-level Lipkin, Hubbard and Picket Fence Models, respectively, are outlined. Extended second RPA (ESRPA) is presented.

PACS numbers: 21.60.Jz, 21.60.Gx, 24.10.Cn

Keywords: Self-Consistent Random Phase Approximation, Equation of motion method, Green function, Three level Lipkin model, Hubbard model, Picket Fence Model,  $\alpha$ -condensate, Extended RPA, Time Dependent Density Method

# CONTENT

- I Introduction
- II The Equation of Motion Method
  - A Rowe's Equation of Motion method, self-consistent RPA (SCRPA), and connection with Coupled Cluster theory
  - B Renormalized RPA
  - C The correlation energy and the boson aspect of the Self-Consistent Random Phase Approximation (SCRPA)
  - D SCRPA in the particle-particle channel
  - E Self-Consistent Quasi-particle RPA (SCQRPA)
  - F Number conserving ph-RPA in superfluid nuclei
  - G Odd-particle number random phase approximation
- III Applications of SCRPA
  - A Picket Fence (pairing) Model
  - B Three level Lipkin model
  - C Hubbard model
  - D Various applications and extensions of the renormalized RPA
- IV The Green's Function Formalism
  - A Static part of the BSE kernel
  - B Dynamic part of the BSE kernel
  - C The ph-channel
  - D The particle-vibration-coupling (PVC) approach
  - E Application of the Green's Function Approach to the pairing model at finite temperature
- V Single-particle Green's function, Dyson equation, and applications to thermodynamic properties of nuclear matter
  - A Relation of the s.p. Green's function to the ground state energy. The tadpole, perturbative particle-vibration coupling, and the spurious mode
  - B An application to the Lipkin model of the coupling constant integration with SCRPA
  - C Inclusion of particle-particle RPA correlations into the self-energy. The T-matrix approximation
  - D Single-particle Green's function from Coupled Cluster Doubles (CCD) wave function. Even-odd self-consistent RPA. Application to the Lipkin model
  - E Cluster expansion of the single-particle self-energy and applications to infinite nuclear matter problems
  - F Applications of the in-medium two nucleon problem and the T-matrix approximation for the s.p. self-energy
- VI Quartetting and  $\alpha$ -particle condensation
  - A Critical temperature for  $\alpha$  condensation
  - B 'Gap' equation for quartet order parameter
- VII Second RPA and extensions
  - A Extended RPA (ERPA) equation
  - B Hermiticity of ERPA matrix
  - C Orthonormal condition
  - D Energy-weighted sum rule
  - E Spurious modes in ERPA and SCRPA
  - F Approximate forms of ERPA
  - G particle-particle ERPA equation
- VIII Applications
  - A Selfconsistent second RPA in the exactly solvable single shell pairing model
  - B Lipkin model
  - C Hubbard model
  - D Damping of giant resonances
- IX Discussion and Conclusions
- References

## I. INTRODUCTION

The solution of the many body problem of quantum gases or quantum fluids is a formidable challenge. In spite of considerable progress and tremendous effort in the past fifty years, we still have no general theory at hand which allows to accurately calculate many properties of strongly correlated many body quantum systems. Of course the Hartree-Fock (HF) or effective mean field approaches [1–5] are well accepted in almost every branch of many body physics as the first basic and necessary step. Many qualitative features can be explained by this method and, if one takes the case of Bardeen-Cooper-Schrieffer (BCS) theory [1–5] as an example for the description of superconducting or superfluid Fermi systems, sometimes even very accurate predictions of the phenomena can be obtained. These one body mean field approaches are in general non perturbative and in the case of the pure HF theory this corresponds to a Rayleigh-Ritz variational principle yielding an upper bound to the true ground state energy which is, of course, a very desirable feature. However, effective mean field theories based on density functionals or effective forces, like they are in use for band structure calculations in condensed matter or for ground state energies of atomic nuclei, usually cannot assure such an upper bound limit of the energy. The consensus which prevails on the level of one body mean field theory, unfortunately, is already lost on the next level of sophistication, when it comes to two body correlations or quantum fluctuations. Indeed, quite a variety of formalisms exist to deal with correlation functions beyond the mean field level. Of course the most ambitious attempt is to calculate two body correlations also from a Rayleigh-Ritz variational principle. Since mean field theory corresponds to a variational wave function of the coherent state type with a one body operator in the exponent, it is natural to extend this to include also a two body operator for two body correlations [1, 6, 7]. However, a most general two-body operator in the exponent is by far too complicated for practical purposes, so that various restrictions on the two-body term have been imposed in the past [1]. A most natural choice is a *local* two body operator leading to the famous Jastrow or Gutzwiller type of variational wave functions [1, 7] together with Quantum Monte Carlo (QMC) methods [8, 9].

However, even these restricted variational ground state wave functions are extremely complicated to be put in full operation. The method of correlated basis functions [10], the hypernetted chain expansion [1, 11] and renormalisation group methods (RGM) [12] are, besides QMC, ways of how to treat this problem. Once the ground state problem is solved, there remains the question of how to obtain the excited states. For this, separate developments based on the previously obtained ground state wave functions are necessary. Though a Rayleigh-Ritz variational method seems conceptually the cleanest way to treat correlations with its nonperturbative and well

controlled aspects, because of its high complexity and numerical difficulties in practical applications, quite a variety of other methods is in use. The oldest but because of its simplicity still very much employed consists of partial resummation of bubbles (Random Phase Approximation, RPA) in the particle-hole (ph) channel [1–5] or of ladders (Bethe-Goldstone equation, Brueckner-Hartree-Fock or Galitskii-Feynman T-matrix equation) in the particle-particle (pp) channel [4, 5].

In spite of the general usefulness of these approaches, they suffer from obvious short comings, like violation of the Pauli principle, uncontrolled (*e.g. non-conserving*) approximations, self-energy but not vertex corrections, etc. Therefore, in order to correct for these short comings, at least partially, more sophisticated approaches have been invented correcting one or several of these deficiencies, but in general not all of them. For example Coupled Cluster Theory (CCT) [1, 6, 13] also starts from an exponential with, as a first correction to HF, a two body operator in the exponent. However, it is not used as a variational wave function but the Schrödinger equation is closed by its projection on the basis of uncorrelated HF states. This leads to a non-Hermitian problem, which lacks the upper bound theorem of the Rayleigh-Ritz variation, but which is otherwise quite general and has been successfully applied to a variety of physics problems [6]. It contains RPA as a limiting case, but in general for excited states and also for finite temperature extra ingredients have to be and have been invented [6]. Usually what makes the problem with a two-body operator in the exponent difficult, is the fact that the corresponding wave function does not correspond to a unitary transformation of some reference state and then the norm of the correlated wave function is very difficult to evaluate. The method of flow equations [14] just tries to establish a unitary transformation going beyond HF in a systematic way. This is a relatively new approach, which is quite general. It seems, however, that correlation functions are very difficult to obtain from this theory. As mentioned, other well established methods are the (Quantum) Monte Carlo, or Path Integral Approaches [3? ?]. For Bose systems they are quite efficient approaching the exact solutions of various quantum many body systems quite accurately, but for correlated Fermi systems the so called sign problem has so far prevented from a real break through and mostly the method is restricted to separable interactions. The methods described above being quite general and applicable practically to any system of interacting fermions or bosons, there also exist numerous methods more or less tailored to specific problems. The Gutzwiller ansatz for the ground state wave function of the Hubbard model is a famous example but again the ansatz can in general not be carried through and is accompanied by the so-called Gutzwiller approximation [7]. Other methods try to attack the many-body fermion problem by diagonalizing huge matrices with more or less sophisticated algorithms like, *e.g.* the one by Lanczos or by different renormalisation group methods [15].

It is, however, not our intention here to be exhaustive in the description of all existing theories. We rather will now give the motivation and a basic outline of the many body formalism which shall be the subject of the present article. Roughly speaking our approach can be characterised by the Equation of Motion (EOM) method in conjunction with extended RPA theories. EOM has, of course, been applied to the many body problem since its early days. However, we believe that the potential of this method has never been fully exploited. In the last couple of years we have developed this formalism and applied it with very good success to various physical problems. In spite of the fact that the theory still can certainly be developed further, we believe that we have explored it sufficiently far by now to present a quite coherent and self contained frame on this subject in this report.

Let us start explaining the physical idea behind our approach. Standard single-particle mean field or HF theory aims at finding the best possible single-particle description of the system. This leads to the well known self consistent HF mean field Hamiltonian, where the two body interaction is averaged over the single-particle density. The idea is now that a many body quantum system not only consists out of a gas of independent mean field quasiparticles but also, in a further step, out of a gas of quantum fluctuations, built out of fermion or boson pairs. These quantum fluctuations then make up their own mean field, in spirit very similar to the ordinary single-particle mean field. As an example, if bound states are formed, they may be considered as new entities producing their own mean field. The formulation of this Cluster Mean-Field (CMF) or Self-Consistent RPA (SCRPA) approach [16–23] will be given below in Sect. II and IV. If the quantum fluctuations can be represented by bosons and the fermion Hamiltonian is mapped into one of interacting bosons, then the concept of a mean field for these bosons can be easily accepted. The difficulty comes from the fact that we want to avoid as far as possible bosonisation and always stay within the original fermion description and then the concept of the mean field for quantum fluctuations (correlated fermion) becomes less evident. In the main text we, however, will show how this concept can be worked out quite rigorously starting from different initial descriptions of the many body system leading, however, to the same final result.

In this review, we will concentrate on interacting Fermi systems while our approach can rather straightforwardly also be applied to Bose systems or to mixed Bose-Fermi ones. Let us here give a short outline of the main ingredients of our approach based on the Equation of Motion method. One particularly simple way to introduce the generalised mean field equations via the EOM is given by the minimisation of the energy weighted sum rules [24]. For pedagogical reasons we want to start out with the rederivation of a well known example which are the Hartree-Fock-Bogoliubov (HFB) equations for interact-

ing fields of bosons  $b_\alpha^\dagger, b_\alpha$  [1, 5]. The Bogoliubov transformation among these operators reads

$$q_\nu^\dagger = \sum_\alpha [U_{\nu\alpha} b_\alpha^\dagger - V_{\nu\alpha} b_\alpha] . \quad (1.1)$$

The transformation shall be unitary and therefore the amplitudes  $U$  and  $V$  obey the usual orthonormality and completeness relations [1, 5].

The coefficients  $U$  and  $V$  will be determined from extremum of the following energy weighted sum rule [24]

$$e_\nu = \frac{1}{2} \frac{\langle 0 | [q_\nu, [H, q_\nu^\dagger]] | 0 \rangle}{\langle 0 | [q_\nu, q_\nu^\dagger] | 0 \rangle} , \quad (1.2)$$

where the ground state  $|0\rangle$  is defined below. Schematically the minimisation leads to the following set of equations

$$\begin{pmatrix} h & \Delta \\ -\Delta^* & -h^* \end{pmatrix} \begin{pmatrix} U \\ V \end{pmatrix} = E \begin{pmatrix} U \\ V \end{pmatrix} , \quad (1.3)$$

with  $h = \langle 0 | [b, [H, b^\dagger]] | 0 \rangle$  and  $\Delta = \langle 0 | [b, [H, b]] | 0 \rangle$ . With  $H$  containing a two body boson interaction of the form  $\sum v b^\dagger b^\dagger b b$  we easily verify that  $h$  and  $\Delta$  are given in terms of single-particle densities  $\langle 0 | b^\dagger b | 0 \rangle$  and  $\langle 0 | b^\dagger b^\dagger | 0 \rangle$ , respectively. In the EOM one always assumes the existence of a ground state  $|0\rangle$ , which is the well known vacuum of the new quasiparticle operators  $q_\nu |0\rangle = 0$ , for all  $\nu$ , see, e.g., [1, 5]. The states  $|\nu\rangle = q_\nu^\dagger |0\rangle$  are then the excited states of the system. Either now one constructs the ground state from the vacuum condition and one evaluates the single-particle densities in terms of the amplitudes  $U$  and  $V$ , or one demands that the transformation (1.1) be unitary in which case this relation can be inverted and the operators  $b^\dagger, b$  can be expressed in terms of  $q^\dagger, q$ . Inserting this into the expression for the densities, moving the destruction operators to the right and exploiting the above mentioned vacuum condition, again one evaluates the densities in terms of the amplitudes  $U$  and  $V$ . The resulting nonlinear and self-consistent equations are, of course, identical with the original HFB equations for bosons [1, 5]. In a very similar way one can derive the HFB equations for fermions.

Let us now indicate how in complete analogy to the HFB equations one derives self consistent equations for e.g. fermion pair operators, or any other clusters of fermion or boson operators, or a mixture of both. As a definite case let us consider the well known example of density fluctuations in a Fermi system. We start with the definition of an RPA-type of excitation operator in the particle-hole channel, i.e. describing density excitations

$$Q_\nu^\dagger = \sum_{ph} [X_{ph}^\nu a_p^\dagger a_h - Y_{ph}^\nu a_h^\dagger a_p] , \quad (1.4)$$

where  $a^\dagger, a$  are fermion creation/destruction operators and the indices  $p, h$  stand for "particle" and "hole" states of a yet to be defined "optimal" single-particle basis. It is recognized that the operators  $Q_\nu^\dagger$  of (1.4) contain a Bogoliubov transformation of fermion pair operators

$a_p^\dagger a_h$ . If they are approximated by ideal Bose operators  $a_p^\dagger a_h \rightarrow B_{ph}^\dagger$ , as in standard RPA [5], (1.4) constitutes a Bogoliubov transformation among bosons quite analogous to (1.1). We, however, want to stress the point that we will avoid "bosonisation" as far as possible and stay with the fermion pair operators, as in (1.4).

Furthermore, the operator of (1.4), as in standard HFB, should have the properties

$$Q_\nu^\dagger |0\rangle = \nu, \quad (1.5)$$

$$Q_\nu |0\rangle = 0, \quad (1.6)$$

that is the application of  $Q_\nu^\dagger$  on the ground state  $|0\rangle$  of the system creates an excited state and at the same time the ground state should be the "vacuum" to the destructors  $Q_\nu$ . In order to determine the amplitudes  $X, Y$  of (1.4) we use in analogy with (1.2) a generalised sum rule

$$\Omega_\nu = \frac{1}{2} \frac{\langle 0 | [Q_\nu, [H, Q_\nu^\dagger]] | 0 \rangle}{\langle 0 | [Q_\nu, Q_\nu^\dagger] | 0 \rangle}, \quad (1.7)$$

which we make stationary with respect to  $X, Y$ . This leads to the RPA-type of equations of the form

$$\begin{pmatrix} \mathcal{A} & \mathcal{B} \\ -\mathcal{B}^* & -\mathcal{A}^* \end{pmatrix} \begin{pmatrix} X \\ Y \end{pmatrix} = \Omega \begin{pmatrix} \mathcal{N} & 0 \\ 0 & -\mathcal{N} \end{pmatrix} \begin{pmatrix} X \\ Y \end{pmatrix}, \quad (1.8)$$

which are the counterpart of the HFB equations for bosons described above. The matrices  $\mathcal{A}$  and  $\mathcal{B}$  contain corresponding double commutators involving the fermion pair operators and the matrix  $\mathcal{N}$  stems from the fact that the fermion pair operators do not have ideal Bose commutation relations. With a Hamiltonian containing a two body interaction, one easily convinces oneself that the matrices  $\mathcal{A}, \mathcal{B}, \mathcal{N}$  contain no more than single-particle and two particle densities of the schematic form  $\langle 0 | a^\dagger a | 0 \rangle$  and  $\langle 0 | a^\dagger a^\dagger a a | 0 \rangle$ . Evaluating these expectation values with the HF ground state leads to the standard HF-RPA equations (as obtained from Time Dependent Hartree-Fock (TDHF) in the small amplitude limit, that is with exchange). However, in general (1.6) is not fulfilled with a HF state but leads to a correlated state containing the  $X$  and  $Y$  amplitudes. Evaluating the one and two particle densities with such correlated ground state leads to matrices  $\mathcal{A}, \mathcal{B}, \mathcal{N}$  which depend on the amplitudes  $X, Y$  and therefore a selfconsistency problem is established quite analogous to the HFB problem for bosons described above. We call these generalised RPA equations the Self-Consistent RPA (SCRPA) equations.

Contrary to the original HFB approach for bosons, the determination of functionals  $\mathcal{A}[X, Y], \mathcal{B}[X, Y], \mathcal{N}[X, Y]$  is, in general, not possible without some approximation. This stems from the fact that Eq. (1.6) can, besides in exceptional model cases, not be solved exactly for the ground state  $|0\rangle$ . However, as we will show in the main text, it is possible to solve (1.6) with a somewhat extended RPA operator and the corresponding ground state wave function will be the well known Coupled-Cluster Doubles (CCD) wave function. We will explain this in detail in

Section II. On the other hand, if one sticks to the usual RPA ph-operator (1.4), in general the condition (1.6) will only be approximately fulfilled. Essentially two strategies are then possible: either one evaluates the one- and two-body densities with an approximate ground state as, e.g. the HF one, or, in the case of a broken symmetry, projected HF, etc. Or one inverts relation (1.4), inserts the  $ph$  pair operators into the densities, commutes the destructors  $Q_\nu$  to the right and uses (1.6). We will show in the main text that the second method, i.e. the one using the inversion of (1.4), leads mostly to much better results. Details of the method and applications also will be given.

We should stress at this point that the above mentioned necessary approximations again lead to certain violation of the Pauli principle. However, as we will show in our examples, SCRPA often quite dramatically improves over standard RPA. Naturally this occurs, for instance, in situations where standard RPA breaks down, i.e. close to a phase transition point or for finite systems with very few number of particles. Let us point out here again that (1.6) can be solved for the ground state if an extension of the operator (1.4) including some specific two body terms is used. We will present this extended approach in section II.B.

The above summary describes the essentials of our method on the example of density fluctuations. However, EOM is not at all restricted to this case. One can in the same way treat pair-fluctuations involving fermion pairs  $a^\dagger a^\dagger$  and  $aa$ . Formally there is no restriction in the choice of the composite operators. To describe quadrupletting, quadruple operators like  $a^\dagger a^\dagger a^\dagger a^\dagger$  shall be used. One can consider second order density fluctuations with  $a^\dagger aa^\dagger a$ , odd numbers of operators as  $a^\dagger a^\dagger a$  and so on. The same can be repeated for Bose systems using clusters of Bose operators [25] Also mixtures of bosonic and fermionic operators can be treated in an analogous way [26–28].

The above formalism can also be derived using many body Green's functions [17, 19, 22, 29]. This has the important advantage that generalisation to finite temperature is straightforward and we will give an example where SCRPA at finite temperature is solved. SCRPA equations can numerically be solved for pairs of fermion operators  $a^\dagger a$  or  $aa$ , since the equations are of the Schroedinger type. They are not more complicated as, e.g., self-consistent Bruckner-HF equations [5]. However, in general, for higher clusters this is not possible at present without drastic approximations. We will further point out that SCRPA is a conserving approach with all the appreciable properties of standard RPA, as, e.g., Ward identities, maintained. We want to point out that the Green's function formalism used, is the one based on so-called two times Green's functions  $-i\langle TA(t)A^\dagger(t') \rangle$  where the operators  $A$  may be clusters of single fermion (or boson) operators. Quite naturally this then leads to Dyson type of equations for those 'cluster' Green's functions which, at equilibrium, depend only on one energy

variable. This is contrary to the usual where many body Green's functions depend on as many times (energies) as there are single-particle operators involved [1]. It has, however, become evident that equations for those many time Green's functions, involving parquet diagram techniques [1], are extremely difficult to solve numerically (besides lowest order equations, this was not achieved) and, therefore, we stick to the above type of propagators depending on only one energy variable. This then leads to Schrödinger type of equations which are much more accessible for a numerical treatment. In this vain we will introduce a Dyson-Bethe-Salpeter Equation (Dyson-BSE) for fermion pairs with an integral kernel which, at equilibrium, depends only on a time difference as the initial pair propagator or, after Fourier transform, this kernel depends only on one frequency, that is, in the case of the response function on the frequency of the external field. The kernel can be expressed by higher correlation functions and, thus, has a definite form ready for well chosen approximations. This one frequency Dyson-BSE is formally as exact as is the usual multi-time BSE.

The review is organized as follows. In Sect. II we will explain the EOM in detail for the example of the response function leading to the self-consistent RPA (SCRPA). A sub product is the renormalized RPA (r-RPA) presented in Sect. II.A. The boson aspect of SCRPA and the SCRPA correlation energy is discussed in Sect. II.B. In Sect. II.C we show how an extended RPA operator can annihilate the CCD wave function. The SCRPA in the particle-particle channel and the self-consistent quasi-particle RPA are outlined in Sects. II.D and II.E, respectively. The very interesting number conserving ph-RPA in superfluid nuclei is presented in Sect. II.F. For odd particle numbers we derive an odd-RPA (o-RPA) in Sect. II.G. In Sections III.A,B,C, we give examples, where SCRPA is applied to the pairing model, the three-level Lipkin model, the Hubbard model, respectively. In Sect. III.D applications of the r-RPA are discussed. In Sect. IV the Green's function formalism with the EOM method is shown to be equivalent to SCRPA with, however, extensions to higher correlations leading to a formally exact Bethe-Salpeter equation of the Dyson form (Dyson-BSE) with an integral kernel depending only on one frequency. The static and dynamic parts of the kernel are presented in Sects. IV.A and IV.B and in Sect. IV.C special attention is paid to the ph-channel. In Sect. IV.D the particle-vibration coupling model and its applications to nuclear structure are presented. In Sect. IV.E an application to the pairing model at finite temperature is given. In Sect. V we discuss the single-particle Green's function and its self-energy, also at finite temperature. In Sects. V.A,B,C the self-energy is presented in various approximate forms including ph-correlation and pp-ones and in general a cluster expansion of the self-energy is discussed. Sect. V.D is devoted to the cluster expansion of the single-particle self-energy and applications to infinite nuclear matter problems. In Sect. V.E applications of the so-called T-matrix approximation of the self-

energy is applied to several problems of nuclear matter. In Sect. VI we discuss quartet ( $\alpha$  particle) condensation also based on the EOM method. In Sects. VI.A,B the critical temperature and the four-nucleon order parameter are calculated in infinite nuclear matter. In Sect. VII the so-called second RPA with extensions (ERPA) is introduced with a discussion of several interesting properties of this scheme and in Sect. VIII some applications of ERPA are given. Finally, in Sect. IX we present our conclusions and perspectives.

## II. THE EQUATION OF MOTION METHOD

In this section we want to present the details of the Equation of Motion (EOM) method. As in the introduction, we will consider as a specific first example the density excitations of a many-body fermion system (later, we also will consider the two particle, that is the pairing channel). In particular, we want to derive details of the Self-Consistent RPA (SCRPA) scheme. Pioneering work in this direction has been performed about half a century ago by D. Rowe (see e.g. the review article [16]). Numerous other studies have followed [17–19, 21–23, 30–32]. But extensions of RPA have also spread into other fields like chemical physics [33–36] and electronic, that is condensed matter systems [37–39]. Let us now set the detailed frame of the EOM method following D. Rowe and also give a connection with the Coupled Cluster Doubles wave function.

### A. Rowe's Equation of Motion method, self-consistent RPA (SCRPA), and connection with Coupled Cluster theory

The basic observation of D. Rowe [16] was that, given the exact non-degenerate ground state  $|0\rangle$  of a many-body system with  $N$  particles, an excited state of the system can be obtained in applying a creation operator  $Q^\dagger$  on this ground state, which at the same time is the vacuum to the corresponding destruction operator, that is

$$Q^\dagger_\nu|0\rangle = |\nu\rangle, \quad (2.1)$$

with

$$Q_\nu|0\rangle = 0. \quad (2.2)$$

Given that  $|0\rangle$  and  $|\nu\rangle$  are, respectively, exact ground state and excited states of the many body Hamiltonian, i.e.  $H|\nu\rangle = E_\nu|\nu\rangle$  and  $H|0\rangle = E_0|0\rangle$ , one easily can write down such an excitation operator. With  $\langle\nu|0\rangle = 0$  the solution to (2.1) and (2.2) is [16]

$$Q^\dagger_\nu = |\nu\rangle\langle 0|. \quad (2.3)$$

With the help of the Schrödinger equation we then obtain

$$[H, Q^\dagger_\nu]|0\rangle = \Omega_\nu Q^\dagger_\nu|0\rangle, \quad (2.4)$$

with  $\Omega_\nu = E_\nu - E_0$  the excitation energy. Multiplying from the left with an arbitrary variation of the form  $\langle 0|\delta Q$  we obtain

$$\langle 0|[\delta Q, [H, Q_\nu^\dagger]]|0\rangle = \Omega_\nu \langle 0|[\delta Q, Q_\nu^\dagger]|0\rangle. \quad (2.5)$$

In the remainder of the review we will use a two body Hamiltonian of the form

$$H = \sum_{k_1 k_2} H_{0, k_1 k_2} a_{k_1}^\dagger a_{k_2} + \frac{1}{4} \sum_{k_1 k_2 k_3 k_4} \bar{v}_{k_1 k_2 k_3 k_4} a_{k_1}^\dagger a_{k_2}^\dagger a_{k_4} a_{k_3} \\ \equiv H_0 + V, \quad (2.6)$$

with the antisymmetrised matrix element of the two body force  $\bar{v}_{k_1 k_2 k_3 k_4} = \langle k_1 k_2 | v | k_3 k_4 \rangle - \langle k_1 k_2 | v | k_4 k_3 \rangle$ . The use of a three-body force is in principle feasible, but would unnecessarily complicate all formulas. So, we refrain from this. In (2.5) we can use the double commutator because  $\langle 0|Q_\nu^\dagger = \langle 0|H Q_\nu^\dagger = 0$  in the exact case. The variation  $\delta Q^\dagger|0\rangle$ , exhausting the complete Hilbert space (2.5), is equivalent to consider the extremum of the mean excitation energy given by an energy weighted sum rule

$$\Omega_\nu = \frac{1}{2} \frac{\langle 0|[[Q_\nu, [H, Q_\nu^\dagger]]|0\rangle}{\langle 0|[[Q_\nu, Q_\nu^\dagger]]|0\rangle}. \quad (2.7)$$

With the exact operator (2.3), (2.7) is equal to exact excitation energy of the state  $|\nu\rangle$ , i.e.  $\Omega_\nu = E_\nu - E_0$ . However, for restricted operators  $Q_\nu^\dagger$  the minimisation of (2.7) with variations  $\delta Q, \delta Q^\dagger$  (both are independent), one sees that this corresponds to minimise the energy weighted sum rule with respect to the trial operator  $Q^\dagger$ . One directly verifies that this again leads to (2.5). An obvious but important observation is that the creation operator (2.1) is an  $N$ -body operator. It is therefore a natural idea to develop this operator in a series of one, two, ...,  $N$ -body operators as follows

$$Q_\nu^\dagger = \sum_{k_1 k_2} \chi_{k_1 k_2}^\nu a_{k_1}^\dagger a_{k_2} \\ + \frac{1}{4} \sum_{k_1 k_2 k_3 k_4} \chi_{k_1 k_2 k_3 k_4}^\nu : a_{k_1}^\dagger a_{k_2}^\dagger a_{k_3} a_{k_4} : + \dots, \quad (2.8)$$

where  $.....$  means that no contractions of fermion operators are allowed within the double dots. If there are  $N$  particles in the system and one pushes above expansion up to the  $Np - Nh$  configuration, the exact result will be recovered. A demonstration of this is given in [40]. Of course, the more terms are kept in the expansion (2.8), the more difficult it will become to solve the ensuing equations (2.5), for instance, from the numerical point of view. So in the course of this review, we will restrict ourselves to the one-body and two-body terms shown in (2.8).

Before entering the details, it may, however, be instructive to present the theory from a slightly different point of view. From the Thouless theorem, see, e.g., [1, 5] we

know that a general Slater determinant and, in particular, the HF determinant can be written as

$$|\Phi_1\rangle \propto \exp \left( \sum_{ph} z_{ph} K_{ph}^\dagger \right) |\Phi_0\rangle, \quad (2.9)$$

with  $K_{ph}^\dagger = c_p^\dagger c_h$  and  $|\Phi_1\rangle$  not orthogonal to  $|\Phi_0\rangle$ . Obtaining the  $z_{ph}$  from the minimisation of the energy, one arrives at the HF Slater-determinant

$$|\text{HF}\rangle = \Pi_h a_h^\dagger |\text{vac}\rangle, \quad (2.10)$$

where the  $a_k^\dagger, a_k$  represent orthonormalised creators and destructors of the HF-orbitals. As is well known, the standard RPA is based on the HF Slater determinant as ground state [5]. The  $ph$  annihilator in standard RPA is then given by, see (1.4)

$$a_h^\dagger a_p |\text{HF}\rangle = 0. \quad (2.11)$$

For a theory which goes beyond mean-field approximation like RPA with extensions, it is then natural to consider the following wave function

$$|Z\rangle = e^{\hat{Z}} |\text{HF}\rangle, \quad (2.12)$$

with

$$\hat{Z} = \frac{1}{4} \sum_{p_1 p_2 h_1 h_2} z_{p_1 p_2 h_1 h_2} \tilde{K}_{p_1 h_1}^\dagger \tilde{K}_{p_2 h_2}^\dagger. \quad (2.13)$$

with  $\tilde{K}_{ph}^\dagger = a_p^\dagger a_h$  where, instead of a single  $ph$  operator in the exponent, there is in addition a quadratic one. It can be shown that this so-called Coupled Cluster Doubles wave function is the vacuum to the following generalized RPA operator [41, 42].

$$\tilde{Q}_\nu^+ = \sum_{ph} [\tilde{X}_{ph}^\nu \tilde{K}_{ph}^\dagger - \tilde{Y}_{ph}^\nu \tilde{K}_{ph}] \\ + \frac{1}{2} \sum_{ph p_1 p_2} \eta_{ph p_1 p_2} a_{p_1}^\dagger a_{p_2}^\dagger \tilde{K}_{ph}^\dagger \\ - \frac{1}{2} \sum_{ph h_1 h_2} \eta_{h_1 h_2 ph} a_{h_1}^\dagger a_{h_2}^\dagger \tilde{K}_{ph}, \quad (2.14)$$

that is there exists the annihilating condition

$$\tilde{Q}_\nu |Z\rangle = 0, \quad (2.15)$$

with the following relations between the various amplitudes

$$\begin{aligned}
\tilde{Y}_{ph}^\nu &= \sum_{p'h'} z_{pp'hh'} \tilde{X}_{p'h'}^\nu \\
z_{pp'hh'} &= \sum_\nu \tilde{Y}_{ph}^\nu (\tilde{X}^{-1})_{p'h'}^\nu \\
\eta_{p_1 p_2 ph}^\nu &= \sum_{h_1} z_{pp_2 hh_1} \tilde{X}_{p_1 h_1}^\nu \\
\eta_{h_1 h_2 ph}^\nu &= \sum_{p_1} z_{pp_1 hh_2} \tilde{X}_{p_1 h_1}^\nu .
\end{aligned} \tag{2.16}$$

The amplitudes  $z_{pp'hh'}$  are antisymmetric in  $pp'$  and  $hh'$ . With the above relations, the vacuum state is entirely expressed by the RPA amplitudes  $\tilde{X}, \tilde{Y}$ . As mentioned, this vacuum state is exactly the one of coupled cluster theory (CCT) truncated at the two-body level which is called CCD [1, 6]. However, the use we will make of this vacuum is very different from CCT. Of course, for the moment, all remains formal because this generalized RPA operator contains, besides the standard one-body terms, also specific two-body terms, which cannot be handled in a straightforward way. For instance, this non-linear transformation among fermion operators cannot be inverted in a simple manner as this is the case for HF or BCS quasiparticle destructors, which are annihilators of their respective wave functions. And, thus, despite being the vacuum of an annihilating operator, it is not immediately clear how to make calculations with this wave function. However, the mere existence of an exact annihilator of the CCD wave function is quite remarkable and we will see later in Sect. V.C, how this CCD with the generalized RPA may be handled in an approximate but efficient way. One may also notice that the operator (2.14) is part of the extended RPA operator considered in (2.8).

On the other hand, there exists a very suggestive and eventually very valid approximation, which replaces in (2.14) in the  $\eta$  terms the density operators  $a_{p_1}^\dagger a_{p_2}$  and  $a_{h_1}^\dagger a_{h_2}$  by their expectation values

$$a_{p_1}^\dagger a_{p_2} \rightarrow \langle a_{p_1}^\dagger a_{p_2} \rangle \simeq \delta_{p_1 p_2} n_{p_1}$$

and

$$a_{h_1}^\dagger a_{h_2} \rightarrow \langle a_{h_1}^\dagger a_{h_2} \rangle \simeq \delta_{h_1 h_2} n_{h_1}$$

with  $n_k = \langle a_k^\dagger a_k \rangle$  being the single-particle (s.p.) occupation numbers. Of course, replacing operators by c-numbers implies to violate the Pauli principle. There exists, unfortunately, no simple measure which tells in general how severe this violation is. However, in some non-trivial models, where this approximation could be tested, it turned out that the violation stays quite mild [42]. This is, for instance, the case in the Richardson pairing model, where the respect of the Pauli principle is extremely important [43], because the s.p. levels are only two-fold degenerate. In any case, adopting above

approximation leads us immediately to the usual ansatz for the RPA creation operator, which is

$$Q_\nu^\dagger = \sum_{ph} \left[ X_{ph}^\nu a_p^\dagger a_h - Y_{ph}^\nu a_h^\dagger a_p \right], \tag{2.17}$$

and which has already been presented in the Introduction (1.4). Besides the hypothesis that the replacements of density operators by their expectation values, leading to (2.17), is in general a good approximation, we can now also give all the well-known arguments under which the ansatz (2.17) should yield a good description of excited states of a Fermi system. As we know, this is usually the case for collective excitations of the system. For instance, the plasma oscillation in electronic systems or Giant Resonances (GR) in nuclei are, among many other examples, of this kind. Of course, in considering finite systems like finite electronic devices and nuclei the size of those systems also plays a role: the number of particles should be large in order that collectivity can develop.

As we already mentioned, we make the reasonable hypothesis that, considering the reduced RPA operator (2.17), does not violate the Pauli-principle strongly. We, thus, can suppose that the annihilating condition (2.2) is also still valid and Eq. (2.5) can be used to calculate excited states. Before giving the details of the equations, we, however, want to proceed to a generalisation. Since Eq. (2.5) implies ground state correlations, the s.p. occupation numbers  $n_k$  will not be any longer of the step function form like with the HF approach but will be rounded close to the Fermi surface. Then, there is no need any longer to restrict the summation in the RPA operator to the  $ph$  domain, but the amplitudes  $X, Y$  can also contain  $hh'$  and  $pp'$  configurations. Consequently, we will choose the amplitudes in (2.8)  $\chi_{mi}^\nu \equiv \tilde{X}_{mi}^\nu$  with  $m > i$  different from the amplitudes  $\chi_{im}^\nu \equiv -\tilde{Y}_{im}^\nu$  with  $i < m$  and all  $\chi_{kk}^\nu \equiv 0$ . We then write for the one body part of (2.8) (unless otherwise stated, we will hitherto make the convention that indices  $m, n > i, j$ )

$$Q_\nu^\dagger = \sum_{m>i} \left[ \tilde{X}_{mi}^\nu a_m^\dagger a_i - \tilde{Y}_{mi}^\nu a_m^\dagger a_i \right]. \tag{2.18}$$

It is, of course, evident, that the operator (2.18) depends very much on the single-particle basis, since any change of the basis will again create a hermitian part  $\chi_{kk} a_k^\dagger a_k$ . Therefore, it is very important to write down the operator  $Q_\nu^\dagger$  of (2.18) in a single-particle basis, which is optimal. As usual, we will choose the one which minimises the ground state energy. It turns out that the ensuing equation is given by  $\langle 0 | [H, Q_\nu] | 0 \rangle = 0$ . How this goes in detail will be demonstrated below. It is, however, clear that this relation is just another equation of motion, fulfilled in the exact case. This single-particle basis will be given by a generalised single-particle mean-field Hamiltonian. It may be instructive to divide for a moment the space into occupied levels ( $h$ : holes) and unoccupied levels ( $p$ : particles). To be definite let



us consider 4 levels with the Fermi energy in the middle. We then order the states according to this energy  $p_4 > p_3 > h_2 > h_1$ . We thus have six  $X^\nu$  amplitudes:  $X_{p_4 p_3}^\nu$ ,  $X_{h_2 h_1}^\nu$ ,  $X_{p_4 h_2}^\nu$ ,  $X_{p_4 h_1}^\nu$ ,  $X_{p_3 h_2}^\nu$ ,  $X_{p_3 h_1}^\nu$  and corresponding six  $Y^\nu$  amplitudes. We anticipate that in the standard RPA [1–5] only the  $ph$  amplitudes survive. However, as we will see, in the more general approach of SCRPA also all other amplitudes can, in principle, be included, which may give non-negligible contributions. This will, for instance, become important later, when we shall discuss conservation laws and the Goldstone theorem in the case of spontaneously broken symmetries.

From (2.18) we see that this leads to an excited state  $|\nu\rangle = Q_\nu^\dagger|0\rangle$ , which is not normalised, i.e.  $\langle\nu|\nu\rangle = \langle 0|[Q_\nu, Q_\nu^\dagger]|0\rangle \neq 1$ . We therefore introduce slightly modified amplitudes and write

$$Q_\nu^\dagger = \sum_{m>i} \left( X_{mi}^\nu \delta Q_{mi}^\dagger - Y_{mi}^\nu \delta Q_{mi} \right), \quad (2.19)$$

where

$$\delta Q_{mi}^\dagger = \frac{A_{mi}}{\sqrt{n_i - n_m}}, \quad A_{mi} = a_m^\dagger a_i, \quad (2.20)$$

are the normalised pair creation operators and

$$n_i = \langle 0|a_i^\dagger a_i|0\rangle, \quad (2.21)$$

are the single-particle occupation numbers. With this choice one immediately verifies that with

$$\sum_{m>i} \left( |X_{mi}^\nu|^2 - |Y_{mi}^\nu|^2 \right) = 1, \quad (2.22)$$

the excited states  $|\nu\rangle$  are normalised under the assumption that the single-particle density matrix only has diagonal elements that is  $\rho_{kk'} = \langle 0|a_k^\dagger a_{k'}|0\rangle = n_k \delta_{kk'}$ , a fact which will become clear in a moment, see after Eq. (2.32). With this we finally can write for Eq. (2.5)

$$\begin{pmatrix} \mathcal{A}_{mim'i'} & \mathcal{B}_{mim'i'} \\ -\mathcal{B}_{mim'i'}^* & -\mathcal{A}_{mim'i'}^* \end{pmatrix} \begin{pmatrix} X_{m'i'}^\nu \\ Y_{m'i'}^\nu \end{pmatrix} = \Omega_\nu \begin{pmatrix} X_{mi}^\nu \\ Y_{mi}^\nu \end{pmatrix}, \quad (2.23)$$

where

$$\mathcal{A}_{mim'i'} = \langle 0| \left[ \delta Q_{mi} \left[ H, \delta Q_{m'i'}^\dagger \right] \right] |0\rangle, \quad (2.24)$$

and

$$\mathcal{B}_{mim'i'} = -\langle 0| \left[ \delta Q_{mi}^\dagger \left[ H, \delta Q_{m'i'}^\dagger \right] \right] |0\rangle. \quad (2.25)$$

We realise that (2.23) has exactly the same mathematical structure as the standard RPA equations (see e.g. [1–5]). Therefore in this respect all standard RPA properties are preserved [1–5]. For instance we see that the eigenvectors  $\begin{pmatrix} X^\nu \\ Y^\nu \end{pmatrix}$  form a complete orthonormal set. It is useful to introduce the matrices

$$\mathcal{X} = \begin{pmatrix} X & Y^* \\ Y & X^* \end{pmatrix}, \quad \mathcal{N} = \begin{pmatrix} 1 & 0 \\ 0 & -1 \end{pmatrix}. \quad (2.26)$$

Equation (2.23) can then be written as

$$\mathcal{S}\mathcal{X} = \mathcal{N}\mathcal{X}\Omega, \quad (2.27)$$

where  $\mathcal{S} = \begin{pmatrix} \mathcal{A} & \mathcal{B} \\ \mathcal{B}^* & \mathcal{A}^* \end{pmatrix}$ , and the diagonal matrix  $\Omega$  contains the eigenvalues  $\begin{pmatrix} \Omega_\nu \\ -\Omega_\nu \end{pmatrix}$ , if  $\mathcal{S}$  is a positive definite matrix. Simple matrix algebra shows that

$$\begin{aligned} [\Omega, \mathcal{X}^\dagger \mathcal{N} \mathcal{X}] &= (\mathcal{N} \mathcal{X} \Omega)^\dagger \mathcal{X} - \mathcal{X}^\dagger (\mathcal{N} \mathcal{X} \Omega) \\ &= \mathcal{X}^\dagger (\mathcal{S}^\dagger - \mathcal{S}) \mathcal{X} = 0, \end{aligned} \quad (2.28)$$

that is,  $\Omega$  commutes with  $\mathcal{X}^\dagger \mathcal{N} \mathcal{X}$ , and thus  $\mathcal{X}^\dagger \mathcal{N} \mathcal{X}$  is diagonal together with  $\Omega$ . The normalisation (2.22) corresponds to the more general orthogonality relations

$$\mathcal{X}^\dagger \mathcal{N} \mathcal{X} = \mathcal{N}. \quad (2.29)$$

This closure condition is obtained by multiplying (2.29) with  $\mathcal{N}$ , which shows that  $\mathcal{N} \mathcal{X} \mathcal{N}$  is the inverse of  $\mathcal{X}^\dagger$ , or

$$\mathcal{X} \mathcal{N} \mathcal{X}^\dagger = \mathcal{N}, \quad (2.30)$$

which gives explicitly

$$\sum_\nu (X_{mi}^\nu X_{m'i'}^{\nu*} - Y_{mi}^{\nu*} Y_{m'i'}^\nu) = \delta_{mm'} \delta_{ii'}. \quad (2.31)$$

These orthonormality relations allow us to invert the operator (2.19)

$$a_m^\dagger a_i = \sqrt{n_i - n_m} \sum_\nu (X_{mi}^{\nu*} Q_\nu^\dagger + Y_{mi}^{\nu*} Q_\nu). \quad (2.32)$$

With (2.2), it then follows that the density matrix  $\langle 0|a_k^\dagger a_{k'}|0\rangle$  only has diagonal elements, as postulated after eq.(2.22).

The matrix  $\mathcal{S}$  in (2.27) can be written in the following way [44].

$$\begin{aligned} \tilde{\mathcal{S}}_{minj} &= \sqrt{n_i - n_m} \mathcal{S}_{minj} \sqrt{n_j - n_n} \\ &= (\epsilon_m - \epsilon_i) N_{mi} \delta_{ij} \delta_{mn} + N_{mi} \bar{v}_{mj} n N_{nj} + \\ &\quad \left[ -\frac{1}{2} \sum_{ll'} (\delta_{ij} \bar{v}_{ml' l''} C_{ll' nl} + \delta_{mn} \bar{v}_{ll' i' l''} C_{jl' l'' l'}) \right. \\ &\quad \left. + \sum_{ll'} (\bar{v}_{ml nl'} C_{jl' il} + \bar{v}_{jl il'} C_{ml' nl}) \right. \\ &\quad \left. - \frac{1}{2} \sum_{ll'} (\bar{v}_{mj ll'} C_{ll' in} + \bar{v}_{ll' in} C_{mj ll'}) \right], \end{aligned} \quad (2.33)$$

where  $\epsilon_k$  are the HF s.p. energies,  $N_{mi} = n_i - n_m$ , and

$$C_{mim'i'} = \langle a_m^\dagger a_{i'}^\dagger a_i a_m \rangle - n_m n_i \delta_{mi, m'i'}. \quad (2.34)$$

With the inversion (2.32) and the annihilating condition (2.2) the RPA matrix can entirely be expressed by the  $X, Y$  amplitudes which then will depend in a very non-linear way of those amplitudes. This then constitutes the

most general SCRPA scheme.

It can immediately be verified that, if all expectation values in (2.23) are evaluated with the HF ground state, then the standard RPA equations are recovered with, in particular, only  $X_{ph}$  and  $Y_{ph}$  amplitudes surviving.

Before we come to the explicit evaluation of the matrix elements  $\mathcal{A}, \mathcal{B}$  in (2.23) in terms of  $X, Y$  we first shall deal with the already mentioned and very important question of the optimal single-particle basis. This basis is to be determined from the minimisation of the ground state energy. However, as shown in [23, 45], there exists a very elegant but equivalent way which we now will explain. If, instead of closing the EOM (2.4) from the left with a variation, we project from the left with the ground state, we obtain with (2.2)

$$\langle 0|[H, Q_\nu^\dagger]|0\rangle = \langle 0|[H, Q_\nu]|0\rangle = 0. \quad (2.35)$$

Because there are as many operators  $Q_\nu^\dagger, Q_\nu$  as there are components  $a_m^\dagger a_i, a_i^\dagger a_m$  we also can write for (2.35)

$$\langle 0|[H, a_m^\dagger a_i]|0\rangle = \langle 0|[H, a_i^\dagger a_m]|0\rangle = 0, \quad (2.36)$$

where we again recall our convention  $m > i$ . One also checks that with these relations the eventual non-hermiticity of the off-diagonal matrices in the RPA matrix (2.23) disappears. It also implies that the time derivative of the single-particle density matrix is zero at equilibrium, that is, it is stationary.

Equations (2.36) are of the one-body type and one can directly verify that with a Slater determinant as a ground state they reduce to the HF equations. However, with the RPA ground state the single-particle basis becomes coupled to the two-body RPA correlations as follows

$$\sum_{m'} H_{mm'} C_{m'\alpha} = \epsilon_\alpha n_\alpha C_{m\alpha}, \quad (2.37)$$

where  $C_{m\alpha}$  are the transformation coefficients defining the basis in which the density matrix is diagonal, the so-called canonical basis, that is

$$a_{k\mu}^\dagger = \sum_\alpha C_{k\alpha} c_{\alpha\mu}^\dagger. \quad (2.38)$$

We also introduced as short-hand notation

$$\begin{aligned} H_{mm'} &\equiv n_m \sum_\mu \epsilon_\mu C_{m\mu} C_{m'\mu} \\ &+ \frac{1}{2} \sum_{jkl} \sum_{\mu\beta\gamma\delta} [\langle m j k l \rangle V_{\alpha\beta\gamma\delta} + \langle j m k l \rangle V_{\beta\alpha\gamma\delta} \\ &+ \langle k j m l \rangle V_{\gamma\beta\alpha\delta} + \langle l j k m \rangle V_{\delta\beta\gamma\alpha}] C_{m'\mu} C_{j\beta} C_{k\gamma} C_{l\delta}, \end{aligned} \quad (2.39)$$

where  $\langle i j k l \rangle \equiv \langle a_i^\dagger a_j a_k^\dagger a_l \rangle$  are the two-body densities which, together with occupation numbers  $n_m$ , depend on the RPA amplitudes.

So this is the outline of the most general RPA scheme with a correlated ground state based on a one-body operator to generate excited states. We now will pass to some useful and simplifying approximations.

## B. Renormalized RPA

There exists a first relatively easy to handle approximation of the SCRPA equations which is usually called the renormalized RPA. Due to its simplicity for numerical realisation with existing standard RPA-codes, it has been applied in the past quite frequently. We, therefore, will give in Sect. II.D a summary of applications and possible properties and here we will only present the basics. The so-called renormalized RPA (r-RPA) is a particular version of SCRPA, defined by the factorisation of two-body densities.

$$\langle a_m^\dagger a_n^\dagger a_j a_i \rangle \simeq \langle a_m^\dagger a_i \rangle \langle a_n^\dagger a_j \rangle - \langle a_m^\dagger a_j \rangle \langle a_n^\dagger a_i \rangle. \quad (2.40)$$

It was introduced by Hara [46], but it became popular after the paper of Catara *et al.* [47], introducing a simple boson mapping method to estimate one-body densities in terms of RPA amplitudes (the so-called Catara method).

The r-RPA system of equations has practically the same form as the standard RPA one, but the matrix elements for a Hamiltonian  $H = H_0 + V$  are given by (we suppose that we work in the canonical basis where the s.p. density matrices are diagonal)

$$\begin{aligned} \sum_{k'_1 k'_2} \tilde{\mathcal{S}}_{k_1 k_2 k'_1 k'_2} N_{k'_1 k'_2}^{-1} \chi_{k'_1 k'_2}^\nu &= \\ \sum_{k'_1 k'_2} \epsilon_{k_1 k_2} \delta_{k_1 k'_1} \delta_{k_2 k'_2} + N_{k_1 k_2} \bar{v}_{k_1 k_2 k'_2 k'_1} \chi_{k'_1 k'_2}^\nu &= \Omega_\nu \chi_{k_1 k_2}^\nu, \end{aligned} \quad (2.41)$$

with  $\epsilon_{k_1 k_2} = \epsilon_{k_1} - \epsilon_{k_2}$ . More explicitly in terms of the matrices defined in (2.23) we can write

$$\begin{aligned} \mathcal{A}_{mi, m' i'} &= \frac{1}{2} \left( N_{mi}^{1/2} N_{m' i'}^{-1/2} + N_{m' i'}^{1/2} N_{mi}^{-1/2} \right) \\ &\times (\epsilon_{m' m} \delta_{ii'} - \epsilon_{ii'} \delta_{m m'}) + N_{mi}^{1/2} N_{m' i'}^{1/2} \langle i m' | v | m i' \rangle \\ \mathcal{B}_{mi, m' i'} &= N_{mi}^{1/2} N_{m' i'}^{1/2} \langle i i' | v | m m' \rangle, \end{aligned} \quad (2.42)$$

where the single-particle mean-field (MF) energies are given by

$$\begin{aligned} \epsilon_{m' m} &= \langle m' | H_0 | m \rangle + \sum_k n_k \langle m' k | v | m k \rangle \\ \epsilon_{ii'} &= \langle i | H_0 | i' \rangle + \sum_k n_k \langle k i | v | k i' \rangle, \end{aligned} \quad (2.43)$$

and where  $N_{mi}$  is the metric matrix written in terms of one-body densities  $n_m$

$$N_{mi} = \langle 0 | [A_{im}, A_{mi}] | 0 \rangle = n_i - n_m. \quad (2.44)$$

The one-body quasiparticle density can be expressed in terms of RPA amplitudes up to a fourth order precision,

by using the number operator method [16, 47], i.e.

$$\begin{aligned}
n_p &= \langle 0 | n_p^\dagger n_p | 0 \rangle \\
&\approx \sum_{h\nu\nu'} \left( \delta_{\nu\nu'} - \frac{1}{2} \sum_{p'h'} N_{p'h'} X_{p'h'}^{\nu'} X_{p'h'}^{\nu'*} \right) N_{ph} Y_{ph}^\nu Y_{ph}^{\nu'*} \\
n_h &= \langle 0 | n_h^\dagger n_h | 0 \rangle \approx 1 - \\
&\sum_{p\nu\nu'} \left( \delta_{\nu\nu'} - \frac{1}{2} \sum_{p'h'} N_{p'h'} X_{p'h'}^{\nu'} X_{p'h'}^{\nu'*} \right) N_{ph} Y_{ph}^\nu Y_{ph}^{\nu'*} .
\end{aligned} \tag{2.45}$$

It consists of working only with ph configurations like in the standard RPA and in retaining only in a systematic way the single-particle density matrices. The latter are expressed in a simple way by the  $Y$ -amplitudes of the r-RPA what constitutes a relatively easy to handle self-consistency problem. It is described in several publications and we will skip the details here referring the reader to examples, where the r-RPA method has been applied, in Sect. III.D. Let us only mention here that the r-RPA amplitudes can sustain all indices as SCRPA besides diagonal configurations. In this case r-RPA keeps all desirable properties of standard RPA intact.

### C. The correlation energy and the boson aspect of the Self-Consistent Random Phase Approximation (SCRPA)

We now come to an important aspect of the SCRPA approach as given in (2.23). It namely turns out that, like with standard RPA, also SCRPA is equivalent to a bosonisation. This stems from the fact that (2.23) has exactly the same mathematical structure as standard RPA [5]. Let us sketch shortly how this boson aspect can be made manifest. Since, as said, the structure of (2.23) is exactly the same as the one of standard RPA [5], the former can also be represented by a boson Hamiltonian

$$\begin{aligned}
H_B &= E_{\text{HF}} - \frac{1}{2} \sum_{m>i} \mathcal{A}_{mimi} \\
&+ \frac{1}{2} \begin{pmatrix} B^\dagger & B \end{pmatrix} \begin{pmatrix} \mathcal{A} & \mathcal{B} \\ \mathcal{B}^* & \mathcal{A}^* \end{pmatrix} \begin{pmatrix} B \\ B^\dagger \end{pmatrix} ,
\end{aligned} \tag{2.46}$$

where  $B^\dagger, B$  are ideal boson operators. This boson Hamiltonian can be diagonalized with a Bogoliubov transformation

$$\mathcal{O}_\nu^\dagger = \sum_{m>i} [X_{mi}^\nu B_{mi}^\dagger - Y_{mi}^\nu B_{mi}] , \tag{2.47}$$

what yields

$$H_B = E_{\text{RPA}} + \sum_\nu \Omega_\nu \mathcal{O}_\nu^\dagger \mathcal{O}_\nu , \tag{2.48}$$

with

$$\begin{aligned}
E_{\text{RPA}} &= E_{\text{HF}} - \sum_\nu \Omega_\nu \sum_{k>k'} |Y_{kk'}^\nu|^2 \\
&= -\frac{1}{2} \text{Tr} \mathcal{A} + \frac{\hbar}{2} \sum_{\nu>0} \Omega_\nu = -\frac{1}{2} \sum_{\nu>0} (E_\nu^{\text{TDA}} - \Omega_\nu) ,
\end{aligned} \tag{2.49}$$

where  $E_\nu^{\text{TDA}}$  is the corresponding excitation energy in Tamm-Dancoff approximation [5]. It is interesting to transform the  $X, Y$  amplitudes into position  $Q$  and momentum  $P$  amplitudes via, see [5]

$$\begin{aligned}
Q_{mi}^\nu &= \sqrt{\frac{\hbar}{2M_\nu \Omega_\nu}} (X - Y^*)_{mi}^\nu \\
P_{mi}^\nu &= i\hbar \sqrt{\frac{M_\nu \Omega_\nu}{2\hbar}} (X + Y^*)_{mi}^\nu ,
\end{aligned} \tag{2.50}$$

where  $M_\nu$  is the mass parameter defined in [5]. With this the correlation energy is written as

$$E_{\text{RPA}} = \sum_{mi\nu} \left[ \frac{P_{mi}^\nu{}^2}{2M_\nu} + \frac{M_\nu}{2} \Omega_\nu^2 Q_{mi}^\nu{}^2 \right] . \tag{2.51}$$

For example, in the case of the spurious translational mode where  $\Omega_\nu = 0$  and the  $X, Y$  amplitudes diverge, the correlation energy becomes

$$E_{\text{RPA}} = - \sum_{mi} \frac{|\langle m | \hat{p} | i \rangle|^2}{2Am} , \tag{2.52}$$

where  $\hat{p}$  is the momentum operator and  $A$  the total number of nucleons. The correlation energy corresponding to the translational mode is thus just the kinetic energy of the whole system.

The corresponding ground state wave function is

$$|Z\rangle = \exp \left[ \sum_{m>i, n>j} z_{kk'l'l'} B_{mi}^\dagger B_{nj}^\dagger \right] |0\rangle , \tag{2.53}$$

with  $B|0\rangle = 0$  defining the simple boson vacuum and  $\mathcal{O}_\nu|Z\rangle = 0$  the RPA boson vacuum with  $2z_{minj} = [YX^{-1}]_{minj}$ .

Details of the derivation of (2.48) can be found in [5]. The correlation functions in the double commutators of  $\mathcal{A}$  and  $\mathcal{B}$  matrices can also be evaluated with the bosonisation. Most importantly, one obtains for the occupation numbers as with standard RPA

$$n_{p_1} = \sum_{k_2 < p_1, \nu} |Y_{p_1 k_2}^\nu|^2 ; \quad n_{h_2} = 1 - \sum_{k_1 > h_2, \nu} |Y_{k_1 h_2}^\nu|^2 . \tag{2.54}$$

We will give the derivation of this formula later in the Sect. IV of the Green's functions. Actually it is known since long that from boson expansion theory we immediately find [5]

$$\langle |c_h c_{h'}^\dagger\rangle \rightarrow \sum_p (0|B_{ph}^\dagger B_{ph'}|0) = \sum_{p,\nu} Y_{ph}^\nu Y_{ph'}^{\nu*}, \quad (2.55)$$

and

$$\langle |c_p^\dagger c_{p'}\rangle \rightarrow \sum_h (0|B_{ph}^\dagger B_{p'h}|0) = \sum_{h,\nu} Y_{ph}^\nu Y_{p'h}^{\nu*}. \quad (2.56)$$

Also the other correlation functions figuring in the RPA-matrix can be expressed via the bosonisation by the RPA-amplitudes.

Let us trace back from where the fact that we end up with a boson theory took its origin. It clearly is rooted in the fact that with our operator (2.8) we cannot find a ground state wave function which fulfills the annihilating condition (2.2). If there existed a fermionic ground state wave function which fulfills the annihilating condition, the Pauli principle would *not* be violated. We, therefore, will refer to the approximation that we take the annihilating condition as fulfilled, where it is not, as the *boson approximation*. A crucial consequence of this boson approximation is the form, in which the correlation energy (2.49) is given, which again is unaltered from the standard RPA expression. In all of our applications with SCRPA we will use this expression. It is also important, as already shortly mentioned, to realize that the generalized RPA operator with *all possible indices* is necessary to maintain all the appreciated qualities of standard RPA as there are fulfillment of the sum-rule, appearance of the Goldstone mode in case of spontaneously broken symmetries, Ward identities, etc. We will come back to this later in Sect. VII.

#### D. SCRPA in the particle-particle channel

It also shall be clear that the SCRPA approach which we sketched above in the channel of fluctuations of the density operator can, in a very analogous way, also be developed in the particle pair fluctuation channel, i.e. in the particle-particle (*pp*) channel, where the *pp* ladders are summed. This leads e.g. to the Feynman-Galitskii T-matrix [4], as well as to the Thouless criterion for the onset of superfluidity [48]. In this section we will restrict the range of indices to particle states (*p*) and hole states (*h*), despite the fact that a more general domain of indices, analogous to the *ph* channel, is certainly possible. However, in the *pp*-channel this is not studied so far and we will refrain from this generalisation.

The starting point is the definition of the so-called two particle addition operator

$$A_\alpha^\dagger = \frac{1}{2} \sum_{p_1 p_2} X_{p_1 p_2}^\alpha a_{p_1}^\dagger a_{p_2}^\dagger - \frac{1}{2} \sum_{h_1 h_2} Y_{h_1 h_2}^\alpha a_{h_1}^\dagger a_{h_2}^\dagger, \quad (2.57)$$

where *p, h* again refer to the particle and hole states corresponding to an optimal single-particle basis yet to be defined. The  $X^\alpha$ ,  $Y^\alpha$  amplitudes can, as before, be determined from the extremal condition of the generalised sum rule

$$\Omega_\alpha = \frac{\langle 0|[A_\alpha, [H, A_\alpha^\dagger]]|0\rangle}{\langle [A_\alpha, A_\alpha^\dagger] \rangle}, \quad (2.58)$$

which leads to

$$\begin{pmatrix} \mathcal{A} & \mathcal{B} \\ -\mathcal{B} & -\mathcal{C} \end{pmatrix} \begin{pmatrix} X^\rho \\ Y^\rho \end{pmatrix} = \Omega_\rho \begin{pmatrix} X^\rho \\ Y^\rho \end{pmatrix}, \quad (2.59)$$

with

$$\begin{aligned} \mathcal{A}_{p_1 p_2 p'_1 p'_2} &= \langle 0|[\delta P_{p_1 p_2}, [H, \delta P_{p'_1 p'_2}^\dagger]]|0\rangle \\ \mathcal{B}_{p_1 p_2 h_1 h_2} &= \langle 0|[\delta P_{p_1 p_2}, [H, \delta P_{h_1 h_2}^\dagger]]|0\rangle \\ \mathcal{C}_{h_1 h_2 h'_1 h'_2} &= \langle 0|[\delta P_{h_1 h_2}, [H, \delta P_{h'_1 h'_2}^\dagger]]|0\rangle, \end{aligned} \quad (2.60)$$

and

$$\begin{aligned} \delta P_{p_1 p_2}^\dagger &= \frac{a_{p_1}^\dagger a_{p_2}^\dagger}{\sqrt{1 - n_{p_1} - n_{p_2}}} \\ \delta P_{h_1 h_2}^\dagger &= \frac{a_{h_1}^\dagger a_{h_2}^\dagger}{\sqrt{1 - n_{h_1} - n_{h_2}}}. \end{aligned} \quad (2.61)$$

As one verifies, the eigenvalues correspond to those, where one adds or removes two particles from the original ground state  $|0\rangle$  with *N* particles. We again have to assume that the ground state is the vacuum to the addition operators, i.e.  $A_\rho|0\rangle = 0$  (however, an exact annihilating condition can again be found with an extended RPA operator as in Sect. II.C). Also the  $X^\rho$ ,  $Y^\rho$  amplitudes have the orthonormality and completeness relations of standard *pp*-RPA, as described in textbooks [5], so we do not repeat them here. Quite analogously we can define the removal operators

$$R_\rho^\dagger = \frac{1}{2} \sum_{h_1 h_2} X_{h_1 h_2}^\rho a_{h_2} a_{h_1} - \frac{1}{2} \sum_{p_1 p_2} Y_{p_1 p_2}^\rho a_{p_2} a_{p_1}. \quad (2.62)$$

Again amplitudes can be determined from the stationarity of the corresponding sum rule. The resulting RPA equations have a similar structure as in Eqs. (2.59) and (2.60). Actually, the content of RPA equations for removal is the same as the one for addition. Only the amplitudes  $X^\alpha$ ,  $Y^\alpha$  and  $X^\rho$ ,  $Y^\rho$  have subtle relations involving interchange of  $p \leftrightarrow h$  indices and relative phases. There exist quite extended applications to the pairing Hamiltonian of this self-consistent particle-particle RPA

(SCppRPA), where things are explained in detail and which we shortly will review in the Application Sect. III.D.

In analogy to the particle-hole case, there also exists an exact annihilator of the CCD wave function  $|Z\rangle$  in the particle-particle case. We write the  $Z$ -operator (2.13) in a different but equivalent form

$$\hat{Z} = \frac{1}{4} \sum_{p_1 p_2 h_1 h_2} z_{p_1 p_2 h_1 h_2} P_{p_1 p_2}^\dagger P_{h_1 h_2} \quad (2.63)$$

with the pair operators  $P_{k_1 k_2}^\dagger = a_{k_1}^\dagger a_{k_2}^\dagger$ . The annihilation operator then writes

$$\begin{aligned} A_\alpha &= \frac{1}{2} \sum_{p_1 p_2} X_{p_1 p_2}^\alpha P_{p_2 p_1} - \frac{1}{2} \sum_{h_1 h_2} Y_{h_1 h_2}^\alpha P_{h_1 h_2} \\ &+ \frac{1}{2} \sum_{p_1 p_2 h_1 h_2} \eta_{p_1 p_2 h_1 h_2}^\alpha S_{p_1 p_2} P_{h_1 h_2} \end{aligned} \quad (2.64)$$

with  $S_{p_1 p_2} = a_{p_1}^\dagger a_{p_2}$ .

The relations between the various amplitudes are

$$\begin{aligned} \frac{1}{2} \sum_{p_1 p_2} X_{p_1 p_2}^\alpha z_{p_1 p_2 h_1 h_2} &= Y_{h_1 h_2}^\alpha \\ \sum_{p_1} X_{p_2 p_1}^\alpha z_{p_1 p_3 h_1 h_2} &= \eta_{p_3 p_2 h_1 h_2}^\alpha \end{aligned} \quad (2.65)$$

Similar to the SCRPA correlation energy, an analogous expression can be derived for the pp-case

$$\begin{aligned} E_{\text{corr}}^{\text{RPA}} &= -\frac{1}{2} \sum_{\alpha} \Omega_{\alpha} \sum_{hh'} |Y_{hh'}^\alpha|^2 - \frac{1}{2} \sum_{\rho} \Omega_{\rho} \sum_{pp'} |Y_{pp'}^\rho|^2 \\ &= \sum_{\alpha} \Omega_{\alpha} - \text{Tr} \mathcal{A} = \sum_{\rho} \Omega_{\rho} + \text{Tr} \mathcal{C} \\ &= \frac{1}{2} \left[ \sum_{\alpha} \Omega_{\alpha} - \text{Tr} \mathcal{A} \right] - \frac{1}{2} \left[ \sum_{\rho} \Omega_{\rho} + \text{Tr} \mathcal{C} \right]. \end{aligned} \quad (2.66)$$

An application of these equations to the pairing model will be given in Sect. III.

In conclusion of the Sects. II.A-II.D, we explained in some detail how two body correlations can be calculated from the establishment of generalised self-consistent RPA equations, which can be paraphrased as resulting from a Bogoliubov approach for fermion pair operators. As the standard RPA equations, the self-consistent ones are of the Schrödinger type, they, therefore, may be numerically tractable. We should, however, point out that, in spite of the analogy with Bogoliubov theory for ideal bosons, the present approach for fermion pairs is not based on an explicit many-body ground state wave function and, therefore, is not a truly Raleigh-Ritz

variational principle. Also the Pauli principle, though certainly much better treated than in standard RPA, is not rigorously satisfied. This also stems from the fact that, in order to make the SCRPA equations fully self-contained, some approximations had to be introduced, which, for example, for the occupation numbers involve an expansion in powers of the RPA amplitudes. We will below present some applications to model cases, where we will show the progress, which has been achieved with respect to standard RPA. An important aspect of SCRPA also is that conservation laws and Goldstone theorem in case of broken symmetries can be conserved, as this is the case with standard RPA. With Schrödinger type of extensions of RPA theory, this is not at all evident. Also the Raleigh-Ritz variational aspect can still be improved as we will show in Sect. VII, that with an extended RPA operator one can solve (2.2) and give the corresponding ground state wave function explicitly in full generality for interacting Fermi systems.

### E. Self-consistent Quasiparticle RPA (SCQRPA)

It is relatively evident how to generalise SCRPA to the superfluid case, where we want to call it self-consistent quasiparticle RPA (SCQRPA). We pose the same RPA operator as for standard QRPA

$$Q_\nu^\dagger = \sum_{k > k'} [X_{kk'}^\nu \alpha_k^\dagger \alpha_{k'}^\dagger - Y_{kk'}^\nu \alpha_{k'} \alpha_k], \quad (2.67)$$

where  $\alpha^\dagger$  and  $\alpha$  are the usual quasiparticle (q.p.) creation and destruction operators [5]. Formally the SCQRPA equations also are obtained from a minimisation of the energy weighted sum-rule (1.2) with, however, the Hamiltonian written with quasiparticles. The self-consistency for the  $X, Y$  amplitudes can be established as in the non-superfluid case. A point of discussion can be whether one should include to the RPA operator the scattering states. This can be done in adding a  $\alpha_k^\dagger \alpha_{k'}$  term to the operator. The problem of the ground state wave function also can be solved with a further extension. Let us consider the following Coupled Cluster Doubles state

$$|Z\rangle = \exp \left[ \frac{1}{4!} \sum_{k_1 k_2 k_3 k_4} z_{k_1 k_2 k_3 k_4} \beta_{k_1}^\dagger \beta_{k_2}^\dagger \beta_{k_3}^\dagger \beta_{k_4}^\dagger \right] |\text{BCS}\rangle. \quad (2.68)$$

The corresponding exact annihilator can be given as follows

$$\begin{aligned} Q_\nu &= \sum_{k > k'} [X_{kk'}^\nu \beta_k^\dagger \beta_{k'}^\dagger - Y_{kk'}^\nu \beta_{k'} \beta_k] \\ &+ \sum_{k_1 < k_2 < k_3} \eta_{k_1 k_2 k_3}^\nu \beta_{k_1}^\dagger \beta_{k_2}^\dagger \beta_{k_3}^\dagger \beta_{k_4}, \end{aligned} \quad (2.69)$$

with  $X, Y$  antisymmetric in  $k, k'$  and  $\eta$  antisymmetric in first three indices. Applying this operator on our CCD state, we find  $Q_\nu|Z\rangle = 0$ , where the relations between the various amplitudes turn out to be

$$\begin{aligned} Y_{ll'}^\nu &= \sum_{k < k'} X_{kk'}^\nu z_{kk' ll'} \\ \eta_{l_2 l_3 l_4 k'}^\nu &= \sum_k X_{kk'}^\nu z_{kl_2 l_3 l_4} . \end{aligned} \quad (2.70)$$

As before, to work with the extended operator is not much studied and remains, in general, a task for the future. However, some indications of how to tackle this problem at least approximately will be given in Sect. VII.

SCQRPA has only been applied to a very simple two-level pairing model [49]:

$$H = \frac{\epsilon}{2} \sum_j j N_j - g \Omega \sum_{jj'} A_j^\dagger A_{j'} , \quad j = \pm 1 , \quad (2.71)$$

where  $\Omega$  is the degeneracy of upper and lower levels and  $\epsilon$  is the level spacing. The operators  $N_j, A_j^\dagger, A_j$  are the usual ones of the pairing Hamiltonian given below in the Application section III.D. The results are quite encouraging, but more realistic applications have to wait. An instructive result may be how the gap equation becomes renormalized

$$\Delta_i = \sum_j \tilde{g}_{ij} \frac{\Delta_j}{2\sqrt{\xi_j^2 + \Delta_j^2}} , \quad (2.72)$$

where  $\tilde{g}_{ij}$  is the renormalized pairing force containing  $X$  and  $Y$  amplitudes, what is also the case for the single-particle energies  $\xi_i$ . For the detailed expressions the reader may look up the original paper [49]. This gap equation with effective constants is equivalent to the EOM which determines the mean-field:  $\langle [H, \alpha_i \alpha_j] \rangle = 0$ , what is the analogue to the generalized mean-field equation (2.36).

### F. Number conserving ph-RPA (NCphRPA) in superfluid nuclei

Quasiparticle RPA has, of course, the drawback that it violates particle number conservation. Particle-number projection at the RPA level has been earlier proposed in Refs. [50, 51]. The procedure requires the projection of two-quasiparticle states and a subsequent reorthogonalization, mixing particle-hole excitations in the A system with particle-particle in the A-2 system and hole-hole in the A+2 system. For these reasons, it has been seldom used in  $\beta$  and double- $\beta$  decay calculations [52, 53]. It is, thus, very interesting that one can build a ph-RPA on a number projected HFB ground state where the latter is given in the canonical basis by

$$|PHFB\rangle = \Gamma^\dagger |\text{vac}\rangle , \quad \Gamma^\dagger = \sum_{i=1}^L z_i a_i^\dagger \bar{a}_i^\dagger , \quad (2.73)$$

where the  $\bar{a}_i$  are the conjugate orbitals to the s.p. states  $i$ . For axially deformed systems,  $J_z$  is conserved and  $\bar{a}_i$  has the opposite spin to  $i$ . The pair condensate (2.73) is the vacuum of a complete set of annihilator operators [54]. The subset of annihilators that conserves spin is

$$C_{ij} = z_i a_i^\dagger a_j - z_j a_j^\dagger \bar{a}_i , \quad i \neq j . \quad (2.74)$$

Since  $[C_{ij}, \Gamma^\dagger] = 0$ , it follows immediately

$$C_{ij}|PHFB\rangle = 0 . \quad (2.75)$$

We are now exactly in an analogous situation to the HF-RPA approach, where the  $a_h^\dagger a_p$  hp-operators annihilate the HF ground state. Therefore, we now will build a ph-RPA approach, which has  $|PHFB\rangle$  as a reference state

$$Q_\nu^\dagger = \sum_{i>j} X_{ij}^\nu C_{ij}^\dagger - Y_{ij}^\nu C_{ij} . \quad (2.76)$$

Notice that for  $z_i = \Theta(M - i)$ , the pair condensate reduces to a HF Slater determinant and (2.76) is the standard ph-RPA operator. In the general case of a superfluid pair condensate, this definition of the RPA operators allows us to launch the usual EOM machinery and establish the RPA equations with PHFB as the reference state. Of course, it is clear that no particle number violation has occurred. The price to pay is that we must have a correlated PHFB state as input. However, particle number projection is relatively easy and is now performed mostly routinely. Similarly, there are powerful techniques to evaluate the expectation values of the two-body operators in the  $\mathcal{A}$  and  $\mathcal{B}$  matrices. The complete NCphRPA formalism developed in [54] is an adaptation to nuclear physics of the generalized RPA theory proposed in quantum chemistry [55]. The lack of superconducting correlations made the theory inefficient in quantum chemistry, though it could find a fertile area for applications in open shell nuclei.

The Agassi model [56] was chosen for a pilot application of the NCphRPA theory, since it is the simplest model that mixes particle-hole and pairing correlations. The Agassi Hamiltonian combines the Lipkin model with the two-level pairing model

$$H = J_0 - \frac{\Sigma}{2j-1} \sum_{\sigma\sigma'} A_\sigma^\dagger A_{\sigma'} - \frac{\chi}{2(2j-1)} [J_+^2 + J_-^2] , \quad (2.77)$$

where  $\sigma = \pm 1$  labels each of the two single-particle levels and  $\Sigma$  and  $\chi$  are the coupling constants in the pairing, respectively ph-channels. The pair creation operators are

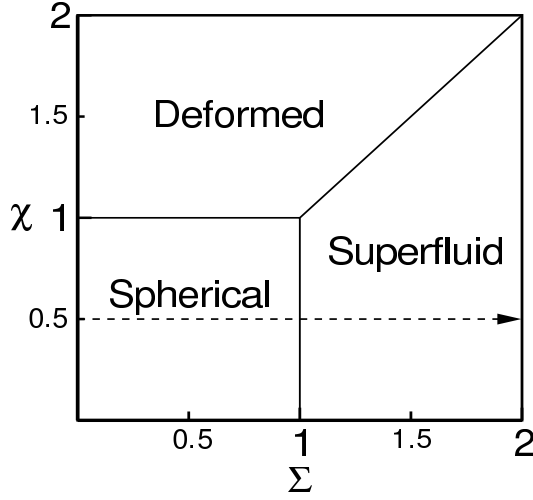


FIG. 1. Phase diagram of the Agassi Hamiltonian (2.77). The dotted line with  $\chi = 1/2$  will be used to benchmark the NCphRPA.

$$A_{\sigma}^{\dagger} = \sum_{m=1}^j a_{\sigma,m}^{\dagger} a_{\sigma,-m}^{\dagger}$$

$$A_0^{\dagger} = \sum_{m=1}^j \left( a_{-1,m}^{\dagger} a_{1,-m}^{\dagger} - a_{-1,-m}^{\dagger} a_{1,m}^{\dagger} \right), \quad (2.78)$$

and the ph operators are

$$J_+ = \sum_{m=-j}^j a_{1m}^{\dagger} a_{-1m} = (J_-)^{\dagger}$$

$$J_0 = \frac{1}{2} \sum_{m=-j}^j \left( a_{1m}^{\dagger} a_{1m} - a_{-1m}^{\dagger} a_{-1m} \right). \quad (2.79)$$

The Agassi model has a rich phase diagram that has been studied in [57, 58] within the HFB approximation. Fig. 1 shows the phase diagram at half filling. It displays a normal (spherical) phase for  $\chi < 1$  and  $\Sigma < 1$ , a ph parity broken (Deformed) phase for  $\chi > 1$  and  $\chi > \Sigma$ , and a superconducting (Superfluid) phase for  $\Sigma > 1$  and  $\Sigma > \chi$ . The horizontal dotted line at  $\chi = 1/2$  represents an ideal path to test the NCphRPA since it has important ph correlations and a phase transition from normal to superconducting. As expected, in NCphRPA the collective ph-RPA excitation shows a smooth behavior across the transition, as opposed to (Q)RPA with the usual kink at the transition point (see [54]). The differences between both approaches can be more readily seen in the transition probabilities that are more sensitive to the wave functions. Fig. 2 shows the transition matrix element of the  $J_x$  operator between the first excited state and the ground state for a finite system with  $j = 10$ ; the inset shows the expectation value of the  $J_0$  operator in

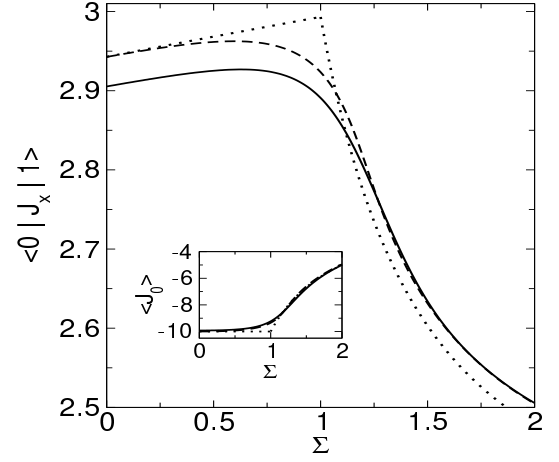


FIG. 2. Transition matrix element of  $J_x$  between the excited state and the GS for level degeneracy  $j = 10$  and  $\chi = 1/2$  as a function of  $\Sigma$ . The inset shows the ground state expectation value of the operator  $J_0$ . The solid line depicts the exact results, the dashed line NCphRPA, and the dotted line (Q)RPA.

the ground state. In both cases the NCphRPA improves over (Q)RPA overcoming the abrupt change at the phase transition of the (Q)RPA for  $\Sigma = 1/2$ . The theory could be extended to describe large amplitude collective motion within a particle-number projected adiabatic time-dependent HFB theory for nuclear fission studies [59]. However, since the theory is very recent, no other applications, e.g., for realistic systems exist so far.

### G. Odd-particle number random phase approximation

The EOM can also be applied to obtain RPA-type of equations for systems with an odd number of particles [60]. We again consider the CCD state of (2.12). We study the following two quasiparticle operators which can be classified, as for the ppRPA, as addition and removal operators

$$q_{\alpha}^{\dagger} = \sum_p u_p^{\alpha} c_p^{\dagger} - \frac{1}{2} \sum_{hh'p} V_{hh'p}^{\alpha} c_h^{\dagger} c_{h'}^{\dagger} c_p$$

$$q_{\rho}^{\dagger} = \sum_h u_h^{\rho} c_h - \frac{1}{2} \sum_{pp'h} V_{pp'h}^{\rho} c_p^{\dagger} c_{p'} c_h. \quad (2.80)$$

It can easily be shown that the corresponding destruction operators  $q_{\alpha}$  and  $q_{\rho}$  annihilate the  $|Z\rangle$  state of (2.12) under the conditions

$$\sum_p u_p^{\alpha*} z_{pp'hh'} = V_{hh'p'}^{\alpha*}$$

$$\sum_h u_h^{\rho*} z_{pp'hh'} = V_{pp'h'}^{\rho*}. \quad (2.81)$$

With our usual EOM technique one obtains the following secular equation for the amplitudes of the, e.g.,  $q_\alpha$  mode

$$\begin{pmatrix} \mathcal{H}_{00} & \mathcal{H}_{01} \\ \mathcal{H}_{10} & \mathcal{H}_{11} \end{pmatrix} \begin{pmatrix} u \\ V \end{pmatrix} = \lambda \begin{pmatrix} n_{00} & n_{01} \\ n_{10} & n_{11} \end{pmatrix} \begin{pmatrix} u \\ V \end{pmatrix}, \quad (2.82)$$

with

$$\begin{aligned} \mathcal{H}_{00} &= \langle \{c_p, [H, c_p^\dagger]\} \rangle \\ \mathcal{H}_{01} &= \mathcal{H}_{10} = \langle \{c_p, [H, c_{h_1}^\dagger c_{h_1'}^\dagger c_{p_1}]\} \rangle \\ \mathcal{H}_{11} &= \langle \{c^\dagger c_{h'} c_h, [H, c_{h_1}^\dagger c_{h_1'}^\dagger c_{p_1}]\} \rangle, \end{aligned} \quad (2.83)$$

and

$$\begin{aligned} n_{00} &= 1 \\ n_{01} &= n_{10} = \langle \{c_p, c_{h_1}^\dagger c_{h_1'}^\dagger c_{p_1}\} \rangle \\ n_{11} &= \langle \{c^\dagger c_{h'} c_h, c_{h_1}^\dagger c_{h_1'}^\dagger c_{p_1}\} \rangle, \end{aligned} \quad (2.84)$$

where  $\{\dots\}$  is the anticommutator and analogous equations hold for the  $q_p$  mode. How this goes in detail, we can see in Ref. [60] from where the matrix elements in (2.83) can be deduced, see also [61], and in the single-particle Green's function section V, since it is evident that this scheme has a direct relation with the s.p. Dyson equation and a specific form of the self-energy. Below, in Sect. V.C we will present an application to the Lipkin model. It is worth mentioning that if Eqs.(2.82) are solved in the full space, they show the appreciable property to fulfill the Luttinger theorem for the s.p. occupation numbers [148].

### III. APPLICATIONS OF SCRPA

In this section, we will show on concrete examples how to go beyond standard RPA in taking into account the fact that the whole medium is correlated and not only the two fermions are explicitly under consideration. This extension is the SCRPA introduced in Sect. II. We first will present the pairing model which has been treated with high dimensional configurations. As a second example, we will consider the three-level Lipkin model which has the interesting feature of a spontaneously broken symmetry. Therefore, the question of the appearance of a Goldstone mode, important for the fulfillment of conservation laws, can be studied. As a third model, the 1D Hubbard model with a finite number of sites is presented. Various applications of the r-RPA will also be discussed at the end of this section.

#### A. Picket Fence (Pairing) Model

As a first example we treat the picket fence model [23]. It is defined as the standard pairing Hamiltonian, specialised, however, to equidistant levels and each level can

accommodate only one pair, let us say spin up/down. This model was exactly solved by Richardson many years back [62].

The picket fence (PF) Hamiltonian is given by

$$H = \sum_{i=1}^{\Omega} (\epsilon_i - \lambda) N_i - G \sum_{i,j=1}^{\Omega} P_i^\dagger P_j, \quad (3.1)$$

with

$$N_i = c_i^\dagger c_i + c_{-i}^\dagger c_{-i}, \quad P_i^\dagger = c_i^\dagger c_{-i}^\dagger, \quad (3.2)$$

where  $c_i^\dagger$  creates a fermion particle in the  $i$ -th level with spin projection  $m = \frac{1}{2}$  and  $c_{-i}^\dagger$  with  $m = -\frac{1}{2}$ .  $\Omega$  is the total number of levels,  $G$  is the pairing interaction strength and the single-particle levels are equally spaced, i.e.  $\epsilon_i = i\epsilon$ . The chemical potential  $\lambda$  will be defined such that the system is completely symmetric with respect to particles and holes.

*Application of EOM to the pairing model.* First we will show how to treat the system by the Equation of Motion Method. We will assume that the system is half filled with number of pairs  $N = \Omega/2$ . The particle and hole states are defined by

$$N_h |HF\rangle = 2, \quad N_p |HF\rangle = 0, \quad (3.3)$$

where  $|HF\rangle$  simply stands for the uncorrelated Slater determinant with  $2N$  particles. The particle states  $p$  correspond to  $\epsilon_p > \lambda$  and the hole states  $h$  to  $\epsilon_h < \lambda$ .

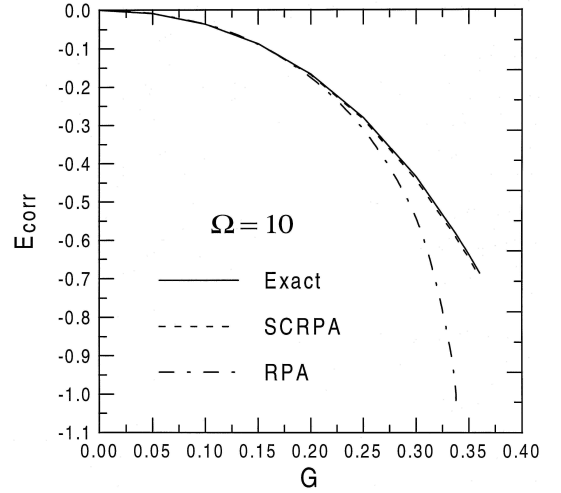


FIG. 3. Ground state correlation energies of the system with  $\Omega = 10$  as a function of the pairing strength  $G$ .

In this case, with no single-particle occupations allowed, the following relation is fulfilled

$$P_i^\dagger P_i + P_i P_i^\dagger = 1, \quad (3.4)$$

which implies

$$N_i = 2P_i^\dagger P_i. \quad (3.5)$$



We can write (3.1) in a more convenient  $ph$  symmetric way defining operators as  $P_h^\dagger = -Q_h$ ,  $P_p^\dagger = Q_p^\dagger$ ,  $N_h = 2 - M_h$ ,  $N_p = M_p$ . Using for the chemical potential

$$\mu = \epsilon(N + \frac{1}{2}) - \frac{G}{2}, \quad (3.6)$$

we arrive at a redefinition of the Hamiltonian (3.1) in the following way

$$\begin{aligned} H = & -\epsilon N^2 + \sum_{p=h=1}^N \left[ \epsilon \left( p - \frac{1}{2} \right) + \frac{G}{2} \right] (M_p + M_h) \\ & - G \sum_{pp'} Q_p^\dagger Q_{p'} - G \sum_{h'} Q_h^\dagger Q_{h'} \\ & - G \sum_{ph} \left( Q_p^\dagger Q_h^\dagger + Q_h Q_p \right). \end{aligned} \quad (3.7)$$

In this form the complete symmetry between particle and hole states becomes evident [23].

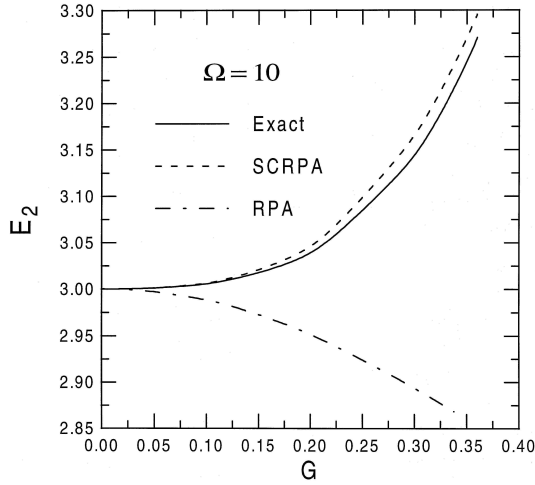


FIG. 4. Second excited state energy of the system with  $\Omega = 10$  and  $N = 12$  particles relative to the ground state of the system with  $\Omega = N = 10$ .

Following the definitions given in Eqs. (2.57) and (2.62), let us now write out the RPA addition and removal operators corresponding to this model,

$$A_\rho^\dagger = \sum_p X_p^\rho \bar{Q}_p^\dagger - \sum_h Y_h^\rho \bar{Q}_h, \quad (3.8)$$

being the addition operator and

$$R_\alpha^\dagger = \sum_h X_h^\alpha \bar{Q}_h^\dagger - \sum_p Y_p^\alpha \bar{Q}_p, \quad (3.9)$$

the removal operator where  $\bar{Q}_p = Q_p / \sqrt{1 - \langle M_p \rangle}$  and  $\bar{Q}_h = Q_h / \sqrt{1 - \langle M_h \rangle}$ . The matrix elements  $\mathcal{A}, \mathcal{B}, \mathcal{C}$  of (2.60) can fully be expressed by the RPA amplitudes with

TABLE I. Excitation energy of the first addition mode as a function of  $G$  obtained with exact calculation, with the RPA,  $SCRPA_1$ , and SCRPA methods, for  $\Omega = 10$ , see [43].

G	Exact	RPA	SCRPA <sub>1</sub>	SCRPA
.00	1.0000	1.0000	1.0000	1.0000
.05	1.0003	0.9940	1.0005	1.0003
.10	1.0011	0.9732	1.0034	1.0014
.20	1.0053	0.8604	1.0279	1.0119
.30	1.0143	0.5257	1.0970	1.0539
.33	1.0184	0.2574	1.1266	1.0758
.34	1.0199	***	1.1372	1.0840
.35	1.0216	***	1.1481	1.0927
.36	1.0233	***	1.1592	1.1018

the help of the techniques outlined in Sect. II. Since they are given by Eqs. (20)-(35) in [43], we will not repeat this here.

In order to fully close the set of SCRPA equations, we still must express the correlation functions  $\langle M_i M_j \rangle$  through the RPA amplitudes, which is the usual somewhat difficult point with SCRPA. In this model, this can also be done exactly, though it is relatively involved. It is explained in Ref. [43]. Here, we will confine ourselves in a first application with the often used approximation  $\langle M_i M_j \rangle \approx \langle M_i \rangle \langle M_j \rangle$ , which in this model is very good. We show the results in Fig. 3 for the ground state correlation energy and in Fig. 4 for the second excited state [23]. In these figures we see the dramatic improvement of SCRPA over standard RPA. Indeed, standard RPA shows the usual collapse of the first excited state at the critical value of the coupling strength. On the contrary, in this case of ten levels the first and second, see [23], excited states of SCRPA show, in agreement with the exact solution, an upward trend signaling that the original attractive force has been overscreened and converted into a repulsive one. This is a very strong feature of the present solution showing that the screening of the force (here actually over-screening) is very well taken into account in SCRPA. The physical origin of the repulsion stems from the very strong action of the Pauli principle in this model, since each level can only be occupied by zero or two particles.

In Table I we show the quality of the various approximations.  $SCRPA_1$  means that the above mentioned factorization approximation of [23] is applied, while SCRPA stands for the full SCRPA solution without approximation of [43]. One point to be mentioned here is the following, see Ref. [43]. Since in this model the SCRPA could be pulled through without any approximations, it shows the possibility to study the fulfillment of the Pauli principle. In Ref. [43] it was shown in studying certain two-body correlation function that the Pauli principle is

slightly violated (remember that the Pauli principle acts very strongly in this model). This feature stems from the fact that the annihilating condition (2.2) has no solution for the ground state with the present RPA operators (3.8) and (3.9) and its use, therefore, implies an approximation in the SCRPA scheme. In this model we, however, see that the deviation from the solution of (2.2) for the ground state is very mild. Since, as mentioned, the Pauli principle plays a crucial role here, we can surmise that the features of SCRPA found in this model can be transposed also to more general cases.

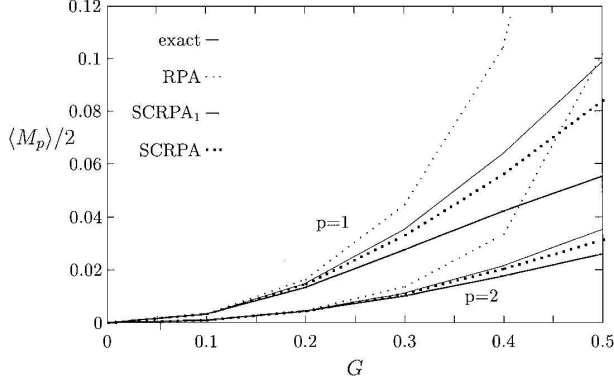


FIG. 5. Occupation numbers  $\langle M_p \rangle / 2$  for the first two particle states  $p = 1, 2$  as a function of  $G$  for  $\Omega = 4$ . Full thin line: exact result; dotted line: standard ppRPA; thick full line: SCRPA1 (meaning with the factorization approximation); thick dots: full SCRPA.

It is also interesting to show some results concerning the occupation numbers like in Fig. 5 [43]. Again, one notices a very strong improvement over standard RPA results.

### B. Three-level Lipkin Model

We have chosen as a next numerical application the three-level Lipkin model, corresponding to an  $SU(3)$  algebra [45]. This model has been widely used in order to test different many-body approximations [63–67]. In analyzing this model we have used a particular form of the Hamiltonian, namely

$$H = \sum_{\alpha=0}^2 \epsilon_{\alpha} K_{\alpha\alpha} - \frac{V}{2} \sum_{\alpha=1}^2 (K_{\alpha 0} K_{\alpha 0} + K_{0\alpha} K_{0\alpha}), \quad (3.1)$$

with

$$K_{\alpha\beta} = \sum_{\mu=1}^N c_{\alpha\mu}^{\dagger} c_{\beta\mu}, \quad (3.2)$$

which are the generators of the  $SU(3)$  algebra. By  $\epsilon_{\alpha}$  we denoted the single-particle energies. According to Ref.

[67], for the three-level Lipkin model the HF transformation matrix defined by

$$a_{k\mu}^{\dagger} = \sum_{\alpha=0}^2 C_{k\alpha} c_{\alpha\mu}^{\dagger}, \quad (3.3)$$

can be written as a product of two rotations, in terms of two angles  $(\phi, \psi)$ . The expectation value of the Hamiltonian (3.1) on the HF vacuum has a very simple form

$$\langle HF | H | HF \rangle = N\epsilon [e_0 \cos^2 \phi + e_1 \sin^2 \phi \cos^2 \psi + e_2 \sin^2 \phi \sin^2 \psi - \chi \sin^2 \phi \cos^2 \phi], \quad (3.4)$$

where we introduced the following dimensionless notations

$$e_k = \frac{\epsilon_k}{\epsilon}, \quad \chi = \frac{V(N-1)}{\epsilon}. \quad (3.5)$$

The Hamiltonian (3.1) has two kinds of HF minima, namely a 'spherical' minimum and a 'deformed' one

$$\begin{aligned} 1) \quad & \phi = 0, \quad \psi = 0, \quad \chi < e_1 - e_0, \\ 2) \quad & \cos 2\phi = \frac{e_1 - e_0}{\chi}, \quad \psi = 0, \quad \chi > e_1 - e_0. \end{aligned} \quad (3.6)$$

According to Ref. [45], for any mean field (MF) minimum one obtains  $\psi = 0$ , independent of which kind of vacuum (correlated or not) we use to estimate the expectation values. We remark, however, that for  $e_1 = e_2$  (3.4) becomes independent of  $\psi$  and therefore we can expect a Goldstone mode in the symmetry broken phase.

For the above mentioned minima one obtains that the standard RPA matrix elements have very simple expressions [67] and the  $\mathcal{A}$  and  $\mathcal{B}$  RPA matrices are diagonal. The RPA frequencies are easy to evaluate

$$\omega_k^2 = \mathcal{A}_{kk}^2 - \mathcal{B}_{kk}^2, \quad k = 1, 2, \quad (3.7)$$

where the indices  $k = 1, 2, 3$  shall be identified with the following configurations

$$10 \rightarrow 1, \quad 20 \rightarrow 2, \quad 21 \rightarrow 3. \quad (3.8)$$

For the ph-amplitudes one gets

$$\begin{pmatrix} X_k^{\nu} \\ Y_k^{\nu} \end{pmatrix} = \frac{1}{\sqrt{2}} \left[ \frac{\mathcal{A}_{kk}}{\omega_k} \pm 1 \right]^{1/2} \delta_{k\nu}. \quad (3.9)$$

We fix the origin of the particle spectrum at  $e_0 = 0$ . Then for a spherical vacuum with  $\phi = 0$  the RPA energies are given by

$$\omega_{\nu} = \epsilon_{\nu} \left[ 1 - \left( \frac{\chi}{e_{\nu}} \right)^2 \right]^{1/2}, \quad \nu = 1, 2, \quad (3.10)$$

with the corresponding RPA amplitudes

$$\begin{pmatrix} X_k^{\nu} \\ Y_k^{\nu} \end{pmatrix} = \frac{1}{\sqrt{2}} \left[ \frac{\epsilon_k}{\omega_k} \pm 1 \right]^{1/2} \delta_{k\nu}. \quad (3.11)$$

As it was shown in Ref. [67], if the upper single-particle levels are degenerate, i.e.  $\Delta\epsilon \equiv \epsilon_2 - \epsilon_1 = 0$ , for the values of the strength  $\chi > e_1$ , in the "deformed region", i.e. with  $\phi \neq 0$  given by HF minimum, one obtains a Goldstone mode. In this case by considering  $e_1 = 1$  one obtains for the excitation energies

$$\begin{aligned}\omega_1 &= \epsilon\sqrt{2(\chi^2 - 1)}, \\ \omega_2 &= 0.\end{aligned}\quad (3.12)$$

*Application of Self-consistent RPA (SCRPA) to the three-level Lipkin model.* The SCRPA operator including scattering terms, see Sect. II, is given by

$$Q_\nu^\dagger = \sum_{m>i} \left( X_{mi}^\nu \frac{A_{mi}}{\sqrt{n_i - n_m}} - Y_{mi}^\nu \frac{A_{mi}}{\sqrt{n_i - n_m}} \right) \quad (3.13)$$

in terms of the pair operators in the MF basis

$$A_{mi} = \sum_{\mu=1}^N a_{m\mu}^\dagger a_{i\mu} = \sum_{\alpha\beta} C_{m\alpha} C_{i\beta} K_{\alpha\beta}. \quad (3.14)$$

Let us first discuss the SCRPA results in the spherical region, i.e. the region where the generalised mean field equation has only the trivial solution  $\phi = 0$ . In comparison with standard HF this region is strongly extended. The content of the spherical region depends on the particle number. For  $N = 20$  the spherical region is typically extended by a factor of 1.5. This comes from the self-consistent coupling of the quantal fluctuations to the mean field and actually corresponds to a weakening (screening) of the force.

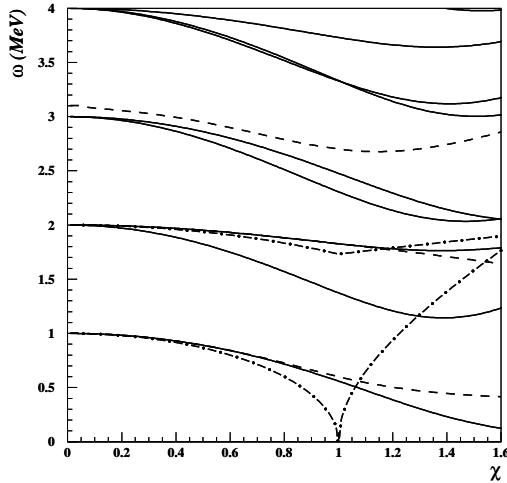


FIG. 6. SCRPA excitation energies versus the strength parameter  $\chi$ , for  $N = 20$  and  $e_0 = 0$ ,  $e_1 = 1$ ,  $e_2 = 2$  (dashed lines). By solid lines are given the lowest exact eigenvalues and by dot-dashes the standard RPA energies.

Let us now consider the definite example  $e_0 = 0$ ,  $e_1 = 1$ ,  $e_2 = 2$  for  $N = 20$ . In Fig. 6 we show by dashed

lines the SCRPA results for the excitation energies, compared with the exact ones (solid lines) and to standard RPA (dot-dashes). We see that SCRPA strongly improves over standard RPA and in fact first and second excited states are excellently reproduced up to  $\chi$ -values of about  $\chi \approx 1.2$ . The third state has no analogue in standard RPA and it must therefore be attributed to the scattering configuration  $A_{21}$ . The SCRPA solution for the the third eigenvalue approximates rather well the fifth exact eigenvalue in the range  $0 < \chi \leq 1.0$ . Concerning the SCRPA result, this seems quite surprising, since naively one would think that for vanishing interaction the SCRPA eigenvalue corresponding to the (21) component should approach to the value  $\omega_3 \rightarrow e_2 - e_1 = 1$ . In Ref. [45] it is shown that this mode indeed corresponds to the fifth exact eigenvalue  $\nu = 5$  as long as  $\chi > 0$ . At exactly  $\chi = 0$  the solution jumps to  $\omega_3 = 1$ .

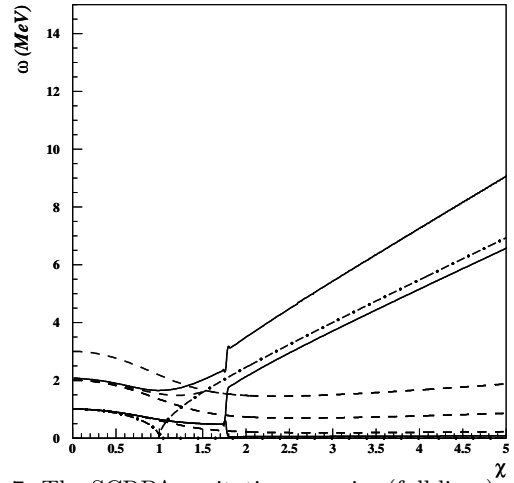


FIG. 7. The SCRPA excitation energies (full lines) compared with the exact solution (broken lines) for  $N = 8$ . Dot-dashed line gives standard RPA values.

In the deformed region a particular situation arises in our model for  $\Delta\epsilon = \epsilon_2 - \epsilon_1 = 0$ , since, as already mentioned, a spontaneously broken symmetry occurs in this case. Here the standard HF-RPA exhibits its real strength because, as shown in (3.12), a zero mode appears, which signifies that the broken symmetry is partially restored, i.e. the conservation laws are fulfilled [1, 5, 68]. This property is also fulfilled in SCRPA under the condition that the scattering terms are included. In this context we mention that the operator

$$\begin{aligned}\hat{L}_0 &= i(K_{21} - K_{12}) = i[A_{20} - A_{02}]\sin\phi \\ &\quad + (A_{21} - A_{12})\cos\phi,\end{aligned}\quad (3.15)$$

where  $A_{ij}$  are the pair operators (3.14) in the HF basis, commutes with the Hamiltonian, i.e.  $[\hat{H}, \hat{L}_0] = 0$ .

It is therefore a symmetry operator which can be identified with the z-component of the rotation operator. The

existence of this symmetry operator is the reason why equation (2.5) produces in the deformed region a Goldstone mode at zero energy (see also Eq. (3.12)).

Indeed, in this case the deformed RPA equations possess a particular solution  $Q^\dagger = \hat{L}_0$  and one has  $\langle 0 | [\delta \hat{L}_0, [H, \hat{L}_0]] | 0 \rangle = 0$ . This means that in the deformed region  $\hat{L}_0$  can be considered as an RPA excitation operator with  $|0\rangle$  not being an eigenstate of  $\hat{L}_0$  and producing a zero excitation energy, i.e. the Goldstone mode. On the contrary, in the spherical region the ground state is an eigenstate of  $\hat{L}_0$  and therefore it cannot be used as an excitation operator.

In standard RPA, where the expectation values of the (double) commutators are evaluated over the deformed HF state, the scattering terms  $A_{12}$  and  $A_{21}$  in  $\hat{L}_0$  automatically decouple from the  $ph$  and  $hp$  space and that is the reason why only  $ph$  ( $hp$ ) components of the symmetry operator suffice to produce the Goldstone mode. On the other hand, if one works with a deformed correlated ground state as in SCRPA, the scattering terms do *not* decouple from the  $ph$  ( $hp$ ) space and therefore the full  $ph$ ,  $hp$ ,  $hh$  and  $pp$  space must be taken into account to produce the Goldstone mode. Since in the latter case the symmetry operator (3.15) is entirely taken into account, this property follows again automatically.

The numerical verification of this desirable quality of SCRPA must, however, be undertaken with care. Indeed, a zero mode contains diverging amplitudes which, injected into the SCRPA matrix, may not lead to self-consistency. The way to overcome this difficulty is to start the calculation with a finite small value of  $\Delta\epsilon$ , i.e. with a slight explicit symmetry breaking, and then to diminish its value step by step. We, in this way, could verify with very high accuracy that the zero eigenvalue occurs in the deformed region for all values of the interaction strength  $\chi$ . This is shown in Fig. 7 by the solid line which parallels very closely the horizontal axis. Here we considered the value  $\Delta\epsilon = 0.001$ , but we were able to reach the value  $\Delta\epsilon = 10^{-6}$ . We, therefore, see that our theoretical expectation is fully verified by the numerical solution. In the same way we checked that the energy weighted sum rule is fulfilled in SCRPA in the symmetry broken phase with the Goldstone mode present.

We also should comment about the other features seen in Fig. 7. Up to about  $\chi = 1.8$ , in the spherical region, the first excited state is two-fold degenerate. After that value the degeneracy becomes suddenly lifted and one state goes into the Goldstone mode and the other more or less joins the upgoing RPA state. If one chooses a larger particle number, both states will become closer and join the second band head of the model. This kind of first order phase transition is an artefact of the theory and does not happen in the exact solution. One probably should include second RPA correlations to cure this, see Sect. VII and also Sect.V.C. However, the appearance of a Goldstone mode is a quite remarkable feature which

we will comment upon in more detail below.

As usual with a continuously broken symmetry, also in the present model a clear rotational band structure is revealed. The exact solution found by a diagonalisation procedure has a definite angular momentum projection  $L_0$ . Moreover, the expectation value of the  $L_0^2$  operator has integer values, namely

$$\sqrt{\langle L_0^2 \rangle} = J = 0, 1, 2, \dots \quad (3.16)$$

The ground state "rotational band"  $J = 0, 1, 2, \dots$  is built on top of the RPA excitation with a vanishing energy (Goldstone mode).

As customary in RPA theory, one also can evaluate the mass parameter of the rotational band within SCRPA. By a straightforward generalisation we obtain for the moment of inertia (see e.g. Ref. [1, 5])

$$M = 2L_0^* (\mathcal{A} - \mathcal{B})^{-1} L_0, \quad (3.17)$$

where  $\mathcal{A}, \mathcal{B}$  are the SCRPA matrices and  $L_0$  is the angular momentum operator (3.15), which should be written in terms of normalised generators  $\delta Q^\dagger$ , i.e.

$$L_0 = i \begin{pmatrix} 0, & N_{20}^{1/2} \sin\phi, & N_{21}^{1/2} \cos\phi \end{pmatrix}. \quad (3.18)$$

For the standard RPA case, by using the corresponding matrix elements, one obtains an analytical solution, namely

$$M = \frac{N(\chi - 1)}{\epsilon\chi(\chi + 1)}, \quad (3.19)$$

where  $N$  is the particle number. The SCRPA mass is also obtained from (3.17) but using the SCRPA expressions for the  $\mathcal{A}$  and  $\mathcal{B}$  matrices. The spectrum of the first three states is shown in Fig. 8 in the range between  $\chi = 2$  and  $\chi = 5$ . We see that the exact spectrum is very well approximated. These states correspond to the ones seen in Fig. 7 in the same range of the coupling constant. The first rotational state for  $\langle L_0 \rangle$  matches rather well with the lowest excited state of SCRPA in the spherical region. However, this is not the case for the higher-lying excitations.

In conclusion of this section, we can say that SCRPA reproduces very well the 'spherical' region of the three-level Lipkin model. What is new is that the inclusion of the scattering configurations allowed to obtain the Goldstone mode in the 'deformed' region where a clear rotational spectrum appears. The calculation of the SCRPA moment of inertia then allowed to get a very accurate reproduction of the rotational ground state band in this model. We would like to point out that the appearance of the Goldstone mode with a theory, which takes into account strong correlation beyond the ones of the standard RPA theory, is highly non-trivial. To the best of our knowledge, we are not aware of any other fully microscopic extension of the RPA approach which has numerically achieved this taking into account self-consistently

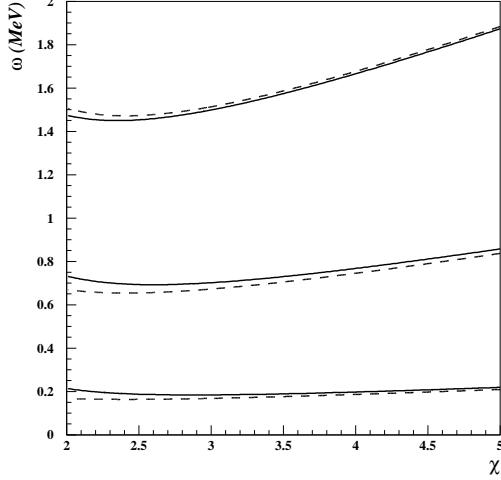


FIG. 8. SCRPA rotational spectrum (dashed lines) and exact energies (solid lines) for  $N = 20$ . The three levels correspond to  $J = 1, 2, 3$ . These levels correspond to the three levels between  $\chi = 2$  and  $\chi = 5$  in Fig. 7.

screening of the interaction. The Kadanoff and Baym formalism would lead even in this very simple model to numerically almost inextricable complications.

### C. Hubbard Model

In this Section we apply the SCRPA scheme to the Hubbard model of strongly correlated electrons, which is one of the most wide spread models to investigate strong electron correlations and high  $T_c$  superconductivity. Its Hamiltonian is given by

$$H = -t \sum_{\langle ij \rangle \sigma} c_{i\sigma}^\dagger c_{j\sigma} + U \sum_i \hat{n}_{i\uparrow} \hat{n}_{i\downarrow} \quad (3.20)$$

where  $c_{i\sigma}^\dagger$ ,  $c_{i\sigma}$  are the electron creation and destruction operators at site ' $i$ ' and the  $\hat{n}_{i\sigma} = c_{i\sigma}^\dagger c_{i\sigma}$  are the number operators for electrons at site ' $i$ ' with spin projection  $\sigma$ . As usual  $t$ , is the nearest neighbour hopping integral and  $U$  the on site Coulomb matrix element.

As an example, we will consider the 1-dimensional 6-sites case at half filling. With the usual transformation to plane waves (we are considering periodic boundary conditions, that is a ring)  $c_{j,\sigma} = \frac{1}{\sqrt{N}} \sum_{\mathbf{k}} a_{\mathbf{k},\sigma} e^{-i\mathbf{k} \cdot \mathbf{x}_j}$ .

This leads to the standard expression for a zero range two body interaction

$$H = \sum_{\mathbf{k},\sigma} (\epsilon_{\mathbf{k}} - \mu) \hat{n}_{\mathbf{k},\sigma} + \frac{U}{2N} \sum_{\mathbf{k},\mathbf{p},\mathbf{q},\sigma} a_{\mathbf{k},\sigma}^\dagger a_{\mathbf{k}+\mathbf{q},\sigma} a_{\mathbf{p},-\sigma}^\dagger a_{\mathbf{p}-\mathbf{q},-\sigma} \quad (3.21)$$

where  $\hat{n}_{\mathbf{k},\sigma} = a_{\mathbf{k},\sigma}^\dagger a_{\mathbf{k},\sigma}$  is the occupation number operator of the mode  $(\mathbf{k}, \sigma)$  and the single-particle energies are given by  $\epsilon_{\mathbf{k}} = -2t \sum_{d=1}^D \cos(k_d)$  with the lattice spacing set to unity.

In the first Brillouin zone  $-\pi \leq k < \pi$  we have for  $N = 6$  the following wave numbers

$$\begin{aligned} k_1 &= 0, & k_2 &= \frac{\pi}{3}, & k_3 &= -\frac{\pi}{3}, \\ k_4 &= \frac{2\pi}{3}, & k_5 &= -\frac{2\pi}{3}, & k_6 &= -\pi. \end{aligned} \quad (3.22)$$

With the HF transformation

$$a_{h,\sigma} = b_{h,\sigma}^\dagger, \quad a_{p,\sigma} = b_{p,\sigma}, \quad (3.23)$$

such that  $b_{k,\sigma}|HF\rangle = 0$  for all  $k$ , we can write the Hamiltonian in the following way (normal order with respect to  $b^\dagger, b$ )

$$H = H_{HF} + H_{|q|=0} + H_{|q|=\frac{\pi}{3}} + H_{|q|=\frac{2\pi}{3}} + H_{|q|=\pi}, \quad (3.24)$$

where the notations are given in [69]. The level scheme is shown in Fig. 9. The hole states are labeled  $h = \{1, 2, 3\}$

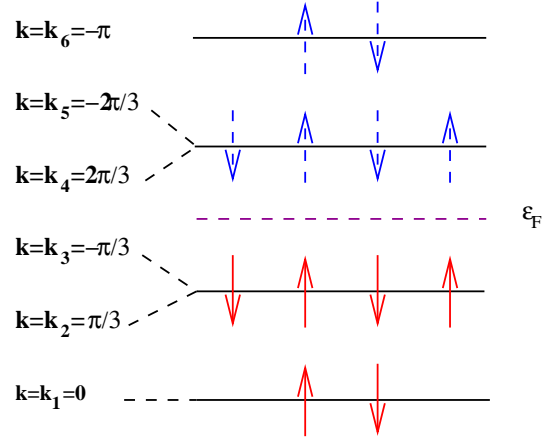


FIG. 9. Excitation spectrum of HF at  $U = 0$  for the chain with 6-sites at half filling and projection of spin  $m_s = 0$ . The occupied states are represented by the full arrows and those not occupied are represented by the dashed arrows.

and the particle states  $p = \{4, 5, 6\}$ . The HF groundstate is

$$|HF\rangle = a_{1,\uparrow}^\dagger a_{1,\downarrow}^\dagger a_{2,\uparrow}^\dagger a_{2,\downarrow}^\dagger a_{3,\uparrow}^\dagger a_{3,\downarrow}^\dagger |-\rangle. \quad (3.25)$$

There are three different absolute values of momentum transfers, as shown in Table II. Since the momentum transfer  $|q|$  is a good quantum number, the RPA equations are block diagonal and can be written down for each  $|q|$ -value separately. For example, for  $|q| = \frac{\pi}{3}$  we have the following RPA operator for charge and longitudinal

TABLE II. The various momentum transfers in the 6 -sites case.

$ q  = \frac{2\pi}{3}$	$ q  = \pi$	$ q  = \frac{\pi}{3}$
$51 \rightarrow q_{51} = -\frac{2\pi}{3}$	$61 \rightarrow q_{61} = -\pi$	$42 \rightarrow q_{42} = +\frac{\pi}{3}$
$41 \rightarrow q_{41} = +\frac{2\pi}{3}$	$52 \rightarrow q_{52} = -\pi$	$53 \rightarrow q_{53} = -\frac{\pi}{3}$
$62 \rightarrow q_{62} = +\frac{2\pi}{3}$	$43 \rightarrow q_{43} = +\pi$	
$63 \rightarrow q_{63} = -\frac{2\pi}{3}$		

spin excitations

$$\begin{aligned}
Q_{|q|=\frac{\pi}{3},\nu}^\dagger = & X_{2\uparrow,4\uparrow}^\nu K_{4\uparrow,2\uparrow}^+ + X_{2\downarrow,4\downarrow}^\nu K_{4\downarrow,2\downarrow}^+ \\
& + X_{3\uparrow,5\uparrow}^\nu K_{5\uparrow,3\uparrow}^+ + X_{3\downarrow,5\downarrow}^\nu K_{5\downarrow,3\downarrow}^+ \\
& - Y_{2\uparrow,4\uparrow}^\nu K_{2\uparrow,4\uparrow}^- - Y_{2\downarrow,4\downarrow}^\nu K_{2\downarrow,4\downarrow}^- \\
& - Y_{3\uparrow,5\uparrow}^\nu K_{5\uparrow,3\uparrow}^- - Y_{3\downarrow,5\downarrow}^\nu K_{5\downarrow,3\downarrow}^-, \quad (3.26)
\end{aligned}$$

where

$$\begin{aligned}
K_{p\sigma,h\sigma}^\pm &= \frac{J_{p\sigma,h\sigma}^\pm}{\sqrt{1 - \langle 0|M_{p\sigma,h\sigma}|0\rangle}} \\
M_{p\sigma,h\sigma} &= \tilde{n}_{p,\sigma} + \tilde{n}_{h,\sigma}. \quad (3.27)
\end{aligned}$$

Here  $J_\sigma^- = b_{1,\sigma} b_{2,\sigma}$ ,  $J_\sigma^+ = (J_\sigma^-)^\dagger$ ,  $\tilde{n}_{k_i,\sigma} = b_{i,\sigma}^\dagger b_{i,\sigma}$ . The operators  $J_\sigma^\pm$  and  $1 - M_\sigma$  form a  $SU(2)$  algebra of spin  $-\frac{1}{2}$  operators and, therefore, using the Casimir relation we obtain

$$M_\sigma = 2 J_\sigma^+ J_\sigma^- . \quad (3.28)$$

We write this RPA operator in short hand notation as

$$Q_\nu^\dagger = \sum_{i=1}^4 \frac{1}{\sqrt{1 - \langle 0|M_i|0\rangle}} (X_i^\nu J_i^+ - Y_i^\nu J_i^-) , \quad (3.29)$$

with the usual properties. The matrix elements in the SCRPA equation are then of the form

$$\mathcal{A}_{i,i'} = \frac{\langle 0|[J_{i'}^- [H, J_i^+]]|0\rangle}{\sqrt{(1 - \langle 0|M_{i'}|0\rangle)(1 - \langle 0|M_i|0\rangle)}} , \quad (3.30a)$$

$$\mathcal{B}_{i,i'} = -\frac{\langle 0|[J_{i'}^- [H, J_i^-]]|0\rangle}{\sqrt{(1 - \langle 0|M_{i'}|0\rangle)(1 - \langle 0|M_i|0\rangle)}} . \quad (3.30b)$$

The expectation values are given in [69]. Let us add that the matrices  $\mathcal{A}$  and  $\mathcal{B}$  are symmetric.

In Fig. 10 we display the excitation energies in the channel  $|q| = \pi$ , as a function of  $U/t$ . The other cases are similar. The exact values are given by the continuous lines, the SCRPA ones by crosses and the ones corresponding to standard RPA by the broken lines. We see that SCRPA results are excellent and strongly improve over standard RPA. As expected, this is particularly important at the phase transition points where the lowest root of standard RPA goes to zero, indicating the onset of a staggered magnetisation on the mean-field level. It is particularly interesting that SCRPA allows to go beyond the mean-field instability point. However, at some values

$U > U_{cr}$  the system still “feels” the phase transition and SCRPA stops to converge and also deteriorates in quality. Up to these values of  $U$  SCRPA shows very good agreement with the exact solution and, in particular, it completely smears the sharp phase transition point of standard RPA, which is an artefact of the linearisation.

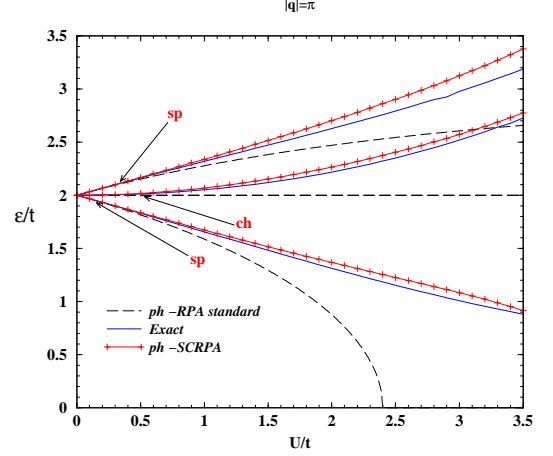


FIG. 10. Energies of excited states in standard RPA, SCRPA, and exact cases as a function of  $U$  for 6 -sites with spin projection  $m_s = 0$  and for  $|q| = \pi$ . States of the charge response and those of the longitudinal spin response are denoted by  $ch$  and  $sp$ , respectively.

A further quantity which crucially tests the ground state correlations are the occupation numbers. We used the so-called Catara approximation, see Sect. II.A, for their evaluation [47], showing an excellent performance of SCRPA, see Fig. 11.

In this section we gave a very short summary of the achievement of SCRPA concerning the Hubbard model. Notably we only considered the symmetry unbroken phase of the model, where SCRPA gives a strong improvement over standard RPA.

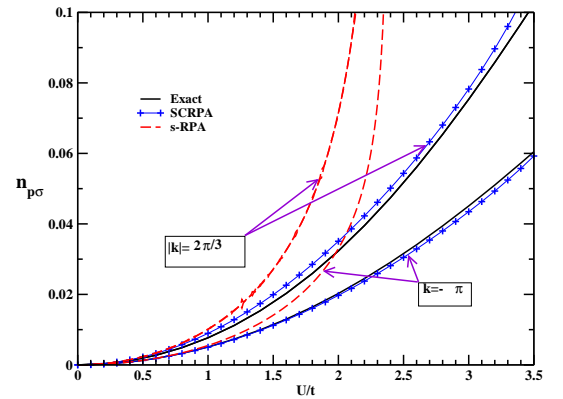


FIG. 11. Occupation numbers for the 5th and 6th state with the SCRPA and the Catara approximation (crosses); full lines represent the exact results and the dots (red) are obtained with the standard RPA approach.

excited states, which are in close agreement with the exact values even somewhat beyond the critical  $U$ , where standard RPA has a break down.

#### D. Various applications and extensions of the renormalized RPA

The renormalized RPA (r-RPA) was applied by many authors to various strongly correlated systems. In Ref. [47] a version of the r-RPA called improved RPA (IRPA) is introduced and applied to the description of the electronic gas in metallic clusters treated within the jellium model. The one- and two-body densities are derived by using the so-called number operator method proposed long time ago by D. Rowe [16]. The corresponding relations are given by Eq. (2.45). IRPA, being considerably simpler from the numerical point of view than SCRPA, represents a significant improvement with respect to standard RPA where uncorrelated occupation numbers are used. The Authors have found that a better treatment of correlations leads to important modifications of single-particle occupation numbers and strength distributions, see Fig. 12 [47]. In Fig. 12 the upper panel shows the fully self-consistent r-RPA (IRPA). With respect to a non-self-consistent solution, i.e., only first iteration (lower panel), the effect is somewhat damped but still strong, maximally 20 percent! Spin singlet and triplet states are included together with orbital angular momenta up to  $L = 6$ . The  $S = 1$  channel gives by far the strongest contribution to the renormalisation. Renormalised RPA has recently also been applied to superfluid strongly polarised Fermi gases with strongly improved results with respect to standard RPA [70].

On the other hand, the two-dimensional electron gas provides a valuable testing ground for microscopical theories of interacting Fermi systems. Compared to the three-dimensional case, the two-dimensional correlations play a more important role, demanding higher precision to theoretical approaches and exposing their weaknesses. In Ref. [32] the Authors propose an iterative procedure, using the momentum distributions for the recalculation of polarization and vertex functions within the RPA, similar to the r-RPA scheme. It is shown that the inclusion of the physical momentum distributions for the calculation of polarization and vertex functions yields significant contributions to the resulting field correction and correlation energies.

An important application of the r-RPA concerns the double beta decay process with emission of two neutrinos ( $2\nu\beta\beta$ ). The second leg of the  $2\nu\beta\beta$  process is very sensitive to changing the relative strength of the particle-particle interaction strength  $g_{pp}$ . It is worth mentioning that the two-body interaction of  $ph$  type is repulsive while that of  $pp$  nature is attractive. Due to this feature there is a critical value for  $g_{pp}$  for which the first root of the proton-neutron QRPA (pnQRPA) equation vanishes. Actually, this is the signal that the pnQRPA approach

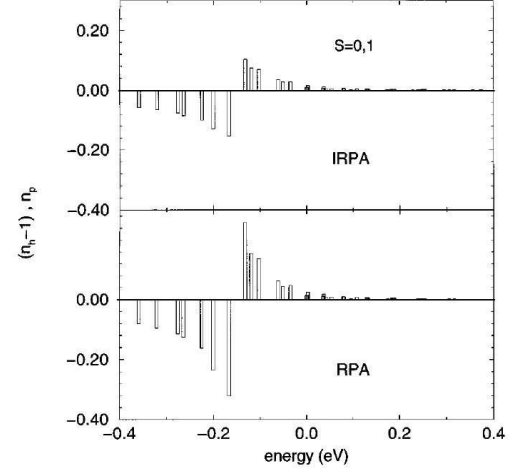


FIG. 12. Occupation numbers  $n_p$  and  $1-n_h$  for particle states and the opposite of depletion numbers  $n_h$  for hole states, respectively. In the lower and in the upper panel the RPA and IRPA results, respectively, are reported. Both spin  $S=0$  and  $S=1$  states are included in the calculations. In the abscissa the single-particle energies in eV are indicated [47].

breaks down. Moreover, the  $g_{pp}$  value, which corresponds to a transition amplitude agreeing with the corresponding experimental data, is close to the mentioned critical value. That means that the result is dependent on adding corrections to the standard RPA picture. The first improvement for the pnQRPA was achieved in Ref. [71] by using a boson expansion (BE) procedure. It is interesting to mention that within the BE formalism transitions to excited state, forbidden in the pnQRPA approach, become possible. A systematic analysis of the double beta transitions for 18 nuclei has been performed.

Later another procedure showed up, which renormalized the dipole two-quasiparticle operators by replacing the scalar components of their commutators by their average values. In Ref. [72] this renormalisation procedure is applied to proton-neutron quasiparticle RPA (r-pnQRPA) in order to describe  $\beta$  and double  $\beta$  ( $\beta\beta$ ) decay processes. The one-body quasiparticle density for protons (p) and neutrons (n) is expressed in terms of QRPA amplitudes by using the Catara method [73], i.e.

$$\begin{aligned} [a_p^\dagger a_p]_{00} &= \sum_{JMn'} A_{JM}^\dagger(pn') A_{JM}(p'n) \\ [a_n^\dagger a_n]_{00} &= \sum_{JMp'} A_{JM}^\dagger(p'n) A_{JM}(p'n) . \end{aligned} \quad (3.31)$$

This ansatz leads to the following equalities for the expectation value on the QRPA vacuum

$$\begin{aligned} N_{pn} &= 1 - \hat{j}_p^{-1} \sum_{n'} N_{pn'} \sum_{J\nu} \hat{j}^2 [Y_{pn'}^{J\nu}]^2 \\ &\quad - \hat{j}_n^{-1} \sum_{p'} N_{p'n} \sum_{J\nu} \hat{j}^2 [Y_{p'n}^{J\nu}]^2 , \end{aligned} \quad (3.32)$$

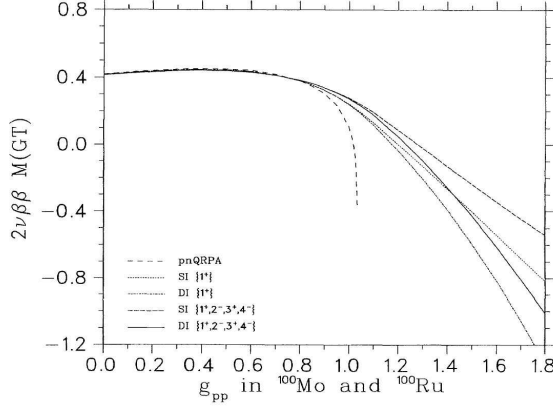


FIG. 13. The transition amplitude of the  $2\nu\beta\beta$  process  $^{100}\text{Mo}(gs) \rightarrow ^{100}\text{Ru}(gs)$  versus the particle-particle strength for various pnQRPA versions. The dashed line corresponds to the standard pnQRPA, while the other lines to various intermediate  $pn$  excitations considered within r-pnQRPA are described in Ref. [72].

where  $\hat{j} = \sqrt{2j+1}$  and the  $N_{pn}$  metric (norm) matrix elements are defined as usual by

$$N_{pn} = \langle 0 | [A_{JM}(pn), A_{JM}^\dagger(pn)] | 0 \rangle. \quad (3.33)$$

In this way the r-pnQRPA system of equations for several multiplicities  $J$  is solved together with (3.32). In calculations the matrix elements of the realistic Bonn interaction [74] are used to describe the two-neutrino ( $2\nu$ )  $\beta\beta$  decay process  $^{100}\text{Mo}(gs) \rightarrow ^{100}\text{Ru}(gs)$ . It was shown that this kind of calculation reduces ground state correlations and prevents the collapse of the standard pnQRPA in the region of physical interest for the particle-particle channel of the interaction, which is very important for double-beta decay processes. This is shown in Fig. 13 for the transition amplitude of the  $2\nu\beta\beta$  process. The dashed line describes the collapse of the transition amplitude versus the particle-particle interaction strength for  $g_{pp} \sim 1$  within the standard pnQRPA, while the other lines give the same dependence within r-pnQRPA. Different lines correspond to various intermediate  $pn$  excitations in the expansion (3.32) and they are described in Ref. [72]. Notice that the matrix element acquires values close to the experimental ones for  $g_{pp} \sim 1$  for all considered versions of r-pnQRPA.

In Ref. [75] this procedure is applied for several  $2\nu\beta\beta$  emitters like  $^{76}\text{Ge}$ ,  $^{78}\text{Kr}$ ,  $^{82}\text{Se}$ ,  $^{96}\text{Zr}$ ,  $^{106}\text{Cd}$  and  $^{130}\text{Te}$  to ground states as well as to excited one- and two-phonon states in daughter nuclei. Later on,  $^{76}\text{Ge}$ ,  $^{82}\text{Se}$  and  $^{128-130}\text{Te}$  emitters were investigated in [76]. A review on this approach is given in Ref. [77].

In Ref. [78] r-RPA is applied to the two-level proton-neutron Lipkin model. The results are compared with the exact diagonalisation procedure, as well as with a

boson mapping. It turned out that in spite of the good agreement of r-RPA eigenvalues compared with the exact solution, the wave function is quite different from the exact one in the region where standard RPA collapses.

In Refs. [79, 80] r-QRPA is applied to the simplest single  $j$ -shell Hamiltonian, describing Fermi  $\beta$ -transitions, namely

$$H = e_p N_p + e_n N_n - G_p S_p^\dagger S_p - G_n S_n^\dagger S_n + 2\chi \beta^- \beta^+ - 2\kappa P^- P^+, \quad (3.34)$$

where the usual notations were used

$$N_i = \sum_{m_i} c_{m_i}^\dagger c_{m_i}, \quad S_i = \sum_{m_i} c_{m_i}^\dagger c_{\bar{m}_i}^\dagger, \\ \beta^- = \sum_{m_p=m_n} c_{m_p}^\dagger c_{m_n}, \quad P^- = \sum_{m_p=m_n} c_{m_p}^\dagger c_{\bar{m}_n}^\dagger. \quad (3.35)$$

In spite of its simplicity, this Hamiltonian is able to describe the main features of a realistic Hamiltonian, describing  $\beta$  and  $\beta\beta$  processes. In particular, the collapse of standard RPA is obtained by increasing the particle-particle strength  $\kappa$ . It was shown that the collapse of QRPA correlates with the presence of an exact eigenvalue at zero energy. It was shown that r-QRPA prevents this collapse. The role of scattering terms was discussed and they were shown to be relevant in getting excitation energies closer to the exact values.  $\beta\beta$ -decay amplitudes were evaluated and compared with other formalisms.

Later on, in Refs. [81, 82] a more complete analysis of this Hamiltonian was performed. The Dyson boson representation ( $b^\dagger, b$ ), together with a coherent representation

$$|\alpha\rangle = N_0 \sum_{l=0}^{2\Omega} \frac{\alpha^l}{l!} (b^\dagger)^l |0\rangle, \quad (3.36)$$

was used to describe phase transitions by using the complex order parameter  $\alpha$ . The spontaneous breaking of the proton-neutron-pair symmetry was induced by the particle-particle strength  $\kappa$  and it manifests in the appearance of the zero-energy mode. It was shown that the coherent state representation is able to describe the phase transition, while r-QRPA is unable to describe correctly the energy and, for instance, the inclusion of the Pauli principle at the Hamiltonian level is crucial to describe the phase transition.

We mention here that the ground state instability versus the particle-particle strength  $\kappa$  of the Hamiltonian (3.34) is analyzed in Ref. [83] within the time-dependent formalism.

In Ref. [84] the r-pnQRPA system of equations is solved consistently with the BCS equations, derived by considering the same RPA vacuum. The normal and pairing densities are written in terms of the quasiparticle density as follows

$$\rho_k = \langle 0 | c_k^\dagger c_k | 0 \rangle = v_k^2 + (u_k^2 - v_k^2) n_k \\ \kappa_k = \langle 0 | c_k^\dagger c_{\bar{k}}^\dagger | 0 \rangle = u_k v_k (1 - 2n_k). \quad (3.37)$$



It is shown that the system of equations (3.32) can be written as a linear system of equations for quasiparticle densities. The case of two neutrino  $\beta\beta$ -decay of  $^{76}\text{Ge}$  is analyzed and it is shown that the inclusion of self-consistency in solving BCS equations leads to more reduction of ground states correlations. In a later Ref. [85] this self-consistent procedure is applied to several emitters in medium-heavy mass region in order to show the systematic reduction of  $\beta\beta$ -decay matrix elements.

In spite of the fact that the Pauli principle is taken into account, the sum rules, in particular the Ikeda sum rule

$$\begin{aligned} S_- - S_+ &= \sum_{\mu} (-)^{\mu} \langle 0 | [\hat{\beta}_{\mu}^+, \hat{\beta}_{-\mu}^-] | 0 \rangle \\ &= 3(N - Z) \end{aligned} \quad (3.38)$$

is not fulfilled within r-pnQRPA, due to the fact that the  $\beta$  decay operators  $\hat{\beta}_{\mu}^{\pm}$  do not contain the scattering terms. This drawback is cured in Refs. [86, 87] within the fully renormalized pnQRPA (FR-pnQRPA), by considering the scattering terms in the structure of the QRPA phonon. Later on, a new method of restoring the gauge symmetry breaking was formulated to cure this drawback within the so-called GPFR-pnQRPA [88].

Let us mention that in Ref. [89] the scattering terms were also included in the phonon operator for a schematic four-level model Hamiltonian. The Authors called this model extended r-QRPA (er-QRPA). The analysis showed that the contribution of  $pp$  and  $hh$  terms to the spectrum and sum rules becomes important and prevent the collapse of standard RPA, if their magnitudes are comparable with the  $ph$  ones.

Unfortunately, small spurious eigenvalues generated within FR-rQRPA by scattering terms are mixed with those of physical eigenstates. An approach to separate these low-lying spurious modes is proposed in Ref. [90]. The idea is to consider the phonon operator not in terms of quasiparticles, but of original particle operators, i.e.

$$Q_{JM}^{\dagger}(\nu) = \sum_{\tau\tau'} X_{\tau\tau'}^{J\nu} \left[ C_{JM}^{\dagger}(\tau\tau') - Y_{\tau\tau'}^{J\nu} \tilde{C}_{JM}(\tau\tau') \right], \quad (3.39)$$

where  $C_{JM}^{\dagger}(\tau\tau') = [c_{\tau}^{\dagger} \tilde{c}_{\tau'}]_{JM}$  and  $\tau$  denote single-particle quantum numbers including isospin. Thus, this phonon operator written in terms of quasiparticles contains scattering terms. It is shown that the spectrum does not contain spurious low-lying states and Ikeda sum rule is analytically fulfilled. A numerical application of the model to  $2\nu\beta\beta$  emitters  $^{76}\text{Ge}$ ,  $^{82}\text{Se}$ ,  $^{100}\text{Mo}$ ,  $^{116}\text{Cd}$ ,  $^{128}\text{Te}$  and  $^{130}\text{Xe}$  is performed in [91]. This model was called by its authors also fully renormalised pnQRPA (fr-pnQRPA).

In all these approaches the expectation values were evaluated without the explicit form of the ground state wave function. It turns out that it can approximately be given only for a limited class of two-level models, like the O(5) model for Fermi transitions, as a superposition of

even number of protons and neutrons similar to (3.36), i.e.

$$|0\rangle = \sqrt{N_0} \sum_{l=0}^{\Omega} a_l z^l (A^{\dagger})^{2l} |BCS\rangle, \quad (3.40)$$

where  $A^{\dagger}$  is the proton-neutron monopole creation operator,  $\Omega = j + 1/2$ ,  $z = Y/X$  and the coefficients  $a_l$  are given in [92]. A similar approach is discussed in reference [93].

An extended RPA phonon of the type

$$Q^{\dagger} = X_1 A^{\dagger} - Y_a A + X_3 A A^{\dagger} A^{\dagger} - Y_3 A A A^{\dagger} \quad (3.41)$$

is discussed in [94] for the two-level proton-neutron Lipkin model, considering the explicit form of the ground state of the form (3.40). It turned out that the inclusion of nonlinear terms in the phonon operator leads to a very good agreement with the exact solution.

In Ref. [95] the ground state is determined as a solution of a variational equation for the proton-neutron Lipkin model mapped onto the boson operators  $B^{\dagger}$  by using the Marumori method. The QRPA phonon operator

$$Q^{\dagger} = X(B^{\dagger} + t^*) - Y(B + t) \quad (3.42)$$

depends upon the variational parameters  $t, t^*$ , which results in a non-vanishing expectation values of  $Q$  on the "deformed ground state"

$$|0\rangle = \exp[t^* B - t B^{\dagger}] \exp[z B^{\dagger} B^{\dagger} - z^* B B] |-\rangle, \quad (3.43)$$

where  $|-\rangle$  is the vacuum state for the boson operator  $B$ . The variational parameters are determined in an optimal way by minimizing the ground state energy.

As a general conclusion, let us point out that the inclusion of the Pauli principle within the renormalized pn-QRPA, describing beta decay processes, reduces the ground state correlations by shifting the collapse of the standard pn-QRPA to larger values of the particle-particle strength, i.e. outside the physical region. Thus, at physical values of the particle-particle strength one obtains a realistic description of the  $2\nu\beta\beta$  transition probability.

#### IV. THE GREEN'S FUNCTION FORMALISM

As is well known, each eigenvalue problem has an analogous Green's function formulation. For convenience, let us start with the particle-particle channel, for which we consider the corresponding two-times propagator

$$G_{k_1 k_2 k'_1 k'_2}^{t-t'} = -i \langle 0 | T(c_{k_1} c_{k_2})_t (c_{k'_2}^{\dagger} c_{k'_1}^{\dagger})_{t'} | 0 \rangle. \quad (4.1)$$

Here  $T$  is the time ordering operator,  $|0\rangle$  stands for the exact ground state and the time dependence of the

fermion pair operators is given by the two body Hamiltonian

$$H = H_0 + V \equiv \sum_{kk'} e_{kk'} c_k^\dagger c_{k'} + \frac{1}{4} \sum_{k_1 k_2 k_3 k_4} \bar{v}_{k_1 k_2 k_3 k_4} c_{k_1}^\dagger c_{k_2}^\dagger c_{k_4} c_{k_3}, \quad (4.2)$$

where  $e_{kk'}$  is the single-particle matrix comprising kinetic energy and external potential, and the antisymmetrised matrix element of the interaction is given after Eq. (2.6).

The two-body propagator obeys the following exact integral equation [22, 96]

$$\begin{aligned} (i\partial_t - \tilde{e}_{k_1} - \tilde{e}_{k_2}) G_{k_1 k_2, k'_1 k'_2}^{t-t'} &= N_{k_1 k_2 k'_1 k'_2} \delta(t-t') \\ &+ \sum_{k_3 k_4} \int dt_1 [K^{pp,0} \delta(t-t_1) + K^{pp,\text{dyn.},t-t_1}]_{k_1 k_2 k_3 k_4} \\ &N_{k_3 k_4}^{pp-1} G_{k_3 k_4 k'_1 k'_2}^{t_1-t'}, \end{aligned} \quad (4.3)$$

where with  $\delta_{k_1 k_2, k'_1 k'_2} = \delta_{k_1 k'_1} \delta_{k_2 k'_2} - \delta_{k_1 k'_2} \delta_{k_2 k'_1}$

$$N_{k_1 k_2 k'_1 k'_2}^{pp} = \delta_{k_1 k_2, k'_1 k'_2} N_{k_1 k_2}^{pp}; \quad N_{k_1 k_2}^{pp} = 1 - n_{k_1} - n_{k_2}, \quad (4.4)$$

and we supposed that we work in the canonical basis, where the density matrix is diagonal, that is

$$\langle 0 | c_{k_1}^\dagger c_{k'_1} | 0 \rangle = \delta_{k_1 k'_1} n_{k_1}. \quad (4.5)$$

Furthermore, the s.p. energies in (4.3) are given by

$$\tilde{e}_k = e_k + V_k^{\text{MF}}, \quad (4.6)$$

where the mean-field shift

$$V_k^{\text{MF}} = \langle 0 | \{c_k, [H, c_k^\dagger]\} | 0 \rangle = \sum_{k'} \bar{v}_{kk'kk'} n_{k'} \quad (4.7)$$

is included and where  $\{..\}$  stands for the anticommutator. We assumed that mean-field energies and density matrix can be diagonalized simultaneously. The integral kernel is given by

$$\begin{aligned} K_{k_1 k_2 k'_1 k'_2}^{pp} &= \langle [A_{k_1 k_2}, [V, A_{k'_1 k'_2}^\dagger]] \rangle \delta(t-t') \\ &+ (-i) \langle T J_{k_1 k_2}(t) J_{k'_1 k'_2}^\dagger(t') \rangle_{\text{irr.}} \\ &\equiv K_{k_1 k_2 k'_1 k'_2}^{pp,0} \delta(t-t') + K_{k_1 k_2 k'_1 k'_2}^{pp,\text{dyn.},t-t'}, \end{aligned} \quad (4.8)$$

where we abbreviated

$$A_{k_1 k_2} = c_{k_1} c_{k_2}, \quad (4.9)$$

and

$$J_{k_1 k_2}^{pp} = [A_{k_1 k_2}, V] = j_{k_1} c_{k_2} + c_{k_1} j_{k_2}, \quad (4.10)$$

with

$$j_k = [c_k, V] = \frac{1}{2} \sum_{k_2 k_3 k_4} \bar{v}_{k k_2 k_3 k_4} c_{k_2}^\dagger c_{k_4} c_{k_3}. \quad (4.11)$$

Please note that the  $K$ -matrix, which after Fourier transform depends only on one frequency can be interpreted as a self-energy for the motion of a fermion pair. As usual, the self-energy is split into a frequency independent, static part and a truly frequency dependent, dynamic part. The latter must be two-line irreducible, hence the index 'irr.'. In [97] (see also [22, 96]) we named Eq.(4.3) with the interaction kernel of Eq. (4.8) Dyson-Bethe-Salpeter Equation (Dyson-BSE). We want again to point out that this Dyson-BSE is an exact equation with a single frequency kernel. Its existence is not often recognized. In fact, it is entirely equivalent to the EOM method.

#### A. Static part of the BSE kernel

Let us now discuss the  $K^{pp,0}$  term of the BSE kernel. To establish an explicit form for  $K^{pp,0}$ , we have to evaluate the double commutator contained in the pair mean-field part of  $K^{pp,0}$  see Eq. (2.59) above. (It is actually the same as given in pp-SCRPA, section II.D).

$$\begin{aligned} K_{k_1 k_2 k'_1 k'_2}^{pp,0} &= N_{k_1 k_2}^{pp} \bar{v}_{k_1 k_2 k'_1 k'_2} N_{k'_1 k'_2}^{pp} \\ &+ \left\{ \left[ \left( \frac{1}{2} \delta_{k_1 k'_1} \bar{v}_{l_1 k_2 l_3 l_4} C_{l_3 l_4 k'_2 l_1} + \bar{v}_{l_1 k_2 l_4 k'_2} C_{l_4 k_1 l_1 k'_1} \right) \right. \right. \\ &\left. \left. - (k_1 \leftrightarrow k_2) \right] - (k'_1 \leftrightarrow k'_2) \right\}, \end{aligned} \quad (4.12)$$

where

$$C_{k_1 k_2 k'_1 k'_2} = \langle 0 | c_{k'_1}^\dagger c_{k'_2}^\dagger c_{k_2} c_{k_1} | 0 \rangle - n_{k_1} n_{k_2} \delta_{k_1 k_2, k'_1 k'_2}, \quad (4.13)$$

which is the fully correlated two-body, or cumulant, form of the density matrix.

We see that  $K^{pp,0}$  involves, besides occupation numbers, static two-body correlation functions. They are of two types: there are single-line corrections with one of the two s.p. motions unaffected by the correlations (those with the Kronecker symbols) and there are exchange terms, where a two-body correlation is exchanged between the two particles. Since our starting point is a two-body propagator, a self-consistent scheme can be established. This is similar to the self-consistency involved with the s.p. mean field, only here, naturally, two-body correlation functions have to be iterated rather than s.p.

densities in the case of the s.p. mean field. We, therefore, call  $K^{pp,0}$  the 'fermion pair mean field'. Of course, there appear also s.p. densities in  $K^{pp,0}$  and we will later show how they can be consistently obtained from the s.p. Green's function.

A closer investigation of the exchange kernel, however, shows that the exchange is rather of the  $ph$  type. At least to lowest order, that is to second order, the exchange is given by a static  $ph$  exchange bubble. It is well known that this  $ph$  exchange screens the pairing force by almost a factor of two as has first been evaluated by Gorkov, Melik-Barkhudarov (GMB) [98, 99]. Actually for systems like the nuclear ones, where there are more than two species of fermions (that is, four species), the screening can eventually also become anti-screening [100, 101]. Also GMB did not use strict second order, but replaced the vertices by the scattering length, that is the vertices have been dressed to  $T$ -matrices in the low-energy limit. Though this resummation can be understood easily by graphical analysis, how this can be derived more analytically will be discussed below in sect. IV.B.

The first term on the r.h.s. of Eq. (4.12) is the usual two-body matrix element of the interaction modified with correlated occupation numbers (the standard particle-particle RPA as described in [5] uses HF occupation numbers). One can pre-sum this term, what leads to the so-called renormalized pp-RPA (see Sect.II.A for renormalized RPA)

$$G_{k_1 k_2 k'_1 k'_2}^{r\text{-ppRPA}} = G_{k_1 k_2 k'_1 k'_2}^{0,r\text{-ppRPA}} + \sum_{k_3 k_4} G_{k_1 k_2 k_3 k_4}^{0,r\text{-ppRPA}} \bar{v}_{k_3 k_4 k'_3 k'_4} G_{k'_3 k'_4 k'_1 k'_2}^{r\text{-ppRPA}}, \quad (4.14)$$

with

$$G_{k_1 k_2 k'_1 k'_2}^{0,r\text{-ppRPA}} = \frac{1 - n_{k_1} - n_{k_2}}{\omega - \tilde{\epsilon}_{k_1} - \tilde{\epsilon}_{k_2}} \delta_{k_1 k_2, k'_1 k'_2}. \quad (4.15)$$

where we omitted the infinitesimal imaginary part(s) in the denominator for brevity. Either one treats a discrete system where they are not needed or one has to add a  $+i\eta$  in the case a retarded Green's function or split the propagator into advanced or retarded parts with alternating signs for the imaginary parts in the case of chronological propagators [4]. The Dyson-BSE can then be written in the following way:

$$G_{k_1 k_2 k'_1 k'_2} = G_{k_1 k_2 k'_1 k'_2}^{r\text{-ppRPA}} + G_{k_1 k_2 k_3 k_4}^{r\text{-ppRPA}} [N^{-1}(K^{pp,0} - N\bar{v}N + K^{pp,\text{dyn.}})N^{-1}]_{k_3 k_4 k'_3 k'_4} G_{k'_3 k'_4 k'_1 k'_2}. \quad (4.16)$$

For brevity, we have replaced  $N^{pp}$  by  $N$  in this equation, Let us stress again that all quantities in (4.16) only de-

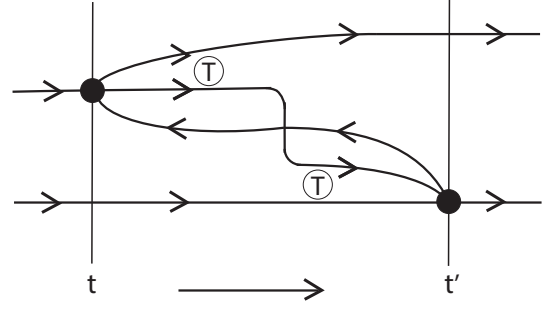


FIG. 14. Second order  $T$ -matrix approximation to the three-particle propagator contained in the 3p-1h correlation function. Together with the first order contribution contained in the uncorrelated 3p-1h propagator, this can be summed to one full  $T$ -matrix. Time flows from left ( $t$ ) to right ( $t'$ ).

pend on a single frequency. Single frequency two-particle propagators have also been considered in [102].

## B. Dynamic part of the BSE kernel

Let us now discuss the time-dependent, *dynamic* part  $K^{\text{dyn.}}$  of the interaction kernel

$$K_{k_1 k_2 k'_1 k'_2}^{pp,\text{dyn.}} = -i \langle 0 | T J_{k_1 k_2}(t) J_{k'_1 k'_2}^+(t') | 0 \rangle_{\text{irr.}}. \quad (4.17)$$

From (4.10) we see that this expression involves four different contributions: two contributions contain the two interaction vertices on the same line and two contributions on opposite lines. The latter, therefore, contain exchange processes while the former are responsible for s.p. self-energy corrections. Approximating the 3p-1h propagator involved in (4.17) by a product of a hole propagator and the three-body propagator in second order  $T$ -matrix approximation, we give a schematic graphical representation of the term in Fig. 14. This illustrates how one can replace in the second order the screening term discussed above, the bare vertices by ladder  $T$ -matrices and then eventually by the scattering lengths as done in GMB [98, 99]. We see that the exchange contributions are of the screening (or anti-screening) type whereas the other two contributions renormalize the s.p. by particle-vibration couplings. Of course, in general, all four lines are correlated.

As a matter of fact the 3p-1h propagator in (4.17) lends itself to several “natural” approximations other than the one we just discussed. For example, instead of considering an uncorrelated ph-propagator exchange, one could take the ph-response function in standard RPA or in SCRPA as discussed in Sect. II. For applications with standard RPA, see [103, 104].

### C. The ph-channel

Since we see that  $ph$  and  $pp$  channels are coupled, we immediately also give the Dyson-BSE in the ph-channel [96]:

$$(\omega - \tilde{\epsilon}_{k_1} + \tilde{\epsilon}_{k_2})R_{k_1 k_2 k'_1 k'_2}(\omega) = N_{k_1 k_2 k'_1 k'_2}^{ph} + \sum_{k_3 k_4} [K_{k_1 k_2 k_3 k_4}^{ph,0} + K_{k_1 k_2 k_3 k_4}^{ph,dyn}(\omega)] N_{k_3 k_4 k'_1 k'_2}^{ph-1} R_{k_3 k_4 k'_1 k'_2}(\omega) \quad (4.18)$$

with

$$N_{k_1 k_2 k'_1 k'_2}^{ph} = \delta_{k_1 k'_1} \delta_{k_2 k'_2} N_{k_1 k_2}^{ph} \equiv \delta_{k_1 k'_1} \delta_{k_2 k'_2} (n_{k_2} - n_{k_1}) \quad (4.19)$$

and the two-time response function defined by (with  $k_1 \neq k_2$  and  $k'_1 \neq k'_2$ )

$$R_{k_1 k_2 k'_1 k'_2}(t - t') = -i \langle 0 | T \{ c_{k_2}^\dagger(t) c_{k_1}(t) c_{k'_1}^\dagger(t') c_{k'_2}(t') \} | 0 \rangle . \quad (4.20)$$

The static part of the integral kernel is given by (again this is same expression as in the ph-SCRPA equation (2.33))

$$K_{k_1 k_2 k_3 k_4}^{ph,0} = N_{k_1 k_2}^{ph} \bar{v}_{k_1 k_4 k_2 k_3} N_{k_3 k_4}^{ph} + \left[ -\frac{1}{2} \sum_{ll'} (\delta_{k_2 k_4} \bar{v}_{k_1 ll' l''} C_{ll' k_2 k_3} + \delta_{k_1 k_3} \bar{v}_{ll' k_2 l''} C_{k_4 l'' ll'}) + \sum_{ll'} (\bar{v}_{k_1 l k_3 l'} C_{k_4 l' k_2 l} + \bar{v}_{k_4 l k_2 l'} C_{k_1 l' k_3 l}) - \frac{1}{2} \sum_{ll'} (\bar{v}_{k_1 k_4 ll'} C_{ll' k_2 k_3} + \bar{v}_{ll' k_2 k_3} C_{k_1 k_4 ll'}) \right] , \quad (4.21)$$

and the dynamic part

$$K_{k_1 k_2 k'_1 k'_2}^{ph,dyn}(t - t') = -i \langle 0 | T \{ J_{k_1 k_2}^{ph}(t) J_{k'_1 k'_2}^{ph\dagger}(t') \} | 0 \rangle^{irr} . \quad (4.22)$$

with

$$J_{k_1 k_2}^{ph} = [c_{k_2}^\dagger c_{k_1}, V] = c_{k_2}^\dagger j_{k_1} + j_{k_2}^\dagger c_{k_1} , \quad (4.23)$$

As in the pp-channel, we can introduce a renormalized ph-propagator

$$R_{k_1 k_2 k'_1 k'_2}^{r-phRPA} = R_{k_1 k_2 k'_1 k'_2}^{0,r} + \sum_{k_3 k_4} R_{k_1 k_2 k_3 k_4}^{0,r} T_{k_3 k'_4 k_4 k'_3} R_{k'_3 k'_4 k'_1 k'_2}^{r-phRPA} , \quad (4.24)$$

with

$$R_{k_1 k_2 k'_1 k'_2}^{0,r} = \frac{n_{k_2} - n_{k_1}}{\omega - \tilde{\epsilon}_{k_1} + \tilde{\epsilon}_{k_2}} \delta_{k_1 k'_1} \delta_{k_2 k'_2} , \quad (4.25)$$

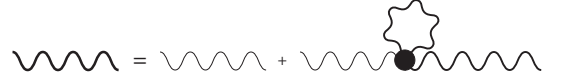


FIG. 15. Mean-field ph-propagator with tad-pole self-interaction.

where with respect to the infinitesimal imaginary parts in the denominator the same remarks hold as for the analog expression in the pp-case, see Eq.(??), and where we introduced the ladder  $T$ -matrix

$$T_{k_1 k_4 k_2 k_3} = \bar{v}_{k_1 k_4 k_2 k_3} + N_{k_1 k_2}^{-1} \times \left[ -\frac{1}{2} \sum_{ll'} (\bar{v}_{k_1 k_4 ll'} C_{ll' k_2 k_3} + \bar{v}_{ll' k_2 k_3} C_{k_1 k_4 ll'}) \right] N_{k_3 k_4}^{-1} , \quad (4.26)$$

which is important when dealing with systems with a hard-core potential.

Keeping from the ph-kernel only the remaining instantaneous part, one arrives at a self-consistent mean-field equation for the ph-propagation

$$R_{k_1 k_2 k'_1 k'_2}^{MF-RPA} = R_{k_1 k_2 k'_1 k'_2}^{r-phRPA} + \sum_{k_3 k_4 k'_3 k'_4} R_{k_1 k_2 k_3 k_4}^{r-phRPA} [N^{-1} \tilde{K}^{ph,0} N^{-1}]_{k_3 k_4 k'_3 k'_4} R_{k'_3 k'_4 k'_1 k'_2}^{MF-RPA} , \quad (4.27)$$

where  $\tilde{K}^{ph,0}$  is the part of (4.21), where only the second, third, fourth, and fifth terms on the r.h.s. are kept. The eigenvalue form of this equation, given below, is the same as the self-consistent RPA (SCRPA) equation (2.23). A schematic graphical representation of Eq. (4.27) is given in Fig. 15.

We want to give the spectral representation of the response function, since it may be important for the following when we discuss the particle-vibration coupling (PVC).

$$R_{k_1 k_2 k'_1 k'_2}(\omega) = \sum_{\nu} \frac{\begin{pmatrix} X^{\nu} \\ Y^{\nu} \end{pmatrix}_{k_1 k_2} (X^{\nu\dagger} \ Y^{\nu\dagger})_{k'_1 k'_2}}{\omega - \Omega_{\nu} + i\eta} - \frac{\left[ \begin{pmatrix} Y^{\nu} \\ X^{\nu} \end{pmatrix}_{k_1 k_2} (Y^{\nu\dagger} \ X^{\nu\dagger})_{k'_1 k'_2} \right]^*}{\omega + \Omega_{\nu} - i\eta} . \quad (4.28)$$

On the pole we get with (4.28) again the eigenvalue equation (SCRPA equation (2.23)).

### D. The particle-vibration-coupling (PVC) approach

The Dyson-BSEs in the  $pp$ - and  $ph$ -channels are a convenient starting point to study the particle-vibration coupling effects, which play a very important role for nuclear and condensed-matter systems [105, 106]. Let us consider the response function in the  $ph$ -channel, which is the quantity describing excitations caused by external perturbations without particle transfer. The model-independent spectral image of this function given by Eq. (4.28) illustrates its direct connection to the observables: its poles correspond to the exact excitation energies and the residues to the respective transition amplitudes.

Already in the static part of the interaction kernel for this response function, see, e.g., (2.33), one discovers an instantaneous exchange of a density-density correlation (vibration). The dynamical part of the kernel defined in Eq. (4.22), after calculating the commutators, leads to four terms with the formally exact two-time two-particle-two-hole ( $2p2h$ ) correlation function contracted with two matrix elements of the bare interaction in four possible ways. The direct way of calculating this  $2p2h$  correlation function would require the solution of the equation of motion for it, however, the latter equation contains even a higher-rank correlation function in its dynamical kernel. Obviously, such a procedure generates a hierarchy of equations for increasing-rank correlation functions, making the many-body problem practically intractable. A variety of approximations to the  $2p2h$  correlation function, however, are known, and the choice of the specific approximation is dictated by the physical constraints. The simplest approximation is given by the replacement of the correlated  $2p2h$ -propagator by the uncorrelated one. This comprises the second random phase approximation, which is quite appropriate for weakly-coupled systems. Other possibilities are given by the cluster expansions, where one can limit the  $2p2h$  propagator by the products of two  $1p1h$  or  $2p$  and  $2h$ -propagators. Here the options are (i) one pair of fermions propagates without interaction, while the other retains correlations and (ii) both fermionic pair configurations form correlated quasiboson states. These states can be associated with the phonons. After identifying the two-fermion correlation functions contracted with the interaction matrix elements with the phonon propagators and vertices, as shown in Fig. 16, the interaction kernel of type (i) can be illustrated by Fig. 17, while the kernel of type (ii) with two correlation functions corresponds to the one displayed in Fig. 18. Note that in these figures we show explicitly only the normal particle-hole phonons, however, the terms with the pairing phonons look analogously with the only difference that they carry couplings between  $ph$  and  $hp$  correlation functions in the Dyson-BSE. Note that in Figs. 17 and 18 we retain the notation  $\Phi$  for the dynamical kernels, which was used in the original works. It corresponds to various approximations to the kernel of Eq. (4.22). The approaches to the dynamical kernels in the phonon-

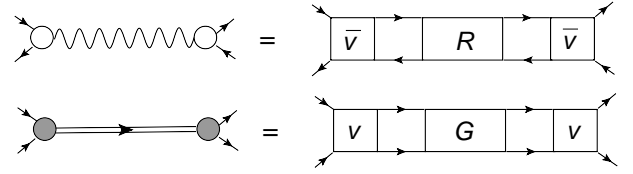


FIG. 16. The emergence of the phonon-exchange interaction: phonon vertices are denoted by circles, and their propagators by wavy lines and double lines for the normal and pairing phonons, respectively. Straight lines stand for the fermionic propagators. Rectangular blocks are associated with the particle-hole ( $R$ ) and particle-particle ( $G$ ) correlation functions, and the square blocks represent the bare interaction. Top: normal (particle-hole) phonon, bottom: pairing (particle-particle) phonon. See Refs. [106, 130] for more details.

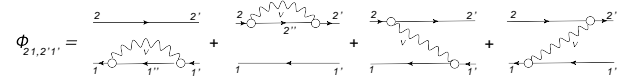


FIG. 17.  $1p1h \otimes \text{phonon}$  approach to the dynamic kernel of the Dyson-BSE for the response function.

coupling form as those shown in Figs. 17, 18 are commonly known in the literature as (quasi)particle-phonon or (quasi)particle-vibration coupling (PVC) [107–128]. It is worth mentioning that very similar expressions as those shown in Fig. 17 have also been used in chemical physics for the purpose of screening the bare electron-electron force [129]. In addition explicit expressions corresponding to Fig. 17 can also be found in [96], Eq. (58).

Similar studies were performed for the  $pp$ -channel [130], where analogous treatments of the static and dynamical kernels were suggested. Considering together the EOM's for both  $ph$  and  $pp$  correlation functions and the factorizations discussed above allows for a truncation of the EOM series on the two-body level. Thus, the many-body problem is reduced to the closed system of coupled equations for one-fermion and two-fermion propagators in the  $pp$  and  $ph$ -channels. The phonon vertices and propagators, which enter the dynamical kernels of these equations, are, in general, model-independent and, ideally, should contain the same correlation functions, which constitute the main variables of these EOM's. As this system of equations is essentially non-linear, it should be solved by iterations with a good initial guess for the sought-for correlation functions. Those could be, in principle, the correlation functions calculated with the only static kernel. However, in strongly-coupled systems, such as atomic nuclei, calculations of the correlation functions with bare interactions and only static kernels can be quite far from the realistic ones [131]. This raises the question about convergence of this approach. Another possibility could be employing the correlation functions calculated in RPA-like approaches with one of the well-known effective interactions at the entrance point. That could potentially provide better convergence, however, this strategy

$$\Phi_{212'1'}^{(n+1)} = \begin{array}{c} \text{Diagram 1} \\ \text{Diagram 2} \\ \text{Diagram 3} \\ \text{Diagram 4} \end{array}$$

FIG. 18. Generic contributions to the dynamical kernel of the Dyson-BSE response function including one phonon and a full response function  $R^{(n)}$ , where the upper index  $n$  indicates the number of phonons it contains. See also [17] where similar processes are discussed.

$$\Phi^{(3)} = \Phi^{(2)} + \begin{array}{c} \text{Diagram 1} \\ \text{Diagram 2} \\ \text{Diagram 3} \\ \text{Diagram 4} \\ \text{Diagram 5} \\ \text{Diagram 6} \\ \text{Diagram 7} \\ \text{Diagram 8} \\ \text{Diagram 9} \\ \text{Diagram 10} \\ \text{Diagram 11} \\ \text{Diagram 12} \\ \text{Diagram 13} \\ \text{Diagram 14} \\ \text{Diagram 15} \\ \text{Diagram 16} \\ \text{Diagram 17} \\ \text{Diagram 18} \\ \text{Diagram 19} \\ \text{Diagram 20} \\ \text{Diagram 21} \\ \text{Diagram 22} \\ \text{Diagram 23} \\ \text{Diagram 24} \\ \text{Diagram 25} \\ \text{Diagram 26} \\ \text{Diagram 27} \\ \text{Diagram 28} \\ \text{Diagram 29} \\ \text{Diagram 30} \\ \text{Diagram 31} \\ \text{Diagram 32} \\ \text{Diagram 33} \\ \text{Diagram 34} \\ \text{Diagram 35} \\ \text{Diagram 36} \\ \text{Diagram 37} \\ \text{Diagram 38} \\ \text{Diagram 39} \\ \text{Diagram 40} \\ \text{Diagram 41} \\ \text{Diagram 42} \\ \text{Diagram 43} \\ \text{Diagram 44} \\ \text{Diagram 45} \\ \text{Diagram 46} \\ \text{Diagram 47} \\ \text{Diagram 48} \\ \text{Diagram 49} \\ \text{Diagram 50} \\ \text{Diagram 51} \\ \text{Diagram 52} \\ \text{Diagram 53} \\ \text{Diagram 54} \\ \text{Diagram 55} \\ \text{Diagram 56} \\ \text{Diagram 57} \\ \text{Diagram 58} \\ \text{Diagram 59} \\ \text{Diagram 60} \\ \text{Diagram 61} \\ \text{Diagram 62} \\ \text{Diagram 63} \\ \text{Diagram 64} \\ \text{Diagram 65} \\ \text{Diagram 66} \\ \text{Diagram 67} \\ \text{Diagram 68} \\ \text{Diagram 69} \\ \text{Diagram 70} \\ \text{Diagram 71} \\ \text{Diagram 72} \\ \text{Diagram 73} \\ \text{Diagram 74} \\ \text{Diagram 75} \\ \text{Diagram 76} \\ \text{Diagram 77} \\ \text{Diagram 78} \\ \text{Diagram 79} \\ \text{Diagram 80} \\ \text{Diagram 81} \\ \text{Diagram 82} \\ \text{Diagram 83} \\ \text{Diagram 84} \\ \text{Diagram 85} \\ \text{Diagram 86} \\ \text{Diagram 87} \\ \text{Diagram 88} \\ \text{Diagram 89} \\ \text{Diagram 90} \\ \text{Diagram 91} \\ \text{Diagram 92} \\ \text{Diagram 93} \\ \text{Diagram 94} \\ \text{Diagram 95} \\ \text{Diagram 96} \\ \text{Diagram 97} \\ \text{Diagram 98} \\ \text{Diagram 99} \\ \text{Diagram 100} \\ \text{Diagram 101} \\ \text{Diagram 102} \\ \text{Diagram 103} \\ \text{Diagram 104} \\ \text{Diagram 105} \\ \text{Diagram 106} \\ \text{Diagram 107} \\ \text{Diagram 108} \\ \text{Diagram 109} \\ \text{Diagram 110} \\ \text{Diagram 111} \\ \text{Diagram 112} \\ \text{Diagram 113} \\ \text{Diagram 114} \\ \text{Diagram 115} \\ \text{Diagram 116} \\ \text{Diagram 117} \\ \text{Diagram 118} \\ \text{Diagram 119} \\ \text{Diagram 120} \\ \text{Diagram 121} \\ \text{Diagram 122} \\ \text{Diagram 123} \\ \text{Diagram 124} \\ \text{Diagram 125} \\ \text{Diagram 126} \\ \text{Diagram 127} \\ \text{Diagram 128} \\ \text{Diagram 129} \\ \text{Diagram 130} \\ \text{Diagram 131} \\ \text{Diagram 132} \\ \text{Diagram 133} \\ \text{Diagram 134} \\ \text{Diagram 135} \\ \text{Diagram 136} \\ \text{Diagram 137} \\ \text{Diagram 138} \\ \text{Diagram 139} \\ \text{Diagram 140} \\ \text{Diagram 141} \\ \text{Diagram 142} \\ \text{Diagram 143} \\ \text{Diagram 144} \\ \text{Diagram 145} \\ \text{Diagram 146} \\ \text{Diagram 147} \\ \text{Diagram 148} \\ \text{Diagram 149} \\ \text{Diagram 150} \\ \text{Diagram 151} \\ \text{Diagram 152} \\ \text{Diagram 153} \\ \text{Diagram 154} \\ \text{Diagram 155} \\ \text{Diagram 156} \\ \text{Diagram 157} \\ \text{Diagram 158} \\ \text{Diagram 159} \\ \text{Diagram 160} \\ \text{Diagram 161} \\ \text{Diagram 162} \\ \text{Diagram 163} \\ \text{Diagram 164} \\ \text{Diagram 165} \\ \text{Diagram 166} \\ \text{Diagram 167} \\ \text{Diagram 168} \\ \text{Diagram 169} \\ \text{Diagram 170} \\ \text{Diagram 171} \\ \text{Diagram 172} \\ \text{Diagram 173} \\ \text{Diagram 174} \\ \text{Diagram 175} \\ \text{Diagram 176} \\ \text{Diagram 177} \\ \text{Diagram 178} \\ \text{Diagram 179} \\ \text{Diagram 180} \\ \text{Diagram 181} \\ \text{Diagram 182} \\ \text{Diagram 183} \\ \text{Diagram 184} \\ \text{Diagram 185} \\ \text{Diagram 186} \\ \text{Diagram 187} \\ \text{Diagram 188} \\ \text{Diagram 189} \\ \text{Diagram 190} \\ \text{Diagram 191} \\ \text{Diagram 192} \\ \text{Diagram 193} \\ \text{Diagram 194} \\ \text{Diagram 195} \\ \text{Diagram 196} \\ \text{Diagram 197} \\ \text{Diagram 198} \\ \text{Diagram 199} \\ \text{Diagram 200} \\ \text{Diagram 201} \\ \text{Diagram 202} \\ \text{Diagram 203} \\ \text{Diagram 204} \\ \text{Diagram 205} \\ \text{Diagram 206} \\ \text{Diagram 207} \\ \text{Diagram 208} \\ \text{Diagram 209} \\ \text{Diagram 210} \\ \text{Diagram 211} \\ \text{Diagram 212} \\ \text{Diagram 213} \\ \text{Diagram 214} \\ \text{Diagram 215} \\ \text{Diagram 216} \\ \text{Diagram 217} \\ \text{Diagram 218} \\ \text{Diagram 219} \\ \text{Diagram 220} \\ \text{Diagram 221} \\ \text{Diagram 222} \\ \text{Diagram 223} \\ \text{Diagram 224} \\ \text{Diagram 225} \\ \text{Diagram 226} \\ \text{Diagram 227} \\ \text{Diagram 228} \\ \text{Diagram 229} \\ \text{Diagram 230} \\ \text{Diagram 231} \\ \text{Diagram 232} \\ \text{Diagram 233} \\ \text{Diagram 234} \\ \text{Diagram 235} \\ \text{Diagram 236} \\ \text{Diagram 237} \\ \text{Diagram 238} \\ \text{Diagram 239} \\ \text{Diagram 240} \\ \text{Diagram 241} \\ \text{Diagram 242} \\ \text{Diagram 243} \\ \text{Diagram 244} \\ \text{Diagram 245} \\ \text{Diagram 246} \\ \text{Diagram 247} \\ \text{Diagram 248} \\ \text{Diagram 249} \\ \text{Diagram 250} \\ \text{Diagram 251} \\ \text{Diagram 252} \\ \text{Diagram 253} \\ \text{Diagram 254} \\ \text{Diagram 255} \\ \text{Diagram 256} \\ \text{Diagram 257} \\ \text{Diagram 258} \\ \text{Diagram 259} \\ \text{Diagram 260} \\ \text{Diagram 261} \\ \text{Diagram 262} \\ \text{Diagram 263} \\ \text{Diagram 264} \\ \text{Diagram 265} \\ \text{Diagram 266} \\ \text{Diagram 267} \\ \text{Diagram 268} \\ \text{Diagram 269} \\ \text{Diagram 270} \\ \text{Diagram 271} \\ \text{Diagram 272} \\ \text{Diagram 273} \\ \text{Diagram 274} \\ \text{Diagram 275} \\ \text{Diagram 276} \\ \text{Diagram 277} \\ \text{Diagram 278} \\ \text{Diagram 279} \\ \text{Diagram 280} \\ \text{Diagram 281} \\ \text{Diagram 282} \\ \text{Diagram 283} \\ \text{Diagram 284} \\ \text{Diagram 285} \\ \text{Diagram 286} \\ \text{Diagram 287} \\ \text{Diagram 288} \\ \text{Diagram 289} \\ \text{Diagram 290} \\ \text{Diagram 291} \\ \text{Diagram 292} \\ \text{Diagram 293} \\ \text{Diagram 294} \\ \text{Diagram 295} \\ \text{Diagram 296} \\ \text{Diagram 297} \\ \text{Diagram 298} \\ \text{Diagram 299} \\ \text{Diagram 300} \\ \text{Diagram 301} \\ \text{Diagram 302} \\ \text{Diagram 303} \\ \text{Diagram 304} \\ \text{Diagram 305} \\ \text{Diagram 306} \\ \text{Diagram 307} \\ \text{Diagram 308} \\ \text{Diagram 309} \\ \text{Diagram 310} \\ \text{Diagram 311} \\ \text{Diagram 312} \\ \text{Diagram 313} \\ \text{Diagram 314} \\ \text{Diagram 315} \\ \text{Diagram 316} \\ \text{Diagram 317} \\ \text{Diagram 318} \\ \text{Diagram 319} \\ \text{Diagram 320} \\ \text{Diagram 321} \\ \text{Diagram 322} \\ \text{Diagram 323} \\ \text{Diagram 324} \\ \text{Diagram 325} \\ \text{Diagram 326} \\ \text{Diagram 327} \\ \text{Diagram 328} \\ \text{Diagram 329} \\ \text{Diagram 330} \\ \text{Diagram 331} \\ \text{Diagram 332} \\ \text{Diagram 333} \\ \text{Diagram 334} \\ \text{Diagram 335} \\ \text{Diagram 336} \\ \text{Diagram 337} \\ \text{Diagram 338} \\ \text{Diagram 339} \\ \text{Diagram 340} \\ \text{Diagram 341} \\ \text{Diagram 342} \\ \text{Diagram 343} \\ \text{Diagram 344} \\ \text{Diagram 345} \\ \text{Diagram 346} \\ \text{Diagram 347} \\ \text{Diagram 348} \\ \text{Diagram 349} \\ \text{Diagram 350} \\ \text{Diagram 351} \\ \text{Diagram 352} \\ \text{Diagram 353} \\ \text{Diagram 354} \\ \text{Diagram 355} \\ \text{Diagram 356} \\ \text{Diagram 357} \\ \text{Diagram 358} \\ \text{Diagram 359} \\ \text{Diagram 360} \\ \text{Diagram 361} \\ \text{Diagram 362} \\ \text{Diagram 363} \\ \text{Diagram 364} \\ \text{Diagram 365} \\ \text{Diagram 366} \\ \text{Diagram 367} \\ \text{Diagram 368} \\ \text{Diagram 369} \\ \text{Diagram 370} \\ \text{Diagram 371} \\ \text{Diagram 372} \\ \text{Diagram 373} \\ \text{Diagram 374} \\ \text{Diagram 375} \\ \text{Diagram 376} \\ \text{Diagram 377} \\ \text{Diagram 378} \\ \text{Diagram 379} \\ \text{Diagram 380} \\ \text{Diagram 381} \\ \text{Diagram 382} \\ \text{Diagram 383} \\ \text{Diagram 384} \\ \text{Diagram 385} \\ \text{Diagram 386} \\ \text{Diagram 387} \\ \text{Diagram 388} \\ \text{Diagram 389} \\ \text{Diagram 390} \\ \text{Diagram 391} \\ \text{Diagram 392} \\ \text{Diagram 393} \\ \text{Diagram 394} \\ \text{Diagram 395} \\ \text{Diagram 396} \\ \text{Diagram 397} \\ \text{Diagram 398} \\ \text{Diagram 399} \\ \text{Diagram 400} \\ \text{Diagram 401} \\ \text{Diagram 402} \\ \text{Diagram 403} \\ \text{Diagram 404} \\ \text{Diagram 405} \\ \text{Diagram 406} \\ \text{Diagram 407} \\ \text{Diagram 408} \\ \text{Diagram 409} \\ \text{Diagram 410} \\ \text{Diagram 411} \\ \text{Diagram 412} \\ \text{Diagram 413} \\ \text{Diagram 414} \\ \text{Diagram 415} \\ \text{Diagram 416} \\ \text{Diagram 417} \\ \text{Diagram 418} \\ \text{Diagram 419} \\ \text{Diagram 420} \\ \text{Diagram 421} \\ \text{Diagram 422} \\ \text{Diagram 423} \\ \text{Diagram 424} \\ \text{Diagram 425} \\ \text{Diagram 426} \\ \text{Diagram 427} \\ \text{Diagram 428} \\ \text{Diagram 429} \\ \text{Diagram 430} \\ \text{Diagram 431} \\ \text{Diagram 432} \\ \text{Diagram 433} \\ \text{Diagram 434} \\ \text{Diagram 435} \\ \text{Diagram 436} \\ \text{Diagram 437} \\ \text{Diagram 438} \\ \text{Diagram 439} \\ \text{Diagram 440} \\ \text{Diagram 441} \\ \text{Diagram 442} \\ \text{Diagram 443} \\ \text{Diagram 444} \\ \text{Diagram 445} \\ \text{Diagram 446} \\ \text{Diagram 447} \\ \text{Diagram 448} \\ \text{Diagram 449} \\ \text{Diagram 450} \\ \text{Diagram 451} \\ \text{Diagram 452} \\ \text{Diagram 453} \\ \text{Diagram 454} \\ \text{Diagram 455} \\ \text{Diagram 456} \\ \text{Diagram 457} \\ \text{Diagram 458} \\ \text{Diagram 459} \\ \text{Diagram 460} \\ \text{Diagram 461} \\ \text{Diagram 462} \\ \text{Diagram 463} \\ \text{Diagram 464} \\ \text{Diagram 465} \\ \text{Diagram 466} \\ \text{Diagram 467} \\ \text{Diagram 468} \\ \text{Diagram 469} \\ \text{Diagram 470} \\ \text{Diagram 471} \\ \text{Diagram 472} \\ \text{Diagram 473} \\ \text{Diagram 474} \\ \text{Diagram 475} \\ \text{Diagram 476} \\ \text{Diagram 477} \\ \text{Diagram 478} \\ \text{Diagram 479} \\ \text{Diagram 480} \\ \text{Diagram 481} \\ \text{Diagram 482} \\ \text{Diagram 483} \\ \text{Diagram 484} \\ \text{Diagram 485} \\ \text{Diagram 486} \\ \text{Diagram 487} \\ \text{Diagram 488} \\ \text{Diagram 489} \\ \text{Diagram 490} \\ \text{Diagram 491} \\ \text{Diagram 492} \\ \text{Diagram 493} \\ \text{Diagram 494} \\ \text{Diagram 495} \\ \text{Diagram 496} \\ \text{Diagram 497} \\ \text{Diagram 498} \\ \text{Diagram 499} \\ \text{Diagram 500} \\ \text{Diagram 501} \\ \text{Diagram 502} \\ \text{Diagram 503} \\ \text{Diagram 504} \\ \text{Diagram 505} \\ \text{Diagram 506} \\ \text{Diagram 507} \\ \text{Diagram 508} \\ \text{Diagram 509} \\ \text{Diagram 510} \\ \text{Diagram 511} \\ \text{Diagram 512} \\ \text{Diagram 513} \\ \text{Diagram 514} \\ \text{Diagram 515} \\ \text{Diagram 516} \\ \text{Diagram 517} \\ \text{Diagram 518} \\ \text{Diagram 519} \\ \text{Diagram 520} \\ \text{Diagram 521} \\ \text{Diagram 522} \\ \text{Diagram 523} \\ \text{Diagram 524} \\ \text{Diagram 525} \\ \text{Diagram 526} \\ \text{Diagram 527} \\ \text{Diagram 528} \\ \text{Diagram 529} \\ \text{Diagram 530} \\ \text{Diagram 531} \\ \text{Diagram 532} \\ \text{Diagram 533} \\ \text{Diagram 534} \\ \text{Diagram 535} \\ \text{Diagram 536} \\ \text{Diagram 537} \\ \text{Diagram 538} \\ \text{Diagram 539} \\ \text{Diagram 540} \\ \text{Diagram 541} \\ \text{Diagram 542} \\ \text{Diagram 543} \\ \text{Diagram 544} \\ \text{Diagram 545} \\ \text{Diagram 546} \\ \text{Diagram 547} \\ \text{Diagram 548} \\ \text{Diagram 549} \\ \text{Diagram 550} \\ \text{Diagram 551} \\ \text{Diagram 552} \\ \text{Diagram 553} \\ \text{Diagram 554} \\ \text{Diagram 555} \\ \text{Diagram 556} \\ \text{Diagram 557} \\ \text{Diagram 558} \\ \text{Diagram 559} \\ \text{Diagram 560} \\ \text{Diagram 561} \\ \text{Diagram 562} \\ \text{Diagram 563} \\ \text{Diagram 564} \\ \text{Diagram 565} \\ \text{Diagram 566} \\ \text{Diagram 567} \\ \text{Diagram 568} \\ \text{Diagram 569} \\ \text{Diagram 570} \\ \text{Diagram 571} \\ \text{Diagram 572} \\ \text{Diagram 573} \\ \text{Diagram 574} \\ \text{Diagram 575} \\ \text{Diagram 576} \\ \text{Diagram 577} \\ \text{Diagram 578} \\ \text{Diagram 579} \\ \text{Diagram 580} \\ \text{Diagram 581} \\ \text{Diagram 582} \\ \text{Diagram 583} \\ \text{Diagram 584} \\ \text{Diagram 585} \\ \text{Diagram 586} \\ \text{Diagram 587} \\ \text{Diagram 588} \\ \text{Diagram 589} \\ \text{Diagram 590} \\ \text{Diagram 591} \\ \text{Diagram 592} \\ \text{Diagram 593} \\ \text{Diagram 594} \\ \text{Diagram 595} \\ \text{Diagram 596} \\ \text{Diagram 597} \\ \text{Diagram 598} \\ \text{Diagram 599} \\ \text{Diagram 600} \\ \text{Diagram 601} \\ \text{Diagram 602} \\ \text{Diagram 603} \\ \text{Diagram 604} \\ \text{Diagram 605} \\ \text{Diagram 606} \\ \text{Diagram 607} \\ \text{Diagram 608} \\ \text{Diagram 609} \\ \text{Diagram 610} \\ \text{Diagram 611} \\ \text{Diagram 612} \\ \text{Diagram 613} \\ \text{Diagram 614} \\ \text{Diagram 615} \\ \text{Diagram 616} \\ \text{Diagram 617} \\ \text{Diagram 618} \\ \text{Diagram 619} \\ \text{Diagram 620} \\ \text{Diagram 621} \\ \text{Diagram 622} \\ \text{Diagram 623} \\ \text{Diagram 624} \\ \text{Diagram 625} \\ \text{Diagram 626} \\ \text{Diagram 627} \\ \text{Diagram 628} \\ \text{Diagram 629} \\ \text{Diagram 630} \\ \text{Diagram 631} \\ \text{Diagram 632} \\ \text{Diagram 633} \\ \text{Diagram 634} \\ \text{Diagram 635} \\ \text{Diagram 636} \\ \text{Diagram 637} \\ \text{Diagram 638} \\ \text{Diagram 639} \\ \text{Diagram 640} \\ \text{Diagram 641} \\ \text{Diagram 642} \\ \text{Diagram 643} \\ \text{Diagram 644} \\ \text{Diagram 645} \\ \text{Diagram 646} \\ \text{Diagram 647} \\ \text{Diagram 648} \\ \text{Diagram 649} \\ \text{Diagram 650} \\ \text{Diagram 651} \\ \text{Diagram 652} \\ \text{Diagram 653} \\ \text{Diagram 654} \\ \text{Diagram 655} \\ \text{Diagram 656} \\ \text{Diagram 657} \\ \text{Diagram 658} \\ \text{Diagram 659} \\ \text{Diagram 660} \\ \text{Diagram 661} \\ \text{Diagram 662} \\ \text{Diagram 663} \\ \text{Diagram 664} \\ \text{Diagram 665} \\ \text{Diagram 666} \\ \text{Diagram 667} \\ \text{Diagram 668} \\ \text{Diagram 669} \\ \text{Diagram 670} \\ \text{Diagram 671} \\ \text{Diagram 672} \\ \text{Diagram 673} \\ \text{Diagram 674} \\ \text{Diagram 675} \\ \text{Diagram 676} \\ \text{Diagram 677} \\ \text{Diagram 678} \\ \text{Diagram 679} \\ \text{Diagram 680} \\ \text{Diagram 681} \\ \text{Diagram 682} \\ \text{Diagram 683} \\ \text{Diagram 684} \\ \text{Diagram 685} \\ \text{Diagram 686} \\ \text{Diagram 687} \\ \text{Diagram 688} \\ \text{Diagram 689} \\ \text{Diagram 690} \\ \text{Diagram 691} \\ \text{Diagram 692} \\ \text{Diagram 693} \\ \text{Diagram 694} \\ \text{Diagram 695} \\ \text{Diagram 696} \\ \text{Diagram 697} \\ \text{Diagram 698} \\ \text{Diagram 699} \\ \text{Diagram 700} \\ \text{Diagram 701} \\ \text{Diagram 702} \\ \text{Diagram 703} \\ \text{Diagram 704} \\ \text{Diagram 705} \\ \text{Diagram 706} \\ \text{Diagram 707} \\ \text{Diagram 708} \\ \text{Diagram 709} \\ \text{Diagram 710} \\ \text{Diagram 711} \\ \text{Diagram 712} \\ \text{Diagram 713} \\ \text{Diagram 714} \\ \text{Diagram 715} \\ \text{Diagram 716} \\ \text{Diagram 717} \\ \text{Diagram 718} \\ \text{Diagram 719} \\ \text{Diagram 720} \\ \text{Diagram 721} \\ \text{Diagram 722} \\ \text{Diagram 723} \\ \text{Diagram 724} \\ \text{Diagram 725} \\ \text{Diagram 726} \\ \text{Diagram 727} \\ \text{Diagram 728} \\ \text{Diagram 729} \\ \text{Diagram 730} \\ \text{Diagram 731} \\ \text{Diagram 732} \\ \text{Diagram 733} \\ \text{Diagram 734} \\ \text{Diagram 735} \\ \text{Diagram 736} \\ \text{Diagram 737} \\ \text{Diagram 738} \\ \text{Diagram 739} \\ \text{Diagram 740} \\ \text{Diagram 741} \\ \text{Diagram 742} \\ \text{Diagram 743} \\ \text{Diagram 744} \\ \text{Diagram 745} \\ \text{Diagram 746} \\ \text{Diagram 747} \\ \text{Diagram 748} \\ \text{Diagram 749} \\ \text{Diagram 750} \\ \text{Diagram 751} \\ \text{Diagram 752} \\ \text{Diagram 753} \\ \text{Diagram 754} \\ \text{Diagram 755} \\ \text{Diagram 756} \\ \text{Diagram 757} \\ \text{Diagram 758} \\ \text{Diagram 759} \\ \text{Diagram 760} \\ \text{Diagram 761} \\ \text{Diagram 762} \\ \text{Diagram 763} \\ \text{Diagram 764} \\ \text{Diagram 765} \\ \text{Diagram 766} \\ \text{Diagram 767} \\ \text{Diagram 768} \\ \text{Diagram 769} \\ \text{Diagram 770} \\ \text{Diagram 771} \\ \text{Diagram 772} \\ \text{Diagram 773} \\ \text{Diagram 774} \\ \text{Diagram 775} \\ \text{Diagram 776} \\ \text{Diagram 777} \\ \text{Diagram 778} \\ \text{Diagram 779} \\ \text{Diagram 780} \\ \text{Diagram 781} \\ \text{Diagram 782} \\ \text{Diagram 783} \\ \text{Diagram 784} \\ \text{Diagram 785} \\ \text{Diagram 786} \\ \text{Diagram 787} \\ \text{Diagram 788} \\ \text{Diagram 789} \\ \text{Diagram 790} \\ \text{Diagram 791} \\ \text{Diagram 792} \\ \text{Diagram 793} \\ \text{Diagram 794} \\ \text{Diagram 795} \\ \text{Diagram 796} \\ \text{Diagram 797} \\ \text{Diagram 798} \\ \text{Diagram 799} \\ \text{Diagram 800} \\ \text{Diagram 801} \\ \text{Diagram 802} \\ \text{Diagram 803} \\ \text{Diagram 804} \\ \text{Diagram 805} \\ \text{Diagram 806} \\ \text{Diagram 807} \\ \text{Diagram 808} \\ \text{Diagram 809} \\ \text{Diagram 810} \\ \text{Diagram 811} \\ \text{Diagram 812} \\ \text{Diagram 813} \\ \text{Diagram 814} \\ \text{Diagram 815} \\ \text{Diagram 816} \\ \text{Diagram 817} \\ \text{Diagram 818} \\ \text{Diagram 819} \\ \text{Diagram 820} \\ \text{Diagram 821} \\ \text{Diagram 822} \\ \text{Diagram 823} \\ \text{Diagram 824} \\ \text{Diagram 825} \\ \text{Diagram 826} \\ \text{Diagram 827} \\ \text{Diagram 828} \\ \text{Diagram 829} \\ \text{Diagram 830} \\ \text{Diagram 831} \\ \text{Diagram 832} \\ \text{Diagram 833} \\ \text{Diagram 834} \\ \text{Diagram 835} \\ \text{Diagram 836} \\ \text{Diagram 837} \\ \text{Diagram 838} \\ \text{Diagram 839} \\ \text{Diagram 840} \\ \text{Diagram 841} \\ \text{Diagram 842} \\ \text{Diagram 843} \\ \text{Diagram 844} \\ \text{Diagram 845} \\ \text{Diagram 846} \\ \text{Diagram 847} \\ \text{Diagram 848} \\ \text{Diagram 849} \\ \text{Diagram 850} \\ \text{Diagram 851} \\ \text{Diagram 852} \\ \text{Diagram 853} \\ \text{Diagram 854} \\ \text{Diagram 855} \\ \text{Diagram 856} \\ \text{Diagram 857} \\ \text{Diagram 858} \\ \text{Diagram 859} \\ \text{Diagram 860} \\ \text{Diagram 861} \\ \text{Diagram 862} \\ \text{Diagram 863} \\ \text{Diagram 864} \\ \text{Diagram 865} \\ \text{Diagram 866} \\ \text{Diagram 867} \\ \text{Diagram 868} \\ \text{Diagram 869} \\ \text{Diagram 870} \\ \text{Diagram 871} \\ \text{Diagram 872} \\ \text{Diagram 873} \\ \text{Diagram 874} \\ \text{Diagram 875} \\ \text{Diagram 876} \\ \text{Diagram 877} \\ \text{Diagram 878} \\ \text{Diagram 879} \\ \text{Diagram 880} \\ \text{Diagram 881} \\ \text{Diagram 882} \\ \text{Diagram 883} \\ \text{Diagram 884} \\ \text{Diagram 885} \\ \text{Diagram 886} \\ \text{Diagram 887} \\ \text{Diagram 888} \\ \text{Diagram 889} \\ \text{Diagram 890} \\ \text{Diagram 891} \\ \text{Diagram 892} \\ \text{Diagram 893} \\ \text{Diagram 894} \\ \text{Diagram 895} \\ \text{Diagram 896} \\ \text{Diagram 897} \\ \text{Diagram 898} \\ \text{Diagram 899} \\ \text{Diagram 900} \\ \text{Diagram 901} \\ \text{Diagram 902} \\ \text{Diagram 903} \\ \text{Diagram 904} \\ \text{Diagram 905} \\ \text{Diagram 906} \\ \text{Diagram 907} \\ \text{Diagram 908} \\ \text{Diagram 909} \\ \text{Diagram 910} \\ \text{Diagram 911} \\ \text{Diagram 912} \\ \text{Diagram 913} \\ \text{Diagram 914} \\ \text{Diagram 915} \\ \text{Diagram 916} \\ \text{Diagram 917} \\ \text{Diagram 918} \\ \text{Diagram 919} \\ \text{Diagram 920} \\ \text{Diagram 921} \\ \text{Diagram 922} \\ \text{Diagram 923} \\ \text{Diagram 924} \\ \text{Diagram 925} \\ \text{Diagram 926} \\ \text{Diagram 927} \\ \text{Diagram 928} \\ \text{Diagram 929} \\ \text{Diagram 930} \\ \text{Diagram 931} \\ \text{Diagram 932} \\ \text{Diagram 933} \\ \text{Diagram 934} \\ \text{Diagram 935} \\ \text{Diagram 936} \\ \text{Diagram 937} \\ \text{Diagram 938} \\ \text{Diagram 939} \\ \text{Diagram 940} \\ \text{Diagram 941} \\ \text{Diagram 942} \\ \text{Diagram 943} \\ \text{Diagram 944} \\ \text{Diagram 945} \\ \text{Diagram 946} \\ \text{Diagram 947} \\ \text{Diagram 948} \\ \text{Diagram 949} \\ \text{Diagram 950} \\ \text{Diagram 951} \\ \text{Diagram 952} \\ \text{Diagram 953} \\ \text{Diagram 954} \\ \text{Diagram 955} \\ \text{Diagram 956} \\ \text{Diagram 957} \\ \text{Diagram 958} \\ \text{Diagram 959} \\ \text{Diagram 960} \\ \text{Diagram 961} \\ \text{Diagram 962} \\ \text{Diagram 963} \\ \text{Diagram 964} \\ \text{Diagram 965} \\ \text{Diagram 966} \\ \text{Diagram 967} \\ \text{Diagram 968} \\ \text{Diagram 969} \\ \text{Diagram 970} \\ \text{Diagram 971} \\ \text{Diagram 972} \\ \text{Diagram 973} \\ \text{Diagram 974} \\ \text{Diagram 975} \\ \text{Diagram 976} \\ \text{Diagram 977} \\ \text{Diagram 978} \\ \text{Diagram 979} \\ \text{Diagram 980} \\ \text{Diagram 981} \\ \text{Diagram 982} \\ \text{Diagram 983} \\ \text{Diagram 984} \\ \text{Diagram 985} \\ \text{Diagram 986} \\ \text{Diagram 987} \\ \text{Diagram 988} \\ \text{Diagram 989} \\ \text{Diagram 990} \\ \text{Diagram 991} \\ \text{Diagram 992} \\ \text{Diagram 993} \\ \text{Diagram 994} \\ \text{Diagram 995} \\ \text{Diagram 996} \\ \text{Diagram 997} \\ \text{Diagram 998} \\ \text{Diagram 999} \\ \text{Diagram 1000} \end{array} + \dots$$

FIG. 19. The simplest time-ordered  $1p1h \otimes 2\text{phonon}$ , or  $2q \otimes 2\text{phonon}$  (two quasiparticles coupled to two phonons), diagrams taken into account in the dynamical kernel. The ellipsis stands for multiple PVC exchange and self-energy contributions as well as for the correlated particle-hole configurations in the internal particle-hole propagators.

has not been explored yet.

PVC studies of the  $ph$ -response in nuclear systems are dominated so far by those based on effective interactions. While in the older works the phonon characteristics were extracted from experimental data, in the last couple of decades the trend has been shifted to fully self-consistent calculations [132–140]. The density functional theory (DFT) allows for calculations of the phonon vertices and energies within the self-consistent RPA, that does not imply any non-linearity as it is confined by the static kernel defined by effective interactions. The advantage of this approach is that, although it is quite simple, the phonon characteristics come out reasonably close to the realistic ones, at least for the most important low-energy phonons. The phonons computed in this way are then used to calculate the dynamical kernels with the subsequent solution of the Dyson-BSE for the full response function. Strictly speaking, this response function with all its components from various channels should be recycled in the dynamical kernel until convergence is achieved. This procedure generates higher-order configurations as it is illustrated in Fig. 18 for the case of  $n = 3$ , where  $n$  stands for the total number of both correlated and non-correlated  $ph$ -pairs of fermions. The latter approach to the dynamical kernel was first proposed in [141] and implemented numerically in Ref. [106]. The higher-order correlations generated in this way were found to

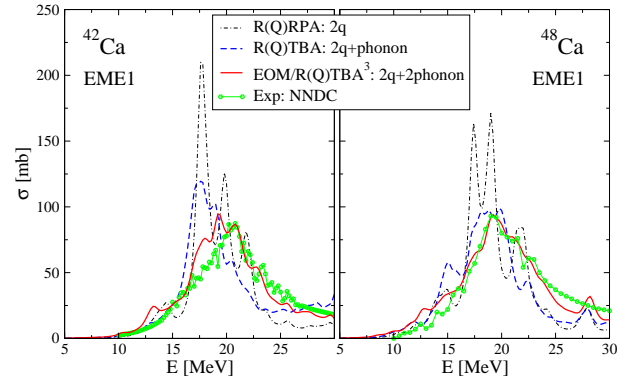


FIG. 20. Giant dipole resonance in  $^{42,48}\text{Ca}$  nuclei calculated within R(Q)RPA, R(Q)TBA and EOM/R(Q)TBA<sup>3</sup>, in comparison to experimental data of Ref. [142]. See text and Ref. [106] for details.

be necessary for nuclear structure calculations, if a certain level of accuracy is required. For instance, astrophysical applications to  $r$ -process nucleosynthesis and to core-collapse supernova require extraction of the radiative neutron capture, beta decay and electron capture rates from the calculated spectra of excitations. These rates are extracted mostly from the low-energy fractions of the dipole, Gamow-Teller and spin-dipole strength distributions, which are very sensitive to the higher-order correlations. It turned out that taking into account only (correlated)  $2p$ - $2h$  configurations, one can not always reproduce the observed spectra of excitations with the required accuracy. Although the results are greatly improved as compared to the RPA calculations and while the gross features of the giant resonances and soft modes can be approximately described by the approaches like  $1p1h \otimes \text{phonon}$  or  $\text{phonon} \otimes \text{phonon}$ , these approaches call for further upgrades in terms of higher-order correlations.

The last major upgrades made recently in Ref. [106] and Ref. [127] included explicitly the  $1p1h \otimes 2\text{phonon}$  configurations. More precisely, Ref. [106] included the  $2q \otimes 2\text{phonon}$  (two quasiparticles coupled to two phonons) configurations, where 'q' stands for 'quasiparticle' in the Bogoliubov's sense, while Ref. [127] analyzed the complex ground state correlations caused by the time-reversed PVC loops (GSC-PVC). The former allowed for significant improvements of the description of the nuclear dipole response in both high and low-energy sectors, while the latter demonstrated how the GSC-PVC's bring the Gamow-Teller strength distribution to a considerably better agreement with data for both proton-neutron and neutron-proton branches.

As an illustration, we display in Fig. 20 the results of the calculations performed in Ref. [106] for the nuclear dipole response with the dynamical kernels of increasing complexity. The dipole response is given in the form of the full photoabsorption cross section for the three approaches: the relativistic (quasiparticle) random

phase approximation (R(Q)RPA), the relativistic (quasi-particle) time blocking approximation (R(Q)TBA) with  $2q \otimes \text{phonon}$  configurations and the upgraded R(Q)TBA, where the  $2q \otimes 2\text{phonon}$  configurations were included (EOM/R(Q)TBA<sup>3</sup>). It turned out that even the use of a fairly large model space of the  $2q \otimes \text{phonon}$  configurations underestimates the experimental value of the width of the giant dipole resonance (GDR). Another problem can be identified on the high-energy shoulder of the GDR above its centroid, where the cross section is systematically underestimated. A similar situation was reported in Ref. [136], which revealed a systematic downshift of the non-relativistic QTBA strength distributions, with respect to the RPA ones, in the calculations with various Skyrme forces. In the EOM/RQTBA<sup>3</sup> calculations with more complex  $2q \otimes 2\text{phonon}$  configurations we see that adding these configurations can resolve those problems. Indeed, Fig. 20 shows that these higher-complexity configurations present in the EOM/RQTBA<sup>3</sup> approach induce a stronger fragmentation of the GDR and reinforce spreading toward both higher and lower energies. A visible shift of the main peak toward higher energies can be associated with the appearance of the new higher-energy complex configurations, which are responsible for higher-energy poles in the resulting response functions. In this way, the energy balance of the overall strength distribution is rearranged, however, with the conservation of the energy-weighted sum rule. The low-energy tail of the GDR was also studied in detail in Ref. [106], which showed that the new correlations bring some important improvements to the description of experimental data also in the low-energy sector.

As already mentioned, in the PVC studies discussed above the static part of the interaction kernel is expressed by phenomenological effective interactions. They are adjusted to nuclear masses and radii on the Hartree or Hartree-Fock level, which means that the effects from dynamical kernels are implicitly included in the parameters of these interactions. The latter indicates that adding the dynamical kernel to the EOM's should be supplemented by a proper subtraction of the double-counting effects. This procedure was developed and discussed in detail in Ref. [143], and since then it is systematically applied in the PVC approaches based on the effective interactions. The fully microscopic approach based on one of the bare nucleon-nucleon interactions remains a task for the future.

More on beyond mean-field and RPA approaches will be discussed below in Sects. VII and VIII. Presently several other groups are also working on multi-configurational extensions of single-particle and RPA states with interesting developments [140, 144–146]. A promising approach on improving on the Pauli principle could be the concept of the generalized optical theorem elaborated in [31, 147]. The whole is a very active field of nuclear physics.

### E. Application of the Green's Function Approach to the pairing model at finite temperature

In order to apply the Green's Function technique for the particle-particle problem at finite temperature to the pairing Hamiltonian (3.1), we define the following set of two-body Matsubara GF's, see Sect. II.D and Sect. III.A for definitions

$$G_{ji}^\tau = -\langle T_\tau \bar{P}_j(\tau) \bar{P}_i^\dagger(0) \rangle, \quad (4.29)$$

where  $T_\tau$  is the time ordering operator for imaginary times [4] and

$$\bar{P}_j = \frac{P_j}{\sqrt{\langle |1 - N_j| \rangle}}. \quad (4.30)$$

By using the static kernel of the Dyson-BSE defined in (4.12) one obtains

$$i\omega_n G_{ji}^{SCRPA} = \delta_{ji} + \sum_k \mathcal{H}_{jk}^{(0)} G_{ki}^{SCRPA}, \quad (4.31)$$

with

$$\begin{aligned} \mathcal{H}_{jk}^{(0)} = & 2\delta_{jk} \left( e_j + \frac{G}{\langle 1 - N_j \rangle} \sum_{j'} \langle P_j^\dagger P_{j'} \rangle \right) \\ & - G \frac{\langle (1 - N_j)(1 - N_k) \rangle}{\sqrt{\langle |1 - N_j| \rangle \langle |1 - N_k| \rangle}}. \end{aligned} \quad (4.32)$$

As remarked in Sect. III A, a good approximation of the two-body correlation function in the above relation is given by the factorisation  $\langle M_i M_j \rangle \simeq \langle M_i \rangle \langle M_j \rangle$ . One then obtains as solution for the particle-particle Green's function

$$\begin{aligned} G_{ji}^{SCRPA} = & \delta_{ji} \frac{1}{z - C_j} \\ & - \frac{G \sqrt{|D_j D_i|}}{(z - C_j)(z - C_i)} \left[ 1 + G \sum_k \frac{D_k}{z - C_k} \right]^{-1}, \end{aligned} \quad (4.33)$$

where

$$\begin{aligned} z = & i\omega_n \\ D_i = & \langle 1 - N_i \rangle \\ C_j = & 2 \left( e_j - G n_j + \frac{G}{D_j} \sum_{j' \neq j} \langle P_j^\dagger P_{j'} \rangle \right). \end{aligned} \quad (4.34)$$

By equating to zero the denominator of (4.33) one obtains the excitation spectrum. Knowing the poles  $E_\mu$  of the GF one obtains its spectral representation with the corresponding residua. They allow us to obtain also the two-body correlation functions [4] in terms of RPA amplitudes for particle (p) and hole (h) states, defined as follows

$$\begin{aligned} X_p^\mu = & \frac{\sqrt{G D_p}}{|C_p| - E_\mu} F_\mu, \quad Y_h^\mu = \frac{\sqrt{-G D_h}}{|C_h| + E_\mu} F_\mu, \\ X_h^\mu = & \frac{\sqrt{-G D_h}}{|C_h| - E_\mu} F_\mu, \quad Y_p^\mu = \frac{\sqrt{G D_p}}{|C_p| + E_\mu} F_\mu, \end{aligned} \quad (4.35)$$

with

$$F_\mu^{-2} = \frac{\partial}{\partial z} \left[ 1 + G \sum_k \frac{D_k}{z - C_k} \right]_{z=E_\mu} . \quad (4.36)$$

In order to close SCRPA equations it is necessary to determine the occupation numbers  $n_k = \langle c_k^\dagger c_k \rangle$ . To achieve this one has to find a single-particle GF,  $G_k^\tau$ , consistent with the SCRPA scheme. The single-particle self-energy  $\Sigma_k$  has the exact representation in terms of the two body T-matrix (see e.g. [22]) and then an appropriate approximation for the  $G_k^\tau$  can be obtained. It consists in using the self-energy  $\tilde{\Sigma}_k$  calculated through the T-matrix found by SCRPA. As the relation between T-matrix and the sum of all irreducible Feynman graphs in the  $pp$  channel is also known, one obtains

$$\tilde{\Sigma}_k = G \sum_{k_1 k_2} G_k^{0(\tau'_1 - \tau_1)} G_{k_1 k_2}^{(\tau'_1 - \tau_1)} \tilde{\mathcal{H}}_{k_2 k}^{(0)} , \quad (4.37)$$

where

$$\begin{aligned} \tilde{\mathcal{H}}_{kk'}^{(0)} &= \mathcal{H}_{kk'}^{(0)} - 2\delta_{kk'} \epsilon_k \\ \epsilon_k &= e_k - G f_k \frac{f_k}{n_k} \frac{D_k}{D_k^0} \end{aligned} \quad (4.38)$$

with  $f_k = \frac{1}{1 + e^{\epsilon_k \beta}}$  being the Fermi-Dirac distribution and  $D_k^0 = 1 - f_k - f_{\bar{k}}$ . The expectation value of the Hamiltonian can be computed by using the two-body GF's and, alternatively, the following relation involving the single-particle Green's function

$$\langle H \rangle = -\frac{1}{2} \lim_{\tau' - \tau \rightarrow 0^+} \sum_k \left( \frac{\partial}{\partial \tau} - e_k \right) \left( G_k^{(\tau - \tau')} + G_{\bar{k}}^{(\tau - \tau')} \right) . \quad (4.39)$$

In order to get the same expressions with both procedures, in Ref. [148] it was shown that one has to expand the single-particle GF to first order in the self-energy (4.37), i.e. in the above relation one has to use (see also discussion below in Sect.V.B)

$$\begin{aligned} G_k &= G_k^0 + G_k^0 \Sigma_k^{SCRPA} G_k^0 \\ \Sigma_k^{SCRPA} &= \frac{\sqrt{D_k}}{D_k^0} \tilde{\Sigma}_k . \end{aligned} \quad (4.40)$$

In principle, this is the same procedure as used by Nozières and Schmitt-Rink [149], only extended to SCp-RPA, see also Sect. V.A.

Finally, one gets a closed expression for the single-particle self-energy  $\Sigma_p^{SCRPA}$  and, therefore, for the occupation numbers by using this GF

$$n_k = \langle c_k^\dagger c_k \rangle = \lim_{\tau \rightarrow 0^-} G_k^\tau . \quad (4.41)$$

In order to check the accuracy of this theory, in Ref. [150]  $\langle H \rangle$  is plotted as a function of particle number  $N$  and temperature  $T$ , and the exact results are compared with the standard thermal RPA (TRPA), thermal mean

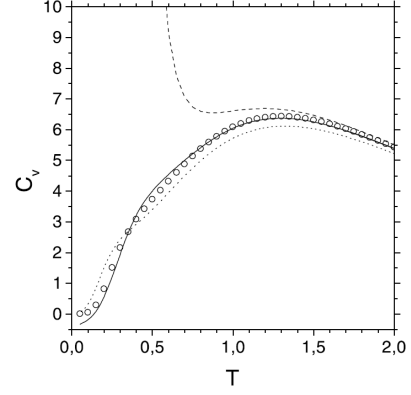


FIG. 21. The heat capacity  $C_v$  as a function of temperature for  $\Omega = N = 10$  and  $G = 0.4$ . The exact results - open circles, the BCS results - dotted line, the TRPA results - dashed line and the TSCRPA results - solid line.

field (TMF) and thermal SCRPA (TSCRPA). One concludes that, when the number of levels  $\Omega$  increases (together with the number of particles  $N$ ), the agreement with the exact solution improves, so that for  $N = \Omega = 10$  the TSCRPA results practically coincide with the exact ones. Concerning the excitation energies, one also obtains a very good agreement between exact and SCRPA versus the coupling constant at zero temperature, at variance with the lowest RPA mode, which collapses when crossing the critical strength from normal to the superfluid phase at  $G_{cr} \approx 0.33$ . A similar behaviour is present for finite temperatures: the TSCRPA reproducing the exact results, while the TRPA values giving qualitatively wrong results.

In order to analyse the behaviour of the system near the critical point, in Fig. 21 [150] we plot the heat capacity

$$C_v = \frac{\partial \langle H \rangle}{\partial T} \quad (4.42)$$

as a function of temperature for  $G = 0.4$ . One sees that TSCRPA values (solid curve) follow the exact results (open circles), while TRPA values are in a total disagreement around the critical temperature. It is remarkable that the TSCRPA results are accurate down to practically zero temperature, in spite of the fact that within the standard BCS theory one enters the superfluid regime. A quasiparticle formulation of SCRPA will only be necessary for stronger  $G$  values driving the system more deeply into the symmetry broken phase.

It is also instructive to consider the spectral function given in [150]. The dependence of this function upon  $\omega$  for different temperatures shows that the distance between the two quasiparticle peaks around Fermi energy ( $\omega = 0$ ) increases by decreasing the temperature. This reminds the *pseudo gap* feature which will be discussed in Sect. V.D. Apparently, it is quite a generic property that



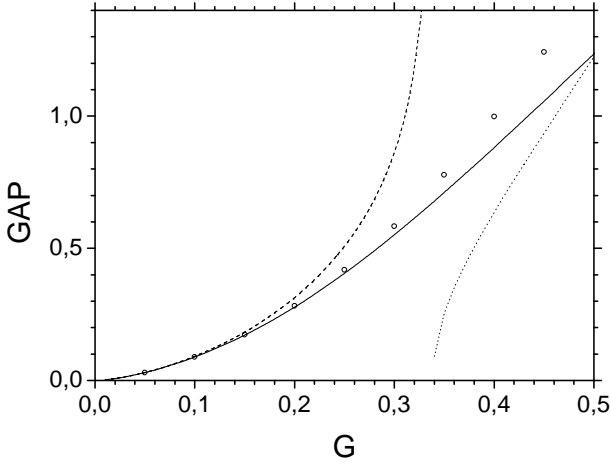


FIG. 22. The effective gap  $\Delta$  as a function of the interaction constant  $G$  for  $\Omega = N = 10$  and  $T = 0$ . Same line and symbol assignments as in Fig. 21 are applied.

pair correlations diminish the density of levels around the Fermi level whereas  $ph$  correlations give rise to an increase. In order to make the temperature dependence

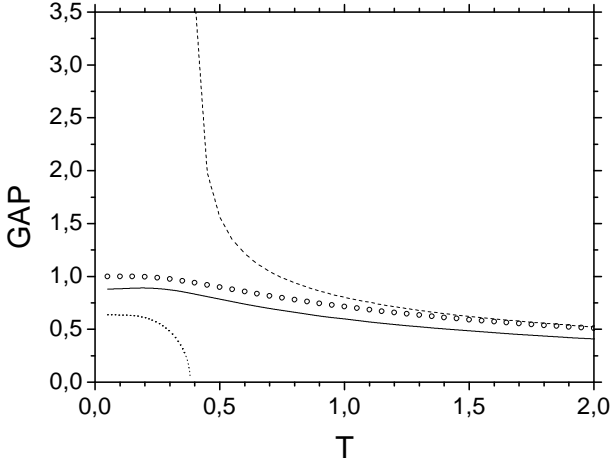


FIG. 23. The effective gap  $\Delta$  as a function of temperature calculated for  $\Omega = N = 10$  and  $G = 0.4$ . Same line and symbol assignments as in Fig. 21 are applied.

of the gap more transparent, it is useful to introduce an effective gap as follows

$$\Delta = G \sqrt{\sum_{ik} \left( \langle P_i^\dagger P_k \rangle - \langle c_i^\dagger c_k \rangle \langle c_i^\dagger c_k^\dagger \rangle \right)}. \quad (4.43)$$

In the BCS approximation the effective gap coincides with the grand canonical BCS gap, i.e.

$$\Delta_0 = G \sum_k \langle P_k \rangle_{BCS}. \quad (4.44)$$

The dependencies of the effective gap on the interaction strength  $G$  at zero temperature and on temperature  $T$  for

$G = 0.4$  are shown in Figs. 22 and 23, respectively [150]. The SCRPA results give a very good description in both cases compared with the exact values. It is clearly seen that the SCRPA and exact calculations do not display the phase transition at the point where BCS gap vanishes. Anyway, we notice in Fig. 22 that SCRPA results deteriorate for values of  $G$  well beyond the critical value. We stress again that in this regime a quasiparticle generalisation of the SCRPA is necessary because one enters deeply into the superfluid region.

In conclusion of this section, we see that SCRPA also works very well at finite temperature. To perform similar studies for other models like the Lipkin and Hubbard models remains a task for the future.

## V. SINGLE-PARTICLE GREEN'S FUNCTION, DYSON EQUATION, AND APPLICATIONS TO THERMODYNAMIC PROPERTIES OF NUCLEAR MATTER

So far we have considered fermion pair problems with SCRPA employing secular equations or Dyson-Bethe-Salpeter equations. Both formulations are equivalent at zero temperature, but the Dyson-BSE has an advantage at finite temperature. However, together with the two-body problems one must also consider the single-particle Green's function and its Dyson equation. At zero temperature we use the chronological Green's function

$$G_{kk'}^{t-t'} = -i \langle T c_k(t) c_{k'}^\dagger(t') \rangle, \quad (5.1)$$

where we used the same notation as for the two-particle GF in Sect. IV. The s.p. Green's function (5.1) obeys the Dyson equation

$$[i\partial_t - e_k] G_{kk'} = \delta_{kk'} \delta(t-t') + \sum_{k_1} \int dt_1 \Sigma_{kk_1}^{t-t_1} G_{k_1 k'}^{t_1-t'}, \quad (5.2)$$

where  $\Sigma$  is the single-particle self-energy and  $e_k$  is a s.p. energy supposedly in an external field. The self-energy can be split into two terms

$$\Sigma_{kk'}^{t-t'} = V_{kk'}^{\text{MF}} \delta(t-t') - i \langle 0 | T j_k(t) j_{k'}^\dagger(t') | 0 \rangle_{\text{irr.}}, \quad (5.3)$$

with

$$j_k = [c_k, V] = \frac{1}{2} \sum_{k_2 k_3 k_4} \bar{v}_{k k_2 k_3 k_4} c_{k_2}^\dagger c_{k_4} c_{k_3}, \quad (5.4)$$

and where the index 'irr.' indicates that the corresponding correlation function should be one-line irreducible.

The time-dependent part of the self-energy contains the following 3-body propagator:

$$G_{k_2 k_3 k_4; k_2' k_3' k_4'}^{t-t'} = -i \langle 0 | T (c_{k_2}^\dagger c_{k_4} c_{k_3} :)_t (c_{k_3'}^\dagger c_{k_4'} c_{k_2'} :)_{t'} | 0 \rangle_{\text{irr.}}, \quad (5.5)$$

where :  $c_{k_2}^\dagger c_{k_4} c_{k_3} := c_{k_2}^\dagger c_{k_4} c_{k_3} - [c_{k_3} \langle 0 | c_{k_2}^\dagger c_{k_4} | 0 \rangle - (k_3 \leftrightarrow k_4)]$ . This is to avoid self-contractions at the same time-level which is to be eliminated. We want to establish an integral equation for this propagator. As usual, we employ the equation of motion and approximate the integral kernel in first approximation by the static part. We obtain (since the following equation will have an irreducible kernel, we will drop the index 'irr.')

$$(i\partial_t - e_{k_3} - e_{k_4} + e_{k_2})G_{k_2 k_3 k_4; k_2' k_3' k_4'}^{t-t'} = N_{k_2 k_3 k_4; k_2' k_3' k_4'} + \sum_{l_2 l_3 l_4, l_2' l_3' l_4'} K_{k_2 k_3 k_4; l_2 l_3 l_4}^0 N_{l_2 l_3 l_4; l_2' l_3' l_4'}^{-1} G_{l_2' l_3' l_4'; k_2' k_3' k_4'}^{t-t'}, \quad (5.6)$$

where

$$N_{k_2 k_3 k_4; k_2' k_3' k_4'} = \langle 0 | \{ \{ c_{k_2}^\dagger c_{k_4} c_{k_3} :, c_{k_3'}^\dagger c_{k_4'} c_{k_2'} : \} | 0 \rangle, \quad (5.7)$$

and

$$K_{k_2 k_3 k_4; k_2' k_3' k_4'}^0 = \langle 0 | \{ \{ c_{k_2}^\dagger c_{k_4} c_{k_3} :, [V, : c_{k_3'}^\dagger c_{k_4'} c_{k_2'} :] \} | 0 \rangle. \quad (5.8)$$

The approach outlined above is the Green's function equivalent to Sect.II.G, see also [60]. A slightly subtle point is that, if we had started the EOM in differentiating with respect to  $t'$  instead of  $t$ , we would not necessarily get the the same integral kernel. Of course, this should not be so. This asymmetry is naturally eliminated by demanding that the time derivative of the two-particle density matrix must vanish at equilibrium. It turns out that this equation is just the difference of the present kernel with its hermitian conjugate form. See for this also the Sect. VII on second RPA equations (7.2). If we want to be consistent with our ground state wave

function (2.12), we have to restrict the indices of  $K^0$  to particles or holes like in Sect. II.D. Evaluating the norm matrix and the interaction kernel in the HF ground state leads to the following eigenvalue equation for the three-fermion transition amplitudes  $\chi^\nu$  [151]

$$(\omega_\nu - \tilde{e}_n - \tilde{e}_m + \tilde{e}_l) \chi_{l, nm}^\nu = (n_l^0 - n_n^0) \bar{v}_{nrlk} \chi_{r, mk}^\nu - (n_l^0 - n_m^0) \bar{v}_{mrlk} \chi_{r, nk}^\nu + \frac{1}{2} (\bar{n}_n^0 \bar{n}_m^0 - n_n^0 n_m^0) \bar{v}_{nmpq} \chi_{l, pq}^\nu, \quad (5.9)$$

where  $\bar{n} = 1 - n$  and repeated indices shall be summed over. The  $n_i^0$  are the mean-field occupancies. They can be replaced by the correlated occupations, similar to the renormalized RPA. However, the use of the HF ground state in this equation is inconsistent, because it does not correspond to a linearized time-dependent equation with the time-dependent HF wave function. This fact leads to some difficulties which have been pointed out in [152]. It is then better to split the equation into two independent TDA equations, one for 2p-1h amplitudes, and one for 2h-1p ones. This is also the case if we want to be consistent with the  $|Z\rangle$  ground state wave function (2.12). In this case we can write the Dyson equation in the following form, see [60]

$$G_{kk'}^\omega = G_k^0 \delta_{kk'} + G_k^0 \sum_{k_1} \Sigma_{kk_1}^\omega G_{k_1 k'}^\omega, \quad (5.10)$$

where

$$G_k^0 = \frac{1 - n_k}{\omega - \tilde{e}_k + i\eta} + \frac{n_k}{\omega - \tilde{e}_k - i\eta} \quad (5.11)$$

is the Green's function which sums up the static mean-field contribution with the occupation numbers  $n_k$  containing in principle ground state correlations. The self-energy is given by

$$\Sigma_{kk'} = \sum_{\rho h h' p_1 p_2 p_1' p_2'} \langle kh | v | p_1 p_2 \rangle \frac{\tilde{V}_{p_1 p_2; h}^\rho \tilde{V}_{p_1' p_2'; h'}^{\rho*}}{\omega - (E_\rho^{N+1} - E_0^N) + i\eta} \langle p_1' p_2' | v | p' k' \rangle + \sum_{\alpha p p' h_1 h_2 h_1' h_2'} \langle kp | v | h_1 h_2 \rangle \frac{\tilde{V}_{h_1 h_2; p}^\alpha \tilde{V}_{h_1' h_2'; p'}^{\alpha*}}{\omega - (E_0^N - E_\alpha^{N-1}) - i\eta} \langle h_1' h_2' | v | p' k' \rangle, \quad (5.12)$$

where  $\tilde{V}^{\alpha, \rho}$  are the correctly normalised 2p-1h and 2h-1p amplitudes and  $\lambda^+ = E_\rho^{N+1} - E_0^N$ ,  $\lambda_- = E_0^N - E_\alpha^{N-1}$  are the eigenvalues obtained from the corresponding equations (2.82). In the case, where we strictly work with the odd-RPA corresponding to the ground state Eq. (2.12), the coupled system of particle and hole propagators in above Dyson equation decouples into two

separate Dyson equations, one for the particles and one for the holes. It may certainly be rewarding to work with an approach which is based on a correlated ground state wave function as in (2.12). Applications of the general formalism to  $^{16}\text{O}$  are given in [60].

In the double commutator of (5.8), each of the two

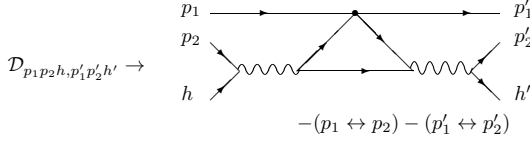


FIG. 24. Schematic view of the PVC interaction vertex which contains itself a selfconsistent PVC process. The full dot stands for the antisymmetrized matrix element and the wiggly line for the vibration. Please note that contrary to the graphical impression, the vertex is instantaneous.

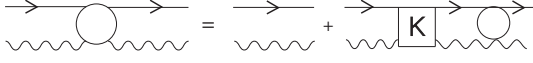


FIG. 25. Representation of the fermion-vibration scattering equation. The kernel is the one of Fig. 24 with all Pauli exchanges included.

triples of  $2p$ - $1h$  fermion operators contracts a particle state to the interaction. Naturally, from each triple then only a  $ph$  pair remains. We can express those  $ph$  pairs via the  $Q^\dagger, Q$  operators of (2.19) using the inverse relation (2.32). Commuting then the destructors to the right, we exploit the annihilating property (2.15) and then  $K^0$  is expressed by (self-consistent) RPA amplitudes  $X, Y$  and occupation numbers. A graphical representation of this PVC vertex is shown in Fig. 24.

On the other hand, the occupation numbers are directly related to the s.p. Green's function (5.11) and then via the dynamical part of the s.p. self-energy which is related to the solution of (5.6), we have a closed system of equations for the SCRPA amplitudes, via the SCRPA equations, and the s.p. occupation probabilities. We want to call this system of equations the even-odd-SCRPA (eo-SCRPA). It has been solved for the Lipkin and 1D Hubbard model with very good success [61].

Of course, the solution of the  $2p - 1h(2h - 1p)$  equations will in general be quite demanding because of the eventually large configuration space. However, presently in nuclear physics quite routinely in the so-called second RPA huge configuration  $2p - 2h$  spaces are considered, so that a  $2p - 1h$  space should be a less difficult problem. We should also point out that the  $2p - 1h$  integral equation (5.6) can be interpreted as a particle-vibration scattering equation with full respect of the Pauli principle. This is schematically shown in Fig. 25. The vibrations (wiggly lines) here are the solutions of the SCRPA equation.

#### A. Relation of the s.p. Green's function to the ground state energy. The tadpole, perturbative particle-vibration coupling, and the spurious mode

The s.p. Green's function has the important property that it is related to the ground state energy  $E_0$  of the system in the following way [4, 5]

$$-\frac{i}{2} \lim_{t' \rightarrow t} \text{Tr}[i\partial_t + \tilde{e}_k] G_{kk}(t - t') = E_0. \quad (5.13)$$

where we supposed that the interaction term of the Hamiltonian does not contain any mean field contribution, since it is already included in  $\tilde{e}_k$ . A useful variant of the relation (5.13) is a formula deduced from the Hellman-Feynman theorem, see [4]

$$E_0 - E_0^{\text{HF}} = -\frac{i}{2} \int_0^1 \frac{d\lambda}{\lambda} \lim_{t' \rightarrow t} \text{Tr}[i\partial - \tilde{e}_k] G_{kk}^\lambda(t - t') \quad (5.14)$$

where the  $\lambda$  dependence of  $G^\lambda$  stems from multiplying the matrix element  $\bar{v}_{k_1 k_2 k_3 k_4}$  in the Hamiltonian with the factor  $\lambda$ . We have seen in Sect. II.A that SCRPA also gives an expression for  $E_0$ . Then, there exists an important consistency property: the ground state energy which one obtains from SCRPA and from the s.p. Green's function should be the same. This entails, for instance, that one should find an expression of the self-energy which is conform with this property. However, since, as we have seen, SCRPA corresponds to a linear boson theory, we must expect that the self-energy also must be linear in this boson and additionally that the self-energy in the solution of the Dyson equation also should only be kept to linear order. We will elaborate on this now.

As just mentioned, keeping with a theory which is linear in the  $ph$ -correlations, we only should consider the self-energy to linear order. We will then see that this leads to the RPA correlation energy in (5.13) and, thus, the above demanded consistency in the two ways to calculate the ground state energy will be fulfilled.

Therefore, we postulate the following form of the s.p. Green's function, where for simplicity we suppose that the Green's function is diagonal

$$G_k = G_k^{(0)} + G_k^{(0)} \Sigma_k^{\text{PVC}} G_k^{(0)}, \quad (5.15)$$

with

$$\Sigma_k^{\text{PVC}} = - \sum_l G_l^{(0)}(t'_1 - t_1) \langle 0 | T \hat{F}_{kl}(t'_1) \hat{F}_{lk}^\dagger(t_1) | 0 \rangle, \quad (5.16)$$

and

$$\hat{F}_{kl}(t) = \sum_{nn'} [\mathcal{B}_{kl nn'} B_{nn'}(t) + \mathcal{A}'_{kl nn'} B_{nn'}^\dagger(t)] \quad (5.17)$$

with  $\mathcal{A}'$  being the matrix element in (2.23), where the MF part is missing. The fermion propagators correspond actually to ideal fermions, that is

$$G_k^{(0)}(t - t') = -i[\Theta(t - t') \bar{n}_k^0 - \Theta(t' - t) n_k^0] e^{-i\tilde{e}_k(t - t')}, \quad (5.18)$$

where the occupation numbers  $n_k^0$  ( $\bar{n}_k^0 = 1 - n_k^0$ ) are step functions serving only to distinguish states from below

and above the Fermi level. The fact that those fermion propagators are ideal ones can already be seen in considering the SCRPA equations (2.23). Let us take the equation for  $Y$ . Then, schematically,

$$Y_{mi}^\nu = -\frac{1}{\Omega_\nu + \tilde{e}_{mi}} F_{mi}^\nu, \quad (5.19)$$

with  $\tilde{e}_{mi} = \tilde{e}_m - \tilde{e}_i$ . We see that the ph-propagator is the Fourier transform of the product

$$G_m^{(0)}(t-t') G_i^{(0)}(t'-t). \quad (5.20)$$

The vertex function is obtained as

$$\begin{aligned} F_{mi}^\nu &= [BX^\nu + A'Y^\nu]_{mi} = \langle 0 | \hat{F}_{mi}(0) | \nu \rangle \\ &= \langle 0 | [\hat{F}_{mi}(0), \mathcal{O}_\nu^\dagger] | 0 \rangle, \end{aligned} \quad (5.21)$$

where we used the inversion (2.47), that is,  $B_{mi}(t) = \sum_\nu [X_{mi}^\nu \mathcal{O}_\nu(t) + Y_{mi}^\nu \mathcal{O}_\nu^\dagger(t)]$  with  $\mathcal{O}(t) = \mathcal{O}(0)e^{-i\Omega_\nu t}$  and the annihilating condition  $\mathcal{O}_\nu|0\rangle = 0$ .

The upper index PVC on the self-energy in Eq. (5.16) shall indicate that this approximation corresponds to (a lowest order) particle-vibration coupling scheme. We then obtain for the correlated parts of the occupation numbers

$$\begin{aligned} -i \lim_{t' \rightarrow t} G_p(t-t') &= \delta n_p = \sum_{k' < p} |Y_{pk'}^\nu|^2 \\ i \lim_{t \rightarrow t'} G_h(t-t') &= \delta n_h = \sum_{k > h} |Y_{kh}^\nu|^2, \end{aligned} \quad (5.22)$$

as well as the following relation for the correlated part of the ground state energy

$$\begin{aligned} E_{corr} &= -\sum_h \tilde{e}_h - \frac{i}{2} \lim_{t' \rightarrow t} \sum_k [i\partial_t + \tilde{e}_k] G_k(t-t') \\ &= -\frac{i}{2} \lim_{t' \rightarrow t} \sum_k [(i\partial_t - \tilde{e}_k) G_k(t-t') + 2\tilde{e}_k G_k(t-t')] \\ &= -\sum_{\nu, k > k'} \Omega_\nu |Y_{kk'}^\nu|^2, \end{aligned} \quad (5.23)$$

which is the same as obtained from SCRPA. The inverse of the free s.p. GF is  $i\partial_t - \tilde{e}_k = G_k^{0-1}$ . Using Eq. (5.15) for  $G_k$  and since

$$-\frac{i}{2} \lim_{t' \rightarrow t} G_k^{0-1} G_k = \sum_{l\nu} \frac{|F_{kl}^\nu|^2}{\Omega_\nu + \tilde{e}_k - \tilde{e}_l}, \quad (5.24)$$

we obtain with Eq.(5.19) the result (5.23) for the correlation energy.

So, since we have from the s.p. Green's function the same ground state energy as obtained from SCRPA in

Sect. II.A, we conclude that the form (5.15) with (5.16) of  $G_{kk'}$  is also consistent with the occupation numbers (5.22). We also realise that the Luttinger theorem, that is  $\sum_h n_h + \sum_p n_p = N$ , is fulfilled.

It is worth mentioning that the boson-fermion scheme just outlined can also be derived from the following boson-fermion coupling Hamiltonian

$$H_{B-F} = \sum_k \tilde{e}_k a_k^\dagger a_k + H_B + \sum_{kk'} (\hat{F}_{kk'} a_k^\dagger a_{k'} + h.c.), \quad (5.25)$$

where  $H_B$  is given in (2.46).

We now can also read off a more explicit form of the self-energy given in frequency space

$$\begin{aligned} \Sigma_k^{\text{PVC}}(\omega) &= \sum_{k'\nu} |F_{kk'}^\nu|^2 \\ &\times \left[ \frac{\bar{n}_{k'}^0}{\omega - \tilde{e}_{k'} - \Omega_\nu + i\eta} + \frac{n_{k'}^0}{\omega - \tilde{e}_{k'} + \Omega_\nu - i\eta} \right] \end{aligned} \quad (5.26)$$

Though it will not be consistent, it may be tempting to use the above expression (5.16) with (5.26) of the self-energy in the full solution of the Dyson equation. We then not only have to consider the self-energy, but also the correction to the HF s.p. energies coming from the correlated part of the occupation numbers

$$\begin{aligned} \delta \tilde{e}_q &= \sum_p v_{qpqp}^{eff} \delta n_p - \sum_h v_{qhqh}^{eff} \delta n_h \\ &= \sum_{kk'} v_{qkqk}^{eff} (n_{k'}^0 - n_k^0) \sum_\nu |Y_{kk'}^\nu|^2, \end{aligned} \quad (5.27)$$

where the effective force is, e.g., obtained from a second variation with respect to the density of a density functional of the Skyrme or Gogny type. In addition, we supposed that the correction to the occupation numbers also stays diagonal. The above correction to the mean-field potential is known as the so-called Tad-pole [128, 153, 154]. It is an important contribution to the PVC scheme because it weakens the contribution of the energy-dependent part  $\Sigma^{\text{PVC}}$ . It is for instance crucial for the 'spurious' translational mode at zero energy, which has diverging amplitudes  $X, Y$ . As a matter of fact the tad-pole and PVC contributions exactly cancel. Let us dwell on this important aspect a little more. We shall work in the canonical basis.

*The spurious mode.* For the translational mode, we have  $Y_{kk'} = -C \langle k' | \hat{p} | k \rangle$  where  $C$  is the diverging normalization constant [5]. Then

$$\delta \tilde{e}_q = \sum_{kk'} v_{qkqk}^{eff} (n_{k'}^0 - n_k^0) \langle k | \hat{p} | k' \rangle \langle k' | \hat{p} | k \rangle C^2, \quad (5.28)$$

with  $\langle k|\hat{\rho}|k'\rangle = \delta_{kk'}n_k^0$ , further

$$\begin{aligned}\delta\tilde{e}_q &= \sum_{kk'} v_{qkqk}^{eff} \langle k|[\hat{p}, \hat{\rho}]|k'\rangle \langle k'|\hat{p}|k\rangle C^2 \\ \delta\tilde{e}_q &= \sum_k v_{qkqk}^{eff} \langle k|[\hat{p}, \hat{\rho}]\hat{p}|k\rangle C^2 .\end{aligned}\quad (5.29)$$

For simplicity but without loss of generality, we discard the exchange term and suppose a translational-invariant finite-range force. Then

$$\delta\tilde{e}_q = N^2 \int d^3r \phi_q^*(r) \phi_{q'}(r) \int d^3r_1 v^{eff}(\mathbf{r} - \mathbf{r}_1) \langle \mathbf{r}_1 | [\hat{p}, \hat{\rho}] \hat{p} | \mathbf{r}_1 \rangle , \quad (5.30)$$

$$\delta\tilde{e}_q = N^2 \int d^3r \phi_q^*(r) \phi_{q'}(r) \int d^3r_1 v^{eff}(\mathbf{r} - \mathbf{r}_1) \frac{\partial \rho(\mathbf{r}_1)}{\partial \mathbf{r}_1} \frac{\partial}{\partial \mathbf{r}_1} . \quad (5.31)$$

With a simple mean field  $U(\mathbf{r})$ , we have  $v(\mathbf{r} - \mathbf{r}_1) = \frac{\delta U(\mathbf{r})}{\delta \rho(\mathbf{r}_1)}$  and, thus, with a partial integration, we get

$$\delta\tilde{e}_q = -C^2 \langle q | \Delta U | q \rangle . \quad (5.32)$$

From Baldo et al. [128], we know that part of the dynamic self energy has the same expression with opposite sign. So, the diverging term cancels as can be seen from the following.

From (5.26) we have (as long as there is no resonance)

$$\Sigma_k^{\text{PVC}}(\omega) = \sum_{k'\nu} |F_{kk'}^\nu|^2 \frac{\omega - \tilde{e}_{k'} + (1 - 2n_{k'}^0)\Omega_\nu}{(\omega - \tilde{e}_{k'})^2 - \Omega_\nu^2} . \quad (5.33)$$

Let us now consider the spurious translational mode with  $\Omega_0 = 0$ . Then

$$\begin{aligned}\Sigma_q^{\text{PVC}}(\omega = \tilde{e}_q) &= \sum_{k'\nu=0} \frac{|F_{qk'}^0|^2}{\tilde{e}_q - \tilde{e}_{k'}} \\ &+ \lim_{\Omega_0 \rightarrow 0} \sum_{k'\nu} |F_{kk'}^0|^2 \frac{(1 - 2n_{k'}^0)\Omega_0}{(\tilde{e}_q - \tilde{e}_{k'})^2} \\ &= \sum_{k'\nu=0} \frac{|F_{qk'}^0|^2}{\tilde{e}_q - \tilde{e}_{k'}} + \sum_{k'} \frac{|\langle k' | \hat{p} | q \rangle|^2}{2Am} (\bar{n}_{k'}^0 - n_{k'}^0) ,\end{aligned}\quad (5.34)$$

where  $A$  is the total nucleon number and we again used (5.19) to simplify the second term. It is the recoil term which is finite, since  $C^2 = \frac{1}{2Am\Omega_0}$ . It is positive for particles and negative for holes. The first part cancels (5.32) and this has to be explained a little. The vertex (5.21) can be written for the spurious mode where  $X_{kq} = C \langle k | \hat{p} | q \rangle$  and  $Y_{kq} = -C \langle q | \hat{p} | k \rangle$  as the commutator of the effective force with the momentum operator, as

long as we consider the  $\mathcal{A}'$  and  $\mathcal{B}$  matrices based on this effective force, which we already have introduced above (the inverse way seems more difficult). Introducing the force as originating from the variational derivative with respect to the density of the mean field potential  $U(r)$  leads then to the expression (see also [128, 153, 154]):

$$\begin{aligned}F_{kq} &= -\langle k | \nabla U | q \rangle = -\langle k | [U, \nabla] | q \rangle \\ &= -\langle k | [H_0, \nabla] | q \rangle = (\tilde{e}_k - \tilde{e}_q) \langle k | \nabla | q \rangle .\end{aligned}\quad (5.35)$$

With this and the second vertex function we obtain that

$$\sum_{k'\nu=0} \frac{|F_{qk'}^0|^2}{\tilde{e}_q - \tilde{e}_{k'}} = C^2 \langle q | \Delta U | q \rangle , \quad (5.36)$$

that is the opposite of expression (5.32).

This shows that the PVC self-energy, which is by itself diverging, stays together with the tadpole finite. It was not clear since long what to do with the spurious mode in the optical potential for elastic nucleon-nucleus scattering, strongly related to the self-energy, because of its divergency. Most of the time it just was not considered despite it is a member of the complete set of states. We now see that this prescription is almost correct. Only the recoil term is missed. It is positive for particle states and negative for hole states. Nevertheless, we should remember that our self-energy used in the full Dyson equation is not completely consistent and, e.g., the Luttinger theorem is violated. Only in SCRPA (r-RPA) scheme this deficiency is overcome. It would be interesting to repeat this derivation in the case of collective rotation.

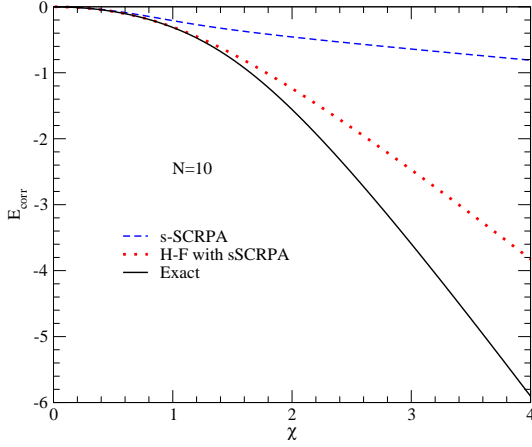


FIG. 26. Demonstration of the positive effect of the coupling constant integration for the correlation energy  $E_{\text{corr}}$ . s-SCRPA, broken line: standard SCRPA; H-F with sSCRPA, dotted line: coupling constant integration; full line: exact result.

### B. An application to the Lipkin model of the coupling constant integration with SCRPA

The Lipkin model will be introduced in Sect.V.D just below. The SCRPA is trivially applied, with good success [21]. It is interesting to apply the coupling constant integration of (5.14) to this case. The general formula can be deduced from (5.23)

$$E_{\text{corr}} = - \sum_{ph,\nu} \int_0^1 \frac{d\lambda}{\lambda} |Y_{ph}^\nu|^2 [\Omega_\nu(\lambda) + \tilde{e}_p - \tilde{e}_h] \quad (5.37)$$

It is immediately verified that if in this formula the standard RPA expressions are used, this leads back to the usual, see [5]. On the contrary, if we use the SCRPA approach, this can lead to substantial improvements. This is shown for the Lipkin model in Fig. 26. One, indeed sees a quite strong improvement over the SCRPA result via the  $\lambda$  integration.

This method is also applied in theoretical chemistry, see, e.g., [36, 155],

### C. Inclusion of particle-particle RPA correlations into the self-energy. The $T$ -matrix approximation

We just have treated the self-energy including  $ph$ -RPA correlations. Of course, there exists also the analogous situation for  $pp$ -RPA correlations. This will lead to the so-called  $T$ -matrix approximation of the self-energy which has been elaborated in a work by Nozières-Schmitt-Rink [149]. We write for the s.p. Green's function

$$G_{kk'} = G_{kk'}^{(0)} + \sum_{k_1} G_{kk_1}^{(0)} \Sigma_{k_1 k_1'}^{pp} G_{k_1' k'}^{(0)}, \quad (5.38)$$

with for the self-energy

$$\Sigma_{kk'}^{pp}(\omega) = -i \sum_{k_1} \int \frac{d\omega'}{2\pi} G_{k_1}^{(0)}(\omega') T_{kk_1 k_1' k_1}(\omega + \omega'), \quad (5.39)$$

where we assumed that  $G_{kk'}^{(0)}$  is diagonal and the  $pp$   $T$ -matrix is related to the  $pp$  Green's function (4.1) by

$$T_{k_1 k_2 k_1' k_2'}(\omega) = \frac{1}{4} \sum_{k_3 k_4 k_3' k_4'} \bar{v}_{k_1 k_2 k_3 k_4} G_{k_3 k_4 k_3' k_4'}(\omega) \bar{v}_{k_3' k_4' k_1' k_2'}. \quad (5.40)$$

where the two-particle Green's function is given in (4.1) and we assumed that the uncorrelated Green's function contains the HF potential. All considerations we have outlined above for the  $ph$ -case shall also apply analogously to the  $pp$ -case. Only  $ph$  correlation functions have been exchanged by  $pp$  correlations. This scheme has for instance been applied by Nozières and Schmitt-Rink [149] to treat the famous BCS-BEC (Bose-Einstein condensation) transition. Below we will give some applications of the  $pp$ -case to nuclear matter.

### D. Single-particle Green's function from the CCD wave function. Application to the Lipkin model

In this section we want to elaborate on the odd-particle number SCRPA, see Sect. II.G. Specifically, we want to study how far one can go with the s.p. self-energy (5.12) entirely based on the CCD wave function. In order not to develop the whole general formalism, which would be quite lengthy, we immediately switch to the Lipkin model, however. It is sufficiently general so that the full many-body formalism with, e.g., a realistic two body force can be deduced. The full formalism will be published in a separate work [156]

#### 1. Calculating with the CCD wave function as a quantum vacuum. Application to the Lipkin model

The standard two-level Lipkin model, see, e.g., [5], can be seen as a one site quasi-spin model with the following Hamiltonian (analogous to the 3-level model of Sect. III.B)

$$H = eJ_0 - \frac{V}{2} [J_+ J_+ + J_- J_-], \quad (5.41)$$

where

$$J_+ = \sum_m c_{1m}^\dagger c_{0m}; \quad J_- = [J_+]^\dagger; \quad 2J_0 = n_1 - n_0$$

$$n_i = \sum_m c_{im}^\dagger c_{im}, \quad (5.42)$$

with the following SU(2) commutation relations among the quasi-spin operators

$$[J_-, J_+] = -2J_0 ; \quad [J_0, J_\pm] = \pm J_\pm . \quad (5.43)$$

According to the spin algebra, the model is easily diagonalisable exactly for any spin value where  $\langle \text{HF} | J_0 | \text{HF} \rangle = -N/2$  and  $N$  the particle number or degeneracy of each of the two levels which have a distance of  $e$ . The model is non-trivial and cited, besides in nuclear physics where it was invented [157], in several other fields [158–161]. For instance, the Lipkin model shows in the strong coupling limit a spontaneously (discrete) broken symmetry, what makes it particularly useful for testing new many-body approaches.

In the Lipkin model the CDD wave function writes

$$|Z\rangle = e^{\frac{z}{2}J_+J_-} |\text{HF}\rangle , \quad (5.44)$$

with  $z$  an in principle complex number. This CCD wave function is the vacuum of the following addition ( $\alpha$ ) and retrieval ( $\rho$ ) annihilators, see (2.80)

$$\begin{aligned} q_{1,\alpha} &= \frac{1}{N} u_1^\alpha \sum_m c_{1m} + V_1^\alpha \frac{1}{N} \sum_m J_+ c_{0m} / \sqrt{n_{11}} \\ q_{0,\rho} &= \frac{1}{N} u_0^\rho \sum_m c_{0m}^\dagger + V_0^\rho \frac{1}{N} \sum_m c_{1m}^\dagger J_+ / \sqrt{n_{11}} , \end{aligned} \quad (5.45)$$

with  $n_{11} = -\langle \{J_- c_{1m}, c_{1m}^\dagger J_+\} \rangle = \langle \{c_{0m}^\dagger J_-, J_+ c_{0m}\} \rangle$  a norm factor. This yields the following norm relations  $|u_0^\rho|^2 + |V_0^\rho|^2 = |u_1^\alpha|^2 + |V_1^\alpha|^2 = 1$ . The various amplitudes are related by  $z = \frac{V_0^\rho}{u_0^\rho \sqrt{n_{11}}} = -\frac{V_1^\alpha}{u_1^\alpha \sqrt{n_{11}}}$ .

Applying the EOM leads to the eigenvalue equation outlined in (2.82) equivalent to the Dyson equation of the s.p. Green's function in (5.10, 5.12). The matrix elements of this equation contain three-body correlation functions.

It does not seem to be very easy to work with these operators (5.45), since they do not represent a canonical transformation and, thus, cannot be inverted and the killing property cannot directly be exploited. However, there exists a way around which allows, due to the annihilating condition,  $q|Z\rangle = 0$ , to reduce the order of the correlations [162]. For example, it is clear that the secular problem (2.82) involves, as mentioned, maximally three-body correlation functions. They can be reduced to two-body correlation functions in the following way. For this, we use the annihilating conditions which directly yield

$$\begin{aligned} J_0 |Z\rangle &= [-\frac{N}{2} + 2zJ_+^2] |Z\rangle \\ J_- |Z\rangle &= [2z(N-1)J_+ - 4z^2J_+^3] |Z\rangle . \end{aligned} \quad (5.46)$$

These are the basic two relations relating higher operators to lower ones. We multiply the first equation from left with  $J_+^2$  and the second one with  $J_+$ . This gives two equations containing  $J_+^4$ . Isolating and equalling leads to an equation for  $\langle J_+^2 J_0 \rangle$  in terms of  $\langle J_+^2 \rangle$  and  $\langle J_+ J_- \rangle$ . We multiply first equation with  $J_0$  what helps to find the Casimir relation  $J_+ J_- = \frac{1}{4}N(N+2) - J_0^2 + J_0$ . From where we get

$$\begin{aligned} 2z\langle J_+^2 \rangle &= \frac{N}{2} + \langle J_0 \rangle \\ z\langle J_+^2 J_0 \rangle &= \frac{1}{2}(N-2)z\langle J_+^2 \rangle - \langle J_+ J_- \rangle \\ 2z\langle J_+ J_- J_0 \rangle &= zN(N+2) - \langle J_+^2 \rangle + z(N-6)\langle J_+ J_- \rangle \\ &\quad - 2z(N-4)\langle J_0 \rangle . \end{aligned} \quad (5.47)$$

In the last formula also the Casimir relation has been used. Then all the matrix elements in the equation corresponding to (2.82) for the Lipkin model can be given as a function of  $\langle J_0 \rangle$  and  $\langle J_0^2 \rangle$ .

Usually, it is a very good approximation to take  $\langle J_0^2 \rangle \simeq \langle J_0 \rangle^2$  so that the whole becomes simply a self-consistency relation for  $\langle J_0 \rangle$ . It seems to be also very valid here: for  $N = 4$  the solution becomes exact and for  $N = 6$  the solution is quite good throughout the whole domain of couplings. However, we will take this only for the initialisation of the iterative cycle because there exists a still better procedure. One can demand that the time derivative of the two-body density matrix be zero, that is stationary at equilibrium

$$\begin{aligned} \langle [H, J_- J_-] \rangle &= 2e\langle J_-^2 \rangle - V\langle (2J_0 + 4J_0^2 - 4J_+ J_- J_0) \rangle \\ &= 0 . \end{aligned} \quad (5.48)$$

This gives an extra relation linking  $\langle J_0 \rangle$  with  $\langle J_0^2 \rangle$  so that, together with (5.47) the system of equations obtained from the EOM is closed together with the relation for the occupation numbers obtainable from (2.82) adapted to the Lipkin model

$$\langle J_0 \rangle = \frac{N}{2} \frac{4z^2 n_{11} - 1}{4z^2 n_{11} + 1} . \quad (5.49)$$

The results for different quantities are excellent throughout the whole domain of coupling constants as can be seen in Fig. 27. One can say that this approach solves the Lipkin model for the correlation energy for all values of  $N$  and  $\chi$  with an error not larger than four percent in the transition region and better elsewhere. This is a very satisfying result. It is quite remarkable that one can work with a nonlinear transformation like in (2.80) very efficiently. For the collective states in the even systems one may try to perform a Tamm-Dancoff or RPA approach with the new quasiparticle operators (5.45), but this remains a task for the future.

In Fig. 28 we show the eigenvalues  $\lambda_\pm$  of the odd-RPA matrix. It is seen that they are also reproduced with good quality over the whole range of  $\chi$ -values.

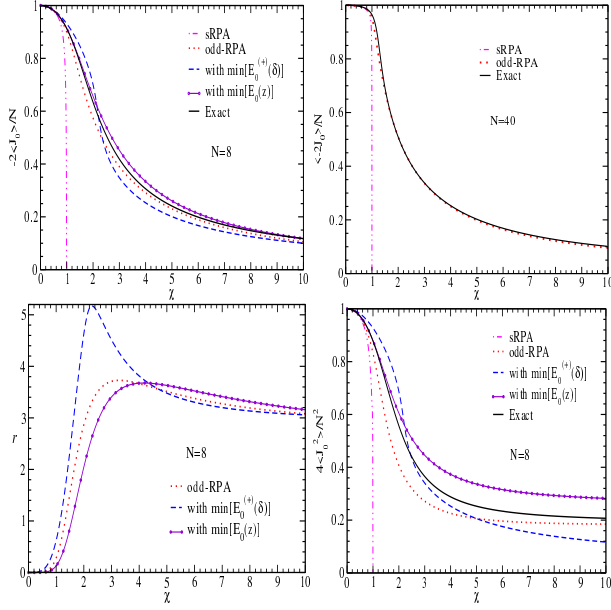


FIG. 27. Upper left panel: the occupation number difference between upper and lower levels,  $\langle -2J_0 \rangle$ , for  $N = 8$  with standard RPA (sRPA) (double dot broken line), present odd-RPA (dotted line), projected HF  $\min[E_0^{(+)}(\delta)]$  (broken line), CCD variational wave function  $\min[E_0(z)]$  (continuous line with dots), and exact solution (full line) as function of the intensity of interaction  $\chi = \frac{V}{e}(N-1)$ . Upper right panel:  $\langle -2J_0 \rangle$ , for  $N = 40$  with sRPA, odd-RPA, and exact solution. Lower left panel: percentage error of the correlation energy as  $r = 100 \times \frac{(E_0^{\text{odd-RPA}} - E_0^{\text{Exact}})}{E_0^{\text{Exact}}}$  (dotted line),  $r = 100 \times \frac{(\min[E_0(z)] - E_0^{\text{Exact}})}{E_0^{\text{Exact}}}$  (continuous line with dots) and  $r = 100 \times \frac{(\min[E_0^{(+)}(\delta)] - E_0^{\text{Exact}})}{E_0^{\text{Exact}}}$  (broken line) as function of the intensity of interaction  $\chi = \frac{V}{e}(N-1)$ . Lower right panel: occupation fluctuation  $\langle 4J_0^2 \rangle$  for  $N = 8$  with same ingredients as upper left panel.

One may wonder from where this high performance in the whole parameter space comes. For this we remark that if one replaces in (5.45) the operator  $J_+$  by its expectation value  $\langle J_+ \rangle$ , the equation for  $q$  just represents a HF transformation to a new symmetry broken s.p. basis. To keep the operator  $J_+$  means that good parity is kept during this transformation. We want to coin it quantum-mean-field (qu-mf) transformation. In spirit it is very similar to symmetry projected mean-field calculation. The results for the Lipkin model with projected HF are also quite close to the present results, see Fig. 27. Also using CCD as a variational wave function yields results rather close to the present odd-RPA method. The method can be seen as a variant to the usual mean field projection techniques [5]. It would be very interesting to apply this technique to the case of rotations.

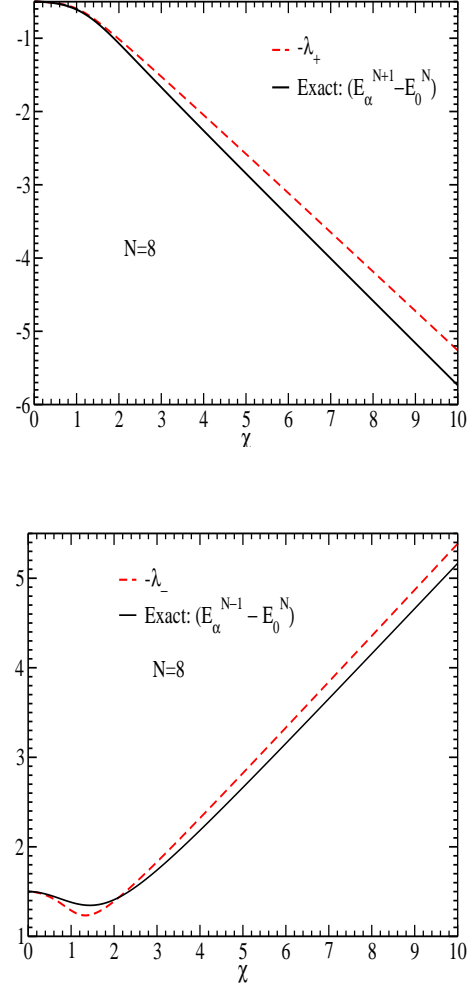


FIG. 28. The eigenvalues  $\lambda_+$  and  $\lambda_-$  of the odd-RPA matrix compared to the exact values as a function of  $\chi$ .

### E. Cluster expansion of the single-particle self-energy and applications to infinite matter problems

In the preceding section we have outlined how to construct a s.p. GF to reproduce the SCRPA correlation energy in the  $ph$  and  $pp$  channels. However, the self-energy contains also higher than two-body correlations. We will, therefore, use the EOM to include three-body and four-body correlations to the self-energy and construct self-energies tailored to treat cluster phenomena in nuclear physics. We are specially interested in four-body correlations, since in nuclear physics, at low densities, besides the triton ( $t$ ,  ${}^3\text{H}$ ) and the helion ( $h$ ,  ${}^3\text{He}$ ), the  $\alpha$  particles play a particularly strong role. This implies that we will have to treat not only more body correlation, but also corresponding cluster bound states.

Within the present section, starting from the s.p. Green's function, we are in addition interested in the equation of state of symmetric nuclear matter expressing the nucleon density  $\rho(T, \mu)$  as a function of tempera-



ture  $T = 1/k_B\beta$  and chemical potential  $\mu$ . Note that for asymmetric nuclear matter different chemical potentials for neutrons ( $\mu_n$ ) and protons ( $\mu_p$ ) have to be introduced. In the Green's functions approach, the density of the system is given by

$$\rho(\beta, \mu) = \sum_{k_1} \int \frac{d\omega}{2\pi} \frac{1}{e^{\beta(\hbar\omega - \mu_1)} + 1} S(k_1, \omega), \quad (5.50)$$

where the *spectral function*  $S(k, \omega)$ , depending upon single-particle coordinate  $k_1 = \{p_1, \sigma_1, \tau_1\}$  describing momentum, spin, and isospin, is defined by [2–4]

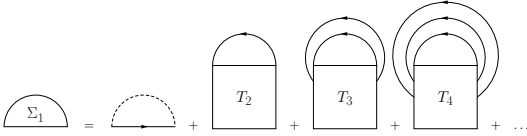
$$S(k_1, \omega) = \frac{1}{i} [G_{k_1}^{\omega_n} |_{i\omega_n \rightarrow \omega - i\eta} - G_{k_1}^{\omega_n} |_{i\omega_n \rightarrow \omega + i\eta}] . \quad (5.51)$$

Starting from the equation of state  $\rho(\beta, \mu)$ , all thermodynamic properties can be calculated after determining the thermodynamic potentials  $f(T, \rho) = \int_0^\rho \mu(\beta, \rho') d\rho'$  or  $p(T, \mu) = \int_{-\infty}^\mu \rho(\beta, \mu') d\mu'$ .

The evaluation of the spectral function or the single-particle Matsubara Green's function, respectively, can be performed with the single-particle self-energy  $\Sigma(k, \omega)$  according to

$$S(k, \omega) = \frac{2\text{Im}\Sigma(k, \omega - i0)}{(\omega - (\hbar k)^2/2m - \text{Re}\Sigma(k, \omega))^2 + (\text{Im}\Sigma(k, \omega - i0))^2} . \quad (5.52)$$

For the self-energy, under certain assumptions, see below, a cluster decomposition [102] is possible,



The  $T_A$  matrices are related to the  $A$ -particle Green functions obtainable from the EOM. They, therefore only depend on one energy

$$T_A(k_1 \dots k_A, k'_1 \dots k'_A, z) = V_A(k_1 \dots k_A, k'_1 \dots k'_A) + V_A(k_1 \dots k_A, k''_1 \dots k''_A) G_A(k''_1 \dots k''_A, k'''_1 \dots k'''_A, z) \times V_A(k'''_1 \dots k'''_A, k'_1 \dots k'_A), \quad (5.53)$$

with the potential  $V_A(k_1 \dots k_A, k'_1 \dots k'_A) = \sum_{i < j} v_{ij, i'j'} \prod_{k \neq i, j} \delta_{k, k'}$ , and subtraction of double counting diagrams when inserting the  $T$  matrices into the self-energy. The solution of the  $A$ -particle propagator in the low-density limit is given by

$$G_A(k_1 \dots k_A, k'_1 \dots k'_A, z) = \sum_{n, P} \frac{\psi_{A, n, P}(k_1 \dots k_A) \psi_{A, n, P}^*(k'_1 \dots k'_A)}{z - E_{A, n, P}}, \quad (5.54)$$

using the eigenvalues  $E_{A, n, P}$  and wave functions  $\psi_{A, n, P}(k_1 \dots k_A)$  of the  $A$ -particle Schrödinger equation,  $P$  denotes the total momentum, and the internal quantum number  $n$  covers bound as well as scattering states.

The evaluation of the equation of state in the low-density limit is straightforward. Considering only the

bound-state contributions, we have the result

$$\rho(\beta, \mu) = \sum_{A, n, P} \frac{1}{e^{\beta(E_{A, n, P} - A\mu)} - (-1)^A}, \quad (5.55)$$

which is an *ideal mixture of components* obeying Fermi or Bose statistics. This equation of state which describes nuclear matter in the low-density limit is denoted as nuclear statistical equilibrium (NSE) and is a standard approach to heavy ion collisions and the astrophysics of compact objects, where the composition of dense nuclear matter and the yields of clusters is of relevance.

In the nondegenerate (classical) limit, the integrals over  $P$  can be carried out for the respective bound states, and one obtains the mass-action law that determines the matter composition at given temperature and total particle density. At low densities, quantum effects become

relevant. The most dramatic is Bose-Einstein condensation (BEC), which occurs for bound states in the channels with even  $A$  when  $E_{A,n,P} - A\mu = 0$ . Usually this happens first for  $P = 0$  and  $n = 0$  (ground state). At low, but fixed temperature, with increasing density BEC occurs first for those clusters with the largest binding energy per particle. If we consider the problem of clustering in nuclear matter, the two-particle (deuteron) binding energy per nucleon is 1.11 MeV, while the four-particle (alpha) binding energy is 7.1 MeV. One, therefore, anticipates that a quantum condensate of  $\alpha$  particles is formed first. At very low temperatures heavier nuclei can be formed with even a higher binding energy per nucleon, so that in the low density regime considered here nuclei of the iron region would form the condensate at low temperatures. However, the formation of iron may be retarded with respect to  $\alpha$  particles because of the much more complex structure of the former. In any case, we will restrict ourselves only to two-nucleon and four-nucleon correlations in the present review article.

An important problem is the modification of the single-particle and bound-state properties at higher nucleon densities, when *medium effects* have to be taken into account [17, 163]. The change of the cluster energies due to self-energy and Pauli-blocking contributions will be investigated in the following subsections. In addition, the inclusion of scattering states [169] would slightly change the composition as well as the equation of state, see also [165].

Concluding, we emphasize that the calculation of the single-particle self-energy, e.g. using the technique of cluster expansion and the EOM, allows to evaluate any thermodynamic property. It should be mentioned that cluster expansions can also be developed for other quantities, such as the polarization function [102], that are of interest in calculating transport properties. Also the hole lines in the cluster expansion of the self-energy can themselves correlate to clusters. For example, the three-hole lines in the four-particle  $T$ -matrix contribution can form a triton or a helion [166]. We will expose  $\alpha$  clustering in nuclear matter in Sect.VI.

We have shown how the formation of correlations, in particular bound states, can be implemented in the equation of state via the cluster decomposition of the single-particle self energy. A well-known approach to nuclear

matter is the Fermi liquid theory of Landau, Migdal and Pomeranchuk considering the linear response function, which is related to the dynamical structure factor. This also allows to derive an equation of state and, in particular, the search for instabilities. The inclusion of correlations was an open problem for a long time but has been considered recently [167], so that the equivalence of both approaches has been shown. The approach to nuclear matter properties via the dynamical structure factor is based on an extension of the RPA including correlations, see [102] and [168], which has been worked out for partially ionized plasmas to investigate the dielectric function. Further considerations of how to incorporate small nuclear clusters into the equation of state of nuclear matter will be discussed in Sect.VI.

## F. Applications of the in-medium two-nucleon problem and the $T$ -matrix approximation for the s.p. self-energy

### 1. Equation of state and critical temperature

With increasing density of nuclear matter, medium modifications of single-particle states as well as of few-nucleon states become of importance. The self-energy of an  $A$ -particle cluster can, in principle, be deduced from contributions describing the single-particle self-energies as well as medium modifications of the interaction and the vertices. A guiding principle in incorporating medium effects is the construction of *consistent* (“conserving”) approximations, which treat medium corrections in the self-energy and in the interaction vertex at the same level of accuracy. This can be achieved in a systematic way using the two-times cluster Green’s functions formalism presented in this article. At the mean-field level, we have only the Hartree-Fock self-energy  $\Gamma^{\text{HF}}(k_1) = \sum_{k_2} \bar{v}_{k_1 k_2, k_1 k_2} f(k_2)$  together with the Pauli blocking factors, which modify the interaction from  $\bar{v}_{k_1 k_2, k'_1 k'_2}$  to  $\bar{v}_{k_1 k_2, k'_1 k'_2} [1 - f(k_1) - f(k_2)]$ . In the case of the in-medium two-nucleon system ( $A = 2$ ), the resulting effective wave equation which includes the mean-field corrections reads

$$[\epsilon_{k_1} + \epsilon_{k_2} - E_{2,n,P}] \psi_{2,n,P}(k_1 k_2) + \sum_{k'_1 k'_2} [1 - f(k_1) - f(k_2)] \bar{v}_{k_1 k_2, k'_1 k'_2} \psi_{2,n,P}(k'_1 k'_2) = 0. \quad (5.56)$$

Here  $\epsilon_{k_1}$  denotes the single-nucleon quasiparticle energy, which in Hartree-Fock approximation reads  $\epsilon_{k_1} = p_1^2/2m + \Gamma^{\text{HF}}(k_1)$ . Both the self-energy and the Pauli blocking have a similar structure, a product of the interaction with the distribution function, and have to be con-

sidered together to find a consistent approximation. Note that correlations in the surrounding nuclear matter are neglected. How those correlations can be considered has been shown in Sect. III.A within SCppRPA applied to the pairing model. Contributions of two-nucleon bound

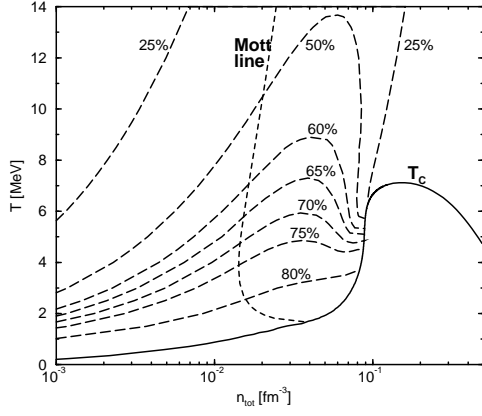


FIG. 29. Phase diagram of symmetric nuclear matter showing lines of equal concentration  $\rho_{\text{corr}}/\rho$  of correlated nucleons, the Mott line, and the critical temperature  $T_c$  of the onset of superfluidity.

states (deuterons) to the effective Hamiltonian are taken into account within the Cluster Mean-Field Approximation [17].

This *effective wave equation* (5.56) is of great interest. It describes not only bound states, but as well scattering states in nuclear matter at arbitrary density, in particular, the merging of a bound state with the continuum of scattering states due to Pauli blocking (Mott effect). The Gor'kov equation describing the appearance of a quantum condensate is reproduced when the deuteron ( $d$ ) binding energy  $E_{d,P=0}$  coincides with  $2\mu$ . The investigation of Eq. (5.56) yields also the crossover from BEC of deuterons to BCS pairing if the nucleon density increases.

Solutions of the effective two-nucleon wave equation (5.56) have been investigated for separable nucleon-nucleon interactions [169, 170] in nuclear physics. With the corresponding  $T$  matrix, the self-energy  $\text{Im}\Sigma(k_1, \omega)$ , the spectral function and the equation of state  $\rho(\beta, \mu)$  (5.50) can be calculated. We are interested in the virial expansion that follows in the limit where the imaginary part of the self-energy is small.

For small  $\text{Im}\Sigma(k_1, \omega)$ , there will be a contribution to the density from the quasiparticle peak at  $\omega - p_1^2/2m - \text{Re}\Sigma(k_1, \omega) = 0$ . In addition, contributions to the total nucleon density arise from the bound cluster states.

This approach was followed in Refs. [169, 170] under the restriction to two-particle contributions (through the  $T_2$ -matrix), but otherwise implementing a full treatment including scattering states. In this way a generalized Beth-Uhlenbeck formula was derived, namely

$$\begin{aligned} \rho(\beta, \mu) &= \rho_{\text{qp}}(\beta, \mu) + \rho_{\text{corr}}(\beta, \mu) \\ &= \rho_{\text{qp}}(\beta, \mu) + \rho_{\text{bound}}(\beta, \mu) + \rho_{\text{scatt}}(\beta, \mu), \end{aligned} \quad (5.57)$$

with (see Refs. [169, 170])

$$\begin{aligned} \rho_{\text{qp}}(\beta, \mu) &= \sum_{k_1} f_1(E_{\text{qp}}(k_1)) \\ \rho_{\text{bound}}(\beta, \mu) &= \sum_{P > P^{\text{Mott}}} f_2(E_{d,P}) \\ \rho_{\text{scatt}}(\beta, \mu) &= \sum_P \int \frac{dE}{\pi} f_2\left(\frac{P^2}{4m} + E\right) \\ &\quad \times \frac{d}{dE} \left[ \delta_{2,P}(E) - \sin \delta_{2,P}(E) \cos \delta_{2,P}(E) \right]. \end{aligned} \quad (5.58)$$

The distribution functions appearing here are

$$f_1(E) = [\exp \beta(E - \mu) + 1]^{-1} \quad (\text{Fermi}), \quad (5.59)$$

and

$$f_2(E) = [\exp \beta(E - 2\mu) - 1]^{-1} \quad (\text{Bose}). \quad (5.60)$$

The quasiparticle energy is determined implicitly from

$$E_{\text{qp}}(k_1) = p_1^2/2m + \text{Re}\Sigma(k_1, E_{\text{qp}}(k_1)). \quad (5.61)$$

As already mentioned, evaluation of the Beth-Uhlenbeck formula (5.57) including two-particle correlations has been carried out in Ref. [165, 169, 170] based on a separable nucleon-nucleon potential. The result [171] for the composition of nuclear matter as function of density and temperature is shown in Fig. 29. Two aspects of this study of two-particle condensation deserve special attention.

(i) The contribution of the correlated density, which is determined both from deuterons as bound states in the isospin-singlet channel and from scattering states, is found to increase with decreasing temperature, in accordance with the law of mass action. This law also predicts the increase of correlated density with increasing nucleon density (as also seen in Fig. 29 for the low-density limit).

However, with increasing density, the binding energy of the bound state (deuteron) decreases due to Pauli blocking (*Mott effect*). At the Mott density  $\rho_{A,n,P(T)}^{\text{Mott}}$ , the bound states with vanishing center-of-mass (c.o.m.) momentum are dissolved into the continuum of scattering states, see discussion below in Sect. V.D and [172]. Bound states with higher c.o.m. momentum merge with the continuum at higher densities. According to Levinson's theorem, if a bound state merges with the continuum, the scattering phase shift in the corresponding channel exhibits a discontinuity by a phase jump of 180 degrees, such that no discontinuity appears in the equation of state. Accordingly, the contribution of the correlated density will remain finite at the Mott density, but will be strongly reduced at somewhat higher densities.

Thus, one salient result is the disappearance of bound states and correlated density already well below the saturation density of nuclear matter. The underlying cause of the Mott effect is Pauli blocking, which prohibits the

formation of bound states if the phase space is already occupied by the medium (Fermi sphere), and hence no longer available for the formation of the wave function of the bound state (momentum space). This effect holds also for higher- $A$  bound states, such as the triton, helium, and  $\alpha$  particle, which disappear at corresponding densities (see Fig. 33 below).

$$T(k_1, k_2, k'_1, k'_2; 2\mu) = \frac{1 - f(k_1) - f(k_2)}{2\mu - \epsilon(k_1) - \epsilon(k_2)} \sum_{k'_1 k'_2} v_{k_1 k_2 k'_1 k'_2} T(k'_1, k'_2, k'_1, k'_2; 2\mu). \quad (5.62)$$

This Thouless condition is not restricted to the presence of bound states, but also holds for the contribution of scattering states, describing BCS pairing of interacting nucleons in single-particle states. Consequently, the transition temperature for the onset of a quantum condensate appears as a smooth function of density, as shown in Fig. 30.

At low densities, where the two-body bound states (deuterons) are well-defined composite particles, the mass action law implies that the deuterons will dominate the composition in the low-temperature region. In this region, the critical temperature for the transition to the quantum condensate coincides with the Bose-Einstein condensation of deuterons as known for ideal Bose systems. At high densities, where bound states are absent, the transition temperature coincides with the solution of the Gor'kov equation describing the formation of Cooper pairs. Thus, BEC and BCS scenarios characterize the low- and high-density regimes, respectively. We observe a smooth *crossover transition* from BEC to BCS behavior – as predicted generally for fermion systems by Nozières and Schmitt-Rink in Ref. [149]. It should be mentioned that the work in Ref. [149] exactly follows what was discussed in the preceding section, namely that the single-particle mass operator in  $T$ -matrix approximation only should be evaluated in first order perturbation theory in order to respect conservation laws, when the  $T$ -matrix itself is evaluated with the ppRPA approach.

Below the transition temperature, the  $T$ -matrix approach is no longer applicable. However, a mean-field approach becomes possible in this regime after performing a Bogoliubov transformation. Even so, the proper inclusion of correlations below the critical temperature remains a challenging problem. To date, only the first steps have been undertaken [174–176] toward solving this problem for general quantum many-particle systems.

Already at the mean-field level, the calculation of the transition temperature should include the quasiparticle shifts in the Hartree-Fock approximation. In general, the *effective-mass approximation* in nuclear matter will reduce the transition temperature [170, 177]. A noteworthy case is the reduction of the transition temperature in

(ii) The Bose pole in the correlated density signals the onset of a quantum condensate. As is well known, for the bound-state (deuteron channel) contribution the  $T$ -matrix approach breaks down, when the pole corresponding to the bound-state energy coincides with twice the chemical potential. This is a consequence of the Thouless condition [48] embodied in the in-medium two-body  $T$ -matrix equation (equivalent to (5.56) for  $E_{2,n,P} = 2\mu$ )

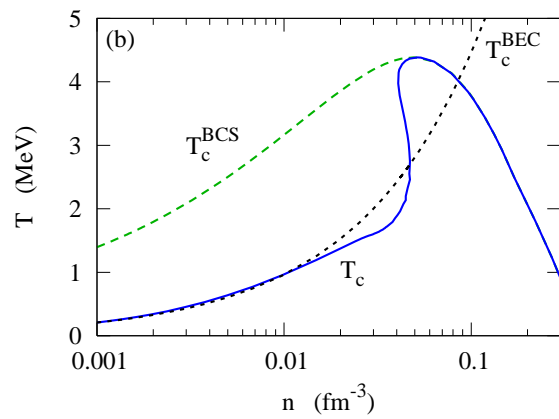


FIG. 30. Superfluid critical temperature as a function of the (total) density. The solid line is the full calculation, while the long dashes correspond to the BCS result. The short dashes show the critical temperature of Bose-Einstein condensation of a deuteron gas. Demonstration of the crossover BEC to BCS. Figure adapted from Fig. 7 in [170], see also [173].

the isospin-singlet channel for asymmetric matter [178]. We shall not discuss further effects that can be described in mean-field approximation, such as the shift and/or deformation of the Fermi surfaces [179], e.g. the LOFF phases.

## 2. Pseudo gap in nuclear matter

Going beyond the mean-field approximation, the first remarkable feature [180] emerging at the two-particle level is the formation of a *pseudogap* in the density of states (DOS) above the critical temperature  $T_c$ . Compared with the orthodox BCS solution, for which a gap opens in the DOS below  $T_c$ , a quite different situation is present in strongly correlated Fermi systems. The full treatment of the (two-body)  $T$ -matrix in the single-particle self-energy with full solution of the Dyson equation and self-consistently calculated single-particle spectral functions leads to a reduction of the single-particle

DOS near the Fermi energy already *above*  $T_c$ , within an energy interval of the same order as the BCS gap at zero temperature. This behavior may be traced to pair fluctuations above  $T_c$  that presage the transition to the superfluid state. Similar precursor behavior is known to occur in other systems of strongly correlated fermions. In the Hubbard model, for example, the formation of local magnetic moments already begins above the critical temperature, at which long-range order of the moments becomes manifest. The pseudogap phenomenon is, of course, a widely discussed aspect of compounds exhibiting high  $T_c$  superconductivity [181], see also Sect. IV.D, where we mention that a pseudogap also forms in the pairing model at finite temperature. In the context of nuclear matter,

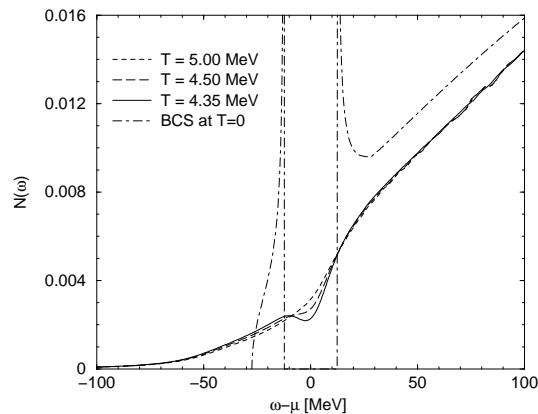


FIG. 31. Nucleon level density as a function of the energy  $\omega - \mu$ , relative to the chemical potential  $\mu$ , given for the density  $\rho = \rho_0/3$  and three values of the temperature. For comparison, the BCS result at zero temperature is shown.

the occurrence of a pseudogap phase was first considered by Schnell et al. [180] in the quasiparticle approximation, as noted above. They showed that this effect is partially washed out if a self-consistent approximation for the spectral function is implemented, but a full description should take vertex corrections into account. A similar assessment applies to a recent self-consistent solution of the Gor'kov equation in terms of the spectral function [182], which shows a reduction of the transition temperature for quantum condensation. However, vertex corrections should also be included in this case and may partially compensate the self-energy effects.

In general, it is necessary to take account *all bosonic clusters* to gain a complete picture of the onset of superfluidity. The picture developed in the preceding section only includes the effects of two-particle correlations leading to deuteron clusters. However, as is well known, the deuteron (binding energy 2.225 MeV) is weakly bound compared to other nuclei. Higher- $A$  clusters can arise that are more stable. In the following subsection, we will consider the formation of  $\alpha$  particles, which are of special importance because of their large binding energy per nucleon (7 MeV). We will not include tritons or helions, which are fermions and not so tightly bound. Moreover,

we will not consider nuclei in the iron region, which have even larger binding energy per nucleon than the  $\alpha$  and thus comprise the dominant component at low temperatures and densities. The latter are complex structures of many particles and are strongly affected by the medium as the density increases. We assume, that in the temperature and density region considered here, these more complex condensates are not of relevance.

## VI. QUARTETTING AND $\alpha$ PARTICLE CONDENSATION

The thermodynamic Green's function method described above can be extended from the two-particle problem to arbitrary numbers of particles in a cluster, i.e. to incorporate few-body correlations with  $A > 2$ . Here we will proceed with the method of equation of motion and focus on the inclusion of four-particle correlations.

The self consistent RPA scheme may be reliable numerically for the case of two body correlation functions, i.e. for  $ph$  or  $pp$  ( $hh$ ) - RPA's. For higher correlation functions the self consistent scheme is at present not feasible in its full generality and one must be satisfied if higher and more particle in-medium equations can be solved on the standard RPA level or with relatively strong other approximations. Actually, the solution of in-medium equations for more than two particles is far from trivial. Even on the purely theoretical side the structure of the equations often has not been worked out completely in the past. We will discuss this in the context of second RPA, see Sect.VII, in the symmetry broken phase, where the appearance of a double spurious mode at zero energy is one of the issues of importance. We here want to consider the in-medium four-particle problem.

In-medium four-particle correlations, for example, appear, if one adds an  $\alpha$ -particle on top of a doubly-magic nucleus, such as  $^{208}\text{Pb}$  and  $^{100}\text{Sn}$  [183, 184], or in semiconductors, where in the gas of excitons, i.e.  $ph$  bound states, may appear bi-excitations, i.e. bound states of two  $ph$  pairs. The effective wave equation contains in mean-field approximation the Hartree-Fock self-energy shift of the single-particle energies as well as the Pauli blocking of the interaction.

Let us try to set up an analogous BCS procedure for quartets. Obviously we should write for the wave function

$$|Z\rangle = \exp \left[ \frac{1}{4!} \sum_{k_1 k_2 k_3 k_4} Z_{k_1 k_2 k_3 k_4} c_{k_1}^\dagger c_{k_2}^\dagger c_{k_3}^\dagger c_{k_4}^\dagger \right] |\text{vac}\rangle, \quad (6.1)$$

where the quartet amplitudes  $Z$  are fully antisymmetric (symmetric) with respect to an odd (even) permutation of the indices. The task will now be to find an annihilating operator for this quartet condensate state. Whereas in the pairing case the partitioning of the pair operator into a linear combination of a fermion creator and a fermion

destructor is unambiguous, in the quartet case there exist two ways to partition the quartet operator, that is into a single plus a triple or into two doubles. Let us start with the superposition of a single and a triple. As a matter of fact it is easy to show that (in the following, we always will assume that all amplitudes are real)

$$\begin{aligned} q_\nu &= \sum_{k_1} u_{k_1}^\nu c_{k_1} - \frac{1}{3!} \sum v_{k_2 k_3 k_4}^\nu c_{k_1}^\dagger c_{k_2}^\dagger c_{k_3}^\dagger \\ &= \sum_{k_1} u_{k_1}^\nu [c_{k_1} - \frac{1}{6} \sum_{k_2 k_3 k_4} Z_{k_1 k_2 k_3 k_4}] , \end{aligned} \quad (6.2)$$

annihilates the quartet state under the condition

$$Z_{k_1 k_2 k_3 k_4} = \sum_\nu (u^{-1})_{k_1}^\nu v_{k_2 k_3 k_4}^\nu . \quad (6.3)$$

However, so far, we barely have gained anything, since the above quartet destructor contains a non-linear fermion transformation which, a priori, cannot be handled (see, however, Sect. V.C). Therefore, let us first try with a superposition of two fermion pair operators which is, in a way, the natural extension of the Bogoliubov transformation in the pairing case, i.e. with  $Q = \sum [XP - YP^\dagger]$  where  $P^\dagger = c^\dagger c^\dagger$  is a fermion pair creator. We will, however, find out that such an operator cannot annihilate the quartet state of Eq. (6.1). In analogy to the Self-Consistent RPA (SCRPA) approach in Sect. II.C [42], we will introduce a slightly more general operator, that is

$$\begin{aligned} Q_\nu &= \sum_{k < k'} [X_{kk'}^\nu c_k c_{k'} - Y_{kk'}^\nu c_{k'}^\dagger c_k^\dagger] \\ &\quad - \sum_{k_1 < k_2 < k_3 < k_4} \eta_{k_1 k_2 k_3 k_4}^\nu c_{k_1}^\dagger c_{k_2}^\dagger c_{k_3}^\dagger c_{k_4} , \end{aligned} \quad (6.4)$$

with  $X, Y$  antisymmetric in  $k, k'$ .

Applying this operator on our quartet state, we find  $Q_\nu |Z\rangle = 0$  where the relations between the various amplitudes turn out to be

$$\begin{aligned} Y_{ll'}^\nu &= \sum_{k < k'} X_{kk'}^\nu Z_{kk' ll'} \\ \eta_{l_2 l_3 l_4; k'}^\nu &= \sum_k X_{kk'}^\nu Z_{kl_2 l_3 l_4} . \end{aligned} \quad (6.5)$$

These relations are quite analogous to the ones which hold in the case of the SCRPA approach discussed in Sect. II.C [42]. One also notices that the relation between  $X, Y, Z$  amplitudes is similar in structure to the one of BCS theory for pairing. As with SCRPA, in order to proceed, we have to approximate the additional  $\eta$ -term. The quite suggestive recipe is to replace in the  $\eta$ -term of Eq. (6.4) the density operator  $c_{k'}^\dagger c_k$  by its

mean value  $\langle Z | c_{k'}^\dagger c_k | Z \rangle / \langle Z | Z \rangle \equiv \langle c_{k'}^\dagger c_k \rangle = \delta_{kk'} n_k$ , i.e.  $c_{k_1}^\dagger c_{k_2}^\dagger c_{k_3}^\dagger c_{k_4} \rightarrow c_{k_1}^\dagger c_{k_2}^\dagger n_{k_3} \delta_{k_3 k_4}$ , where we supposed that we work in the basis where the single particle density matrix is diagonal, that is, it is given by the occupation probabilities  $n_k$ . This approximation, of course, violates the Pauli principle but, as it was found in applications of SCppRPA [29] and SCRPA [42], we suppose that also here this violation will be quite mild (of the order of a couple of percent). With this approximation, we see that the  $\eta$ -term only renormalises the  $Y$  amplitudes and, thus, the annihilating operator boils down to a linear superposition of a fermion pair destructor with a pair creator. This can then be seen as a Hartree-Fock-Bogoliubov (HFB) transformation of fermion pair operators, i.e., pairing of 'pairs'. Replacing the pair operators by ideal bosons as done in RPA, would lead to a standard bosonic HFB approach (see [5], Ch. 9 and Appendix). Here, however, we will stay with the fermionic description and elaborate an HFB theory for fermion pairs. For this, we will suppose that we can use the annihilating property  $Q_\nu |Z\rangle = 0$  even with the approximate  $Q$ -operator. As already mentioned, we assume that this violation of consistency is weak (in the future one may try to work with (6.4) in a similar way as done in Sect. V.C).

Let us continue with elaborating our just defined frame. We will then use for the pair-annihilating operator

$$Q_\nu = \sum_{k < k'} [X_{kk'}^\nu c_k c_{k'} - Y_{kk'}^\nu c_{k'}^\dagger c_k^\dagger] / N_{kk'}^{1/2} , \quad (6.6)$$

with (the approximate) property  $Q|Z\rangle = 0$  and the first relation in (6.5). The normalisation factor  $N_{kk'} = \bar{n}_k \bar{n}_{k'} - n_k n_{k'} = 1 - n_k - n_{k'}$  has been introduced ( $\bar{n}_k = 1 - n_k$ ), so that  $\langle [Q, Q^\dagger] \rangle = \frac{1}{2} \sum (X^2 - Y^2) = 1$ , i.e., the quasi-pair state  $Q^\dagger |Z\rangle$  and the  $X, Y$  amplitudes being normalised to one. Of course, the indices  $k'$  have to be chosen so that  $\sqrt{N_{kk'}}$  stays real. We now will minimise the following energy weighted sum rule:

$$\Omega_\nu = \frac{\langle Z | [Q_\nu, [H - 2\mu\hat{N}, Q_\nu^\dagger]] | Z \rangle}{\langle Z | [Q_\nu, Q_\nu^\dagger] | Z \rangle} . \quad (6.7)$$

The minimisation with respect to  $X, Y$  amplitudes leads to

$$\begin{pmatrix} \mathbf{H} & \mathbf{\Delta}^{(22)} \\ -\mathbf{\Delta}^{(22)+} & -\mathbf{H}^* \end{pmatrix} \begin{pmatrix} X^\nu \\ Y^\nu \end{pmatrix} = \Omega_\nu \begin{pmatrix} X^\nu \\ Y^\nu \end{pmatrix} , \quad (6.8)$$

with (we eventually will consider a symmetrized double commutator in  $\mathbf{H}$ )

$$\begin{aligned}
& \mathbf{H}_{k_1 k_2, k'_1 k'_2} \\
&= \langle [c_{k_2} c_{k_1}, [H - 2\mu\hat{N}, c_{k'_1}^\dagger c_{k'_2}^\dagger]] \rangle / (N_{k_1 k_2}^{1/2} N_{k'_1 k'_2}^{1/2}) \\
&= (\xi_{k_1} + \xi_{k_2}) \delta_{k_1 k_2, k'_1 k'_2} \\
&+ N_{k_1 k_2}^{-1/2} N_{k'_1 k'_2}^{-1/2} \{ N_{k_1 k_2} \bar{v}_{k_1 k_2 k'_1 k'_2} N_{k'_1 k'_2} \\
&+ [\frac{1}{2} \delta_{k_1 k'_1} \bar{v}_{l_1 k_2 l_3 l_4} C_{l_3 l_4 k'_2 l_1} + \bar{v}_{l_1 k_2 l_4 k'_2} C_{l_4 k_1 l_1 k'_1}] \\
&- (k_1 \leftrightarrow k_2) - [k'_1 \leftrightarrow k'_2] \} , \quad (6.9)
\end{aligned}$$

where

$$\begin{aligned}
C_{k_1 k_2 k'_1 k'_2} &= \langle c_{k'_1}^\dagger c_{k'_2}^\dagger c_{k_2} c_{k_1} \rangle \\
&- n_{k_1} n_{k_2} [\delta_{k_1 k'_1} \delta_{k_2 k'_2} - \delta_{k_1 k'_2} \delta_{k_2 k'_1}] , \quad (6.10)
\end{aligned}$$

is the two body correlation function and

$$\begin{aligned}
& \Delta_{k_1 k_2, k'_1 k'_2}^{(22)} \\
&= -\langle [c_{k_2} c_{k_1}, [H - 2\mu\hat{N}, c_{k'_1}^\dagger c_{k'_2}^\dagger]] \rangle / (N_{k_1 k_2}^{1/2} N_{k'_1 k'_2}^{1/2}) \\
&= N_{k_1 k_2}^{-1/2} [(\Delta_{k_1 k'_2, k'_1 k_2} - k_1 \leftrightarrow k_2) - (k'_1 \leftrightarrow k'_2)] N_{k'_1 k'_2}^{-1/2} , \quad (6.11)
\end{aligned}$$

with the quartet order parameter field

$$\Delta_{k_1 k'_2, k'_1 k_2} = \sum_{l < l'} \bar{v}_{k_1 k'_2 l l'} \langle c_{k'_1}^\dagger c_{k_2} c_{l'} c_l \rangle . \quad (6.12)$$

In (6.8) the matrix multiplication is to be understood as  $\sum_{k'_1 < k'_2}$  for restricted summation (or as  $\frac{1}{2} \sum_{k'_1 k'_2}$  for unrestricted summation). We see from (6.11) and (6.12) that the bosonic gap  $\Delta^{(22)}$  involves the quartet order parameter  $\langle c_{k'_1}^\dagger c_{k_2} c_{l'} c_l \rangle$  quite in analogy to the usual gap field in the BCS case. The  $\mathbf{H}$  operator in (6.8) has already been discussed in Sect. II.D in connection with SCRPA in the particle-particle channel. Equation (6.8) has the typical structure of a bosonic HFB equation but, here, for fermion pairs, instead of bosons. It remains the task to close those HFB equations in expressing all expectation values involved in the  $\mathbf{H}$  and  $\Delta^{(22)}$  fields by the  $X, Y$  amplitudes. This goes in the following way. Because of the HFB structure of (6.8), the  $X, Y$  amplitudes obey the usual orthonormality relations, see [5]. Therefore, one can invert relation (6.6) to obtain (see the corresponding inversion relation (2.32))

$$c_{k'}^\dagger c_k^\dagger = N_{kk'}^{1/2} \sum_\nu [X_{kk'}^\nu Q_\nu^\dagger + Y_{kk'}^\nu Q_\nu] \quad (k < k') , \quad (6.13)$$

and by conjugation the expression for  $cc$ . With this relation, we can calculate all two-body correlation functions in (6.11) and (6.9) in terms of  $X, Y$  amplitudes.

This is achieved in commuting the destruction operators  $Q$  to the right hand side and use the annihilating property. For example, the quartet order parameter in the gap-field (6.12) is obtained as  $\langle c_{k'_1}^\dagger c_{k_2} c_{l'} c_l \rangle = N_{k'_1 k_2}^{1/2} \sum_\nu X_{k_2 k'_1}^\nu Y_{l' l}^\nu N_{l' l}^{1/2}$ . The task remains how to link the occupation numbers  $n_k = \langle c_k^\dagger c_k \rangle$  to the  $X, Y$  amplitudes. Of course, that is where our partitioning of the quartet operator into singles and triples comes into play. Therefore, let us try to work with the operator (6.2). First, as a side-remark, let us notice that if in (6.2) we replace  $c_{k_1}^\dagger c_{k_2}^\dagger$  by its expectation value which is the pairing tensor, we are back to the standard Bogoliubov transformation for pairing. Here we want to consider quartetting and, thus, we have to keep the triple operator fully. Minimising, as in (6.7), an average single-particle energy, we arrive at the following equation for the amplitudes  $u, v$  in (6.2)

$$\begin{pmatrix} \xi & \Delta^{(13)} \\ \Delta^{(13)+} & -\mathcal{N}\mathcal{H}^* \end{pmatrix} \begin{pmatrix} u \\ v \end{pmatrix} = E \begin{pmatrix} 1 & 0 \\ 0 & \mathcal{N} \end{pmatrix} \begin{pmatrix} u \\ v \end{pmatrix} , \quad (6.14)$$

with (we disregard pairing, i.e.,  $\langle cc \rangle$  amplitudes)

$$\Delta_{k; k_1 k_2 k_3}^{(13)} = \Delta_{k k_3; k_2 k_1} - [(k_2 \leftrightarrow k_3) - (k_1 \leftrightarrow k_2)] , \quad (6.15)$$

and

$$\begin{aligned}
(\mathcal{N}\mathcal{H}^*)_{k_1 k_2 k_3; k'_1 k'_2 k'_3} &= \langle \{c_{k_3}^\dagger c_{k_2}^\dagger c_{k_1}^\dagger, [H - 3\mu\hat{N}, c_{k'_1}^\dagger c_{k'_2}^\dagger c_{k'_3}^\dagger]\} \rangle \\
\mathcal{N}_{k_1 k_2 k_3; k'_1 k'_2 k'_3} &= \langle \{c_{k_3}^\dagger c_{k_2}^\dagger c_{k_1}^\dagger, c_{k'_1}^\dagger c_{k'_2}^\dagger c_{k'_3}^\dagger\} \rangle , \quad (6.16)
\end{aligned}$$

with  $\{\dots\}$  the anticommutator. We will not give  $\mathcal{H}$  in full because it is a very complicated expression involving self-consistent determination of three-body densities [60]. To lowest order in the interaction it is given by

$$\begin{aligned}
\mathcal{H}_{k_1 k_2 k_3; k'_1 k'_2 k'_3} &= (\xi_{k_1} + \xi_{k_2} + \xi_{k_3}) \delta_{k_1 k_2 k_3, k'_1 k'_2 k'_3} \\
&+ [(1 - n_{k_1} - n_{k_2}) \bar{v}_{k_1 k_2 k'_1 k'_2} \delta_{k_3 k'_3} + \text{permutations}] , \quad (6.17)
\end{aligned}$$

where  $\delta_{k_1 k_2 k_3, k'_1 k'_2 k'_3}$  is the fully antisymmetrised three-fermion Kronecker symbol. Even this operator is still rather complicated for numerical applications and mostly one will replace the correlated occupation numbers by their free Fermi-Dirac function steps, i.e.,  $n_k \rightarrow n_k^0$ . To this order the three-body norm in (6.16) is given by

$$\mathcal{N}_{k_1 k_2 k_3; k'_1 k'_2 k'_3} \simeq [\bar{n}_{k_1}^0 \bar{n}_{k_2}^0 \bar{n}_{k_3}^0 + n_{k_1}^0 n_{k_2}^0 n_{k_3}^0] \delta_{k_1 k_2 k_3, k'_1 k'_2 k'_3} , \quad (6.18)$$

with  $\bar{n}^0 = 1 - n^0$ . In principle, this effective three-body Hamiltonian leads to three-body bound and scattering states. In our application to nuclear matter given below, we will make an even more drastic approximation and completely neglect the interaction term in the three-body

Hamiltonian. Eliminating under this condition the  $v$ -amplitudes from (6.14), one can write down the following effective single-particle equation

$$\begin{aligned} & \xi_k u_k^{(\nu)} + \\ & \sum_{k_1 < k_2 < k_3 k'} \frac{\Delta_{kk_1 k_2 k_3}^{(13)} (\bar{n}_{k_1}^0 \bar{n}_{k_2}^0 \bar{n}_{k_3}^0 + n_{k_1}^0 n_{k_2}^0 n_{k_3}^0) \Delta_{k_3 k_2 k_1 k'}^{(13)*}}{E_\nu + \xi_{k_1} + \xi_{k_2} + \xi_{k_3}} u_{k'}^{(\nu)} \\ & = E_\nu u_k^{(\nu)}. \end{aligned} \quad (6.19)$$

The occupation numbers are given by

$$n_k = 1 - \sum_\nu |u_k^{(\nu)}|^2. \quad (6.20)$$

Of course, one could also replace the uncorrelated occupation numbers in the three-body term by the correlated ones, but we want to refrain from this complication here. The effective single-particle field in (6.19) is graphically interpreted in Fig. 35 below in Sect. VI.B. The gap-fields in (6.19) are then to be calculated as in (6.15) and (6.12) with (6.13) and the system of equations is fully closed. This is quite in parallel to the pairing case. It is clear that the solution of this complicated self-consistent quartet problem is at present hardly envisageable. In cases, where the quartet consists out of four different fermions, which, in addition, is rather strongly bound, as this will be the case for the  $\alpha$ -particle in nuclear physics, one still can make a very good, but drastic simplification: one writes the quartic order parameter as a translationally invariant product of four times the same single-particle wave function in momentum space. We will see right below, how this goes when we apply our theory to  $\alpha$  particle condensation in nuclear matter for the simpler case of the determination of the critical temperature. Comparing the effective single-particle field in (6.19) with the one of standard pairing [4], we find strong analogies, but also several structural differences. The most striking is that in the quartet case Pauli factors figure in the numerator of (6.19), whereas this is not the case for pairing. In principle, in the pairing case, they are also there, but since  $\bar{n}_k + n_k = 1$ , they drop out. This difference between the pairing and the quartetting cases has quite dramatic consequences. Namely when the chemical potential  $\mu$  changes from negative (binding) to positive, the implicit three-hole level density passes through zero at  $\omega - 3\mu = 0$ , because phase space constraints and energy conservation cannot be fulfilled simultaneously at that point. So, we will see that as soon as with increasing density the chemical potential turns positive, quartet condensation is suppressed. More details can be found in Sect. VI.B below. It is also rather evident that the three hole lines in Fig. 35 can further be correlated, eventually also to bound states of helions ( ${}^3\text{He}$ ) or tritons ( ${}^3\text{H}$ ). This is illustrated in Fig. 32 where also the possibility of deuteron pairing is indicated. It remains a task for the future to include all these processes in a coherent approach of  $\alpha$  particle condensation.

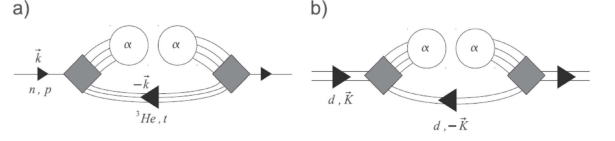


FIG. 32. Inclusion of two and three body clusters in the formation of  $\alpha$  particle condensation.

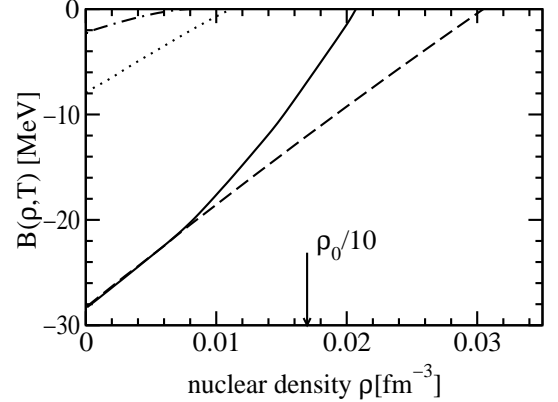


FIG. 33. Shift of binding energy of the light clusters ( $d$  - dash dotted,  $t/h$  - dotted, and  $\alpha$  - dashed: perturbation theory, full line: non-perturbative Faddeev-Yakubovski equation) in symmetric nuclear matter as a function of density for given temperature  $T = 10$  MeV [186].

#### A. Critical temperature for $\alpha$ condensation

We are interested in an example of nuclear physics, where the  $\alpha$ -particle constitutes a particularly strongly bound cluster of four nucleons. One can ask the question how, for a fixed temperature, the binding energy of the  $\alpha$ -particle varies with increasing temperature.

The effective wave equation has been solved using separable potentials for  $A = 2$  by integration. For  $A = 3, 4$  we can use a *Faddeev approach* [185]. The shifts of binding energy can also be calculated approximately via perturbation theory. In Fig. 33 we show the shift of the binding energy of the light clusters ( $d$ ,  $t/h$  and  $\alpha$ ) in symmetric nuclear matter as a function of density for temperature  $T = 10$  MeV [186]. It is found that the cluster binding energy decreases with increasing density. Finally, at the *Mott density*  $\rho_{A,n,P}^{\text{Mott}}(T)$  the bound state is dissolved. The clusters are not present at higher densities, merging into the nucleonic medium. It is found that the  $\alpha$  particle at  $T = 10$  MeV already dissolves at a density  $\rho_\alpha^{\text{Mott}} \approx \rho_0/10$ , see Fig. 33. For a given cluster type characterized by  $A, n$ , we can also introduce the Mott momentum  $P_{A,n}^{\text{Mott}}(\rho, T)$  in terms of the ambient temperature  $T$  and nucleon density  $\rho$ , such that the bound states exist only for  $P \geq P_{A,n}^{\text{Mott}}(\rho, T)$ . We do not present an example here, but it is intuitively clear that a cluster with



high c.o.m. momentum with respect to the medium is less affected by the Pauli principle than a cluster at rest.

Since Bose condensation only is of relevance for  $d$  and  $\alpha$ , and the fraction of  $d$ ,  $t$  and  $h$  becomes low compared with that of  $\alpha$  with increasing density, we can neglect the contribution of them to the equation of state in a first approximation. Consequently, if we further neglect the contribution of the four-particle scattering phase shifts in the different channels, we can now construct an equation of state

$$\rho(T, \mu) = \rho^{\text{free}}(T, \mu) + \rho^{\text{bound}, d}(T, \mu) + \rho^{\text{bound}, \alpha}(T, \mu), \quad (6.21)$$

such that  $\alpha$ -particles determine the behavior of symmetric nuclear matter at densities below  $\rho_{\alpha}^{\text{Mott}}$  and temperatures below the binding energy per nucleon of the  $\alpha$ -particle. The formation of deuteron clusters alone gives an incorrect description because the deuteron binding en-

ergy is small, and, thus, the abundance of  $d$ -clusters is small compared with that of  $\alpha$ -clusters. In the low density region of the phase diagram,  $\alpha$ -matter emerges as an adequate model for describing the nuclear matter equation of state.

With increasing density, the medium modifications, especially Pauli blocking, will lead to a deviation of the critical temperature  $T_c(\rho)$  from that of an ideal Bose gas of  $\alpha$ -particles (the analogous situation holds for deuteron clusters, i.e., in the isospin-singlet channel), see Sect. IV.B.

Symmetric nuclear matter is characterized by the equality of the proton and neutron chemical potentials, i.e.,  $\mu_p = \mu_n = \mu$ . Then an extended Thouless condition based on the relation for the four-body T-matrix (in principle, equivalent to (6.29) below)

$$\begin{aligned} T_4(k_1 k_2 k_3 k_4, k'_1 k'_2 k'_3 k'_4, 4\mu) = & \sum_{k'_1 k'_2 k'_3 k'_4} \left\{ \frac{v_{k_1 k_2, k'_1 k'_2} [1 - f(k_1) - f(k_2)]}{4\mu - \epsilon_{k_1} - \epsilon_{k_2} - \epsilon_{k_3} - \epsilon_{k_4}} \delta(k_3, k'_3) \delta(k_4, k'_4) \right. \\ & \left. + \text{permutations} \right\} T_4(k'_1 k'_2 k'_3 k'_4, k''_1 k''_2 k''_3 k''_4, 4\mu) \end{aligned} \quad (6.22)$$

serves to determine the onset of Bose condensation of  $\alpha$ -like clusters, noting that the existence of a solution of this relation signals a divergence of the four-particle correlation function. An approximate solution has been obtained by a variational approach, in which the wave function is taken as Gaussian incorporating the correct solution for the two-particle problem [187].

Eq. (6.22) at eigenvalue  $4\mu$  has been solved numerically exactly by the Faddeev-Yakubovsky method employing the Malfliet-Tjon force [188]. The results for the critical temperature of  $\alpha$ -condensation is presented in Fig. 34 as a function of the chemical potential  $\mu$ . The exact solution is a numerical challenge and could only be obtained for negative  $\mu$ , i.e. when there exists a bound cluster. It is, therefore, important to try another, approximate, solution of the in-medium four-body equation. Since the  $\alpha$ -particle is strongly bound, we make a momentum projected mean-field ansatz [5] for the quartet wave function [189]

$$\Psi_{1234} = (2\pi)^3 \delta^{(3)}(\mathbf{k}_1 + \mathbf{k}_2 + \mathbf{k}_3 + \mathbf{k}_4) \prod_{i=1}^4 \varphi(\mathbf{k}_i) \chi^{ST}, \quad (6.23)$$

where  $\chi^{ST}$  is the spin-isospin function which we suppose to be the one of a scalar ( $S = T = 0$ ). We will not further mention it from now on. We work in momentum space and  $\varphi(\mathbf{k})$  is the as-yet unknown single-particle  $0S$  wave function. In position space, this leads to the usual formula [5]  $\Psi_{1234} \rightarrow \int d^3 R \prod_{i=1}^4 \tilde{\varphi}(\mathbf{r}_i - \mathbf{R})$

where  $\tilde{\varphi}(\mathbf{r}_i)$  is the Fourier transform of  $\varphi(\mathbf{k}_i)$ . If we take for  $\varphi(\mathbf{k}_i)$  a Gaussian shape, this gives:  $\Psi_{1234} \rightarrow \exp[-c \sum_{1 \leq i < k \leq 4} (\mathbf{r}_i - \mathbf{r}_k)^2]$  which is the translationally invariant ansatz often used to describe  $\alpha$ -clusters in nuclei. For instance, it is also employed in the  $\alpha$ -particle condensate wave function of Tohsaki, Horiuchi, Schuck, Röpke (THSR) in Ref. [190].

Inserting the ansatz (6.23) into the 4-body wave equation equivalent to (6.22) and integrating over superfluous variables, or minimizing the energy, we arrive at a Hartree-Fock type of equation for the single-particle  $0S$  wave function  $\varphi(k) = \varphi(|\mathbf{k}|)$  which can be solved. However, for a general two body force  $v_{\mathbf{k}_1 \mathbf{k}_2, \mathbf{k}'_1 \mathbf{k}'_2}$ , the equation to be solved is still rather complicated. We, therefore, proceed to the last simplification and replace the two-body force by a unique separable one, that is

$$v_{\mathbf{k}_1 \mathbf{k}_2, \mathbf{k}'_1 \mathbf{k}'_2} = \lambda e^{-k^2/k_0^2} e^{-k'^2/k_0^2} (2\pi)^3 \delta^{(3)}(\mathbf{K} - \mathbf{K}'), \quad (6.24)$$

where  $\mathbf{k} = (\mathbf{k}_1 - \mathbf{k}_2)/2$ ,  $\mathbf{k}' = (\mathbf{k}'_1 - \mathbf{k}'_2)/2$ ,  $\mathbf{K} = \mathbf{k}_1 + \mathbf{k}_2$ , and  $\mathbf{K}' = \mathbf{k}'_1 + \mathbf{k}'_2$ . This means that we take a spin-isospin averaged two-body interaction and disregard that, in principle, the force may be somewhat different in the  $S, T = 0, 1$  or  $1, 0$  channels. It is important to remark that for a mean field solution the interaction only can be an effective one, very different from a bare nucleon-nucleon force. This is contrary to the usual gap equation for pairs, to be considered below, where, at least in the nuclear context, a bare force can be used as a reasonable first approximation.

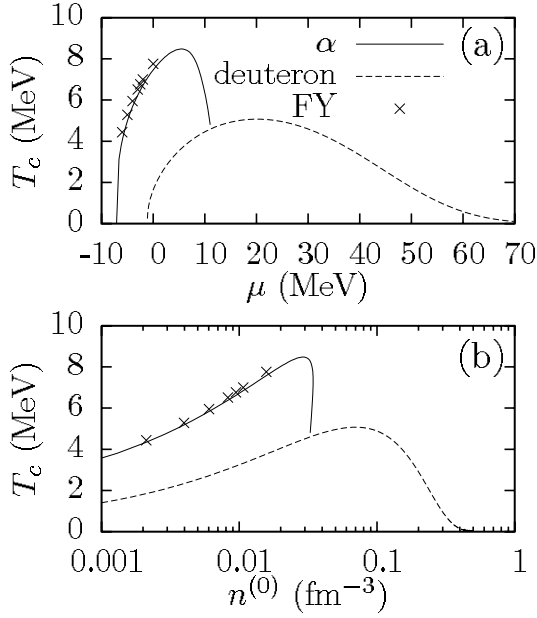


FIG. 34. Critical temperature of alpha and deuteron condensations as functions of (a) chemical potential and (b) density of free nucleon [185]. Crosses (x) correspond to calculation of Eq. (6.22) with the Malfliet-Tjon interaction (MT I-III) using the Faddeev-Yakubovskii method.

We are now ready to study the solution of (6.22) with (6.23) for the critical temperature  $T_c^\alpha$ , defined by the point where the eigenvalue equals  $4\mu$ . For later comparison, the deuteron (pair) wave function at the critical temperature is also deduced from Eqs. (5.56) and (6.24) to be

$$\phi(k) = -\frac{1-2f(\varepsilon)}{k^2/m-2\mu} \lambda e^{-k^2/k_0^2} \int \frac{d^3k'}{(2\pi)^3} e^{-k'^2/k_0^2} \phi(k'), \quad (6.25)$$

where  $\phi(k)$  is the relative wave function of two particles given by  $\Psi_{12} \rightarrow \phi(|\frac{\mathbf{k}_1-\mathbf{k}_2}{2}|) \delta^{(3)}(\mathbf{k}_1+\mathbf{k}_2)$ , and  $\varepsilon = k^2/(2m)$ . We also neglected the momentum dependence of the Hartree-Fock mean field shift in Eq. (6.25). It, therefore, can be incorporated into the chemical potential  $\mu$ . With Eq. (6.25), the critical temperature of pair condensation is obtained from the following equation:

$$1 = -\lambda \int \frac{d^3k}{(2\pi)^3} \frac{1-2f(\varepsilon)}{k^2/m-2\mu} e^{-2k^2/k_0^2}. \quad (6.26)$$

In order to determine the critical temperature for  $\alpha$ -particle condensation, we have to adjust the temperature so that the eigenvalue of (6.22) equals  $4\mu$ . The result is shown in Fig. 34(a). In order to get an idea how this converts into a density dependence, we use for the moment the free gas relation between the density  $n^{(0)}$  of uncorrelated nucleons and the chemical potential

$$n^{(0)} = 4 \int \frac{d^3k}{(2\pi)^3} f(\varepsilon). \quad (6.27)$$

We are well aware of the fact that this is a relatively gross simplification, for instance, at the lowest densities and we intend to generalize our theory in the future so that correlations are included into the density. This may be done along the work of Nozières and Schmitt-Rink [149]. The two open constants  $\lambda$  and  $k_0$  in Eq. (6.24) are determined so that binding energy (28.3 MeV) and radius (1.71 fm) of the free ( $f_i = 0$ )  $\alpha$ -particle come out right. The adjusted parameter values are:  $\lambda = -992 \text{ MeV fm}^3$ , and  $k_0 = 1.43 \text{ fm}^{-1}$ . The results of the calculation are shown in Fig. 34.

In Fig. 34, the maximum of critical temperature  $T_{c,\max}^\alpha$  is at  $\mu = 5.5 \text{ MeV}$ , and the  $\alpha$ -condensation can exist up to  $\mu_{\max} = 11 \text{ MeV}$ . It is very remarkable that the results obtained with (6.23) for  $T_c^\alpha$  very well agree with the exact solution of (6.22) using the Malfliet-Tjon interaction (MT I-III) [188] with the Faddeev-Yakubovskii method also shown by crosses in Fig. 34 (the numerical solution only could be obtained for negative values of  $\mu$ ). This indicates that  $T_c^\alpha$  is essentially determined by the Pauli blocking factors.

In Fig. 34 we also show the critical temperature for deuteron condensation derived from Eq. (6.26). In this case, the bare force is adjusted with  $\lambda = -1305 \text{ MeV fm}^3$  and  $k_0 = 1.46 \text{ fm}^{-1}$  to get experimental energy ( $-2.2 \text{ MeV}$ ) and radius (1.95 fm) of the deuteron. It is seen that at higher densities deuteron condensation wins over the one of  $\alpha$ -particle. The latter breaks down rather abruptly at a critical positive value of the chemical potential. Roughly speaking, this corresponds to the point where the  $\alpha$ -particles start to overlap. This behavior stems from the fact that Fermi-Dirac distributions in the four-body case, see (6.22), can never become step-like, as in the two-body case, even not at zero temperature, since the pairs in an  $\alpha$ -particle are always in motion. Therefore, no threshold effect occurs as with pairing for Cooper pairs at rest. As a consequence,  $\alpha$ -condensation generally only exists as a BEC phase and the weak coupling regime is absent, see also discussion in Sec. VI B.

An important consequence of this study is that at the lowest temperatures, Bose-Einstein condensation occurs for  $\alpha$ -particles rather than for deuterons. As the density increases within the low-temperature regime, the chemical potential  $\mu$  first reaches  $-7 \text{ MeV}$ , where the  $\alpha$ -particles start to Bose-condense. In contrast, Bose condensation of deuterons would not occur until  $\mu$  rises to  $-1.1 \text{ MeV}$ .

The “quartetting” transition temperature sharply drops as the rising density approaches the critical Mott value, at which the four-body bound states disappear. At that point, pair formation in the isospin-singlet deuteron-like channel comes into play, and a deuteron condensate will exist below the critical temperature for BCS pairing up to densities above the nuclear-matter saturation density  $\rho_0$ , as described in the previous Section. Of course, also isovector  $n$ - $n$  and  $p$ - $p$  pairing develops. The critical (Mott) density, at which the  $\alpha$  condensate disappears is estimated to be  $\rho_0/3$ . Therefore,  $\alpha$ -particle

condensation primarily only exists in the Bose-Einstein-Condensed (BEC) phase and there exist no phase, where the quartets acquire a large extension as Cooper pairs do in the weak coupling regime. However, the variational approaches of Ref. [187] and of Eq. (6.23), on which this conclusion is based, represent only first attempts at the description of the transition from quartetting to pairing. The detailed nature of this fascinating transition remains to be clarified. Many different questions arise in relation to the possible physical occurrence and experimental manifestations of quartetting: Can we observe the hypothetical “ $\alpha$  condensate” in nature? What about thermodynamic stability? What happens with quartetting in asymmetric nuclear matter? Are more complex quantum condensates possible? What is their relevance for finite nuclei? As discussed, the special type of microscopic quantum correlations associated with quartetting may be important in nuclei, its role in these finite inhomogeneous systems being similar to that of pairing [190].

On the other hand, if at all,  $\alpha$ -condensation in compact stars occurs at strongly asymmetric matter. It is, therefore, important to generalize the above study for symmetric nuclear matter to the asymmetric case. This can be done straightforwardly again using our momentum projected mean-field ansatz (6.23) generalized to the asymmetric case. This implies to introduce two chemical potentials, one for neutrons and one for protons. We also have to distinguish two single-particle wave functions in our product ansatz. For the results, we refer the reader to [178] and simply state that as a function of asymmetry the  $\alpha$  wins over the deuteron because the latter’s binding is much weaker than the one of the  $\alpha$ -particle.

In conclusion the  $\alpha$ -particle (quartet) condensation was investigated in homogeneous symmetric nuclear matter as well as in asymmetric nuclear matter. We found that the critical density at which the  $\alpha$ -particle condensate appears is estimated to be around  $\rho_0/3$  in the symmetric nuclear matter, and the  $\alpha$ -particle condensation can occur only at low density. This result is consistent with the fact that the Hoyle state ( $0_2^+$ ) of  $^{12}\text{C}$ , which is considered as a three- $\alpha$  condensed state also has a very low density  $\rho \sim \rho_0/3$ . On the other hand, in the asymmetric nuclear matter, the critical temperature  $T_c$  for the  $\alpha$ -particle condensation was found to decrease with increasing asymmetry. However,  $T_c$  stays relatively high for very strong asymmetries, a fact of importance in the astrophysical context. The asymmetry affects deuteron pairing more strongly than  $\alpha$ -particle condensation. Therefore, at high asymmetries, if at all,  $\alpha$ -particle condensate seems to dominate over deuteron-

like pairing at all possible densities.

## B. ‘Gap’ equation for quartet order parameter

In the preceding section, we considered  $\alpha$ -particle condensation at finite temperature, specifically we determined the critical temperature for the onset of condensation. We now want to consider  $\alpha$  condensation at zero temperature, where the full non-linear order parameter equation has to be solved, similar to the solution of the gap equation in the case of pairing. For macroscopic  $\alpha$  condensation it is, of course, not conceivable to work with a number projected  $\alpha$ -particle condensate wave function as we did, when in finite nuclei only a couple of  $\alpha$  particles were present [190]. We rather have to develop an analogous procedure to BCS theory, but generalized for quartets. In principle, a wave function of the already mentioned type  $|\alpha\rangle = \exp[\sum_{1234} z_{1234} c_1^\dagger c_2^\dagger c_3^\dagger c_4^\dagger] |\text{vac}\rangle$  would be the ideal generalization of the BCS wave function for the case of quartets. However, unfortunately, it is unknown so far (see, however, Ref. [42] and Sect. V.C) how to treat such a complicated many-body wave function mathematically in a reasonable way. So, we rather attack the problem from the other end, that is with a Gor’kov type of approach, well known from pairing, but here extended to the quartet case. Since, naturally, the formalism is complicated, we only will outline the main ideas and refer for details to the literature.

Actually, one part of the problem is written down easily. Let us guide from a particular form of the gap equation in the case of pairing. We have at zero temperature (see also eq.(5.56))

$$(\varepsilon_{k_1} + \varepsilon_{k_2})\kappa_{k_1 k_2} + (1 - n_{k_1} - n_{k_2})\frac{1}{2} \sum_{k'_1 k'_2} \bar{v}_{k_1 k_2 k'_1 k'_2} \kappa_{k'_1 k'_2} = 2\mu\kappa_{k_1 k_2} , \quad (6.28)$$

where  $\kappa_{k_1 k_2} = \langle c_{k_1} c_{k_2} \rangle$  is the pairing tensor,  $n_i = \langle c_i^\dagger c_i \rangle$  are the BCS occupation numbers, and  $\bar{v}_{k_1 k_2 k'_1 k'_2}$  denotes the antisymmetrized matrix element of the two-body interaction. The  $\varepsilon_i$  are the usual mean-field energies. Equation (6.28) is equivalent to the usual gap equation in the case of zero total momentum and opposite spin, i.e. in short hand:  $k_2 = \bar{k}_1$ , where the bar stands for ‘time reversed conjugate’. With the EOM, the extension of (6.28) to the quartet case is formally written down without problem. It is a direct consequence of our self-consistent quartet equations derived above. As in the pairing case, we then linearize to large extent the problem keeping only the occupation numbers coupled to the quartet condensate in the self-consistent cycle. We write for zero temperature

$$\begin{aligned}
(\varepsilon_{1234} - 4\mu)\kappa_{1234} &= (1 - n_1 - n_2) \frac{1}{2} \sum_{k'_1 k'_2} \bar{v}_{k_1 k_2 k'_1 k'_2} \kappa_{k'_1 k'_2 k_3 k_4} \\
&+ (1 - n_{k_1} - n_{k_3}) \frac{1}{2} \sum_{k'_1 k'_3} \bar{v}_{k_1 k_3 k'_1 k'_3} \kappa_{k'_1 k'_3 k_2 k_4} + \text{all permutations} ,
\end{aligned} \tag{6.29}$$

with  $\kappa_{k_1 k_2 k_3 k_4} = \langle c_{k_1} c_{k_2} c_{k_3} c_{k_4} \rangle$  the quartet order parameter. This is formally the same equation as Eq. (6.22) with, however, the Fermi-Dirac occupation numbers replaced by the zero temperature quartet correlated single-particle occupation numbers, similar to the BCS case. For the quartet case, the crux lies in the determination of those occupation numbers. However, as we have seen, they can very naturally be determined from the generalized s.p. self-energy in (6.19).

Let us discuss some properties of the s.p. self-energy in the case of  $\alpha$ -particles with respect to the one of pairing, see Fig. 35. Put aside the difficulty to derive a manageable expression for this 'quartet' s.p. self-energy, what immediately strikes is that instead of only one 'backward going line' with  $(-\mathbf{p}, -\sigma)$  as in the pairing case, we now have three backwards going lines. As a consequence, the three momenta  $\mathbf{k}_1, \mathbf{k}_2, \mathbf{k}_3$  in these lines are only constrained so that their sum is equal to  $\mathbf{k}_1 + \mathbf{k}_2 + \mathbf{k}_3 = -\mathbf{p}$

in order that the total momentum of the order parameter is zero and, thus, the remaining freedom has to be summed over. This is in strong contrast to the pairing case, where the single backward-going line is constrained by momentum conservation to have momentum  $-\mathbf{p}$ , so that together with the incoming particle at  $\mathbf{p}$  the total momentum of the gap function is zero, see also Fig. 35. So, no internal summation occurs in the self-energy belonging to pairing. The consequence of this additional momentum summation in the mass operator for quartetting leads, with respect to pairing, to a completely different analytic structure of the self-energy in case of quartetting. This is best studied with the so-called three-hole level density  $g_{3h}(\omega)$ , which is related to the imaginary part of the three-hole Green's function  $G^{3h}(k_1, k_2, k_3; \omega) = (\bar{f}_1 \bar{f}_2 \bar{f}_3 + f_1 f_2 f_3)/(\omega + \varepsilon_{123})$  with  $\varepsilon_{123} = \varepsilon_1 + \varepsilon_2 + \varepsilon_3$  figuring in the self-energy, see Fig. 35

$$\begin{aligned}
g_{3h}(\omega) &= - \int \frac{d^3 k_1}{(2\pi)^3} \frac{d^3 k_2}{(2\pi)^3} \frac{d^3 k_3}{(2\pi)^3} \text{Im} G^{(3h)}(k_1, k_2, k_3; \omega + i\eta) \\
&= \int \frac{d^3 k_1}{(2\pi)^3} \frac{d^3 k_2}{(2\pi)^3} \frac{d^3 k_3}{(2\pi)^3} (\bar{f}_1 \bar{f}_2 \bar{f}_3 + f_1 f_2 f_3) \pi \delta(\omega + \varepsilon_1 + \varepsilon_2 + \varepsilon_3) .
\end{aligned} \tag{6.30}$$

In Fig. 36 we show the level density at zero temperature ( $f(\omega) = \theta(-\omega)$ ), where it is calculated with the proton mass  $m = 938.27$  MeV [178]. Two cases have to be considered, chemical potential  $\mu$  positive or negative. In the latter case we have binding of the quartet. Let us first discuss the case  $\mu > 0$ . We remark that, in this case, the  $3h$  level density goes through zero at  $\omega = 0$ , i.e., since we are measuring energies with respect to the chemical potential  $\mu$ , just in the region where the quartet correlations should appear. This is at strong variance with the pairing case where the  $1h$  level density,  $g_{1h}(\omega) = \int \frac{d^3 k}{(2\pi\hbar)^3} (\bar{f}_k + f_k) \delta(\omega + \varepsilon_k) = \int \frac{d^3 k}{(2\pi\hbar)^3} \delta(\omega + \varepsilon_k)$ , does not feel any influence from the medium and, therefore, the corresponding level density varies (neglecting the mean field for the sake of the argument) like in free space with the square root of energy. In particular, this means that the level density is *finite* at the Fermi level. This is a dramatic difference with the quartet case and explains why Cooper pairs can strongly overlap whereas for quartets this is impossible as we will see below. We also would like to point out that the  $3h$  level density is just the mirror to the  $3p$  level density, which has been

discussed in Ref. [191].

For the case  $\mu < 0$ , where anyway the  $f_i$ 's are zero at  $T=0$ , there is nothing very special, besides the fact that the level density is non-vanishing only for negative values of  $\omega$  and that the upper boundary is given by  $\omega = 3\mu$ . Therefore, the level density of Eq. (6.30) is zero for  $\omega > 3\mu$ . Therefore, in the BEC regime ( $\mu < 0$ ), there is no marked difference between the pairing and quartetting cases.

The complexity of the calculation in Eq. (6.29) is much reduced using for the order parameter  $\langle cccc \rangle$  our mean-field ansatz projected onto zero total momentum, as it was already very successfully employed with Eq. (6.23),

$$\begin{aligned}
\langle c_1 c_2 c_3 c_4 \rangle &\rightarrow \phi_{\mathbf{k}_1 \mathbf{k}_2, \mathbf{k}_3 \mathbf{k}_4} \chi_0, \\
\phi_{\mathbf{k}_1 \mathbf{k}_2, \mathbf{k}_3 \mathbf{k}_4} &= \varphi(|\mathbf{k}_1|) \varphi(|\mathbf{k}_2|) \varphi(|\mathbf{k}_3|) \varphi(|\mathbf{k}_4|) \\
&\times (2\pi)^3 \delta(\mathbf{k}_1 + \mathbf{k}_2 + \mathbf{k}_3 + \mathbf{k}_4) ,
\end{aligned} \tag{6.31}$$

where  $\chi_0$  is the spin-isospin singlet wave function. It should be pointed out that this product ansatz with four identical  $0S$  single-particle wave functions is typical for a ground state configuration of the  $\alpha$  particle. Excited con-

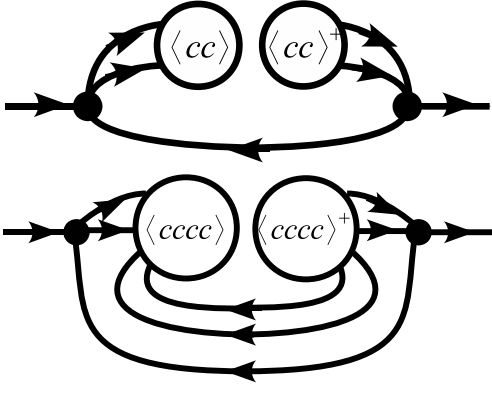


FIG. 35. Graphical representation of the BCS self-energy (top) and the approximate  $\alpha$ -BEC self-energy  $M^{\text{quartet}}$  (bottom) of Eq. (6.19).

figurations with wave functions of higher nodal structures may eventually be envisaged for other physical situations. We also would like to mention that the momentum conserving  $\delta$ -function induces strong correlations among the four particles and (6.31) is, therefore, a rather non-trivial variational wave function.

For the two-body interaction  $v_{k_1 k_2, k_3 k_4}$  in Eq. (6.29), we employ the same separable form as done already for the quartet critical temperature.

As already mentioned, in this pilot application of our self-consistent quartet theory, we only will consider the zero temperature case. As a definite physical example, we will treat the case of nuclear physics with the particularly strongly bound quartet, the  $\alpha$  particle. It should be pointed out, however, that, if scaled appropriately, all energies and lengths can be transformed to other physical systems. For the nuclear case it is convenient to measure energies in Fermi energies  $\varepsilon_F = 35$  MeV and lengths in inverse Fermi momentum  $k_F^{-1} = 1.35^{-1}$  fm which are the values at nuclear saturation.

We are now in a position to solve, as in the BCS case, the coupled equations (6.20, 6.29) for the quartet order parameter and the single-particle occupation numbers from the single-particle Dyson equation with the self-energy (6.19) self-consistently. The single-particle wave functions and occupation numbers obtained from the above cycle are shown in Fig. 37. We also insert the Gaussian wave function with the same r.m.s. momentum as the single-particle wave function in the left figures in Fig. 37. As shown in Fig. 37, the single-particle wave function is sharper than a Gaussian.

We could not obtain a convergent solution for  $\mu > 0.55$  MeV. This difficulty has precisely its origin in the fact that the three-hole level density goes through zero at  $3\mu > 0$ , just where the four-body correlations should build up, as this was discussed above. In the r.h.s. panels of Fig. 37 we also show the corresponding occupation numbers. We see that they are very small. However, they increase for increasing values of the chemical potential.

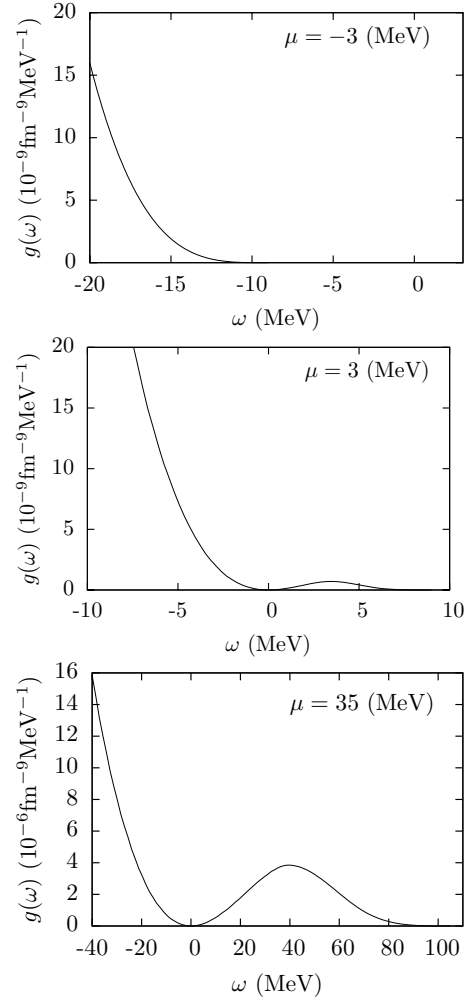


FIG. 36.  $3h$  level densities defined in Eq. (6.30) for various values of the chemical potential  $\mu$  at a zero temperature [178].

For  $\mu = 0.55$  MeV the maximum of the occupation still only attains 0.35 what is far away from the saturation value of one. What really happens for larger values of the chemical potential, is unclear. Surely, as discussed above, the situation for the quartet case is completely different from the standard pairing case. This is due to the just mentioned particular behavior of the  $3h$  level density. Due to this fact, the inhibition to go into the positive  $\mu$  regime is here even stronger than in the case of the critical temperature [185]. This transition is akin to a Quantum Phase Transition (QPT), where the density plays the role of a control parameter [192].

In conclusion of this quartet condensation section, let us say that we could build with the help of the EOM method a self-consistent scheme for the quartet order parameter, quite in analogy to the pairing case. Strong differences with the latter have been revealed. In first place comes the fact that quartet condensation occurs only as long as the quartet is bound, that is as long as the corresponding chemical potential  $\mu$  is negative. Contrary

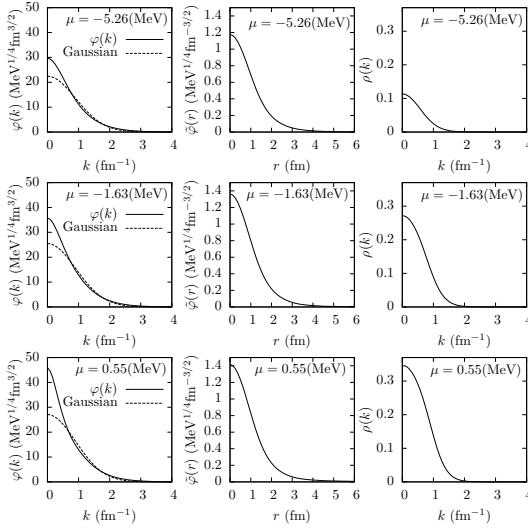


FIG. 37. Single-particle wave function  $\varphi(k)$  in  $k$ -space (left) and  $r$ -space  $\tilde{\varphi}(r)$  (middle), and occupation numbers (right) at  $\mu = -5.26$  (top),  $-1.63$  (middle) and  $0.55$  (bottom). The  $r$ -space wave function  $\tilde{\varphi}(r)$  is derived from the Fourier transform of  $\varphi(k)$  by  $\tilde{\varphi}(r) = \int d^3k e^{i\mathbf{k}\cdot\mathbf{r}} \varphi(k) / (2\pi)^3$ . The dashed line in the left panels correspond to the Gaussian with same norm and r.m.s. momentum as  $\varphi(k)$  [178].

to the pairing case, there exists no quartet condensation effect for states in the continuum. This stems from a radically different behavior of the level densities involved in both cases, as explained above. It is very rewarding that in finite nuclei, there seems to exist the  $\alpha$ -particle condensation phenomenon. As we have investigated, the famous Hoyle state of  $^{12}\text{C}$  seems to be well described by a three- $\alpha$  condensate type of wave function (THSR). It remains a challenge to find other quartet condensates in nature [193].

## VII. SECOND RPA AND EXTENSIONS

RPA and SCRPA are designed to describe the excitation of one-phonon states. For the description of properties of two-phonon states and the coupling of one-phonon states to two-phonon states, we need to use extensions of RPA, which enable us to calculate two-body transition amplitudes in addition to one-body transition amplitudes. One of such extended RPA theories is the second RPA (SRPA) [194] which has been used for the study of decay properties of giant resonances [195]. However, the original formulation of SRPA is not complete as will be demonstrated in this section. Also the effects of ground-state correlations are not included in SRPA. Recently, we have developed a more general Extended RPA (ERPA) which contains the effects of ground-state correlations and meets the requirement of hermiticity [196]. In this section we present the formulation of our ERPA and show

recent applications.

We consider the Hamiltonian

$$H = \sum_{kk'} t_{kk'} a_k^\dagger a_{k'} + \frac{1}{2} \sum_{k_1 k_2 k'_1 k'_2} v_{k_1 k_2 k'_1 k'_2} a_{k_1}^\dagger a_{k_2}^\dagger a_{k'_2} a_{k'_1} . \quad (7.1)$$

### A. Ground state

The ground state  $|0\rangle$ , which is used to evaluate various matrices in ERPA, is given by the stationary conditions of the occupation matrix  $n_{\alpha\alpha'}$ , the two-body correlation matrix  $C_{klk'l'}$  and the three-body correlation matrix  $C_{klmk'l'm'}$  defined as

$$\begin{aligned} n_{kk'} &= \langle 0 | a_k^\dagger a_k | 0 \rangle \\ C_{klk'l'} &= \langle 0 | a_k^\dagger a_l^\dagger a_l a_k | 0 \rangle - \mathcal{A}(n_{kk'} n_{ll'}) \\ C_{klmk'l'm'} &= \langle 0 | a_k^\dagger a_l^\dagger a_m^\dagger a_m a_l a_k | 0 \rangle \\ &\quad - \mathcal{A}(n_{kk'} n_{ll'} n_{mm'} + \mathcal{S}(n_{kk'} C_{lml'm'})) , \end{aligned} \quad (7.2)$$

where  $\mathcal{A}$  and  $\mathcal{S}$  mean that the products in the parentheses are properly antisymmetrized and symmetrized under the exchange of single-particle indices [197]. The stationary conditions whose significance will become clear immediately below are written as

$$\begin{aligned} F_1(kk') &= \langle 0 | [a_k^\dagger a_k, \hat{H}] | 0 \rangle = 0 \\ F_2(klk'l') &= \langle 0 | [a_k^\dagger a_l^\dagger a_l a_k, \hat{H}] | 0 \rangle = 0 \\ F_3(klmk'l'm') &= \langle 0 | [a_k^\dagger a_l^\dagger a_m^\dagger a_m a_l a_k, \hat{H}] | 0 \rangle = 0 . \end{aligned} \quad (7.3)$$

Since a four-body correlation matrix is neglected, the expectation values of four-body operators in Eq.(7.3) are approximated by the products of  $n_{kk'}$ ,  $C_{klk'l'}$  and  $C_{klmk'l'm'}$ . Evaluation of the above conditions is straightforward and is given in Ref. [196] using the single-particle states which satisfy the HF-like mean-field hamiltonian

$$h(\rho)\phi_k(1) = \epsilon_k \phi_k(1) . \quad (7.4)$$

Here,  $h(\rho)$  is the mean-field Hamiltonian and  $\rho$  is the one-body density matrix given by  $\rho(1,1') = \sum_{kk'} n_{kk'} \phi_k(1) \phi_k^*(1')$  and numbers indicate spatial, spin and isospin coordinates. The three-body correlation matrix  $C_{klmk'l'm'}$  is necessary to make ERPA hermitian, as will be discussed below. To obtain the ground state implies that all quantities  $n_{kk'}$ ,  $C_{klk'l'}$ ,  $C_{klmk'l'm'}$  and  $\phi_k$  are determined under the conditions (7.3-7.4). It was found [198] that this task can be achieved using the gradient method: Starting from a simple ground state, such as the HF ground state, where  $n_{kk'}$ ,  $C_{klk'l'}$  and  $C_{klmk'l'm'}$

can be easily evaluated, we iterate

$$\begin{pmatrix} n(i+1) \\ C_2(i+1) \\ C_3(i+1) \end{pmatrix} = \begin{pmatrix} n(i) \\ C_2(i) \\ C_3(i) \end{pmatrix} - \alpha \begin{pmatrix} \frac{\delta F_1}{\delta n} & \frac{\delta F_1}{\delta C_2} & 0 \\ \frac{\delta F_2}{\delta n} & \frac{\delta F_2}{\delta C_2} & \frac{\delta F_2}{\delta C_3} \\ \frac{\delta F_3}{\delta n} & \frac{\delta F_3}{\delta C_2} & \frac{\delta F_3}{\delta C_3} \end{pmatrix}^{-1} \begin{pmatrix} F_1(i) \\ F_2(i) \\ F_3(i) \end{pmatrix}, \quad (7.5)$$

until convergence is achieved. Here,  $n$ ,  $C_2$  and  $C_3$  imply  $n_{kk'}$ ,  $C_{klk'l'}$ ,  $C_{klmk'l'm'}$ , respectively. Equation (7.5) is coupled to  $h\phi_k = \epsilon_k\phi_k$ , because  $h$  depends on  $n_{kk'}$ . The convergence process is controlled using a small parameter ( $\alpha$ ). The matrix consisting of the functional derivatives of  $F_1$ ,  $F_2$  and  $F_3$  has a close relation with the hamiltonian matrix of ERPA [198]. Therefore, the ground state is not independent of the excited states in ERPA. Of course, the equations (7.3) can also be written out explicitly and one can try to solve for the implied correlation functions. How this can be achieved is demonstrated in Sect.V.C with the very simple Lipkin model.

### B. Extended RPA (ERPA) equation

We consider an excitation operator consisting of one-body and two-body operators

$$\hat{Q}_\mu^\dagger = \sum_{kk'} x_{kk'}^\mu : a_k^\dagger a_{k'} : + \sum_{k_1 k_2 k'_1 k'_2} X_{k_1 k_2 k'_1 k'_2}^\mu : a_{k_1}^\dagger a_{k_2}^\dagger a_{k'_2} a_{k'_1} : , \quad (7.6)$$

where  $: :$  implies that uncorrelated parts consisting of lower-level operators are to be subtracted; for example,

$$\begin{aligned} : a_{k'}^\dagger a_k : &= a_{k'}^\dagger a_k - n_{kk'} \\ : a_{k'}^\dagger a_{l'}^\dagger a_l a_k : &= a_{k'}^\dagger a_{l'}^\dagger a_l a_k - \mathcal{AS}(n_{kk'} : a_{l'}^\dagger a_l : ) \\ &\quad - [\mathcal{A}(n_{kk'} n_{ll'}) + C_{klk'l'}] . \end{aligned} \quad (7.7)$$

where  $\mathcal{AS}$  stands for properly antisymmetrized and symmetrized. The ERPA equations are derived using the EOM method minimizing, as usual, the energy weighted sum-rule (2.7). In the evaluation of the matrix elements we approximate the ERPA ground state with  $|0\rangle$  which satisfy Eqs. (7.3)-(7.4). The ERPA equations are written as

$$\begin{pmatrix} A & C \\ B & D \end{pmatrix} \begin{pmatrix} x^\mu \\ X^\mu \end{pmatrix} = \Omega_\mu \begin{pmatrix} S_1 & T_1 \\ T_2 & S_2 \end{pmatrix} \begin{pmatrix} x^\mu \\ X^\mu \end{pmatrix}, \quad (7.8)$$

where the matrix elements are given by

$$\begin{aligned} A(kk' : mm') &= \langle 0 | [[ : a_{k'}^\dagger a_k : , \hat{H} ], : a_m^\dagger a_{m'} : ] | 0 \rangle \\ B(klk'l' : mm') &= \langle 0 | [[ : a_{k'}^\dagger a_{l'}^\dagger a_l a_k : , \hat{H} ], : a_m^\dagger a_{m'} : ] | 0 \rangle \\ C(kk' : m_1 m_2 m'_1 m'_2) &= \langle 0 | [[ : a_{k'}^\dagger a_k : , \hat{H} ], : a_{m_1}^\dagger a_{m_2}^\dagger a_{m'_2} a_{m'_1} : ] | 0 \rangle \\ D(klk'l' : m_1 m_2 m'_1 m'_2) &= \langle 0 | [[ : a_{k'}^\dagger a_{l'}^\dagger a_l a_k : , \hat{H} ], : a_{m_1}^\dagger a_{m_2}^\dagger a_{m'_2} a_{m'_1} : ] | 0 \rangle , \end{aligned} \quad (7.9)$$

$$\begin{aligned} S_1(kk' : mm') &= \langle 0 | [ : a_{k'}^\dagger a_k : , : a_m^\dagger a_{m'} : ] | 0 \rangle \\ T_1(kk' : m_1 m_2 m'_1 m'_2) &= \langle 0 | [ : a_{k'}^\dagger a_k : , : a_{m_1}^\dagger a_{m_2}^\dagger a_{m'_2} a_{m'_1} : ] | 0 \rangle \\ T_2(klk'l' : mm') &= \langle 0 | [ : a_{k'}^\dagger a_{l'}^\dagger a_l a_k : , : a_m^\dagger a_{m'} : ] | 0 \rangle \\ S_2(klk'l' : m_1 m_2 m'_1 m'_2) &= \langle 0 | [ : a_{k'}^\dagger a_{l'}^\dagger a_l a_k : , : a_{m_1}^\dagger a_{m_2}^\dagger a_{m'_2} a_{m'_1} : ] | 0 \rangle . \end{aligned} \quad (7.10)$$

When the ground-state correlations are neglected, Eq. (7.8) and the one-body section of Eq. (7.8),  $Ax^\mu = \Omega_\mu S_1 x^\mu$ , are equivalent to SRPA and RPA, respectively.

Above equations give the ERPA scheme in its most general form. Below we will discuss some of the important properties of these equations, notably that they conserve all desirable and nice properties of standard RPA

as conservation laws, sum-rules, Goldstone modes, etc.

### C. Hermiticity of ERPA matrix

The hamiltonian matrix on the left hand side of Eq. (7.8) is hermitian. This is because the following opera-

tor identity for  $\hat{A}$  and  $\hat{B}$ , which are either  $:a_{k'}^\dagger a_k:$  or  $:a_{k'}^\dagger a_{l'}^\dagger a_l a_k:$ ,

$$\begin{aligned} & \langle 0 | [[\hat{B}, \hat{H}], \hat{A}] | 0 \rangle - \langle 0 | [[\hat{A}, \hat{H}], \hat{B}] | 0 \rangle \\ &= \langle 0 | [\hat{H}, [\hat{A}, \hat{B}]] | 0 \rangle = 0, \end{aligned} \quad (7.11)$$

is satisfied due to the ground-state conditions of Eqs. (7.3). We show this explicitly for the matrix  $D$  where  $\hat{A}$  and  $\hat{B}$  are both two-body operators  $:a_{k'}^\dagger a_l^\dagger a_l a_k:$  and  $:a_{m_1}^\dagger a_{m_2}^\dagger a_{m_2'} a_{m_1'}:$ , respectively. Since  $[\hat{A}, \hat{B}]$  consists of at most three-body operators, Eq. (7.11) holds because of Eqs. (7.3). This means

$$D(klk'l' : m_1 m_2 m_1' m_2') = D(m_1' m_2' m_1 m_2 : k'l'kl). \quad (7.12)$$

From its definition the hermitian conjugate of  $D$  is

$$D(m_1 m_2 m_1' m_2' : klk'l')^* = D(m_1' m_2' m_1 m_2 : k'l'kl). \quad (7.13)$$

Eqs. (7.12) and (7.13) imply that  $D$  is hermitian, namely,

$$D(klk'l' : m_1 m_2 m_1' m_2') = D(m_1 m_2 m_1' m_2' : klk'l')^*. \quad (7.14)$$

The following symmetries of other matrices  $A$ ,  $B$  and  $C$  are shown in a similar way:

$$\begin{aligned} A(kk' : mm') &= A(m'm : k'k) = A(mm' : kk')^* \\ C(kk' : m_1 m_2 m_1' m_2') &= B(m_1' m_2' m_1 m_2 : k'k) \\ &= B(m_1 m_2 m_1' m_2' : kk')^*. \end{aligned} \quad (7.15)$$

Therefore, the hamiltonian matrix in Eq. (7.8) is hermitian. The three-body correlation matrix is necessary for Eq. (7.14), whereas Eqs. (7.15) hold without it. The matrices  $S_1$ ,  $T_1$ ,  $T_2$  and  $S_2$  have the following properties

$$\begin{aligned} S_1(kk' : mm')^* &= S_1(mm' : kk') = -S_1(k'k : m'm) \\ T_1(kk' : m_1 m_2 m_1' m_2')^* &= T_2(m_1 m_2 m_1' m_2' : kk') = -T_1(k'k : m_1' m_2' m_1 m_2) \\ T_2(klk'l' : mm')^* &= T_1(mm' : klk'l') = -T_2(k'l'kl : m'm) \\ S_2(klk'l' : m_1 m_2 m_1' m_2')^* &= S_2(m_1 m_2 m_1' m_2' : klk'l') = -S_2(k'l'kl : m_1' m_2' m_1 m_2). \end{aligned} \quad (7.16)$$

Therefore, also the norm matrix in Eq. (7.8) is hermitian. Taking hermitian conjugate of Eq. (7.8) and using the above symmetries, we can show that when

$$\begin{pmatrix} x_{kk'}^\mu \\ X_{klk'l'}^\mu \end{pmatrix}$$

is a positive energy solution with  $\Omega_\mu(>0)$ ,

$$\begin{pmatrix} x_{k'k}^{\mu *} \\ X_{k'l'kl}^{\mu *} \end{pmatrix}$$

is a negative energy solution with  $-\Omega_\mu$  as in RPA and other extended RPA theories [195].

#### D. Orthonormal condition

For a hermitian hamiltonian matrix the orthonormal condition is given as [199]

$$(x^{\mu *} \ X^{\mu *}) \begin{pmatrix} S_1 & T_1 \\ T_2 & S_2 \end{pmatrix} \begin{pmatrix} x^{\mu'} \\ X^{\mu'} \end{pmatrix} = \pm \delta_{\mu\mu'}, \quad (7.17)$$

where the negative sign is for a negative-energy solution. Accordingly, the closure relation is written as

$$\begin{aligned} & \sum_{\Omega_\mu > 0} \begin{pmatrix} x^\mu \\ X^\mu \end{pmatrix} (x^{\mu *} \ X^{\mu *}) \begin{pmatrix} S_1 & T_1 \\ T_2 & S_2 \end{pmatrix} \\ & - \sum_{\Omega_\mu > 0} \begin{pmatrix} x_{k'k}^{\mu *} \\ X_{k'l'kl}^{\mu *} \end{pmatrix} (x_{k'k}^\mu \ X_{k'l'kl}^\mu) \begin{pmatrix} S_1 & T_1 \\ T_2 & S_2 \end{pmatrix} = I, \end{aligned} \quad (7.18)$$

where  $I$  is the unit matrix.

#### E. Energy-weighted sum rule

We discuss the energy-weighted sum rule and show that the Thouless theorem [200] is satisfied. We consider a hermitian operator

$$\begin{aligned} \hat{F} &= F_0 + \sum_{mm'} f_{mm'} : a_m^\dagger a_{m'} : \\ &+ \sum_{m_1 m_2 m_1' m_2'} F_{m_1 m_2 m_1' m_2'} : a_{m_1}^\dagger a_{m_2}^\dagger a_{m_2'} a_{m_1'} : , \end{aligned} \quad (7.19)$$

where  $F_0$  is  $\langle 0 | \hat{F} | 0 \rangle$ . Since the one-body and two-body transition amplitudes  $z_{kk'}^\mu = \langle 0 | : a_{k'}^\dagger a_k : | \mu \rangle$  and



$Z_{klk'l'}^\mu = \langle 0 | : a_{k'}^\dagger a_{l'}^\dagger a_l a_k : | \mu \rangle$  are given by

$$\begin{pmatrix} z^\mu \\ Z^\mu \end{pmatrix} = \begin{pmatrix} S_1 & T_1 \\ T_2 & S_2 \end{pmatrix} \begin{pmatrix} x^\mu \\ X^\mu \end{pmatrix}, \quad (7.20)$$

the energy-weighted strength  $m_1$  is written as

$$\begin{aligned} m_1 &= \sum_{\Omega_\mu > 0} \Omega_\mu |\langle 0 | \hat{F} | \mu \rangle|^2 \\ &= \sum_{\Omega_\mu > 0} \Omega_\mu (f \ F) \begin{pmatrix} z^\mu \\ Z^\mu \end{pmatrix} (z^{\mu*} \ Z^{\mu*}) \begin{pmatrix} f \\ F \end{pmatrix}. \end{aligned} \quad (7.21)$$

Taking into account the contribution of negative-energy solutions and using Eqs. (7.8) and (7.18), we can show [201] that the Thouless theorem holds, that is,

$$m_1 = \frac{1}{2} \langle 0 | [[\hat{F}, \hat{H}], \hat{F}] | 0 \rangle. \quad (7.22)$$

The important point is that  $\hat{F}$  can be both one-body and two-body operators.

### F. Spurious modes in ERPA and SCRPA

We show that ERPA gives zero excitation energy to spurious modes associated with operators  $\hat{F}$  which commute with the hamiltonian, that is,  $[\hat{F}, \hat{H}] = 0$ . This actually holds for situations for which the ground state determined by Eqs. (7.3)-(7.4) has a spontaneously broken symmetry. The operator  $\hat{F}$  can be both one-body

and two-body operators

$$\hat{F} = F_0 + \sum_{kk'} f_{k'k} : a_{k'}^\dagger a_k : + \sum_{klk'l'} F_{k'l'kl} : a_{k'}^\dagger a_{l'}^\dagger a_l a_k :. \quad (7.23)$$

This means that our discussion holds for spurious modes associated with two-body operators, such as double excitation of translational motion. We consider  $\Omega_\mu \langle 0 | \hat{F} | \mu \rangle$ , where  $\langle 0 | \hat{F} | \mu \rangle \neq 0$  because the ground state has a broken symmetry. Using Eqs. (7.8), we obtain [201]

$$\begin{aligned} \Omega_\mu \langle 0 | \hat{F} | \mu \rangle &= \Omega_\mu (f \ F) \begin{pmatrix} S_1 & T_1 \\ T_2 & S_2 \end{pmatrix} \begin{pmatrix} x^\mu \\ X^\mu \end{pmatrix} \\ &= (f \ F) \begin{pmatrix} A & C \\ B & D \end{pmatrix} \begin{pmatrix} x^\mu \\ X^\mu \end{pmatrix} \\ &= \langle 0 | [[\hat{F}, \hat{H}], \hat{Q}_\mu^\dagger] | 0 \rangle = 0. \end{aligned} \quad (7.24)$$

This implies  $\Omega_\mu = 0$  for spurious modes. Equation (7.24) also implies that the transition amplitudes of the symmetry operator  $\hat{F}$  vanish for physical excited states, because  $\Omega_\mu \neq 0$  in such cases.

### G. Approximate forms of ERPA

The calculation of the three-body correlation matrix for realistic hamiltonians is very difficult. We derive two approximate forms of ERPA without the three-body correlation matrix, which can be used for realistic applications.

#### 1. Hamiltonian matrix of ERPA

We rewrite the hamiltonian matrix in ERPA in a different way using the commutation relations between the hamiltonian and one-body and two-body operators, which are written as

$$[: a_{k'}^\dagger a_k :, \hat{H}] = \sum_{mm'} a(kk' : mm') : a_{m'}^\dagger a_m : + \sum_{m_1 m_2 m'_1 m'_2} c(kk' : m_1 m_2 m'_1 m'_2) : a_{m'_1}^\dagger a_{m'_2}^\dagger a_{m_2} a_{m_1} : , \quad (7.25)$$

$$\begin{aligned} [: a_{k'}^\dagger a_{l'}^\dagger a_l a_k :, \hat{H}] &= \sum_{mm'} b(klk'l' : mm') : a_{m'}^\dagger a_m : + \sum_{m_1 m_2 m'_1 m'_2} d(klk'l' : m_1 m_2 m'_1 m'_2) : a_{m'_1}^\dagger a_{m'_2}^\dagger a_{m_2} a_{m_1} : \\ &+ \sum_{m_1 m_2 m_3 m'_1 m'_2 m'_3} e(klk'l' : m_1 m_2 m_3 m'_1 m'_2 m'_3) : a_{m'_1}^\dagger a_{m'_2}^\dagger a_{m'_3}^\dagger a_{m_3} a_{m_2} a_{m_1} : . \end{aligned} \quad (7.26)$$

The matrices  $a$ ,  $b$ ,  $c$ ,  $d$  and  $e$  are explicitly given in Ref. [196]. The ground-state conditions of Eqs. (7.3) and (7.4) are employed in the derivation of these matrices. The matrices  $a$ ,  $b$ ,  $c$ ,  $d$  and  $e$  are equivalent to  $\delta F_1/\delta n$ ,  $\delta F_2/\delta n$ ,  $\delta F_1/\delta C_2$ ,  $\delta F_2/\delta C_2$ ,  $\delta F_2/\delta C_3$  in Eq. (7.5), respectively

[196]. Using  $a$ ,  $b$ ,  $c$ ,  $d$  and  $e$ , the matrices  $A$ ,  $B$ ,  $C$  and

$D$  in ERPA are written as

$$\begin{aligned}
A &= \langle 0 | [ [ a_{k'}^\dagger a_k :, \hat{H} ], : a_m^\dagger a_{m'} : ] | 0 \rangle \\
&= aS_1 + cT_2 \\
B &= \langle 0 | [ [ a_{k'}^\dagger a_l^\dagger a_l a_k :, \hat{H} ], : a_m^\dagger a_{m'} : ] | 0 \rangle \\
&= bS_1 + dT_2 + eT_{31} \\
C &= \langle 0 | [ [ a_{k'}^\dagger a_k :, \hat{H} ], : a_{m_1}^\dagger a_{m_2}^\dagger a_{m_2'} a_{m_1'} : ] | 0 \rangle \\
&= aT_1 + cS_2 \\
D &= \langle 0 | [ [ a_{k'}^\dagger a_l^\dagger a_l a_k :, \hat{H} ], : a_{m_1}^\dagger a_{m_2}^\dagger a_{m_2'} a_{m_1'} : ] | 0 \rangle \\
&= bT_1 + dS_2 + eT_{32} , \tag{7.27}
\end{aligned}$$

where

$$\begin{aligned}
T_{31} &= \langle 0 | [ [ a_{k'}^\dagger a_l^\dagger a_{m'}^\dagger a_m a_l a_k :, : a_m^\dagger a_{m'} : ] | 0 \rangle \\
T_{32} &= \langle 0 | [ [ a_{k'}^\dagger a_l^\dagger a_{m'}^\dagger a_m a_l a_k :, : a_{m_1}^\dagger a_{m_2}^\dagger a_{m_2'} a_{m_1'} : ] | 0 \rangle . \tag{7.28}
\end{aligned}$$

Since a four-body correlation matrix is not considered, expectation values of four-body operators in  $T_{32}$

are approximated by the products of  $n_{\alpha\alpha'}$ ,  $C_{klk'l'}$  and  $C_{klmk'l'm'}$ .

## 2. STDDM

Here we discuss the relation of ERPA and the Small amplitude limit of the Time-Dependent Density-Matrix (STDDM) theory [202] which has been used for realistic cases [203, 204]. When the three-body correlation matrix  $C_{klmk'l'm'}$  and the matrix  $e$  in Eq. (7.26) are neglected, the ERPA equations in this approximation are written as

$$\begin{pmatrix} A & C' \\ B' & D' \end{pmatrix} \begin{pmatrix} x^\mu \\ X^\mu \end{pmatrix} = \Omega_\mu \begin{pmatrix} S_1 & T_1 \\ T_2 & S_2' \end{pmatrix} \begin{pmatrix} x^\mu \\ X^\mu \end{pmatrix} , \tag{7.29}$$

where  $S_2'$  does not have the three-body correlation matrix, and  $B'$ ,  $C'$  and  $D'$  are given by  $B' = bS_1 + dT_2$ ,  $C' = aT_1 + cS_2'$  and  $D' = bT_1 + dS_2'$ , respectively. Other matrices in Eq.(7.29) are the same as those in ERPA.

Equation (7.29) can be written in a different form as

$$\begin{aligned}
\begin{pmatrix} A & C' \\ B' & D' \end{pmatrix} \begin{pmatrix} x^\mu \\ X^\mu \end{pmatrix} &= \begin{pmatrix} aS_1 + cT_2 & aT_1 + cS_2' \\ bS_1 + dT_2 & bT_1 + dS_2' \end{pmatrix} \begin{pmatrix} x^\mu \\ X^\mu \end{pmatrix} \\
&= \begin{pmatrix} a & c \\ b & d \end{pmatrix} \begin{pmatrix} S_1 & T_1 \\ T_2 & S_2' \end{pmatrix} \begin{pmatrix} x^\mu \\ X^\mu \end{pmatrix} = \Omega_\mu \begin{pmatrix} S_1 & T_1 \\ T_2 & S_2' \end{pmatrix} \begin{pmatrix} x^\mu \\ X^\mu \end{pmatrix} . \tag{7.30}
\end{aligned}$$

Using the transition amplitude

$$\begin{pmatrix} z^\mu \\ Z^\mu \end{pmatrix} = \begin{pmatrix} S_1 & T_1 \\ T_2 & S_2' \end{pmatrix} \begin{pmatrix} x^\mu \\ X^\mu \end{pmatrix} , \tag{7.31}$$

Eq.(7.29) is written as

$$\begin{pmatrix} a & c \\ b & d \end{pmatrix} \begin{pmatrix} z^\mu \\ Z^\mu \end{pmatrix} = \Omega_\mu \begin{pmatrix} z^\mu \\ Z^\mu \end{pmatrix} . \tag{7.32}$$

This is the form derived as the small amplitude limit of TDDM. The effects of ground-state correlations are included in STDDM, because the matrices  $a$ ,  $b$  and  $d$  in Eq. (7.32) contain  $n_{kk'}$  and  $C_{klmk'l'm'}$ .

## 3. Modified STDDM

When we keep the matrix  $e$  and neglect the three-body correlation matrix  $C_{klmk'l'm'}$  in Eq. (7.8), we obtain

$$\begin{pmatrix} A & C' \\ B' & D'' \end{pmatrix} \begin{pmatrix} x^\mu \\ X^\mu \end{pmatrix} = \Omega_\mu \begin{pmatrix} S_1 & T_1 \\ T_2 & S_2' \end{pmatrix} \begin{pmatrix} x^\mu \\ X^\mu \end{pmatrix} , \tag{7.33}$$

where  $D'' = bT_1 + dS_2' + eT_{32}'$ . Here  $T_{32}'$  does not contain the three-body correlation matrix. The last term in  $D''$  gives significant improvement of the description of two-phonon states [205]. We refer to this approximation of ERPA as mSTDDM (modified STDDM). In STDDM and mSTDDM, the hermiticity of  $D'$  and  $D''$  is lost. However, non-hermiticity does not cause any serious problems in the following applications.

## H. particle-particle ERPA equation

In this subsection we present very briefly an extended particle-particle RPA which can be formulated in a way similar to the particle-hole RPA using EOM method. We consider an excitation operator consisting of one-body and two-body parts

$$\hat{Q}_\mu^\dagger = \sum_{kk'} x_{kk'}^\mu a_k^\dagger a_{k'}^\dagger + \sum_{k_1 k_2 k_2' k_1'} \mathcal{X}_{k_1 k_2 k_2' k_1'}^\mu : a_{k_1}^\dagger a_{k_2}^\dagger a_{k_2'}^\dagger a_{k_1'}^\dagger : . \tag{7.34}$$

In the evaluation of the matrix elements we approximate the ppERPA ground state with  $|0\rangle$  which satisfy Eqs.

(7.3-7.4). The ERPA equations are written as

$$\begin{pmatrix} \mathcal{A} & \mathcal{C} \\ \mathcal{B} & \mathcal{D} \end{pmatrix} \begin{pmatrix} x^\mu \\ \mathcal{X}^\mu \end{pmatrix} = \Omega_\mu \begin{pmatrix} \mathcal{S}_1 & \mathcal{T}_1 \\ \mathcal{T}_2 & \mathcal{S}_2 \end{pmatrix} \begin{pmatrix} x^\mu \\ \mathcal{X}^\mu \end{pmatrix}, \quad (7.35)$$

where the matrix elements are given by

$$\begin{aligned} \mathcal{A}(kk' : mm') &= \langle 0 | [[a_{k'} a_k, \hat{H}], a_m^\dagger a_{m'}^\dagger] | 0 \rangle \\ \mathcal{B}(klk'l' : mm') &= \langle 0 | [[a_{k'}^\dagger a_{l'} a_l a_k, \hat{H}], a_m^\dagger a_{m'}^\dagger] | 0 \rangle \\ \mathcal{C}(kk' : m_1 m_2 m'_1 m'_2) &= \langle 0 | [[a_{k'} a_k, \hat{H}], a_{m_1}^\dagger a_{m_2}^\dagger a_{m'_1}^\dagger a_{m'_2}^\dagger] | 0 \rangle \\ \mathcal{D}(klk'l' : m_1 m_2 m'_1 m'_2) &= \langle 0 | [[a_{k'}^\dagger a_{l'} a_l a_k, \hat{H}], a_{m_1}^\dagger a_{m_2}^\dagger a_{m'_1}^\dagger a_{m'_2}^\dagger] | 0 \rangle, \end{aligned} \quad (7.36)$$

$$\begin{aligned} \mathcal{S}_1(kk' : mm') &= \langle 0 | [a_{k'} a_k, a_m^\dagger a_{m'}^\dagger] | 0 \rangle \\ \mathcal{T}_1(kk' : m_1 m_2 m'_1 m'_2) &= \langle 0 | [a_{k'} a_k, a_{m_1}^\dagger a_{m_2}^\dagger a_{m'_1}^\dagger a_{m'_2}^\dagger] | 0 \rangle \\ \mathcal{T}_2(klk'l' : mm') &= \langle 0 | [a_{k'}^\dagger a_{l'} a_l a_k, a_m^\dagger a_{m'}^\dagger] | 0 \rangle \\ \mathcal{S}_2(klk'l' : m_1 m_2 m'_1 m'_2) &= \langle 0 | [a_{k'}^\dagger a_{l'} a_l a_k, a_{m_1}^\dagger a_{m_2}^\dagger a_{m'_1}^\dagger a_{m'_2}^\dagger] | 0 \rangle. \end{aligned} \quad (7.37)$$

Similar considerations and approximations as in the *ph* case can also be performed in this *pp* case, but nothing has been worked out so far in the literature and, thus, we will also not go further here. Nonetheless, a small application will be given in the next section.

## VIII. APPLICATIONS

### A. Self-consistent second RPA in the exactly solvable single shell pairing model

As a first small, but instructive exercise we want to solve the single shell pairing (seniority) model [5, 206]. This model is usually easily solved with angular momentum algebra. However, here we want to solve it with the EOM technique, which is a new rather interesting many-body way of solution. The Hamiltonian of the single shell seniority model is

$$H = -GS_+ S_- , \quad (8.1)$$

where

$$S_+ = \sum_{m>0} c_m^\dagger c_{-m} , \quad (8.2)$$

with  $S_- = (S_+)^\dagger$  and  $m$  being the magnetic quantum numbers of the  $j$ -shell. The sum over the magnetic quantum numbers runs over  $\Omega = j + 1/2$  states. We make the following ppERPA ansatz for the pair addition operator which is a simplified form of (7.34)

$$\begin{aligned} A^\dagger &= X_1 S_+ + X_2 S_+ S_0 \\ A &= X_1 S_- + X_2 S_0 S_- , \end{aligned} \quad (8.3)$$

and for the removal operator

$$\begin{aligned} R^\dagger &= Z_1 S_- + Z_2 S_0 S_- \\ R &= Z_1 S_+ + Z_2 S_+ S_0 . \end{aligned} \quad (8.4)$$

It is not difficult to see that with certain relations among the variational amplitudes, one can fulfill the exact annihilating conditions

$$A|0\rangle = R|0\rangle = 0 . \quad (8.5)$$

These operators obey the following orthonormalization conditions

$$\begin{aligned} \langle [A, A^\dagger] \rangle &= X_1^2 N_{11} + X_1 X_2 (N_{12} + N_{21}) + X_2^2 N_{22} = 1 \\ \langle [R, R^\dagger] \rangle &= Z_1^2 N_{11} + Z_1 Z_2 (N_{12} + N_{21} + Z_2^2 N_{22}) = -1 , \end{aligned} \quad (8.6)$$

where

$$\begin{aligned} N_{11} &= \langle [S_-, S_+] \rangle = -2\langle S_0 \rangle \\ N_{12} &= N_{21} = \langle S_-, S_+ S_0 \rangle = -2\langle S_0^2 \rangle + \langle S_+ S_- \rangle \\ N_{22} &= \langle S_0 S_-, S_+ S_0 \rangle = -2\langle S_0^3 \rangle + \langle S_+ S_- (2S_0 - 1) \rangle . \end{aligned} \quad (8.7)$$

By simple manipulations with backward and forward amplitudes we can invert (8.3) and (8.4) and obtain the following expressions for  $S_+$  and  $S_+S_0$

$$S_+ = \frac{Z_2 A^\dagger - X_2 R}{Z_2 X_1 - X_2 Z_1}; \quad S_+ S_0 = \frac{Z_1 A^\dagger - X_1 R}{Z_1 X_2 - X_1 Z_2}, \quad (8.8)$$

and  $S_-$  and  $S_0 S_-$  are obtained by hermitian conjugation. From above relations we obtain

$$\langle S_+ S_- \rangle = \frac{X_2^2}{(Z_2 X_1 - X_2 Z_1)^2}. \quad (8.9)$$

Applying the EOM method to the addition and removal mode in the usual way we obtain

$$\begin{pmatrix} A & B \\ B & C \end{pmatrix} \begin{pmatrix} X_1 \\ X_2 \end{pmatrix} = \omega_a \begin{pmatrix} N_{11} & N_{12} \\ N_{21} & N_{22} \end{pmatrix} \begin{pmatrix} X_1 \\ X_2 \end{pmatrix}, \quad (8.10)$$

and same for removal mode

$$\begin{pmatrix} A & B \\ B & C \end{pmatrix} \begin{pmatrix} Z_1 \\ Z_2 \end{pmatrix} = -\omega_r \begin{pmatrix} N_{11} & N_{12} \\ N_{21} & N_{22} \end{pmatrix} \begin{pmatrix} Z_1 \\ Z_2 \end{pmatrix}, \quad (8.11)$$

where

$$\begin{aligned} A &= \langle [S_-, [H, S_+]] \rangle = 2GN_{12} \\ B &= \langle [S_0 S_-, [H, S_+]] \rangle = 2GN_{22} \\ C &= \langle [S_0 S_-, [H, S_+ S_0]] \rangle \\ &= 2G \langle -2S_0^4 + S_+ S_- (3S_0^2 - 3S_0 + 1) \rangle. \end{aligned} \quad (8.12)$$

The system of equations contains the operator  $S_0$  which in the seniority model is expressed as [5]  $2S_0 = \hat{N} - \Omega$ . Therefore, in all expressions  $\hat{N}$  can be replaced by the appropriate particle number. At this moment the system of equations (8.10, 8.11) is closed and can be solved with the usual methods. It turns out that the exact solution is obtained. It may be worthwhile to notice that the seniority model also can be solved with the corresponding Dyson-BSE. It just corresponds to the transcription of the eigenvalue problem into the Green's function approach.

Actually, the seniority model can also be solved with the s.p. Dyson equation in evaluating the 2p-1h Green's function figuring in the self-energy with the EOM method as described in Sect. V and in [206]. So, in this simple case of the seniority model even and odd SCRPA's are decoupled. However, already on the level of the Lipkin model both equations become coupled and then constitute together a powerful system of equations for the solution of the many-body problem.

Next, we present the results for the Lipkin model [157] and the Hubbard model using the original form of ERPA with the three-body correlation matrix. We also review the main results for the quadrupole states in  $^{16}\text{O}$  and  $^{40}\text{Ca}$  calculated using STDDM.

## B. Lipkin model

We consider the standard two-level Lipkin model of Eq. (5.41). The excitation energies of the first and second excited states are displayed in Fig. 38 as functions of  $\chi = (N-1)|V|/\epsilon$  for  $N=4$  [207]. We see that ERPA (squares) performs extremely well for the first excited state, even far beyond the RPA instability point of  $\chi=1$ . SCRPA (circles) also is very good, but deteriorate after the instability point. In the case of the second excited state which can be obtained with ERPA, deviation from the exact solution becomes larger with increasing  $\chi$ . This can be explained either by the neglect of the coupling to higher amplitudes or by the fact that in ERPA non-collective amplitudes are not included. The occupation probabilities of the upper state are also reasonably well reproduced in ERPA and SCRPA as shown in Fig. 39.

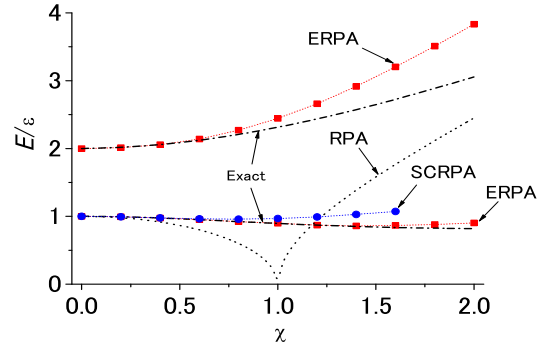


FIG. 38. Excitation energies of the first and second excited states in the Lipkin model calculated in ERPA (squares), SCRPA (circles) and RPA (dotted line) as functions of  $\chi = (N-1)|V|/\epsilon$  for  $N=4$ . The exact solutions are shown with the dot-dashed lines. Readapted from Ref. [207].

## C. Hubbard model

As the next model we consider the one-dimensional six-site Hubbard model with half-filling (see Eq. (3.21)). In the ERPA calculations we take only the 2p-2h and 2h-2p components of  $X_{\alpha\beta\alpha'\beta'}^\mu$  to facilitate the numerics. The excitation energy of the first excited state, which is the spin mode with momentum transfer  $|q| = \pi$ , is shown in Fig. 40 as a function of  $U/t$  [207]. The results in ERPA (squares) show good agreement with the exact values (dot-dashed line). The SCRPA results (filled circles) are reasonable and avoid the instability of RPA (open circles). The SCRPA results in Fig. 40 are, however, less good than the ones in [42], that is, no SCRPA solutions exist beyond  $U/t = 3$ . This is due to the fact

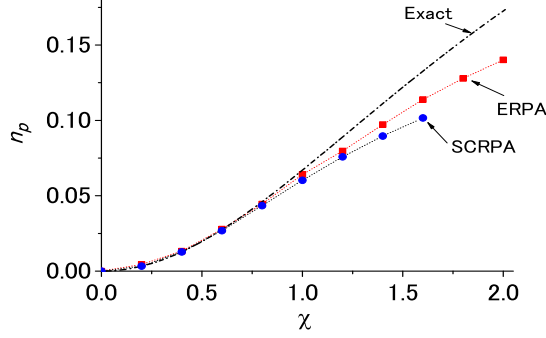


FIG. 39. Occupation probabilities of the upper state in the Lipkin model calculated in ERPA (squares) and SCRPA (circles) as functions of  $\chi$  for  $N = 4$ . The exact solutions are shown with the dot-dashed lines. Readapted from Ref. [207].

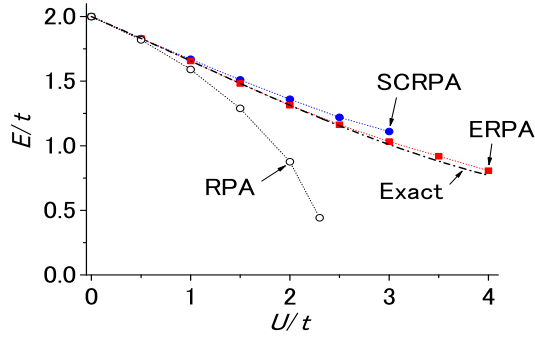


FIG. 40. Excitation energy of the first excited state (the spin mode with momentum transfer  $|q| = \pi$ ) calculated in ERPA (squares) and SCRPA (circles) as a function of  $U/t$  for the six-site Hubbard model with half-filling. The exact values are shown with the dot-dashed line. The open circles depict the results in RPA. Readapted from Ref. [207].

that the implicit cross excitation mode couplings involved in  $n_{\alpha\alpha}$  and  $C_{\alpha\beta\alpha'\beta'}$  are neglected in [42].

Let us mention that ERPA can only be tackled at the moment for simple models. In realistic cases this approach becomes numerically too complicated and has to be simplified as, e.g., in STDDM or mSTDDM or even more drastic approximations.

#### D. Damping of giant resonances

Applications to the Isoscalar Giant Quadrupole Resonances (ISGQR) in  $^{16}\text{O}$  [204] and  $^{40}\text{Ca}$  [208] have been done using the simplified version of ERPA, that is, STDDM. A simplified Skyrme force has been adapted as the effective interaction for the mean-field potential and also as the residual interaction. Assuming that single-

particle states around the Fermi energy are most important for ground-state correlations, we use the  $1p_{3/2}$ ,  $1p_{1/2}$ ,  $1d_{5/2}$  and  $2s_{1/2}$  states to calculate  $n_{\alpha\alpha'}$ ,  $C_{\alpha\beta\alpha'\beta'}$  and  $X_{\alpha\beta\alpha'\beta'}^\mu$  for  $^{16}\text{O}$  and the  $1d_{5/2}$ ,  $2s_{1/2}$ ,  $1d_{3/2}$  and  $1f_{1/2}$  states for  $^{40}\text{Ca}$ , and only the 2p-2h and 2h-2p components of  $C_{\alpha\beta\alpha'\beta'}$  and  $X_{\alpha\beta\alpha'\beta'}^\mu$  are considered to facilitate the numerics. To satisfy the energy weighted sum rule, we use a large number of single-particle states to calculate the one-body transition amplitude: The continuum states are discretized by confining the single-particle wave functions in a sphere of radius 20 fm and all single-particle states with  $\epsilon \leq 40$  MeV and the orbital angular momentum  $\ell \leq 5\hbar$  are taken. In Figs. 41 and

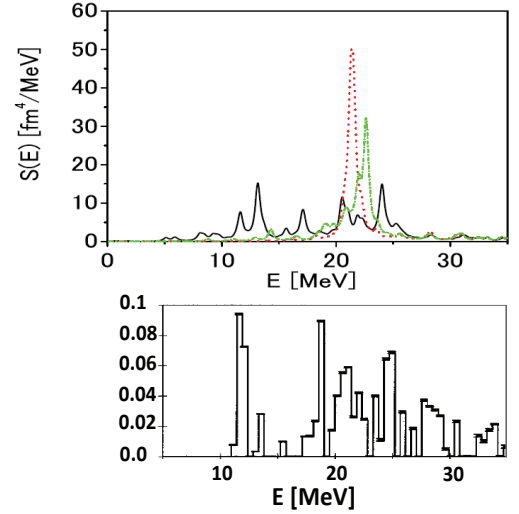


FIG. 41. Upper panel: strength functions for the isoscalar quadrupole states in  $^{16}\text{O}$  calculated in STDDM (solid line), SRPA (dot-dashed line) and RPA (dotted line). The strength functions are smoothed with  $\Gamma = 0.5$  MeV. Adopted from Ref. [204]; lower panel: experimental strength function for the ISGQR from [209].

42 the strength functions for ISGQR in  $^{16}\text{O}$  and  $^{40}\text{Ca}$  calculated in STDDM are compared with the results of RPA and SRPA. The sharp peak in RPA corresponds to the ISGQR. STDDM gives much larger fragmentation of the quadrupole strength than SRPA. In the lower panel of Fig. 41 the experimental distribution [209] is reproduced. Good agreement with theory can be seen. This large fragmentation, especially the concentration of the strength in the region below ISGQR, is also consistent with experiment for  $^{40}\text{Ca}$  [211, 212]. Main components of the peaks located below ISGQR are 2p-2h configurations. In the case of  $^{16}\text{O}$ , for example, they are either  $[1d_{5/2}(p)1d_{5/2}(n)(1p_{3/2}(p))^{-1}(1p_{1/2}(n))^{-1}]$  or  $[1d_{5/2}(p)1d_{5/2}(n)(1p_{1/2}(p))^{-1}(1p_{3/2}(n))^{-1}]$ , where  $(p)$  and  $(n)$  denote proton and neutron states, respectively. This means that proton-neutron correlations play an im-

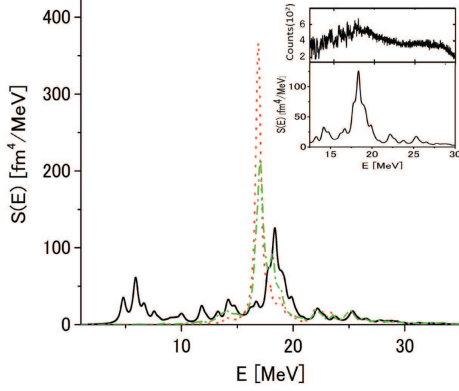


FIG. 42. Strength functions calculated in STDDM (solid line), SRPA (dot-dashed line) and RPA (dotted line) for the isoscalar quadrupole excitation in  $^{40}\text{Ca}$ . The distributions are smoothed with an artificial width  $\Gamma = 0.5$  MeV. In the inset the STDDM strength distribution (lower part) is compared with the experimental data from  $(p, p')$  experiments at  $E_p = 200$  MeV and  $\theta_{\text{Lab}} = 11^\circ$  [210] (upper part). Adopted from Ref. [208].

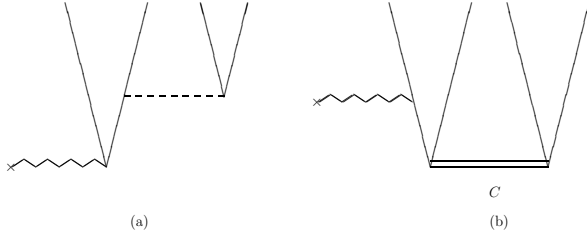


FIG. 43. (a) Damping process both in STDDM and SRPA. (b) Process only in STDDM. The wavy line means an external field (the quadrupole field in this case), the dashed line is the interaction and the vertical lines indicate either particle states or hole states. The double line with  $C$  means  $C_{\alpha\beta\alpha'\beta'}$ .

portant role in the splitting of ISGQR in  $^{16}\text{O}$  and also in  $^{40}\text{Ca}$ . The difference between the STDDM and SRPA results also indicates the importance of ground-state correlations. In fact, the process shown diagrammatically in Fig. 43(b), which involves the ground-state correlations, is responsible for the enhancement of the strength in the low-energy region [204, 208]. In the inset of Fig. 42 the STDDM strength distribution in the ISGQR region (lower part) is compared with the experimental data from  $(p, p')$  experiments [210] (upper part). Although the peak position in STDDM corresponds to the experimental data, STDDM cannot describe the large fragmentation of ISGQR. The result of the large-scale SRPA calculation [213] suggests the importance of higher configurations. There are 19 states below 10 MeV in STDDM, which are compared with experiment [211] in Figure 44.

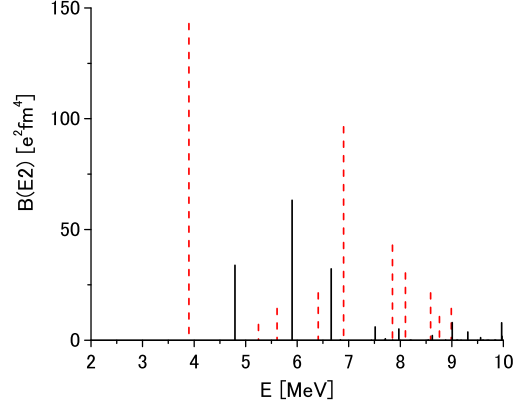


FIG. 44. Distribution of  $B(E2)$  strength below 10 MeV calculated in STDDM for  $^{40}\text{Ca}$ . Experimental data (dashed line) are taken from Ref. [211].

The first  $2^+$  state in  $^{40}\text{Ca}$  cannot be described in RPA and STDDM because it mainly consists of  $4p$ – $4h$  states. The summed strength below 10 MeV is  $166 e^2\text{fm}^4$  in STDDM, which explains about two thirds of the experimental value  $263 \pm 46 e^2\text{fm}^4$ , where the first  $2^+$  state is excluded.

In summary of this section, we can say that a simplified version of ERPA, that is STDDM, yields quite encouraging results. However, the numerical challenges are quite enormous and much effort must still be invested in the future to make this promising approach a full success.

## IX. DISCUSSION AND CONCLUSIONS

In this review we gave a survey of recent developments of the equation of motion (EOM) method as applied to the many-body problem of fermions. This method leads essentially to extended RPA equations, which are mostly applied in nuclear physics, but not only. There is some activity on this also in theoretical chemistry, in condensed matter, and in plasma physics which we mention in the main text. In order to point to the distinctive feature with respect to other many-body approaches, we transcribed the EOM approach into formally exact 'Dyson-Bethe-Salpeter' equations (Dyson-BSEs) for two-fermion propagators. These Dyson-BSEs contain an integral kernel which depends only on one frequency which, e.g., in the case of the response function, corresponds to the one of the external photon. This integral kernel contains a static, i.e., frequency independent and a genuinely frequency dependent, i.e., dynamic part. This is analogous to the single-particle Dyson equation, where the self-energy also splits into the static mean-field and the frequency dependent parts. The static part of the integral kernel in the Dyson-BSE can be interpreted as the

mean field for the two-fermion propagation. For example, in the case of  $pp$  propagation, it enters in a natural way the optical potential of elastic deuteron scattering on nuclei. In the many-body community outside nuclear physics it is not well recognized that such formally exact Dyson-BSEs with well-defined single frequency integral kernels in terms of higher correlation functions exist. Bethe-Salpeter equations (BSEs) are mainly constructed on the basis of Green's functions with four time dependencies, that is, as many as there are fermion operators in, e.g., the response function. Taking into account the time homogeneity, the kernels still depend on three frequencies, which makes a numerical solution other than for the most basic approximations practically impossible. The popularity of this multi-frequency approach, probably, stems from the fact that in the past it has been shown that corresponding BSEs can be constructed, which fulfill all basic properties as there are conservation laws and Ward identities. In condensed matter and theoretical chemistry, for example, the GW approximation is based on the so-called Hedin equations [214] or else conserving approximations can also be derived from the Kadanoff-Baym so-called  $\phi$ -derivable functionals [215, 216]. All these techniques lead, besides lowest order approximations, like HF-RPA, to integral kernels which depend on more than one frequency, which in most cases cannot be treated numerically without further quite drastic approximations in order to reduce the integral kernel to a one frequency dependence. However, we have shown that most of the time those one frequency forms can directly be obtained from our explicit expression of the one-frequency kernel, see, e.g., [96]. In addition, as we show in this review, also EOM equations and corresponding Dyson-BSEs can be formulated so as to *fulfill conservation laws and Ward identities*. Since the corresponding equations are of the Schroedinger type, the access to numerical solutions is much improved and physically motivated non-trivial approximations are straightforwardly elaborated. We give an example with the three-level Lipkin model, where the numerical solution clearly shows the appearance of a Goldstone mode in the spontaneously broken symmetry phase. Even in this simple model, to solve the Kadanoff-Baym approach including screening, that is, vertex corrections, would be extremely difficult from the numerical point of view. In Section VII and in [196, 217] it is shown in complete generality that conservation laws and Goldstone theorem are fulfilled with appropriate EOM equations.

After these general remarks let us be more specific on the objectives and content of this review. Our basic aim is to improve on the standard HF-RPA approach (we always include exchange in our equations, so HF-RPA means linearised time dependent HF equations). It is well known that, besides nice properties, HF-RPA also suffers from sometimes severe shortcomings. One of those is that HF-RPA corresponds to a bosonisation, see Sect.II.B and [5], of the  $ph$  fermion pairs, which stems from the fact that the RPA matrix is constructed with

the HF vacuum. RPA treats two-body correlations, so using an uncorrelated ground state is clearly an inconsistency. We remedy to this problem in showing that the Coupled Cluster Doubles (CCD) wave function is actually the vacuum to an extended RPA operator containing a specific two-body term, see Sect.II.C. Because of this extra term the approach is a little difficult to handle, but first results are very promising, see Sect.V.C. It is clear that with the CCD wave function as vacuum the Pauli principle is entirely respected. However, in the recent past, because of this difficulty, the two-body term was neglected, which lead to a (relatively mild) violation of the Pauli principle, see [43], within Richardson's pairing model which contains one of the most severe Pauli principle constraints possible since each s.p. level is only two fold degenerate. However, also in other models as, e.g., Lipkin and Hubbard models, it turned out that the Pauli principle violations are surprisingly weak [42]. In this way, with a correlated ground state, the RPA approach turns into a Hartree-Fock Bogoliubov approach for fermion pairs, where the RPA matrix depends in a quite non-linear way on the usual RPA amplitudes  $X$  and  $Y$ . It was named Self-Consistent RPA (SCRPA). Results on some non-trivial models (Richardson model, three-level Lipkin model, Hubbard model) show very strong improvements, most importantly close to a phase transition point. However, around the phase transition points appeared some slight discontinuities reminiscent of a first order phase transition, which are absent in the exact solutions of those models. In Sect. V.C, in an application to the Lipkin model, we achieved for the first time to keep the vacuum property of the CCD wave function fully. The results are excellent with, e.g., the correlation energy going smoothly through the phase transition region, showing there a 4 percent error while becoming even better in the weak and strong coupling limits. So, this success opens up quite wide perspectives. Of course, the approach is necessarily of some complexity and for problems, which do not demand such sophistication, more easily accessible variants of improved RPA approaches are available. The easiest one and, may be, also the most obvious one, is the so-called renormalised RPA (r-RPA). In standard HF-RPA equations one uses HF occupation numbers which are zero or one. Since RPA calculates two-body correlation functions, it is natural to replace the HF occupation numbers by correlated, rounded ones. There exists indeed, in nuclear physics, since long a correction to the HF occupation numbers, which involves in a direct way the RPA two-body correlation density matrix, see Sect.II.B. With this, in a minimal way, the RPA matrix depends on the RPA solution and a self-consistency problem is created. Because of its numerical simplicity, this form of RPA extension has known quite a number of applications, as outlined in Sect. III.D. In particular, this approach was extensively applied in the investigation of double beta decay processes. By the way, this r-RPA also can be formulated in such a way as to conserve all nice properties of the standard HF-RPA. This

simple extension of RPA has in addition the property that the Luttinger theorem is conserved [148]. The full Hartree-Fock-Bogoliubov approach for fermion pairs was coined, as mentioned, Self-Consistent RPA (SCRPA). It contains much more correlations in the RPA matrix. One of the most important ones is that the bare force becomes screened (or antiscreened). For example, in the Richardson pairing Hamiltonian, for small particle numbers, the Pauli principle is so strong and, thus, screening so important that the originally attractive force is turned into repulsion, see Fig. 4 in Sect.III.A.

Besides the usual two-fermion ( $ph$  and  $pp$ ) problems, RPA-like equations can also be applied to the single-particle propagator, where in the self-energy of the Dyson equation the  $2p - 1h(2h - 1p)$  propagator appears. With the EOM method we find a form of this propagator, which uses again the CCD wave function as the vacuum. This approach was coined odd-self-consistent RPA or, in short, odd-RPA. It is by the way in this way that the aforementioned excellent results for the Lipkin model were obtained in Sect.V.C allowing to pass through the phase transition region in a continuous and accurate way. One-fermion and two-fermion RPA approaches are, of course, complementary to each other. The Dyson equation allows one to calculate the correlated occupation numbers which are also needed in the SCRPA equations.

Those s.p. and two-particle Dyson equations lend themselves in an efficient way to tackle the important aspect of nuclear physics, which is the particle-vibration coupling (PVC) approach. It turns out that for the description of the width of giant resonances it is absolutely necessary to consider self-energy of the Dyson equation and dynamic kernel of the response function to rather high order in the particle-vibration (phonon) couplings. An overview of this is given in Sect. IV.D.

An extremely important aspect of nuclear physics is alpha-particle clustering. Again the EOM method has allowed to tackle this difficult subject in a very efficient way. It was shown by an in-medium four-body equation that  $\alpha$ -particle condensation occurs only below a certain critical density which corresponds to the point where the chemical potential turns from negative (bound state) to positive (scattering states). We explain that this has to do with the four-body level density which for positive chemical potentials  $\mu$  goes through zero at the Fermi-energy. This entails that there is no  $\alpha$ -particle condensation possible at those higher densities. The density, therefore, is the control parameter of this nuclear quantum phase transition (QPT). We explain why this is opposite to deuteron condensation or, more generally, to pairing where the BCS solution exists at all densities as long as there is an attractive force. This hinges on the unique situation that for pairs at rest the two-particle level density does not go through zero at the Fermi energy. This quartet condensation approach entailed that the enigmatic structure of the Hoyle state in  $^{12}\text{C}$  at 7.65 MeV, so important for the carbon production in the universe and, thus, for life on earth, could be explained as a

state where three  $\alpha$ -particles move almost freely in an extended volume within their 0S center of mass wave function, being a forerunner of  $\alpha$ -particle condensation in nuclear matter, see [193].

In the last two Sections VII and VIII, we illustrate another extension of RPA theory in including to the density-density (response) function the next higher configurations, which contain the squares of the density ( $2p - 2h$ ). The corresponding equations are also consistently constructed on a corresponding correlated ground state. It is demonstrated that the approach, including the SCRPA one, is *conserving* and keeps all good properties of standard HF-RPA intact. The numerical applications to simple models show very good accuracy. A pilot calculation in a very restricted space for giant resonances in  $^{16}\text{O}$  and  $^{40}\text{C}$  shows interesting spreading effects. In a much more rudimentary, that is, phenomenological form this theory in nuclear physics is known as the 'second RPA' (SRPA). It is still numerically very demanding because of the extremely high dimensions of the matrices to be diagonalized. However, nice successes using phenomenological effective forces have in the mean-time appeared in nuclear physics [127, 128, 213]. The theory outlined in this review has as final objectives *ab initio calculations*. However, because of the numerical complexity of the equations, applications are still very rare and remain for the future.

Let us also mention that the EOM can naturally be applied in almost the same way to Bose systems [25, 218, 219], or to mixtures of bosons and fermions [27, 220].

In summary, we outlined progress in the *equation of motion method* and demonstrated its great utility. We, for instance, pointed out that a Bethe-Salpeter equation for, e.g., the response function can be derived with a single frequency kernel which yields, in principle, the exact solution for the response function. The same holds for the two fermion propagator in the pairing channel. It is argued that this Dyson-BSE approach is much more amenable to numerical solutions than the multi-frequency BSE, since the former leads to equations of the Schrödinger type. Also the explicit form of the integral kernels in terms of higher correlation functions lends itself to physically well motivated approximations which are difficult to obtain from the multi-frequency formulation. Additionally the advocated equations can be formulated in such a way that all conservation laws, sum-rules, Goldstone theorem and Ward identities are fulfilled, see Sects.VII.D and VII.E. Therefore, we do not see any advantage to start with the much more complicated multi-frequency formulation of the two fermion Green's function which in the past was almost exclusively at the basis of many-body approaches in various fields of physics.

## ACKNOWLEDGEMENTS

This review could not have been accomplished without the help of many recent and less recent collaborators.



We want in particular thank: V. Olevano, J. Toulouse, G. Strinati, U. Lombardo, M. Baldo, M. Urban, A. Pastore, A. Rabhi, T. Sogo, V.V. Baran, R. Lazauskas, A. Storozhenko, J. G. Hirsch, P. Nozières, J. Wambach, M. Beyer, D. Janssen, S. Adachi, P. Danielewicz, S. Ethofer. Special thanks go to Markus Holzmann for valuable comments on the manuscript. D.S.D. was sup-

ported by the grant PN-18090101/2019-2021 of the Romanian Ministry of Education and Research, J.D. was supported by the Spanish Ministerio de Ciencia, Innovación y Universidades and the European regional development fund (FEDER), Project No. PGC2018-094180-B-I00, and E.L. was supported by the US-NSF Career Grant PHY-1654379.

- 
- [1] J.P. Blaizot and G. Ripka, *Quantum Theory of Finite Systems* (MIT Press, Cambridge, 1986).
  - [2] G.D. Mahan, *Many Particle Physics* (Plenum Press, New York, 1981).
  - [3] J.W. Negele, H. Orland, *Quantum Many Particle Systems, Frontiers in Physics* (Addison Wesley, New York, 1988).
  - [4] A.L. Fetter and J.D. Walecka, *Quantum Theory of Many particle Systems* (McGraw-Hill, New York, 1971).
  - [5] P. Ring and P. Schuck, *The Nuclear Many-body Problem* (Springer-Verlag, Berlin, 1980).
  - [6] R. J. Bartlett and M. Musial, *Rev. Mod. Phys.* **79**, 291 (2007); G. Hagen, T. Papenbrock, M. Hjorth-Jensen, and D. J. Dean, *Coupled-cluster computations of atomic nuclei*, *Rep. Prog. Phys.* **77**, 096302 (2014).
  - [7] P. Fulde, *Electron Correlations in Molecules and Solids*, (Springer Series in Solid State Sciences, Gebhardt book, 1995).
  - [8] L. K. Wagner and D. M. Ceperley, *Discovering correlated fermions using quantum Monte Carlo*, *Rep. Prog. Phys.* **79** 094501 (2016).
  - [9] J. Carlson, S. Gandolfi, F. Pederiva, Steven C. Pieper, R. Schiavilla, K.E. Schmidt, and R.B. Wiringa, *Quantum Monte Carlo methods for nuclear physics*, *Rev. Mod. Phys.* **87**, 1067 (2015).
  - [10] J. W. Clark, P. Westhaus, *Phys. Rev.* **141** (1966) 833.
  - [11] A. Fabrocini, S. Fantoni, E. Krotscheck (Editors), *Introduction to Modern Methods of Quantum Many Body Theory*, Vol.7, World Scientific, Singapore (2002).
  - [12] R. Bauerschmidt, D. C. Bydges, and G. Slade, *Lecture Notes in Mathematics*, (Springer 2019).
  - [13] R. F. Bishop, *Theor. Chem. Acta* **80** (1991) 95.
  - [14] S. Kehrein, *The Flow Equation Approach to Many-Particle Systems*, (Springer Tracts in Modern Physics, 2006).
  - [15] U. Schollwöck, *Rev. Mod. Phys.* **77**, 259 (2005).
  - [16] D.J. Rowe, *Rev. Mod. Phys.* **40**, 153 (1968); *Phys. Rev.* **175**, 1283 (1968).
  - [17] G. Röpke, T. Seifert, H. Stolz, and R. Zimmermann, *Phys. Stat. Sol. (b)* **100**, 215 (1980); G. Röpke, M. Schmidt, L. Münchow, and H. Schulz, *Nucl. Phys. A* **399**, 587 (1983).
  - [18] G. Röpke, *Z. Phys.* **B99**, 83 (1995) and the references therein.
  - [19] G. Röpke, *Phys. Rev. C* **79**, 014002 (2009).
  - [20] H. Hergert, S. K. Bogner, T. D. Morris, A. Schwenk, and K. Tsukiyama, *Phys. Rep.* **621**, 165 (2016).
  - [21] J. Dukelsky and P. Schuck, *Nucl. Phys. A* **512**, 466 (1990).
  - [22] J. Dukelsky, G. Röpke, and P. Schuck, *Nucl. Phys. A* **628**, 17 (1998).
  - [23] J. Dukelsky and P. Schuck, *Phys. Lett. B* **464**, 164 (1999).
  - [24] M. Baranger, *Nucl. Phys. A* **149** (1970) 225.
  - [25] J. Dukelsky and P. Schuck, *Mod. Phys. Lett. A* **26**, 2429 (1991).
  - [26] T. Sogo, P. Schuck, and M. Urban, *Phys. Rev. A* **88**, 023613 (2013).
  - [27] T. Watanabe, T. Suzuki, and P. Schuck, *Phys. Rev. A* **78**, 033601 (2008).
  - [28] A. Storozhenko, P. Schuck, T. Suzuki, H. Yabu, and J. Dukelsky, *Phys. Rev. A* **71**, 063617 (2005).
  - [29] P. Krüger and P. Schuck, *Europhys. Lett.* **27** (1994) 395; J. G. Hirsch, A. Mariano, J. Dukelsky, and P. Schuck, *Ann. Phys. (NY)* **296**, 187 (2002).
  - [30] P. Schuck, S. Ethofer, *Nucl. Phys. A* **212**, 269 (1973); J. Dukelsky, G. Röpke, P. Schuck, *Nucl. Phys. A* **628**, 17 (1998).
  - [31] S. Adachi and P. Schuck, *Nucl. Phys. A* **496**, 485 (1989).
  - [32] H.-J. Schulze, P. Schuck, and N. Van Giai, *Phys. Rev. B* **61**, 8026 (2000); P. Schuck, H.-J. Schulze, and N. Van Giai, and M. Zverev, *Phys. Rev. B* **67**, 233404 (2003).
  - [33] K. Chatterjee and K. Pernal, *J. Chem. Phys.* **137**, 204109 (2012).
  - [34] H. Eshuis, J. Bates, and F. Furche, *Theor. Chem. Acc.* **131**, 1084 (2012).
  - [35] K. Pernal, K. Chatterjee, and P. H. Kowalski, *J. Chem. Phys.* **140**, 014101 (2014).
  - [36] K. Pernal, *Phys. Rev. Lett.* **120**, 013001 (2018).
  - [37] T. Shibuya, V. McKoy, *Phys. Rev. A* **2**, 2208 (1970).
  - [38] T. Shibuya, J. Rose, and V. McKoy, *J. Chem. Phys.* **58**, 500 (1973).
  - [39] A. C. Lasaga and M. Karplus, *Phys. Rev. A* **16**, 807 (1977).
  - [40] J. Terasaki, A. Smetana, F. Simkovic, and M. I. Krivoruchenko, *Int. J. Mod. Phys. E* **26**, 1750062 (2017).
  - [41] M. Jemai and P. Schuck, *Phys. At. Nucl.* **74**, No 8, 1139 (2011).
  - [42] M. Jemai, D.S. Delion, and P. Schuck, *Phys. Rev. C* **88**, 044004 (2013).
  - [43] J.G. Hirsch, A. Mariano, J. Dukelsky, and P. Schuck, *Ann. Phys. (NY)* **296**, 187 (2002).
  - [44] P. Schuck and M. Tohyama, *Phys. Rev. B* **93**, 165117 (2016).
  - [45] D.S. Delion, P. Schuck, and J. Dukelsky, *Phys. Rev. C* **72**, 064305 (2005).
  - [46] K. Hara, *Progr. Theor. Phys.* **32**, 88 (1964).
  - [47] F. Catara, G. Piccitto, M. Sambataro, and N. Van Giai, *Phys. Rev. B* **54**, 17536 (1996); F. Catara, M. Grasso, G. Piccitto, and M. Sambataro, *Phys. Rev. B* **58**, 16070 (1998).

- [48] D. J. Thouless *The Quantum Mechanics of Many-Body Systems*, Academic Press Inc., New York and London (1961).
- [49] A. Rabhi, R. Bennaceur, G. Chanfray, and P. Schuck, Phys. Rev. C **66**, 064315 (2002).
- [50] C. Federsmidt, P. Ring, Nucl. Phys. A **435**, 110 (1985).
- [51] M. Kyotoku, K.W. Schmid, F. Grümmer, and A. Faessler, Phys. Rev. C **41**, 284 (1990).
- [52] O. Civitarese, A. Faessler, J. Suhonen, and X.R. Wu, Nucl. Phys. A **524**, 404 (1991).
- [53] J. Suhonen, J. Phys. G **19**, 139 (1993).
- [54] J. Dukelsky, J. E. Garcia-Ramos, J. M. Arias, P. Pérez-Fernández, and P. Schuck, Phys. Lett. B **795**, 537 (2019).
- [55] E. Sangfelt, R. Roy Chowduri, B. Weiner, Y. Ahrn, J. Chem. Phys. **86**, 4523 (1987).
- [56] D. Agassi, Nucl. Phys. A **116**, 49 (1968).
- [57] E. D. Davis, W. D. Heiss, J. Phys. G **12**, 805 (1986).
- [58] J. E. Garcia-Ramos, J. Dukelsky, P. Prez-Fernndez, and J. M. Arias, Phys. Rev. C **97**, 054303 (2018).
- [59] M. Bender *et al* arXiv:2005.10216.
- [60] M. Tohyama, and P. Schuck, Phys. Rev. C **87**, 044316 (2013).
- [61] M. Jemai and P. Schuck, Phys. Rev. C **100**, 034311 (2019).
- [62] R.W. Richardson, Phys. Lett. **3**, 277 (1963).
- [63] S.Y. Li, A. Klein and R.M. Dreizler, J. Math. Phys. **11**, 975 (1970).
- [64] N. Meshkov, Phys. Rev. C **3**, 2214 (1971).
- [65] M. Sambataro, Phys. Rev. C **60**, 064320 (1999).
- [66] M. Grasso, F. Catara, and M. Sambataro, Phys. Rev. C **66**, 064303 (2002).
- [67] K. Hagino and G.F. Bertsch, Phys. Rev. C **61**, 024307 (2000).
- [68] D. Forster, *Hydrodynamic fluctuations-broken symmetry and correlation functions*, Frontiers in Physics: A Lecture Note and Reprint Series, No **47** (Benjamin, New York, 1975).
- [69] M. Jemai, P. Schuck, J. Dukelsky, and R. Bennaceur, Phys. Rev. B **71**, 085115 (2005).
- [70] D. Durel and M. Urban, Phys. Rev. A **101**, 013608 (2020).
- [71] A.A.Raduta, A.Faessler, and S.Stoica, Nucl.Phys.A **534**, 149 (1991).
- [72] J. Toivanen and J. Suhonen, Phys. Rev. Lett. **75**, 410 (1995).
- [73] F. Catara, N. Dinh Dang, and M. Sambataro, Nucl. Phys. A **579**, 1 (1994).
- [74] R. Machleidt, K. Holinde, and C. Elster, Phys. Rep. **149**, 1 (1987).
- [75] J. Toivanen and J. Suhonen, Phys. Rev. C **55**, 2314 (1997).
- [76] J. Schwieger, F. Simkovic, and Amand Faessler, Nucl. Phys. A **600**, 179 (1996).
- [77] Amand Faessler and F. Simkovic, J. Phys. G **24**, 2139 (1998).
- [78] O. Civitarese and M. Reboiro, Phys. Rev. C **57**, 3092 (1997).
- [79] J.G. Hirsch, P.O. Hess, and O. Civitarese, Phys. Rev. C **54**, 1976 (1996).
- [80] J.G. Hirsch, P.O. Hess, and O. Civitarese, Phys. Rev. C **56**, 199 (1997).
- [81] J.G. Hirsch, P.O. Hess, and O. Civitarese, Phys. Rev. C **60**, 064303 (1999).
- [82] J.G. Hirsch, O. Civitarese, and M. Reboiro, Phys. Rev. C **60**, 024309 (1999).
- [83] A.A. Raduta, Prog. Part. Nucl. Phys. **48**, 233 (2002).
- [84] A. Bobyk, W.A. Kaminski, and P. Zareba, Eur. Phys. J. A **5**, 385 (1999).
- [85] A. Bobyk, W.A. Kaminski, and P. Zareba, Nucl. Phys. A **669**, 221 (2000).
- [86] A.A. Raduta *et al.*, Nucl. Phys. A **634**, 497 (1998).
- [87] C.M. Raduta and A.A. Raduta, Nucl. Phys. A **756**, 153 (2005).
- [88] C. M. Raduta and A. A. Raduta, Phys. Rev. C **82**, 068501 (2010).
- [89] N. Dinh Dang and A. Arima, Phys. Rev. C **62**, 024303 (2000).
- [90] V. Rodin and A. Fessler, Phys. Rev. C **66**, 051303(R) (2002).
- [91] L. Paceaescu, V. Rodin, F. Simkovic, and A. Faessler, Phys. Rev. C **68**, 064310 (2003).
- [92] F. Krmpotic, E.J.V. Passos, D.S. Delion, J. Dukelsky, and P. Schuck, Nucl. Phys. A **637**, 295 (1998).
- [93] F. Simkovic, A.A. Raduta, M. Veselsky, and A.Faessler, Phys. Rev. C **61**, 044319 (2000).
- [94] F. Simkovic, M. Smotlak, and G. Pantis, Phys. Rev. C **68**, 014309 (2003).
- [95] F. Simkovic, M. Smotlak, and A.A. Raduta, J. Phys. G **27**, 1757 (2001).
- [96] V. Olevano, J. Toulouse, and P. Schuck, J. Chem. Phys. **150**, 084112 (2019).
- [97] P. Schuck, Eur. Phys. J. A **55**, 250 (2019).
- [98] L. P. Gorkov and T. K. Melik-Barkhudarov, Sov. Phys. JETP **13**, 1018 (1961).
- [99] G. Calvanese Strinati, P. Pieri, G. Röpke, P. Schuck, and M. Urban, Phys. Rep. **738**, 1 (2018).
- [100] S. Ramanan and M. Urban, Phys. Rev. C **98**, 024314 (2018).
- [101] C.J. Pethick and H. Smith, *Bose-Einstein Condensation in Dilute Gases* (Cambridge University Press, 2002).
- [102] W. D. Kraeft, D. Kremp, W. Ebeling, and G. Röpke, *Quantum Statistics of Charged Particle Systems* (Berlin, Akademie-Verlag 1986).
- [103] Wenmei Guo, U. Lombardo, and P. Schuck, Phys. Rev. C **99**, 014310 (2019).
- [104] M. Urban and S. Ramanan, Phys. Rev. C **101**, 035803 (2020).
- [105] E. Litvinova, C. Robin, and P. Schuck, EPJ Web Conf. **182**, no. 02075 (2018).
- [106] E. Litvinova and P. Schuck, Phys. Rev. C **100**, 064320 (2019).
- [107] A. Bohr and B. R. Mottelson, *Nuclear structure*, vol. 1 (World Scientific, 1969).
- [108] A. Bohr and B. R. Mottelson, *Nuclear structure*, vol. 2 (Benjamin, New York, 1975).
- [109] R. A. Broglia and P. F. Bortignon, Phys. Lett. B **65**, 221 (1976).
- [110] P. F. Bortignon, R. Broglia, D. Bes, and R. Liotta, Phys. Rep. **30**, 305 (1977).
- [111] G. Bertsch, P. Bortignon, and R. Broglia, Rev. Mod. Phys. **55**, 287 (1983).
- [112] V. Soloviev, *Theory of Atomic Nuclei: Quasiparticles and Phonons* (Institute of Physics Publishing, 1992).
- [113] P. F. Bortignon, R. A. Broglia, and D. R. Bes, Phys. Lett. B **76**, 153 (1978).

- [114] P. F. Bortignon and R. A. Broglia, Nucl. Phys. A **371**, 405 (1981).
- [115] C. Mahaux, P. Bortignon, R. Broglia, and C. Dasso, Phys. Rep. **120**, 1 (1985).
- [116] P. Bortignon, R. Broglia, G. Bertsch, and J. Pacheco, Nucl. Phys. A **460**, 149 (1986).
- [117] P. F. Bortignon and C. H. Dasso, Phys. Rev. C **56**, 574 (1997).
- [118] G. Colò and P.-F. Bortignon, Nucl. Phys. A **696**, 427 (2001).
- [119] V. Tselyaev, Sov. J. Nucl. Phys. **50**, 780 (1989).
- [120] S. P. Kamerdzhiev, G. Y. Tertychny, and V. I. Tselyaev, Physics of Particles and Nuclei **28**, 134 (1997).
- [121] V. Yu. Ponomarev, P. F. Bortignon, R. A. Broglia, and V. V. Voronov, Nucl. Phys. A **687**, 170 (2001).
- [122] V. Yu. Ponomarev et al., Phys. Rev. Lett. **83**, 4029 (1999).
- [123] N. Lo Iudice, V. Y. Ponomarev, C. Stoyanov, A. V. Sushkov, and V. V. Voronov, J. Phys. G **39**, 043101 (2012).
- [124] E. Litvinova, Physics Letters B **755**, 138 (2016).
- [125] C. Robin and E. Litvinova, Eur. Phys. J. A **52**, 205 (2016).
- [126] C. Robin and E. Litvinova, Phys. Rev. C **98**, 051301 (2018).
- [127] C. Robin and E. Litvinova, Phys. Rev. Lett. **123**, 202501 (2019).
- [128] P.F. Bortignon, E.E. Saperstein, and M. Baldo, Eur. Phys. J. A **246**, (2019).
- [129] P. Romaniello, D. Sangalli, J. A. Berger, F. Sottile, L. G. Molinari, and L. Reining, J. Chem. Phys. **130**, 044108 (2009).
- [130] E. Litvinova and P. Schuck, arXiv:1912.12585 (2019).
- [131] P. Papakonstantinou and R. Roth, Phys. Lett. B **671**, 356 (2009).
- [132] E. Litvinova, P. Ring, and V. Tselyaev, Phys. Rev. C **75**, 064308 (2007).
- [133] E. Litvinova, P. Ring, and V. Tselyaev, Phys. Rev. C **78**, 014312 (2008).
- [134] E. Litvinova, P. Ring, and V. Tselyaev, Phys. Rev. Lett. **105**, 022502 (2010).
- [135] E. Litvinova, P. Ring, and V. Tselyaev, Phys. Rev. C **88**, 044320 (2013).
- [136] V. Tselyaev, N. Lyutorovich, J. Speth, S. Krewald, and P. G. Reinhard, Phys. Rev. C **94**, 034306 (2016).
- [137] V. Tselyaev, N. Lyutorovich, J. Speth, and P. G. Reinhard, Phys. Rev. C **97**, 044308 (2018).
- [138] Y. Niu, Z. Niu, G. Colò, and E. Vigezzi, Phys. Rev. Lett. **114**, 142501 (2015).
- [139] Y. Niu, Z. Niu, G. Colò, and E. Vigezzi, Phys. Lett. B **780**, 325 (2018).
- [140] S. Shen, G. Colò, X. Roca-Maza, et al., Phys. Rev. C **101**, 044316 (2020).
- [141] E. Litvinova, Phys. Rev. C **91**, 034332 (2015).
- [142] V. A. Erokhova, M. A. Yolkina, A. V. Izotova, B. S. Ishkhanov, I. M. Kapitonov, E. I. Lileeva, and E. V. Shirokov, Bulletin of the Russian Academy of Science, Physics **67**, 1636 (2003).
- [143] V. I. Tselyaev, Phys. Rev. C **88**, 054301 (2013).
- [144] P. Papakonstantinou and R. Roth, Phys. Rev. C **81**, 024317 (2010).
- [145] F. Raimondi and C. Barbieri, Phys. Rev. C **99**, 054327 (2019).
- [146] M. Grasso and D. Gambacurta, Phys. Rev. C **101**, 064314 (2020).
- [147] D. Danielewicz and P. Schuck, Nucl. Phys. A **567**, 78 (1994).
- [148] M. Urban and P. Schuck, Phys. Rev. C **90**, 023632 (2014).
- [149] P. Nozières and S. Schmitt-Rink, J. Low Temp. Phys. **59**, 159 (1985).
- [150] A. Storozhenko, P. Schuck, J. Dukelsky, G. Röpke, and A. Vdovin, Ann. Phys. (NY) **307**, 308 (2003).
- [151] P. Schuck, F. Villars, and P. Ring, Nucl. Phys. A **208**, 302 (1973).
- [152] G. A. Rijsdijk, W. J. W. Geurts, K. Allaart, Phys. Rev. C **53**, 201 (1996).
- [153] V.A. Khodel and E. E. Saperstein, Phys. Rep. **92**, 183 (1982).
- [154] N.V. Gnezdilov, I.N. Borzov, E.E. Saperstein, and S.V. Tolokonnikov, Phys. Rev. C **89**, 034404 (2014).
- [155] Nam Vu, Ion Mitxelena, and A. E. DePrince, J. Chem. Phys. **151**, 244121 (2019).
- [156] M. Jemai, and P. Schuck (submitted to Eur. Phys. J. A).
- [157] H. J. Lipkin, N. Meshkov and A. J. Glick, Nucl. Phys. A **62**, 188 (1965).
- [158] J. Vidal, G. Palacios, and C. Aslangul, Phys. Rev. A **70**, 062304 (2004).
- [159] P. Ribeiro, J. Vidal, and R. Mosseri, Phys. Rev. Lett. **99**, 050402 (2007).
- [160] G. Colò and S. De Leo, Int. J. Mod. Phys. E **27**, 1850039 (2018).
- [161] S. Campbell, G. De Chiara, M. Paternostro, G. M. Palma, and R. Fazio, Phys. Rev. Lett. **114**, 177206 (2015).
- [162] P. Schuck is very grateful to V.V. Baran who has pointed this out to him.
- [163] G. Röpke, in "Nuclear Particle Correlations and Cluster Physics", edited by W.-U. Schröder (World Scientific, Singapore, 2017).
- [164] M. Schmidt, G. Röpke, and H. Schulz, Ann. Phys. (NY) **202**, 57 (1990).
- [165] C.J. Horowitz and A. Schwenk, Nucl. Phys. A **776**, 55 (2006).
- [166] P. Schuck, Int. J. Mod. Phys. E **17**, 2136 (2008).
- [167] G. Röpke, D. N. Voskresensky, I. A. Kryukov, D. Blaschke, Nucl. Phys. A **970**, 224 (2018).
- [168] G. Röpke, R. Der, Phys. Stat. Sol. (b) **92**, 501 (1979).
- [169] M. Schmidt, G. Röpke, and H. Schulz, Ann. Phys. (NY) **202**, 57 (1990).
- [170] Meng Jin, M. Urban, and P. Schuck, Phys. Rev. C **82**, 024911 (2010).
- [171] T. Alm, G. Röpke, and M. Schmidt, Z. Phys. A **351**, 295 (1995).
- [172] G. Röpke, Phys. Rev. C **92**, 054001 (2015).
- [173] H. Stein, A. Schnell, T. Alm, and G. Röpke, Z. Physik A **351**, 295 (1995).
- [174] G. Röpke, Ann. Physik (Leipzig) **3**, 145 (1994); R. Haussmann, Z. Physik B **91**, 291 (1993).
- [175] P. Bozek, Nucl. Phys. A **657**, 187 (1999).
- [176] R. Haussmann and W. Zwerger, Phys. Rev. A **80**, 063612 (2009).
- [177] U. Lombardo, P. Nozières, P. Schuck, H.-J. Schulze, and A. Sedrakian, Phys. Rev. C **64**, 064314 (2001).
- [178] T. Sogo, G. Röpke, and P. Schuck, Phys. Rev. C **81**, 064310 (2010).

- [179] A. Sedrakian, J. Mur-Petit, A. Polls, and H. Mütter, Phys. Rev. A **72**, 013613 (2005).
- [180] A. Schnell, G. Röpke, and P. Schuck, Phys. Rev. Lett. **83**, 1926 (1999).
- [181] M. Randeria, Varenna Lectures 1997, cond-mat/9710223.
- [182] W. H. Dickhoff and C. Barbieri, Prog. Part. Nucl. Phys. **52**, 377 (2004); A. Schnell, Ph.D. Thesis, Rostock (1996).
- [183] Chang Xu, Z. Ren, G. Röpke, P. Schuck, Y. Funaki, H. Horiuchi, A. Tohsaki, T. Yamada, and Bo Zhou, Phys. Rev. C **93**, 011306 (2016).
- [184] Chang Xu, G. Röpke, P. Schuck, Z. Ren, Y. Funaki, H. Horiuchi, A. Tohsaki, T. Yamada, and Bo Zhou, Phys. Rev. C **95**, 061306 (2017).
- [185] T. Sogo, R. Lazauskas, G. Röpke, and P. Schuck, Phys. Rev. C **79**, 051301 (2009).
- [186] M. Beyer, S.A. Sofianos, C. Kuhrt, G. Röpke, and P. Schuck, Phys. Lett. B **488**, 247 (2000).
- [187] G. Röpke, A. Schnell, P. Schuck, and P. Nozières, Phys. Rev. Lett. **80**, 3177 (1998).
- [188] R.A. Malfliet and J.A. Tjon, Nucl. Phys. A **127**, 161 (1969).
- [189] H. Kamei and K. Miyake, J. Phys. Jpn. **74**, 1911 (2005).
- [190] A. Tohsaki, H. Horiuchi, P. Schuck, and G. Röpke, Phys. Rev. Lett. **87**, 192501 (2001).
- [191] A.H. Blin, R.W. Hasse, B. Hiller, P. Schuck, and C. Yannouleas, Nucl. Phys. A **456**, 109 (1986).
- [192] J.-P. Ebran, M. Girod, R. Lasser, and P. Schuck, Phys. Rev. C **102**, 014305 (2020).
- [193] A. Tohsaki, H. Horiuchi, P. Schuck, and G. Röpke, Rev. Mod. Phys. **89**, 011002 (2017).
- [194] J. Sawicki, Phys. Rev. **126**, 2231 (1962).
- [195] S. Drożdż, S. Nishizaki, J. Speth and J. Wambach, Phys. Rep. **197**, 1 (1990).
- [196] M. Tohyama and P. Schuck, Eur. Phys. J. A **19**, 203 (2004).
- [197] S. J. Wang and W. Cassing, Ann. Phys. **159**, 328 (1985); W. Cassing and S. J. Wang, Z. Phys. A **328**, 423 (1987).
- [198] M. Tohyama, S. Takahara and P. Schuck, Eur. Phys. J. A **21**, 217 (2004).
- [199] K. Takayanagi, K. Shimizu and A. Arima, Nucl. Phys. A **477**, 205 (1988).
- [200] D. J. Thouless, Nucl. Phys. A **22**, 78 (1961).
- [201] M. Tohyama and P. Schuck, Eur. Phys. J. A **32**, 139 (2004).
- [202] M. Tohyama and M. Gong, Z. Phys. A **332**, 269 (1989).
- [203] M. Tohyama, Prog. Theor. Phys. **114**, 1021 (2005).
- [204] M. Tohyama, Phys. Rev. C **75**, 044310 (2007).
- [205] M. Tohyama and P. Schuck, Eur. Phys. J. A **36**, 349 (2008).
- [206] P. Schuck, Int. J. Mod. Phys. E **29**, 2050023 (2020).
- [207] P. Schuck and M. Tohyama, Eur. Phys. J. A **52**, 307 (2016).
- [208] M. Tohyama, Prog. Theor. Exp. Phys. **2017**, 093D06 (2017).
- [209] Y.-W. Lui, H. L. Clark, D. and H. Youngblood, Phys. Rev. C **64**, 064308 (2001).
- [210] I. Usman *et al.*, Phys. Lett. B **698**, 191 (2011).
- [211] T. Hartmann *et al.*, Phys. Rev. Lett. **85**, 274 (2000).
- [212] A. Hotta, K. Itoh and T. Saito, Phys. Rev. Lett. **33**, 790 (1974).
- [213] O. Vasseur, D. Gambacurta and M. Grasso, Phys. Rev. C **98**, 044313 (2018).
- [214] L. Hedin, Phys. Rev. A **139**, 796 (1965).
- [215] G. Baym, L. P. Kadanoff, Phys. Rev. **124**, 287 (1961).
- [216] G. Baym, Phys. Rev. **127**, 1391 (1962).
- [217] D.S. Delion, P. Schuck, and M. Tohyama, Eur. Phys. J. B **89**, 1 (2016).
- [218] Z. Aouissat, G. Chanfray, P. Schuck, and G. Welke, Z. Phys. **340**, 347 (1991).
- [219] Z. Aouissat, P. Schuck, R. Rapp, J. Wambach, and G. Chanfray, Nucl. Phys. A **581**, 471 (1995).
- [220] X. Barillier-Pertuisel, S. Pittel, L. Pollet, and P. Schuck, Phys. Rev. A **77**, 012115 (2008).